Efficient Approaches to Robust and Cooperative Wireless Network Design

by

Tony Q.S. Quek

Submitted to the Department of Electrical Engineering and Computer Science
in partial fulfillment of the requirements for the degree of

Doctor of Philosophy

at the

MASSACHUSETTS INSTITUTE OF TECHNOLOGY

February 2008

Author .....
Department of Electrical Engineering and Computer Science
January 31, 2008

Certified by .....
Moe Z. Win
Associate Professor
Thesis Supervisor

Accepted by .....
T. P. Orlando
Chairman, Department Committee on Graduate Students

Efficient Approaches to Robust and Cooperative Wireless Network Design

by

Tony Q.S. Quek

Submitted to the Department of Electrical Engineering and Computer Science
on January 31, 2008, in partial fulfillment of the
requirements for the degree of
Doctor of Philosophy

Abstract

In wireless networks, relaying and user cooperation offer several attractive benefits such as higher throughput, better power efficiency, and larger coverage. As a result, cooperative networks are regarded as one of the most promising enabling technologies able to meet the increasingly high rate demands and quality of service requirements in wireless networks. In this dissertation, we investigate the efficient design of cooperative wireless networks from the perspectives of robust resource allocation, wideband communications, and energy efficiency.

Given that the primary resource to be allocated is the relay node's transmission power, we propose robust and efficient relay power allocation algorithms when the global channel state information is subject to uncertainty. In addition, we propose practical algorithms that do not require frequent tracking of the global channel state information. This work reveals that ignoring global channel state information uncertainties and solving the relay power optimization problems often lead to poor performance, highlighting the importance of robust algorithm designs in practical wireless networks.

Wideband cooperative networks allow for both higher data rate and higher resistance to interference. Since the gains achieved by using cooperation come at the cost of higher node complexity and substantial coordination overhead, it is important to study practical low-complexity signaling and receiver schemes suitable for wideband networks. In particular, we consider transmitted-reference signaling schemes and provide a unified performance analysis in terms of bit error rate. Since wideband networks are expected to coexist with many existing narrowband systems, it is important to characterize the effect of narrowband interference. We further extend the performance analysis of transmitted-reference signaling schemes to include the effect of narrowband interference.

Finally, we conclude by studying the benefits of cooperation in a wireless sensor network, which aims at detecting the presence or absence of a certain physical phenomenon of interest using geographically dispersed sensor nodes. We propose a consensus flooding protocol and analyze its average energy consumption. We inves-

tigate the tradeoff between the detection reliability and the energy efficiency when nodes are allowed to cooperate.

By addressing the above design challenges, this dissertation will be useful for obtaining insight into the theory and application of cooperative networks in future communication systems.

Thesis Supervisor: Moe Z. Win
Title: Associate Professor

Acknowledgments

Throughout my graduate experience, many people have supported me and this dissertation could not have been completed without their help and guidance.

My advisor, Professor Moe Z. Win, deserves particular attention and many thanks for his inquisitiveness, insight, and inspiration. I have benefited tremendously from his countless efforts and dedication to my intellectual and personal growth. He has helped me to reach my milestones to be a well-rounded researcher. I would also like to thank the other members of my dissertation committee, Professors Dimitri Bertsekas, Davide Dardari, and Vivek Goyal for many useful discussions and for contributing their suggestions to shape this dissertation. The financial support of the Agency of Science, Technology and Research (A*STAR) and the Department of Electrical Engineering and Computer Science are also gratefully acknowledged.

The W-Group and Laboratory of Information and Decision Systems (LIDS) have been a truly enriching environment for me as a graduate student and I am fortunate to have met many talented and amazing people: Professor Hyundong Shin has been a great mentor and collaborator and I have learned a lot from him; Wesley Gifford for his patience and help for reading and correcting many of my manuscripts; W. Suwansantisuk for many technical and non-technical discussions; many thanks also go to Dr. Henk Wymeersch, Dr. Buon Kiong Lau, Dr. Andrew Fletcher, Dr. Damien B. Jourdan, Dr. Wee Peng Tay, Pedro C. Pinto, Yuan Shen, Jaime Lien, Faisal M. Kashif, Ulric Ferner, Kampol Woradit, Stefano Maran, Chiara Falsi, Sy Bor Wang, and Lynette Cheah.

Of many other friends and colleagues, I want to thank my Italian colleagues for hosting me during the summer of 2006 at University of Bologna. In particular, I want to thank Professor Davide Dardari for his support and guidance, which made my stay in Italy both fruitful and enjoyable. In addition, special thanks also go to Professor Marco Chiani, Dr. Andrea Conti, Professor Andrea Giorgetti, Dr. Alberto Zanella, and Professor Roberto Verdone for their many helpful discussions and suggestions. I would also like to thank my Japanese colleagues at NTT DoCoMo Wireless Labo-

ratory during my internship in Summer 2003, particularly Dr. Mamoru Sawahashi, Dr. Nobuyuki Maeda and Dr. Hiroyuki Atarashi for hosting me despite their busy schedules.

Among all my friends at MIT, I want to especially thank Melvyn Sim for his kindness and support during my first few years of graduate study. In addition, my fellow brothers and sisters in Christ from the MIT Chinese Bible Study have been my great spiritual support, constantly praying for me and my family during all the difficulties and hardships at MIT.

As always, I thank my family for inspiring me to pursue an academic career. I also thank my wife's parents for visiting us frequently to help us to take care of our children. Last, my most tender and sincere thanks go to my loving wife, Sandy. Without her, this dissertation would not have been completed, and we would not have two adorable children, Joseph and Esther.

I have realized that it is impossible to pass through life without experiencing times when we cannot see our way through a deep valley. When I persevere through these trials and hardships, God gives me a new insight and something that would not be learned otherwise. Without His grace and faithfulness, I cannot imagine how I could have traveled so far in life. May this dissertation brings glory to His name. Amen!

"Wisdom is the God-given ability to see life with rare objectivity and to handle life with rare stability." - Charles R. Swindoll

Contents

List of Figures

List of Tables

Chapter 1

Introduction

1.1 Motivations

Cooperative wireless networking has recently emerged as one of the most promising enabling technologies, as it is able to address a wide range of application scenarios, including cellular networks, IEEE 802.11 networks, wireless sensor networks (WSNs), and ad-hoc networks, to enhance connectivity, extend coverage, and improve energy efficiency and communication reliability. In these cooperative networks, the main feature is that relay nodes pool their resources in a distributed manner to enhance the reliability of wireless transmission links.

The first design challenge to overcome is the efficient use of resource allocation to increase the throughput or energy efficiency of the cooperative networks. Given that the primary resource to be allocated is the relay node's transmission power, can we design robust and efficient relay power allocation (RPA) algorithms when the global channel state information (CSI) is subject to uncertainty? Can we design practical algorithms that do not require frequent tracking of the global CSI? By addressing these questions in our design, we ensure that our proposed algorithms are robust and practical.

The second issue is the study of ultrawide bandwidth (UWB) as an enabling low-complexity technology for cooperative networks. In particular, we focus on non-coherent UWB communications due to their low-complexity and low-power consump-

tion. Therefore, we are interested in fully understanding the performance limits of such UWB communications for their possible implementation in future wideband cooperative networks.

Finally, we study the benefits of cooperation in a specific type of wireless network, WSN, where it involves the fusion of information about a phenomenon of interest (PoI) at a fusion center. Our goal is to investigate the tradeoff between the detection reliability and the energy efficiency when nodes are allowed to cooperate.

1.2 Robust Resource Allocation

Resource allocation in wireless networks promises significant benefits such as higher throughput, longer network lifetime, better quality-of-service (QoS), and lower network interference. In relay networks, the primary resource is the transmission power because it affects both the lifetime and the scalability of the network. For example, consider a WSN in which both the individual sensor power and the total network power are constrained. These twofold constraints are present since sensor nodes typically have limited power resources, such as a battery or solar cell, resulting in a finite total network power proportional to the number of nodes in the network. To prolong network lifetime, it is important to determine the optimal transmission power of the sensor nodes [1–3]. Furthermore, regulatory agencies may limit the total transmission power to reduce interference to other users. For example, consider a relay-enhanced cellular network, where nodes are deployed to relay transmissions from a base station to a distant user. In such a network, efficient power allocation can be used 1) to minimize network interference while satisfying certain QoS requirements; and 2) to maximize network throughput while controlling the amount of network interference [4–6].

However, the benefits promised by power allocation algorithms depend on the quality of the global CSI, which is rarely perfect in practice. As such, algorithm design should take into account such uncertainties in the global CSI. Nevertheless, it is unclear how to incorporate CSI uncertainties in power allocation algorithm design

with the current optimization frameworks. Moreover, conventional power allocation algorithms require tracking of the global CSI at the timescale of fast-fading. This requires frequent communication between the relay nodes and the central unit to determine new power allocations.[1] Therefore, the following important questions arise in practice:

- How can we control network interference by incorporating individual relay and aggregate power constraints in our RPA algorithms?
- What are the fundamental limits on performance gains that can be achieved with RPA when uncertainties exist in the global CSI?
- Is it possible to design RPA algorithms that are robust to global CSI uncertainty?
- Is it feasible to implement RPA algorithms by tracking only large-scale fading which is on the order of seconds?

To address these issues of robustness, we adopt a robust optimization methodology developed in [7,8]. Specifically, this methodology treats uncertainty by assuming that CSI is a deterministic variable within a bounded set of possible values. The size of the uncertainty set corresponds to the amount of uncertainty about the CSI.[2] This methodology ensures that the robust counterpart of uncertain optimization problem, i.e., optimization problem with uncertain global CSI, leads to feasible solutions and yields good performance in all realizations of CSI within the uncertainty set.

In relay networks, various relaying schemes have been proposed and studied [9,10]. Among these, considerable attention has been given to decode-and-forward (DF) and amplify-and-forward (AF) relaying. In DF relaying, the relay node fully decodes, re-encodes, and retransmits the source messages. In AF relaying, the relay node simply forwards a scaled version of its received signal. To reduce the required cooperation overhead, these relaying schemes can also be implemented with only a subset of active relay nodes, which are appropriately selected [11–14]. Furthermore, many of

[1] As a result, this incurs a power penalty due to intense signal processing.

[2] The singleton uncertainty set corresponds to the case of perfect CSI.

the recent works have focused on RPA. For DF relay networks, [13, 15–18] consider orthogonal relay transmissions while [14, 19] exploit the possibility of performing distributed beamforming over a common bandwidth. The problem formulations include maximizing capacity [16, 19], minimizing outage probability [13, 14], and minimizing transmission power [15, 17]. Similarly, for AF relay networks, [15, 18, 20–23] consider orthogonal relay transmissions while [24] considers relay transmissions over a common bandwidth. The problem formulations include maximizing capacity [18, 21, 22, 24], minimizing outage probability [23], and minimizing transmission power [15, 20]. In all the above works, power allocation is performed without imposing any individual relay power constraint.

Here, we focus on an AF relay network.[3] The AF relaying is attractive due to its simplicity (i.e., complexity and cost of relaying is minimal), security (i.e., relay node does not need to decode any information), power-efficiency (i.e., power consumption is minimal due to simple circuitry), and ability to realize full diversity order. Moreover, the AF relaying has been shown to be optimal in certain situations [26, 27]. We consider that all relay nodes operate in a common frequency band. This allows faster and easier deployment of the relay nodes since the addition of relay nodes to the existing network will have little effect on the source and the destination nodes; e.g., specific relay channel assignments are not necessary. We consider coherent and noncoherent AF relaying, depending on the knowledge of CSI available at each relay node. When an AF relay node has access to its locally-bidirectional CSI, it can perform distributed beamforming so that the relayed signals add up coherently at the destination node, i.e., coherent AF relaying [26–28]. If the relay node cannot perform distributed beamforming, it adopts the noncoherent AF relaying [9, 12, 28].

The goal is to propose a centralized optimization framework for determining the optimal RPA of the relay nodes at the central unit. In a centralized design, the relay nodes need to send their local CSI to the central unit, which determines the transmit power allocation among the relay nodes.[4] However, all previous works assume

[3]The hardware demonstration at the MIT Media Laboratory shows that AF relay nodes can be built easily with existing wireless transceivers [25].

[4]Exactly how this global CSI can be obtained by the central unit is beyond the scope of this

perfect global CSI at the central unit [13–24]. In practice, such an assumption is too optimistic since the knowledge of global CSI is rarely perfect in practice; i.e., uncertainties in CSI arise as a consequence of imperfect channel estimation, quantization, synchronization errors, hardware limitations, implementation errors, or transmission errors in feedback channels. In general, imperfect CSI causes performance degradation of wireless systems [29, 30]. Moreover, the power allocation algorithms proposed in the above works require the central unit to track the global CSI at the time-scale of fast-fading. This requires frequent communication between the relay nodes and the central unit to determine new power allocations.[5]

1.3 Wideband Communications

The emergence of ubiquitous wireless services has prompted the exploration of using increasingly larger transmission bandwidths, often in challenging environments and over portions of bandwidth that are already in use for legacy systems. Current demands in quality and reliability of wireless connections suggest that ever-higher bandwidths in various frequency bands will be made available in an unlicensed manner for unrestricted wireless access. As a result, UWB spread-spectrum systems have received considerable attention from the scientific, commercial, and military sectors [31–34]. UWB technology is known to provide many advantages over traditional narrowband systems. The key motivation for using UWB systems is the ability to highly resolve multipath, as well as the availability of technology to implement and generate UWB signals with relatively low complexity. The fine delay resolution properties make UWB radio a viable candidate for communications [35–38], as well as for ranging and localization in dense multipath environments [39–42].

Wideband cooperative networks allow for both higher data rate and higher resistance to interference. Since the gains achieved by using cooperation come at the cost of higher node complexity and substantial coordination overhead, it is important

dissertation.

[5] As a result, this incurs a power penalty due to intense signal processing.

to study practical low-complexity signaling and receiver schemes suitable for UWB networks. To demodulate UWB signals, the reference signal can be locally generated by the receiver, which requires accurate acquisition and channel estimation. We refer to this class of systems as locally generated reference (LGR) systems. Since LGR systems in wideband channels require a large number of Rake fingers to capture most of the multipath energy [36–38], this greatly increases the complexity of each UWB node. As a result, it is unlikely that these UWB nodes are inexpensive and low-power, and, consequently, may not be appropriate for WSN applications. Moreover, the channel estimation and synchronization requirements can be very stringent for such LGR systems.

As an alternative to LGR systems, a reference signal can be transmitted along with the data. Such a signaling scheme, referred to as transmitted-reference (TR) signaling, was first considered in the early 1950s [43]. TR signaling involves the transmission of a reference and data signal pair, separated either in time [44,45] or in frequency [46,47].[6] Due to its simplicity, there is renewed interest in TR signaling for UWB systems [48–51] which can exploit multipath diversity inherent in the environment without the need for channel estimation and stringent acquisition. The receiver can simply be an autocorrelation receiver (AcR), which can be modified to include noise averaging for better performance.[7] Since TR signaling allocates a significant part of the symbol energy to transmitting reference pulses, differential encoding over consecutive symbols can also be used to alleviate inefficient resource usage. This alternative TR signaling is referred to as differential transmitted-reference (DTR) signaling [52].

A typical approach to analyzing the bit error probability (BEP) performance of TR signaling with AcR in UWB systems is to obtain the conditional BEP, using a Gaussian approximation of the noise components at the output of the AcR [48–50]. The BEP of TR signaling can then be obtained by numerically averag-

[6]In order for this pair of separated signals to experience the same channel, either the time separation must be less than the channel coherence time, or the frequency separation must be less than the channel coherence bandwidth.

[7]Besides using TR signaling with AcR, there has been an emerging interest using energy detection for pulse position signaling schemes for low-data rate UWB applications in the IEEE 802.15.4a standardization process.

ing the conditional BEP with a quasi-analytical/experimental approach [49, 53] or a quasi-analytical/simulation approach [50]. Although one can also use the derived BEP in [54] and [55], these results are only applicable to Rayleigh fading. Since the amplitude distribution of the resolved multipaths in typical UWB channels can be drastically different from the Rayleigh distribution [37,38], there is a compelling need for analytical expressions that are valid for a broad class of fading distributions.

Furthermore, due to its large transmission bandwidth, UWB systems need to coexist and contend with many narrowband communication systems. Therefore, a thorough performance analysis of TR systems in the presence of narrowband systems is essential for successful deployment of UWB systems. Previous work in this area includes the study of the effect of UWB signals on some commercial narrowband communication systems [56–59], the analysis of UWB systems in the presence of narrowband interference (NBI) with conventional receiver structures involving a LGR [60–66], and the development of techniques to suppress NBI in UWB systems [67–71]. However, only a few results are available for the performance of TR and DTR signaling schemes in the presence of NBI [72–74].

1.4 Energy Efficiency

The last part of the dissertation is dedicated to a more specific kind of wireless network - a WSN for sensing a PoI in the sensor field by geographically dispersed nodes. With the development of low-cost and low-power transceivers, sensors, and embedded processors, there has been growing interest in WSNs for a wide variety of applications, from surveillance and security to environmental hazard monitoring [75–78]. In most applications, the intelligent fusion of information from geographically dispersed sensor nodes, commonly known as distributed data fusion, is an important issue. A related problem is the decentralized (or distributed) detection problem, where a network of sensors, together with a global detector (or fusion center), cooperatively undertake the task of identifying a PoI. However, unlike in classical decentralized detection problems [79–82], greater challenges exist in a WSN setting. There are stringent

power constraints for each node [75–77], and communication channels from nodes to the fusion center are severely bandwidth-constrained. In addition, the communication channels are no longer lossless (e.g, fading, noise and, possibly, interference are present) [83–86], and the observation at each sensor node is spatially varying [87, 88]. Motivated by [87, 88], we consider decentralized detection in a dense WSN with randomly deployed, identical sensor nodes. In order to capture uncertainty in the total number of active nodes in the WSN due to node malfunction, node power depletion, or random behavior of data gathering process, we consider the number of activated nodes within the WSN at any particular time to be random.

In addition, unlike previous works in [79–88], we allow the possibility of cooperation among the sensor nodes, where multiple sensor nodes pool their resources in a distributed manner to enhance the reliability of the transmission link. For example, it has been shown in [89] that the capacity of many-to-one data gathering channels, with fixed total average power, scales as $\Theta(\log K)$ in dense WSN, where K is the number of nodes. In fact, this capacity scaling is possible by the use of cooperative diversity. In [90], it has also been shown that cooperation can increase reliability in WSN. Specifically, in the context of decentralized detection, cooperation allows sensor nodes to exchange information and to continuously update their local decisions until consensus is reached across the nodes [91–94]. For example, cooperation in decentralized detection can be accomplished via the use of the Parley algorithm [91]. This algorithm has been shown to converge to a global decision after a sufficient number of iterations when certain conditions are met. However, without a fully-connected network and given that the sensor observations are spatially varying, the Parley algorithm may converge to a wrong decision at most of the nodes.

Since network connectivity and node density greatly affects the reliability and energy efficiency of WSNs, it is not clear *a priori* whether cooperation improves both of these performance measures. More specifically, in our context of decentralized detection in WSN, the designer of the network is confronted with questions: When is cooperation better in terms of reliability and energy efficiency? How do network connectivity, node density, and PoI intensity affect our cooperative protocol?

1.5 Dissertation Outline

The main contribution of this dissertation is to investigate how cooperation among nodes leads to the design of efficient network from the perspectives of robust resource allocation, wideband communications, and energy efficiency. In addition, UWB technology has been investigated as the enabling technology due to its capability to operate with low-complexity and low-power consumption. The organization of the dissertation is as follows:

In Chapter 2, we develop RPA algorithms for coherent and noncoherent AF relay networks [95–97]. The goal is to maximize the output SNR under individual as well as aggregate relay power constraints. We show that these RPA problems, in the presence of perfect global CSI, can be formulated as quasiconvex optimization problems. In such settings, the optimal solutions can be efficiently obtained via a sequence of convex feasibility problems, in the form of second-order cone programs (SOCPs). Furthermore, we develop robust optimization framework for RPA problems in the case of uncertain global CSI. We show that the robust counterparts of our uncertain convex feasibility problems with ellipsoidal uncertainty sets can be formulated as semi-definite programs (SDPs).

In Chapter 3, we formulate the RPA problem as the total transmitted relay power minimization problem subject to a QoS constraint [98].[8] Our algorithms track only the large-scale fading and thereby leading to practical implementations. We show that our optimization problems for coherent and noncoherent AF relay networks can be cast as an SOCP and a linear program (LP), respectively, under perfect knowledge of large-scale fading. Under ellipsoidal uncertainty sets, the robust counterparts of the power minimization problems for coherent and noncoherent AF relay channels can be formulated as an SDP and an SOCP, respectively.

In Chapter 4, we analyze the BEP performance of TR and DTR signaling schemes for a UWB system with AcR in dense multipath channels [99–101]. We develop an analytical framework, based on the sampling expansion approach, to derive closed-

[8]The required QoS is considered to be satisfied when the output SNR at the destination node exceeds a given target value.

form BEP expressions valid for a broad class of fading channels. We consider both AcRs and modified AcRs with noise averaging. We obtain a rule of thumb for the asymptotic SNR penalty which is useful for comparing a TR system to an ideal Rake receiver.

In Chapter 5, we analyze the BEP performance of TR and DTR signaling schemes in the presence of NBI [102–104]. We develop a quasi-analytical method as well as an approximate analytical method to evaluate the BEP of TR and DTR signaling in the presence of NBI. We quantify the effects of NBI and channel power dispersion profile on the optimum integration interval of an AcR.

In Chapter 6, we investigate the problem of binary decentralized detection in a randomly deployed dense WSN, where the communication channels between the nodes and the fusion center are bandwidth constrained [105–108]. We compare two different fusion architectures depending on whether sensor nodes are allowed to collaborate or not. We characterize the effects of PoI intensity, realistic link models, consensus flooding protocol, and network connectivity on the system reliability and average energy consumption for both fusion architectures. We propose a consensus flooding protocol that accounts for scenarios with weak PoI intensity and reduces the possibility of false-alarm flooding.

In Chapter 7, we give our conclusions and some discussions for future work.

Notation: Throughout the dissertation, we use the following notations. Boldface upper-case letters denote matrices, boldface lower-case letters denote column vectors, and plain lower-case letters denote scalars. The notations $\mathbb{E}\{X\}$ and $\mathbb{V}\{X\}$ denote the expectation and variance of a random variable (r.v.) X, respectively. The superscripts $(\cdot)^T$, $(\cdot)^*$, and $(\cdot)^\dagger$ denote the transpose, complex conjugate, and transpose conjugate, respectively. $\boldsymbol{I}_n$ denotes the $n \times n$ identity matrix, $[\boldsymbol{B}]_{ij}$ denotes the (i,j)th element of $\boldsymbol{B}$, $\mathbf{1}$ denotes a vector with all 1 elements, $\mathbf{0}$ denotes a vector with all 0 elements, and $\boldsymbol{e}_k$ denotes a standard basis vector with a 1 at the kth element. $\mathrm{tr}(\cdot)$, $|\cdot|$, and $\|\cdot\|$ denote the trace operator, absolute value, and standard Euclidean norm, respectively. $\mathbb{R}_+^K$ and $\mathbb{R}_{++}^K$ denote the nonnegative and positive orthants in Euclidean vector space of dimension K, respectively. $\boldsymbol{a} \| \boldsymbol{b}$ and $\boldsymbol{a} \nparallel \boldsymbol{b}$ denote that $\boldsymbol{a}$ is parallel to

$\boldsymbol{b}$ and $\boldsymbol{a}$ is not parallel to $\boldsymbol{b}$, respectively. $\boldsymbol{B} \succeq 0$ and $\boldsymbol{B} \succ 0$ denote that $\boldsymbol{B}$ is positive semi-definite and positive definite, respectively. We denote the primal optimization problem as $\mathcal{P}$, its associated dual optimization problem as $\mathcal{DP}$, and its associated robust counterpart as $\mathcal{RP}$.

Chapter 2

Robust Power Allocation Algorithms for Wireless Relay Networks

In this chapter, we develop RPA algorithms for coherent and noncoherent AF relay networks. The goal is to maximize the output SNR under individual as well as aggregate relay power constraints. We show that these RPA problems, in the presence of perfect global CSI, can be formulated as quasiconvex optimization problems. In such settings, the optimal solutions can be efficiently obtained via a sequence of convex feasibility problems in the form of SOCPs. Furthermore, we introduce robust optimization methodology that accounts for uncertainties in the global CSI. We show that the robust counterparts of our convex feasibility problems with ellipsoidal uncertainty sets can be formulated as SDPs.

2.1 Problem Formulation

We consider a wireless relay network consisting of $N_{\mathrm{r}} + 2$ nodes, each with single-antenna: a designated source-destination node pair together with N_{r} relay nodes located randomly and independently in a fixed area (see Fig. 2-1). We consider a scenario in which there is no direct link between the source and destination nodes. All

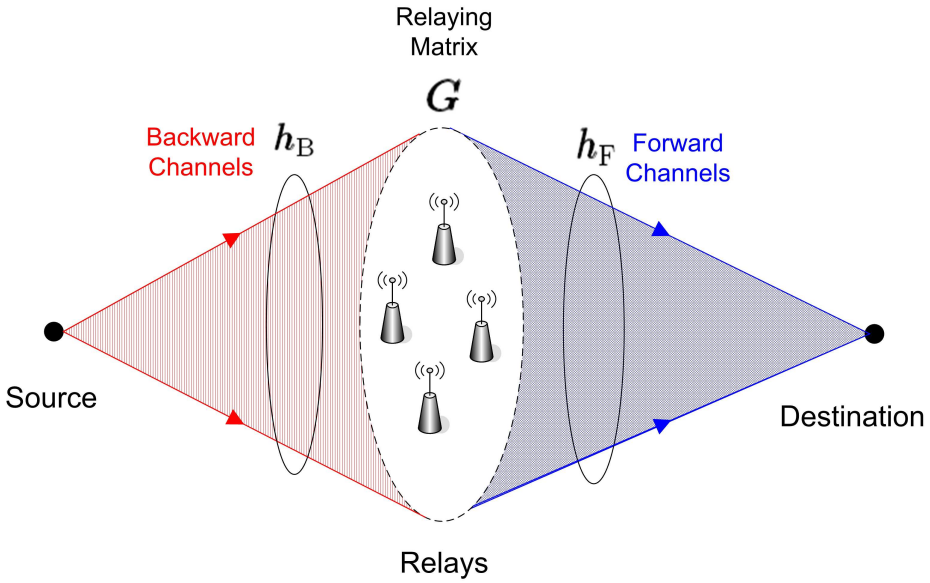

Figure 2-1: Wireless relay network.

nodes operating in a common frequency band are in half-duplex mode, so transmission occurs over two time slots.

In the first time slot, the relay nodes receive the signal transmitted by the source node. After processing the received signals, the relay nodes transmit the processed data to the destination node during the second time slot while the source node remains silent. We assume perfect synchronization at the destination node.[1] The received signals at the relay and destination nodes can then be written as

$$\boldsymbol{y}_{\mathrm{R}} = \boldsymbol{h}_{\mathrm{B}} x_{\mathrm{S}} + \boldsymbol{z}_{\mathrm{R}}, \qquad \text{First slot} \tag{2.1}$$

$$y_{\mathrm{D}} = \boldsymbol{h}_{\mathrm{F}}^{T} \boldsymbol{x}_{\mathrm{R}} + z_{\mathrm{D}}, \qquad \text{Second slot} \tag{2.2}$$

where x_{S} is the transmitted signal from the source node to the relay nodes, $\boldsymbol{x}_{\mathrm{R}}$ is the $N_{\mathrm{r}} \times 1$ transmitted signal vector from the relay nodes to the destination node, $\boldsymbol{y}_{\mathrm{R}}$ is the $N_{\mathrm{r}} \times 1$ received signal vector at the relay nodes, y_{D} is the received signal at the destination node, $\boldsymbol{z}_{\mathrm{R}} \sim \tilde{\mathcal{N}}_K(\boldsymbol{0}, \boldsymbol{\Sigma}_{\mathrm{R}})$ is the $N_{\mathrm{r}} \times 1$ noise vector at the relay nodes, and $z_{\mathrm{D}} \sim \tilde{\mathcal{N}}(0, \sigma_{\mathrm{D}}^2)$ is the noise at the destination node.[2] Note that the different

[1] Exactly how to achieve this synchronization or the effect of small synchronization errors on performance is beyond the scope of this dissertation [27].

[2] $\tilde{\mathcal{N}}(\mu, \sigma_2)$ denotes a complex circularly symmetric Gaussian distribution with mean μ and vari-

noise variances at the relay nodes are reflected in $\boldsymbol{\Sigma}_{\mathrm{R}} \triangleq \mathrm{diag}(\sigma^2_{\mathrm{R},1}, \sigma^2_{\mathrm{R},2}, \ldots, \sigma^2_{\mathrm{R},N_{\mathrm{r}}})$. Moreover, $\boldsymbol{z}_{\mathrm{R}}$ and z_{D} are independent. Furthermore, they are mutually uncorrelated with x_{S} and $\boldsymbol{x}_{\mathrm{R}}$. With perfect global CSI at the destination node, $\boldsymbol{h}_{\mathrm{B}}$ and $\boldsymbol{h}_{\mathrm{F}}$ are $N_{\mathrm{r}} \times 1$ known channel vectors from source to relay and from relay to destination, respectively, where $\boldsymbol{h}_{\mathrm{B}} = [h_{\mathrm{B},1}, h_{\mathrm{B},2}, \ldots, h_{\mathrm{B},N_{\mathrm{r}}}]^T \in \mathbb{C}^{N_{\mathrm{r}}}$ and $\boldsymbol{h}_{\mathrm{F}} = [h_{\mathrm{F},1}, h_{\mathrm{F},2}, \ldots, h_{\mathrm{F},N_{\mathrm{r}}}]^T \in \mathbb{C}^{N_{\mathrm{r}}}$. For convenience, we shall refer to $\boldsymbol{h}_{\mathrm{B}}$ as the backward channel and $\boldsymbol{h}_{\mathrm{F}}$ as the forward channel.

At the source node, we impose an individual source power constraint P_{S}, such that $\mathbb{E}\{|x_{\mathrm{S}}|^2\} \leq P_{\mathrm{S}}$. Similarly, at the relay nodes, we impose both individual relay power constraint P and aggregate relay power constraint P_{R} such that the transmission power allocated to the kth relay node $p_k \triangleq [\boldsymbol{Q}_{\mathrm{R}}]_{k,k} \leq P$ for $k \in \mathcal{N}_{\mathrm{r}}$ and $\mathrm{tr}\,(\boldsymbol{Q}_{\mathrm{R}}) \leq P_{\mathrm{R}}$, where $\boldsymbol{Q}_{\mathrm{R}} \triangleq \mathbb{E}\{\boldsymbol{x}_{\mathrm{R}}\boldsymbol{x}_{\mathrm{R}}^{\dagger} |\ \boldsymbol{h}_{\mathrm{B}}\}$ and $\mathcal{N}_{\mathrm{r}} = \{1, 2, \ldots, N_{\mathrm{r}}\}$.

For AF relaying, the relay nodes simply transmit scaled versions of the exact signals they have received while satisfying power constraints. In this case, $\boldsymbol{x}_{\mathrm{R}}$ in (2.2) is given by

$$\boldsymbol{x}_{\mathrm{R}} = \boldsymbol{G}\boldsymbol{y}_{\mathrm{R}}, \tag{2.3}$$

where $\boldsymbol{G}$ denotes the $N_{\mathrm{r}} \times N_{\mathrm{r}}$ diagonal matrix representing relay gains and thus[3]

$$\boldsymbol{Q}_{\mathrm{R}} = \boldsymbol{G}\left(P_{\mathrm{S}}\boldsymbol{h}_{\mathrm{B}}\boldsymbol{h}_{\mathrm{B}}^{\dagger} + \boldsymbol{\Sigma}_{\mathrm{R}}\right)\boldsymbol{G}^{\dagger}. \tag{2.4}$$

The diagonal structure of $\boldsymbol{G}$ ensures that each relay node only requires the knowledge about its own received signal. When each relay node has access to its locally-bidirectional CSI, it can perform distributed beamforming.[4] As such, this is referred

ance σ^2. Similarly, $\tilde{\mathcal{N}}_K(\boldsymbol{\mu}, \boldsymbol{\Sigma})$ denotes a complex K-variate Gaussian distribution with a mean vector $\boldsymbol{\mu}$ and a covariance matrix $\boldsymbol{\Sigma}$.

[3]Note that in (2.4), the source employs the maximum allowable power P_{S} in order to maximize the SNR at the destination node.

[4]Here, locally-bidirectional CSI refers to the knowledge of $h_{\mathrm{B},k}$ and $h_{\mathrm{F},k}$ at the kth relay node.

to as coherent AF relaying and the kth diagonal element of $\boldsymbol{G}$ is given by [26, 27]

$$g_{\text{coh}}^{(k)} = \sqrt{\beta_k p_k} \frac{h_{\text{B},k}^*}{|h_{\text{B},k}|} \frac{h_{\text{F},k}^*}{|h_{\text{F},k}|}, \tag{2.5}$$

where $\beta_k = 1/(P_{\text{S}}|h_{\text{B},k}|^2 + \sigma_{\text{R},k}^2)$. On the other hand, when forward CSI is absent at each relay node, the relay node simply forwards a scaled version of its received signal without any phase alignment. This is referred to as noncoherent AF relaying and the kth diagonal element of $\boldsymbol{G}$ is given by [9, 12, 22, 109]

$$g_{\text{noncoh}}^{(k)} = \sqrt{\beta_k p_k}. \tag{2.6}$$

Using (2.1)-(2.3), the received signal at the destination node can be written as

$$y_{\text{D}} = \boldsymbol{h}_{\text{F}}^T \boldsymbol{G} \boldsymbol{h}_{\text{B}} x_{\text{S}} + \underbrace{\boldsymbol{h}_{\text{F}}^T \boldsymbol{G} \boldsymbol{z}_{\text{R}} + z_{\text{D}}}_{\triangleq \tilde{z}_{\text{D}}}, \tag{2.7}$$

where $\tilde{z}_{\text{D}}$ represents the effective noise at the destination node. The instantaneous SNR at the destination node conditioned on $\boldsymbol{h}_{\text{B}}$ and $\boldsymbol{h}_{\text{F}}$ is defined as

$$\mathsf{SNR}(\boldsymbol{p}) \triangleq \frac{\mathbb{E}\left\{ |\boldsymbol{h}_{\text{F}}^T \boldsymbol{G} \boldsymbol{h}_{\text{B}} x_{\text{S}}|^2 \, | \boldsymbol{h}_{\text{B}}, \boldsymbol{h}_{\text{F}} \right\}}{\mathbb{E}\left\{ |\tilde{z}_{\text{D}}|^2 \, | \boldsymbol{h}_{\text{F}} \right\}} = \frac{P_{\text{S}} \boldsymbol{h}_{\text{F}}^T \boldsymbol{G} \boldsymbol{h}_{\text{B}} \boldsymbol{h}_{\text{B}}^\dagger \boldsymbol{G}^\dagger \boldsymbol{h}_{\text{F}}^*}{\boldsymbol{h}_{\text{F}}^T \boldsymbol{G} \boldsymbol{\Sigma}_{\text{R}} \boldsymbol{G}^\dagger \boldsymbol{h}_{\text{F}}^* + \sigma_{\text{D}}^2}, \tag{2.8}$$

where $\boldsymbol{p} = [p_1, p_2, \ldots, p_{N_{\text{r}}}]^T$. Our goal is to maximize system performance by optimally allocating transmission power of the relay nodes. We adopt the SNR at the destination node as the performance metric and formulate the RPA problem as follows:

$$\begin{aligned} \max_{\boldsymbol{p}} \quad & \mathsf{SNR}(\boldsymbol{p}) \\ \text{s.t.} \quad & \text{tr}\left(\boldsymbol{Q}_{\text{R}}\right) \leq P_{\text{R}}, \\ & 0 \leq [\boldsymbol{Q}_{\text{R}}]_{k,k} \leq P, \quad \forall k \in \mathcal{N}_{\text{r}}. \end{aligned} \tag{2.9}$$

Note that the optimal solution to the problem in (2.9) maximizes the capacity of the AF relay network under perfect global CSI since this capacity, given by $\frac{1}{2}\log(1+\mathsf{SNR})$, is a monotonically increasing function of SNR.

2.2 Optimal Relay Power Allocation

We provide a framework for formulating coherent and noncoherent AF RPA problems, under perfect global CSI at the destination node, using optimization methods such as quasiconvex optimization and SOCP [110,111]. Details of these optimization methods can be found in Appendix A.

2.2.1 Coherent AF Relaying

It will be apparent that (2.9) is a nonconvex optimization problem. It is generally difficult to solve this class of optimization problems, and, often, we may end up obtaining locally optimal solutions. Here, we show how this difficulty can be alleviated by transforming into another domain.[5] Specifically, we can transform (2.9) for the coherent AF RPA problem into a quasiconvex optimization problem, such that the upper-level set satisfies an SOC constraint. We now present our results in the following:

Proposition 1. *The coherent AF relay power allocation problem can be transformed into a quasiconvex optimization problem as*

$$\begin{aligned} \mathcal{P}_{\text{coh}} : max_{\boldsymbol{\zeta}} \quad & f_{\text{coh}}(\boldsymbol{\zeta}) \triangleq \tfrac{P_{\text{S}}}{\sigma_{\text{D}}^2} \tfrac{(\boldsymbol{c}^T\boldsymbol{\zeta})^2}{\|\boldsymbol{A}\boldsymbol{\zeta}\|^2+1} \\ s.t. \quad & \boldsymbol{\zeta} \in \mathcal{S}, \end{aligned} \tag{2.10}$$

and the feasible set $\mathcal{S}$ is given by

$$\mathcal{S} = \left\{ \boldsymbol{\zeta} \in \mathbb{R}_+^{N_{\text{r}}} : \sum_{k \in \mathcal{N}_{\text{r}}} \zeta_k^2 \leq 1,\ 0 \leq \zeta_k \leq \sqrt{\eta_{\text{p}}},\ \forall k \in \mathcal{N}_{\text{r}} \right\},$$

where $\zeta_k \triangleq \sqrt{\frac{p_k}{P_{\text{R}}}}$ is the optimization variable and $\eta_{\text{p}} \triangleq P/P_{\text{R}}$. In addition, $\boldsymbol{c} = [c_1, c_2, \ldots, c_{N_{\text{r}}}]^T \in \mathbb{R}_+^{N_{\text{r}}}$, and $\boldsymbol{A} = \text{diag}(a_1, a_2, \ldots, a_{N_{\text{r}}}) \in \mathbb{R}_+^{N_{\text{r}} \times N_{\text{r}}}$ are defined for nota-

[5] Our approach follows the general philosophy of solving difficult problems in another domain [112,113].

tional convenience where

$$c_k = \sqrt{\beta_k P_{\mathrm{R}}}\ |h_{\mathrm{B},k}||h_{\mathrm{F},k}|, \tag{2.11}$$

$$a_k = \frac{\sqrt{\beta_k P_{\mathrm{R}}}\ |h_{\mathrm{F},k}|\sigma_{\mathrm{R},k}}{\sigma_{\mathrm{D}}}. \tag{2.12}$$

Proof. First, to show that $\mathcal{P}_{\mathrm{coh}}$ is a quasiconvex optimization problem, we simply need to show that the objective function $f_{\mathrm{coh}}(\boldsymbol{\zeta})$ is quasiconcave and the constraint set in (2.10) is convex. The constraint set in (2.10) is simply the intersection of a hypercube with an SOC. Since the intersection of convex sets is convex, the constraint set in (2.10) is again convex. For any $t \in \mathbb{R}_+$, the upper-level set of $f_{\mathrm{coh}}(\boldsymbol{\zeta})$ that belongs to $\mathcal{S}$ is given by

$$\begin{aligned} U(f_{\mathrm{coh}}, t) &= \left\{ \boldsymbol{\zeta} \in \mathcal{S} : \frac{P_{\mathrm{S}}}{\sigma_{\mathrm{D}}^2} \frac{(\boldsymbol{c}^T\boldsymbol{\zeta})^2}{\|\boldsymbol{A}\boldsymbol{\zeta}\|^2 + 1} \geq t \right\} \\ &= \left\{ \boldsymbol{\zeta} \in \mathcal{S} : \boldsymbol{c}^T\boldsymbol{\zeta}\sqrt{\frac{P_{\mathrm{S}}}{t\sigma_{\mathrm{D}}^2}} \geq \sqrt{(1 + \|\boldsymbol{A}\boldsymbol{\zeta}\|^2)} \right\} \\ &= \left\{ \boldsymbol{\zeta} \in \mathcal{S} : \begin{bmatrix} \boldsymbol{c}^T\boldsymbol{\zeta}\sqrt{\frac{P_{\mathrm{S}}}{t\sigma_{\mathrm{D}}^2}} \\ \begin{pmatrix} 1 \\ \boldsymbol{A}\boldsymbol{\zeta} \end{pmatrix} \end{bmatrix} \succeq_{\mathcal{K}} 0 \right\}. \end{aligned} \tag{2.13}$$

It is clear that $U(f_{\mathrm{coh}}, t)$ is a convex set since it can be represented as an SOC. Since the upper-level set $U(f_{\mathrm{coh}}, t)$ is convex for every $t \in \mathbb{R}_+$, $f_{\mathrm{coh}}(\boldsymbol{\zeta})$ is, thus, quasiconcave. Note that a concave function is also quasiconcave. We now show that $f_{\mathrm{coh}}(\boldsymbol{\zeta})$ is not concave by contradiction. Suppose that $f_{\mathrm{coh}}(\boldsymbol{\zeta})$ is concave. We consider $\boldsymbol{\zeta}_a$ and $\boldsymbol{\zeta}_b$ such that $\boldsymbol{\zeta}_a = \zeta_1\boldsymbol{e}_1$ and $\boldsymbol{\zeta}_b = \delta\zeta_1\boldsymbol{e}_1$ for $0 \leq \zeta_1 \leq \sqrt{\eta_{\mathrm{p}}}$, $\zeta_1^2 \leq 1$, and $0 < \delta < 1$. Clearly, $\boldsymbol{\zeta}_a$ and $\boldsymbol{\zeta}_b \in \mathcal{S}$. For any $\lambda \in [0, 1]$, we have

$$f_{\mathrm{coh}}(\lambda\boldsymbol{\zeta}_a + (1-\lambda)\boldsymbol{\zeta}_b) = \frac{P_{\mathrm{S}}/\sigma_{\mathrm{D}}^2}{\frac{a_1^2}{c_1^2} + \frac{1}{\zeta_1^2[\lambda c_1 + \delta c_1(1-\lambda)]^2}} \triangleq g(\zeta_1), \tag{2.14}$$

where $g(\zeta_1)$ is clearly convex in ζ_1. Due to convexity of $g(\zeta_1)$, the following inequality

must hold

$$g(\lambda\zeta_1^{(1)} + (1-\lambda)\zeta_1^{(2)}) \leq \lambda g(\zeta_1^{(1)}) + (1-\lambda)g(\zeta_1^{(2)}). \tag{2.15}$$

Now, by letting $\zeta_1^{(1)} = \zeta_1/[\lambda + \delta(1-\lambda)]$ and $\zeta_1^{(2)} = \delta\zeta_1/[\lambda + \delta(1-\lambda)]$, we can rewrite (2.15) as

$$f_{\text{coh}}(\lambda\boldsymbol{\zeta}_a + (1-\lambda)\boldsymbol{\zeta}_b) \leq \lambda f_{\text{coh}}(\boldsymbol{\zeta}_a) + (1-\lambda)f_{\text{coh}}(\boldsymbol{\zeta}_b). \tag{2.16}$$

Thus, we have showed that there exists $\boldsymbol{\zeta}_a, \boldsymbol{\zeta}_b \in \mathcal{S}$ and $\lambda \in [0,1]$, such that (2.16) holds. By contradiction, $f_{\text{coh}}(\boldsymbol{\zeta})$ is not concave on $\mathcal{S}$. □

Remark 1. *Note that $f_{\text{coh}}(\boldsymbol{\zeta})$ is a quasiconcave function, ζ_k denotes the fractional power allocated to the kth relay node, and η_{p} denotes the ratio between the individual relay power constraint and the aggregate relay power constraint, where $0 < \eta_{\text{p}} \leq 1$.*

Remark 2. *It is well-known that we can solve $\mathcal{P}_{\text{coh}}$ efficiently through a sequence of convex feasibility problems using the bisection method [111].*[6] *In order for the bisection method to work, it is important that we initialize an interval that contains the optimal solution, i.e., $t_{\min} \leq f_{\text{coh}}(\boldsymbol{\zeta}_{\text{opt}}) \leq t_{\max}$. It takes exactly $\lceil \log_2((t_{\max} - t_{\min})/\varepsilon) \rceil$ iterations before the algorithm terminates, where ε denotes the termination criteria parameter [111]. In our case, we can always let $t_{\min}$ corresponding to the uniform RPA and we only need to choose $t_{\max}$ appropriately. We formalize these results in the following lemma.*

Lemma 1. *The program $\mathcal{P}_{\text{coh}}$ in Proposition 1 can be solved numerically using the bisection method:*

0. *Initialize $t_{\min} = f_{\text{coh}}(\boldsymbol{\zeta}_{\min})$, $t_{\max} = f_{\text{coh}}(\boldsymbol{\zeta}_{\max})$, where $f_{\text{coh}}(\boldsymbol{\zeta}_{\min})$ and $f_{\text{coh}}(\boldsymbol{\zeta}_{\max})$ define a range of relevant values of $f_{\text{coh}}(\boldsymbol{\zeta})$, and set tolerance $\varepsilon \in \mathbb{R}_{++}$.*

[6] Note that the program $\mathcal{P}_{\text{coh}}$ is always feasible as long as $\eta_{\text{p}} > 0$.

1. *Solve the convex feasibility program* $\mathcal{P}_{\text{coh}}^{(\text{SOCP})}(t)$ *in (2.17) by fixing* $t = (t_{\max} + t_{\min})/2$.

2. *If* $\mathcal{S}_{\text{coh}}(t) = \emptyset$, *then set* $t_{\max} = t$ *else set* $t_{\min} = t$.

3. *Stop if the gap* $(t_{\max} - t_{\min})$ *is less than the tolerance* ε. *Go to Step 1 otherwise.*

4. *Output* $\boldsymbol{\zeta}_{\text{opt}}$ *obtained from solving* $\mathcal{P}_{\text{coh}}^{(\text{SOCP})}(t)$ *in Step 1.*

where the convex feasibility program can be written in SOCP form as

$$\begin{aligned} \mathcal{P}_{\text{coh}}^{(\text{SOCP})}(t): \textit{find} \quad & \boldsymbol{\zeta} \\ \textit{s.t.} \quad & \boldsymbol{\zeta} \in \mathcal{S}_{\text{coh}}(t), \end{aligned} \tag{2.17}$$

with the set $\mathcal{S}_{\text{coh}}(t)$ *given by*

$$\mathcal{S}_{\text{coh}}(t) = \left\{ \boldsymbol{\zeta} \in \mathbb{R}_+^{N_{\text{r}}} : \begin{bmatrix} \boldsymbol{c}^T \boldsymbol{\zeta} \sqrt{\frac{P_{\text{S}}}{t\sigma_{\text{D}}^2}} \\ \begin{pmatrix} 1 \\ \boldsymbol{A}\boldsymbol{\zeta} \end{pmatrix} \end{bmatrix} \succeq_{\mathcal{K}} 0, \begin{bmatrix} 1 \\ \boldsymbol{\zeta} \end{bmatrix} \succeq_{\mathcal{K}} 0, \begin{bmatrix} \frac{\eta_{\text{p}}+1}{2} \\ \begin{pmatrix} \boldsymbol{\zeta}^T \boldsymbol{e}_k \\ \frac{\eta_{\text{p}}-1}{2} \end{pmatrix} \end{bmatrix} \succeq_{\mathcal{K}} 0, \forall k \in \mathcal{N}_{\text{r}} \right\}. \tag{2.18}$$

Proof. We first show that for each given t, the convex feasibility program is an SOCP. For each t, the first constraint in (2.18) follows immediately from (2.13), which is an SOC constraint. Clearly, the aggregate relay power constraint in (2.10) can be cast as an SOC constraint using (A.4). Lastly, the individual relay power constraints can be cast as SOC constraints as follows:

$$\begin{aligned} \boldsymbol{\zeta}^T \boldsymbol{e}_k &\leq \sqrt{\eta_{\text{p}}} \\ \Leftrightarrow \sqrt{(\boldsymbol{\zeta}^T \boldsymbol{e}_k)^2 + \frac{(\eta_{\text{p}}-1)^2}{4}} &\leq \frac{\eta_{\text{p}}+1}{2} \\ \Leftrightarrow \left\| \begin{pmatrix} \boldsymbol{\zeta}^T \boldsymbol{e}_k \\ \frac{\eta_{\text{p}}-1}{2} \end{pmatrix} \right\| &\leq \frac{\eta_{\text{p}}+1}{2} \end{aligned} \tag{2.19}$$

In summary, $\mathcal{P}_{\text{coh}}^{(\text{SOCP})}$ is an SOCP since $\mathcal{S}_{(\text{coh})}(t)$ is equivalent to the intersection of $(N_{\text{r}} + 2)$ SOC constraints and the objective function is linear. □

Remark 3. *In Lemma 1, we formulate the convex feasibility problem in the form of SOCP, which can be solved efficiently [114]. Although an SOC constraint can be represented as an LMI, it is always computationally more efficient and stable to solve SOCP rather than SDP [111,114]. Nevertheless, we have included the equivalent SDP representation of such SOCP in the following corollary for comparison with the robust formulation in the subsequent section.*

Corollary 1. *The equivalent SDP representation of our convex feasibility program can be written as*

$$\begin{aligned} \mathcal{P}_{\text{coh}}^{(\text{SDP})}(t): \textit{find} \quad & \boldsymbol{\zeta} \\ \textit{s.t.} \quad & \boldsymbol{\zeta} \in \mathcal{S}_{\text{coh}}(t), \end{aligned} \tag{2.20}$$

where $\mathcal{S}_{\text{coh}}(t)$ *is now given by*

$$\begin{aligned} \mathcal{S}_{\text{coh}}(t) = \Bigg\{ \boldsymbol{\zeta} \in \mathbb{R}_+^{N_\text{r}} : & \begin{bmatrix} \boldsymbol{c}^T\boldsymbol{\zeta}\sqrt{\frac{P_\text{S}}{t\sigma_\text{D}^2}}\boldsymbol{I}_{N_\text{r}+1} & \begin{pmatrix} 1 \\ \boldsymbol{A}\boldsymbol{\zeta} \end{pmatrix} \\ \begin{pmatrix} 1 \\ \boldsymbol{A}\boldsymbol{\zeta} \end{pmatrix}^T & \boldsymbol{c}^T\boldsymbol{\zeta}\sqrt{\frac{P_\text{S}}{t\sigma_\text{D}^2}} \end{bmatrix} \succeq 0, \quad \begin{bmatrix} \boldsymbol{I}_{N_\text{r}} & \boldsymbol{\zeta} \\ \boldsymbol{\zeta}^T & 1 \end{bmatrix} \succeq 0, \\ & \begin{bmatrix} \frac{\eta_\text{p}+1}{2}\boldsymbol{I}_2 & \begin{pmatrix} \boldsymbol{\zeta}^T\boldsymbol{e}_k \\ \frac{\eta_\text{p}-1}{2} \end{pmatrix} \\ \begin{pmatrix} \boldsymbol{\zeta}^T\boldsymbol{e}_k \\ \frac{\eta_\text{p}-1}{2} \end{pmatrix}^T & \frac{\eta_\text{p}+1}{2} \end{bmatrix} \succeq 0, \forall k \in \mathcal{N}_\text{r} \Bigg\}. \end{aligned} \tag{2.21}$$

2.2.2 Noncoherent AF Relaying

Similar to the formulation of coherent AF RPA problem in (2.10), we can expressed the the noncoherent AF RPA problem as

$$\begin{aligned} \mathcal{P}_{\text{noncoh}}: \max\nolimits_{\boldsymbol{\zeta}} \quad & \frac{P_\text{S}}{\sigma_\text{D}^2}\frac{|\boldsymbol{c}^T\boldsymbol{\zeta}|^2}{\|\boldsymbol{A}\boldsymbol{\zeta}\|^2+1} \\ \text{s.t.} \quad & \boldsymbol{\zeta} \in \mathcal{S}, \end{aligned} \tag{2.22}$$

where $\mathcal{S}$ and $\boldsymbol{A}$ are given in Proposition 1. The difference is in $\boldsymbol{c} = [c_1, c_2, \ldots, c_{N_\mathrm{r}}] \in \mathbb{C}^{N_\mathrm{r}}$, where

$$c_k = \sqrt{\beta_k P_\mathrm{R}}\, h_{\mathrm{B},k} h_{\mathrm{F},k}.$$

As a result, we cannot directly apply Lemma 1 to solve $\mathcal{P}_{\mathrm{noncoh}}$ in (2.22). Instead, we introduce the following lemma which enables us to decompose $\mathcal{P}_{\mathrm{noncoh}}$ into $2L$ quasiconvex optimization subproblems, each of which can then be solved efficiently via the algorithm presented in Lemma 1.

Lemma 2 (Linear Approximation of Modulus [115,116])**.** *The modulus of a complex number $Z \in \mathbb{C}$ can be linearly approximated with the polyhedral norm given by*

$$p_L(Z) = \max_{l \in \mathcal{L}} \left\{ \mathfrak{Re}\{Z\} \cos\left(\frac{l\pi}{L}\right) + \mathfrak{Im}\{Z\} \sin\left(\frac{l\pi}{L}\right) \right\},$$

where $\mathcal{L} = \{1, 2, \ldots, 2L\}$, $\mathfrak{Re}\{Z\}$ and $\mathfrak{Im}\{Z\}$ denote the real and imaginary parts of Z, and the polyhedral norm $p_L(Z)$ is bounded by

$$p_L(Z) \leq |Z| \leq p_L(Z) \sec\left(\frac{\pi}{2L}\right).$$

and L is a positive integer such that $L \geq 2$.

Remark 4. *It follows from Lemma 2 that $p_L(Z)$ approaches $|Z|$ quadratically as $L \to \infty$. As a result, we can approximate the modulus of a complex number with arbitrary accuracy by increasing L. Using Lemma 2, we reformulate (2.9) for the noncoherent AF RPA problem in parallel with Proposition 1.*

Proposition 2. *The noncoherent AF relay power allocation problem can be approximately decomposed into $2L$ quasiconvex optimization subproblems. The master problem can be written as*

$$max_{l \in \mathcal{L}} \quad f_{\mathrm{noncoh}}(\boldsymbol{\zeta}_l^{\mathrm{opt}}) \tag{2.23}$$

where

$$f_{\text{noncoh}}(\boldsymbol{\zeta}) \triangleq \frac{P_{\text{S}}}{\sigma_{\text{D}}^2} \frac{\left[\mathfrak{Re}\left\{\boldsymbol{c}^T\boldsymbol{\zeta}\right\}\cos(l\pi/L) + \mathfrak{Im}\left\{\boldsymbol{c}^T\boldsymbol{\zeta}\right\}\sin(l\pi/L)\right]^2}{\|\boldsymbol{A}\boldsymbol{\zeta}\|^2 + 1}$$

and $\boldsymbol{\zeta}_l^{\text{opt}}$ *is the optimal solution of the following subproblem* $\mathcal{P}_{\text{noncoh}}(l)$*:*

$$\begin{aligned} \mathcal{P}_{\text{noncoh}}(l): max_{\boldsymbol{\zeta}_l} \quad & f_{\text{noncoh}}(\boldsymbol{\zeta}_l) \\ s.t. \quad & \mathfrak{Re}\left\{\boldsymbol{c}^T\boldsymbol{\zeta}_l\right\}\cos(l\pi/L) + \mathfrak{Im}\left\{\boldsymbol{c}^T\boldsymbol{\zeta}_l\right\}\sin(l\pi/L) \ \geq \ 0, \\ & \boldsymbol{\zeta}_l \in \mathcal{S}. \end{aligned} \tag{2.24}$$

The feasible set $\mathcal{S}$ *is given by*

$$\mathcal{S} = \left\{\boldsymbol{\zeta} \in \mathbb{R}_+^{N_{\text{r}}} : \sum_{k\in N_{\text{r}}} \zeta_k^2 \leq 1, \ 0 \leq \zeta_k \leq \sqrt{\eta_{\text{p}}}, \ \forall k \in \mathcal{N}_{\text{r}}\right\},$$

where $\zeta_k \triangleq \sqrt{\frac{p_k}{P_{\text{R}}}}$ *is the optimization variable and* $\eta_{\text{p}} \triangleq P/P_{\text{R}}$*. In addition,* $\boldsymbol{c} = [c_1, c_2, \ldots, c_{N_{\text{r}}}]^T \in \mathbb{C}^{N_{\text{r}}}$*, and* $\boldsymbol{A} = \text{diag}(a_1, a_2, \ldots, a_{N_{\text{r}}}) \in \mathbb{R}_+^{N_{\text{r}}\times N_{\text{r}}}$ *are defined as*

$$c_k = \sqrt{\beta_k P_{\text{R}}}\ h_{\text{B},k} h_{\text{F},k}, \tag{2.25}$$

$$a_k = \frac{\sqrt{\beta_k P_{\text{R}}}\ |h_{\text{F},k}|\sigma_{\text{R},k}}{\sigma_{\text{D}}}. \tag{2.26}$$

Proof. Similar to the proof of *Proposition 1.* □

Remark 5. *Note that* $\mathcal{S}$ *and* $\boldsymbol{A}$ *in Proposition 2 are exactly the same as that in Proposition 1. The difference is in* $\boldsymbol{c}$ *only. Unlike* $\mathcal{P}_{\text{coh}}$*, we now need to solve* $2L$ *quasiconvex optimization subproblems due to the approximation of* $|\boldsymbol{c}^T\boldsymbol{\zeta}|$ *using Lemma 2.*

Lemma 3. *Each of the* $2L$ *subproblems* $\mathcal{P}_{\text{noncoh}}(l)$ *in Proposition 2 can be solved efficiently by the bisection method via a sequence of convex feasibility problems in the form of SOCP. The* $2L$ *solutions* $\{\boldsymbol{\zeta}_l^{\text{opt}}\}_{l=1}^{2L}$ *then forms a candidate set for the optimal* $\boldsymbol{\zeta}^{\text{opt}}$ *that maximizes our master problem.*

Proof. Each of the $2L$ quasiconvex optimization problems $\mathcal{P}_{\text{noncoh}}(l), \ l \in \mathcal{L}$, in Proposition 2 can be solved efficiently via a sequence of convex feasibility problems using

the bisection method. For completeness, we present the algorithm for solving $\mathcal{P}_{\text{noncoh}}$ in (2.22), as follows:

0. Initialize $t_{\min} = f_{\text{noncoh}}(\boldsymbol{\zeta}_{\min})$, $t_{\max} = f_{\text{noncoh}}(\boldsymbol{\zeta}_{\max})$, where $f_{\text{noncoh}}(\boldsymbol{\zeta}_{\min})$ and $f_{\text{noncoh}}(\boldsymbol{\zeta}_{\max})$ define a range of relevant values of $f_{\text{noncoh}}(\boldsymbol{\zeta}_l)$, and set tolerance $\varepsilon \in \mathbb{R}_{++}$.

1. For $l \in \mathcal{L}$, solve $\mathcal{P}_{\text{noncoh}}(l)$ using the bisection method as follows:

1-1. Solve the convex feasibility program $\mathcal{P}^{(\text{SOCP})}_{\text{noncoh}}(t, l)$ in (2.27) by fixing $t = (t_{\max} + t_{\min})/2$.

1-2. If $\mathcal{S}_{\text{noncoh}}(t, l) = \emptyset$, then set $t_{\max} = t$ else set $t_{\min} = t$.

1-3. Stop if the gap $(t_{\max} - t_{\min})$ is less than the tolerance ε. Go to Step 1-1 otherwise.

3. Output $\boldsymbol{\zeta}_{\text{opt}}$ with maximum $f_{\text{noncoh}}(\boldsymbol{\zeta}_l^{\text{opt}})$ obtained from solving the $2L$ subproblems in Step 1.

where the convex feasibility program can be written in SOCP form as

$$\begin{aligned} \mathcal{P}^{(\text{SOCP})}_{\text{noncoh}}(t, l) : \text{find} \quad & \boldsymbol{\zeta}_l \\ \text{s.t.} \quad & \boldsymbol{\zeta}_l \in \mathcal{S}_{\text{noncoh}}(t, l), \end{aligned} \tag{2.27}$$

with the set $\mathcal{S}_{\text{noncoh}}(t, l)$ given by

$$\begin{aligned} &\mathcal{S}_{\text{noncoh}}(t, l) \\ &= \Bigg\{ \boldsymbol{\zeta}_l \in \mathbb{R}_+^{N_{\text{r}}} : \begin{bmatrix} \left[\mathfrak{Re}\left\{\boldsymbol{c}^T\boldsymbol{\zeta}_l\right\}\cos(l\pi/L) + \mathfrak{Im}\left\{\boldsymbol{c}^T\boldsymbol{\zeta}_l\right\}\sin(l\pi/L)\right]\sqrt{\frac{P_{\text{S}}}{t\sigma_{\text{D}}^2}} \\ \begin{pmatrix} 1 \\ \boldsymbol{A}\boldsymbol{\zeta}_l \end{pmatrix} \end{bmatrix} \succeq_{\mathcal{K}} 0, \quad \begin{bmatrix} 1 \\ \boldsymbol{\zeta}_l \end{bmatrix} \succeq_{\mathcal{K}} 0, \\ &\qquad \begin{bmatrix} \frac{\eta_{\text{p}}+1}{2} \\ \begin{pmatrix} \boldsymbol{\zeta}_l^T\boldsymbol{e}_k \\ \frac{\eta_{\text{p}}-1}{2} \end{pmatrix} \end{bmatrix} \succeq_{\mathcal{K}} 0, \quad \mathfrak{Re}\left\{\boldsymbol{c}^T\boldsymbol{\zeta}_l\right\}\cos(l\pi/L) + \mathfrak{Im}\left\{\boldsymbol{c}^T\boldsymbol{\zeta}_l\right\}\sin(l\pi/L) \;\geq\; 0, \\ &\qquad \forall k \in \mathcal{N}_{\text{r}} \Bigg\}. \end{aligned}$$

□

2.3 Robust Relay Power Allocation

To account for uncertainties associated with the global CSI of the relay network, we adopt a robust optimization methodology briefly summarized in Appendix A.3 [7,8]. Specifically, this methodology treats uncertainty by assuming that CSI is a deterministic variable within a bounded set of possible values. The size of the uncertainty set corresponds to the amount of uncertainty about the CSI.[7] This methodology ensures that the robust counterparts of our optimization problems lead to feasible solutions and yield good performance in all realizations of CSI within the uncertainty set. As in [7,8], we consider an ellipsoidal uncertainty set for simplicity.[8]

2.3.1 Coherent AF Relaying

Using the robust methodology, we formulate the robust counterpart of our AF RPA problem in *Proposition 1* with uncertainties in $\boldsymbol{A}$ and $\boldsymbol{c}$, as follows:

$$\begin{aligned} &\max_{\boldsymbol{\zeta}} \quad f_{\text{coh}}(\boldsymbol{\zeta}, \boldsymbol{A}, \boldsymbol{c}) \\ &\text{s.t.} \quad \boldsymbol{\zeta} \in \mathcal{S}, \quad \forall\, (\boldsymbol{A}, \boldsymbol{c}) \in \mathcal{U}, \end{aligned} \tag{2.28}$$

where the feasible set $\mathcal{S}$ is given in *Proposition 1* and $\mathcal{U}$ is an uncertainty set that contains all possible realizations of $\boldsymbol{A}$ and $\boldsymbol{c}$. To solve the above optimization problem, we incorporate the uncertainties associated with $\boldsymbol{A}$ and $\boldsymbol{c}$ into the convex feasibility program in (2.17) of Lemma 1. Since $(\boldsymbol{A}, \boldsymbol{c})$ only appears in the first constraint of (2.18), we simply need to focus on this constraint and build its robust counterpart as

[7] The singleton uncertainty set corresponds to the case of perfect CSI.

[8] Besides resulting in mathematical simplification, the ellipsoidal uncertainty set is well-motivated by practical CSI error models [117]. The size of the ellipsoidal uncertainty set can be known *a priori* from preliminary knowledge of the imperfect CSI estimation and/or from extensive wireless channel measurement campaigns.

follows:

$$\boldsymbol{c}^T\boldsymbol{\zeta} \geq \sqrt{\frac{t\sigma_{\mathrm{D}}^2}{P_{\mathrm{S}}}\left(1+\|\boldsymbol{A}\boldsymbol{\zeta}\|^2\right)}, \qquad \forall(\boldsymbol{A},\boldsymbol{c}) \in \mathcal{U}. \tag{2.29}$$

However, we adopt a conservative approach which assumes that $\mathcal{U}$ affecting (2.29) is sidewise, i.e., the uncertainty affecting the right-hand side in (2.29) is independent of that affecting the left-hand side. Specifically, we have $\mathcal{U} = \mathcal{U}_{\mathrm{R}} \times \mathcal{U}_{\mathrm{L}}$. Without such an assumption, it is known that a computationally tractable robust counterpart for (2.29) does not exist, which makes the conservative approach rather attractive [118]. Our results are summarized in the next theorem.

Theorem 1. *The robust coherent AF relay power allocation problem in (2.28) can be solved numerically via Lemma 1, except that the convex feasibility program is now conservatively replaced by its robust counterpart given as follows:*

$$\begin{aligned} \mathcal{P}_{\mathrm{coh}}^{(\mathrm{robust})}(t): \textit{find} \quad & \boldsymbol{\zeta} \\ \textit{s.t.} \quad & \boldsymbol{\zeta} \in \mathcal{S}_{\mathrm{coh}}(t,\boldsymbol{A},\boldsymbol{c}), \quad \forall \boldsymbol{A} \in \mathcal{U}_{\mathrm{R}}, \boldsymbol{c} \in \mathcal{U}_{\mathrm{L}}, \end{aligned} \tag{2.30}$$

with the sidewise independent ellipsoidal uncertainty sets $\mathcal{U}_{\mathrm{R}}$ and $\mathcal{U}_{\mathrm{L}}$ are given by

$$\mathcal{U}_{\mathrm{R}} = \left\{ \boldsymbol{A} = \boldsymbol{A}_0 + \sum_{j\in\mathcal{N}_A} z_j \boldsymbol{A}_j : \|\boldsymbol{z}\| \leq \rho_1 \right\} \tag{2.31}$$

$$\mathcal{U}_{\mathrm{L}} = \left\{ \boldsymbol{c} = \boldsymbol{c}_0 + \sum_{j\in\mathcal{N}_c} u_j \boldsymbol{c}_j : \|\boldsymbol{u}\| \leq \rho_2 \right\}, \tag{2.32}$$

where $\mathcal{N}_A = \{1,2,\ldots,N_A\}$, $\mathcal{N}_c = \{1,2,\ldots,N_c\}$, and N_A and N_c are the dimensions of $\boldsymbol{z}$ and $\boldsymbol{u}$, respectively. Then, the approximate robust convex feasibility program $\mathcal{P}_{\mathrm{coh}}^{(\mathrm{robust})}(t)$ can be written in SDP form as:

$$\begin{aligned} \textit{find} \quad & (\boldsymbol{\zeta},\tau,\mu) \\ \textit{s.t.} \quad & (\boldsymbol{\zeta},\tau,\mu) \in \mathcal{W}_{\mathrm{coh}}(t), \end{aligned} \tag{2.33}$$

such that $(\boldsymbol{\zeta}, \tau, \mu) \in \mathbb{R}_+^{N_\mathrm{r}} \times \mathbb{R}_+ \times \mathbb{R}_+$ *and the feasible set* $\mathcal{W}_{\mathrm{coh}}(t)$ *is given by*

$$\mathcal{W}_{\mathrm{coh}}(t) = \Bigg\{ \boldsymbol{\zeta} \in \mathbb{R}_+^{N_\mathrm{r}} : \begin{bmatrix} \mu \boldsymbol{I}_{N_A} & \boldsymbol{0}_{N_A} & \breve{\boldsymbol{A}}^T \\ \boldsymbol{0}_{N_A}^T & \lambda - \mu\rho_1^2 & \boldsymbol{\zeta}^T \boldsymbol{A}_0^T \\ \breve{\boldsymbol{A}} & \boldsymbol{A}_0 \boldsymbol{\zeta} & \lambda \boldsymbol{I}_{N_\mathrm{r}} \end{bmatrix} \succeq 0, \quad \begin{bmatrix} \frac{\boldsymbol{c}_0^T \boldsymbol{\zeta} - \tau}{\rho_2} \boldsymbol{I}_{N_c} & \breve{\boldsymbol{c}} \\ \breve{\boldsymbol{c}}^T & \frac{\boldsymbol{c}_0^T \boldsymbol{\zeta} - \tau}{\rho_2} \end{bmatrix} \succeq 0,$$
$$\begin{bmatrix} \frac{\eta_\mathrm{p}+1}{2} \boldsymbol{I}_2 & \begin{pmatrix} \boldsymbol{\zeta}^T \boldsymbol{e}_k \\ \frac{\eta_\mathrm{p}-1}{2} \end{pmatrix} \\ \begin{pmatrix} \boldsymbol{\zeta}^T \boldsymbol{e}_k \\ \frac{\eta_\mathrm{p}-1}{2} \end{pmatrix}^T & \frac{\eta_\mathrm{p}+1}{2} \end{bmatrix} \succeq 0, \begin{bmatrix} \boldsymbol{I}_{N_\mathrm{r}} & \boldsymbol{\zeta} \\ \boldsymbol{\zeta}^T & 1 \end{bmatrix} \succeq 0,$$
$$\begin{bmatrix} \tau & \sqrt{\frac{t\sigma_\mathrm{D}^2}{P_\mathrm{S}}} \\ \sqrt{\frac{t\sigma_\mathrm{D}^2}{P_\mathrm{S}}} & \tau \end{bmatrix} \succeq 0, \quad \forall k \in \mathcal{N}_\mathrm{r} \Bigg\},$$

where $\lambda = \tau\sqrt{P_\mathrm{S}/t\sigma_\mathrm{D}^2} - 1$, $\breve{\boldsymbol{A}} = [\boldsymbol{A}_1\boldsymbol{\zeta}, \boldsymbol{A}_2\boldsymbol{\zeta}, \ldots, \boldsymbol{A}_{N_A}\boldsymbol{\zeta}]$ *and* $\breve{\boldsymbol{c}} = \left[\boldsymbol{c}_1^T\boldsymbol{\zeta}, \boldsymbol{c}_2^T\boldsymbol{\zeta}, \ldots, \boldsymbol{c}_{N_c}^T\boldsymbol{\zeta}\right]^T$.

Proof. Under sidewise independence assumption, $\boldsymbol{\zeta}$ is robust feasible for (2.29) if there exists $\tau \in \mathbb{R}_+$ such that [7, 118, 119]

$$\sqrt{\frac{t\sigma_\mathrm{D}^2}{P_\mathrm{S}}\left(1 + \|\boldsymbol{A}\boldsymbol{\zeta}\|^2\right)} \leq \tau, \qquad \forall \boldsymbol{A} \in \mathcal{U}_\mathrm{R} \tag{2.34}$$
$$\tau \leq \boldsymbol{c}^T\boldsymbol{\zeta}, \qquad \forall \boldsymbol{c} \in \mathcal{U}_\mathrm{L}. \tag{2.35}$$

First, we consider (2.34) by rewriting it as follows:

$$\left\| \begin{pmatrix} 1 \\ \boldsymbol{A}\boldsymbol{\zeta} \end{pmatrix} \right\| \leq \tau\sqrt{\frac{P_\mathrm{S}}{t\sigma_\mathrm{D}^2}}, \qquad \forall \boldsymbol{A} \in \mathcal{U}_\mathrm{R}. \tag{2.36}$$

We now replace the constraint in (2.36) by

$$1 + \|\boldsymbol{A}\boldsymbol{\zeta}\| \leq \tau\sqrt{\frac{P_\mathrm{S}}{t\sigma_\mathrm{D}^2}}, \qquad \forall \boldsymbol{A} \in \mathcal{U}_\mathrm{R}. \tag{2.37}$$

Indeed, if (2.37) is satisfied, then (2.36) is always satisfied since

$$\left\| \begin{pmatrix} 1 \\ \boldsymbol{A\zeta} \end{pmatrix} \right\| \leq 1 + \|\boldsymbol{A\zeta}\|, \tag{2.38}$$

By letting $\lambda = \tau\sqrt{P_{\mathrm{S}}/t\sigma_{\mathrm{D}}^2} - 1$, we have

$$\begin{aligned} 0 &\leq \lambda, \\ \left\| \boldsymbol{A}_0\boldsymbol{\zeta} + \breve{\boldsymbol{A}}\boldsymbol{z} \right\| &\leq \lambda, \qquad \forall \boldsymbol{z} \in \{\boldsymbol{z} : \|\boldsymbol{z}\| \leq \rho_1\}, \end{aligned} \tag{2.39}$$

where we have substituted $\boldsymbol{A}$ defined by the uncertainty set $\mathcal{U}_{\mathrm{R}}$ in (2.31). Note that when $\lambda = 0$, we have $\boldsymbol{A}_0\boldsymbol{\zeta} = \boldsymbol{0}$ and $\breve{\boldsymbol{A}} = \boldsymbol{0}$ for (2.39) to hold. Now, by expanding (2.39) in terms of a quadratic form of $\boldsymbol{z}$, we have

$$\begin{aligned} &0 \leq \lambda, \\ &0 \leq q_0(\boldsymbol{z}) \quad \forall \boldsymbol{z} \in \{\boldsymbol{z} : 0 \leq q_1(\boldsymbol{z})\}, \end{aligned} \tag{2.40}$$

where

$$\begin{aligned} q_0(\boldsymbol{z}) &= -\boldsymbol{z}^T\breve{\boldsymbol{A}}^T\breve{\boldsymbol{A}}\boldsymbol{z} - 2\left(\breve{\boldsymbol{A}}^T\boldsymbol{A}_0\boldsymbol{\zeta}\right)^T\boldsymbol{z} - \boldsymbol{\zeta}^T\boldsymbol{A}_0^T\boldsymbol{A}_0\boldsymbol{\zeta} + \lambda^2 \\ q_1(\boldsymbol{z}) &= \rho_1^2 - \boldsymbol{z}^T\boldsymbol{z}. \end{aligned} \tag{2.41}$$

We exploit the following lemma to express the quadratic constraints in (2.40) in terms of matrix inequality.

Lemma 4 (S-procedure [111])**.** *Let $q_0(\boldsymbol{z}) = \boldsymbol{z}^T\boldsymbol{B}_0\boldsymbol{z} + 2\boldsymbol{b}_0^T\boldsymbol{z} + c_0$ and $q_1(\boldsymbol{z}) = \boldsymbol{z}^T\boldsymbol{B}_1\boldsymbol{z} + 2\boldsymbol{b}_1^T\boldsymbol{z} + c_1$ be two quadratic functions of $\boldsymbol{z}$, where $\boldsymbol{B}_0$ and $\boldsymbol{B}_1$ are symmetric, and there exists some $\boldsymbol{z}_0$ satisfying $q_1(\boldsymbol{z}_0) > 0$. Then, we have*

$$\begin{aligned} q_1(\boldsymbol{z}) \geq 0 \Rightarrow q_0(\boldsymbol{z}) \geq 0 \quad &\textit{iff} \\ \exists\, \alpha \in \mathbb{R}_+ : &\begin{bmatrix} \boldsymbol{B}_0 & \boldsymbol{b}_0 \\ \boldsymbol{b}_0^T & c_0 \end{bmatrix} - \alpha \begin{bmatrix} \boldsymbol{B}_1 & \boldsymbol{b}_1 \\ \boldsymbol{b}_1^T & c_1 \end{bmatrix} \succeq 0. \end{aligned}$$

From Lemma 4, it follows that (2.40) is satisfied if and only if there exists $\alpha \in \mathbb{R}_+$ such that

$$\begin{bmatrix} -\breve{\boldsymbol{A}}^T\breve{\boldsymbol{A}} & -\breve{\boldsymbol{A}}^T\boldsymbol{A}_0\boldsymbol{\zeta} \\ \left(-\breve{\boldsymbol{A}}^T\boldsymbol{A}_0\boldsymbol{\zeta}\right)^T & \lambda^2 - \boldsymbol{\zeta}^T\boldsymbol{A}_0^T\boldsymbol{A}_0\boldsymbol{\zeta} \end{bmatrix} - \alpha \begin{bmatrix} -\boldsymbol{I}_{N_A} & \boldsymbol{0}_{N_A} \\ \boldsymbol{0}_{N_A}^T & \rho_1^2 \end{bmatrix} \succeq 0. \tag{2.42}$$

In the case of $\lambda = 0$, it is easy to see that (2.42) is satisfied only when $\alpha = 0$. To convert the above quadratic matrix inequality into a linear matrix inequality (LMI), we first let $\alpha = \lambda\mu$ for some $\mu \in \mathbb{R}_+$. Rearranging (2.40), we have[9]

$$\Delta_{\boldsymbol{D}} \triangleq \lambda \begin{bmatrix} \mu\boldsymbol{I}_{N_A} & \boldsymbol{0}_{N_A} \\ \boldsymbol{0}_{N_A}^T & \lambda - \mu\rho_1^2 \end{bmatrix} - \begin{bmatrix} \breve{\boldsymbol{A}}^T \\ \boldsymbol{\zeta}^T\boldsymbol{A}_0^T \end{bmatrix} \boldsymbol{I}_{N_\mathrm{r}} \begin{bmatrix} \breve{\boldsymbol{A}}^T \\ \boldsymbol{\zeta}^T\boldsymbol{A}_0^T \end{bmatrix}^T \succeq 0. \tag{2.43}$$

To linearize (2.43), we rely on the following lemma:

Lemma 5 (Schur Complement [111])**.** *Let*

$$\boldsymbol{M} = \begin{bmatrix} \boldsymbol{A} & \boldsymbol{B} \\ \boldsymbol{B}^T & \boldsymbol{D} \end{bmatrix}$$

be a symmetric matrix with $\boldsymbol{D} \succ 0$. Then, $\boldsymbol{M} \succeq 0$ if and only if the Schur complement of $\boldsymbol{D}$ in $\boldsymbol{M}$, i.e., $\Delta_{\boldsymbol{D}} = \boldsymbol{A} - \boldsymbol{B}\boldsymbol{D}^{-1}\boldsymbol{B}^T \succeq 0$.

If $\lambda > 0$, it follows that $\frac{1}{\lambda}\Delta_{\boldsymbol{D}}$ in (2.43) is the Schur complement of $\lambda\boldsymbol{I}_{N_\mathrm{r}}$ in

$$\boldsymbol{M} \triangleq \begin{bmatrix} \mu\boldsymbol{I}_{N_A} & \boldsymbol{0}_{N_A} & \breve{\boldsymbol{A}}^T \\ \boldsymbol{0}_{N_A}^T & \lambda - \mu\rho_1^2 & \boldsymbol{\zeta}^T\boldsymbol{A}_0^T \\ \breve{\boldsymbol{A}} & \boldsymbol{A}_0\boldsymbol{\zeta} & \lambda\boldsymbol{I}_{N_\mathrm{r}} \end{bmatrix}, \tag{2.44}$$

and by Lemma 5, $\boldsymbol{M} \succeq 0$ since $\frac{1}{\lambda}\Delta_{\boldsymbol{D}} \succeq 0$. For $\lambda = 0$, $\boldsymbol{M} \succeq 0$ holds if and only if $\mu = 0$, $\boldsymbol{A}_0\boldsymbol{\zeta} = \boldsymbol{0}$ and $\breve{\boldsymbol{A}} = \boldsymbol{0}$. Thus, we have the first LMI in $\mathcal{W}_{\mathrm{coh}}(t)$. In summary, a pair $(\boldsymbol{\zeta}, \tau)$ satisfies (2.34) if there exists some $\mu \in \mathbb{R}_+$ and $\tau \geq \sqrt{t\sigma_\mathrm{D}^2/P_\mathrm{S}}$ such that the triple $(\boldsymbol{\zeta}, \tau, \mu)$ satisfies the LMI in (2.44).

[9] When $\lambda = 0$, we have $\mu = 0$.

Next, we turn to the condition (2.35). By substituting $\boldsymbol{c}$ defined by the uncertainty set $\mathcal{U}_{\mathrm{L}}$ in (2.32) into (2.35), we have equivalently

$$-\left(\boldsymbol{c}_0^T\boldsymbol{\zeta}-\tau\right) \leq \breve{\boldsymbol{c}}^T\boldsymbol{u}, \qquad \forall \boldsymbol{u} \in \{\boldsymbol{u} : \|\boldsymbol{u}\| \leq \rho_2\}, \tag{2.45}$$

and the robust constraint in (2.45) can be expressed as

$$-\left(\boldsymbol{c}_0^T\boldsymbol{\zeta}-\tau\right) \leq \min_{\boldsymbol{u}:\|\boldsymbol{u}\|\leq\rho_2} \left\{\breve{\boldsymbol{c}}^T\boldsymbol{u}\right\}. \tag{2.46}$$

From the Cauchy-Schwartz inequality, the minimum value on the right-hand side of (2.46) is equal to $-\rho_2\|\breve{\boldsymbol{c}}\|$, and hence we obtain an SOC constraint, as follows:

$$\begin{bmatrix} \frac{\boldsymbol{c}_0^T\boldsymbol{\zeta}-\tau}{\rho_2} \\ \breve{\boldsymbol{c}} \end{bmatrix} \succeq_{\mathcal{K}} 0. \tag{2.47}$$

Using (A.6), we can represent (2.47) as

$$\begin{bmatrix} \frac{\boldsymbol{c}_0^T\boldsymbol{\zeta}-\tau}{\rho_2}\boldsymbol{I}_{N_c} & \breve{\boldsymbol{c}} \\ \breve{\boldsymbol{c}}^T & \frac{\boldsymbol{c}_0^T\boldsymbol{\zeta}-\tau}{\rho_2} \end{bmatrix} \succeq 0, \tag{2.48}$$

which is the second LMI in $\mathcal{W}_{\mathrm{coh}}(t)$. The third and fourth LMIs in $\mathcal{W}_{\mathrm{coh}}(t)$ follow straightforwardly from the results in (2.21), and the last LMI is easily obtained by representing the constraint $\tau \geq \sqrt{t\sigma_{\mathrm{D}}^2/P_{\mathrm{S}}}$ in terms of an LMI. □

Remark 6. *The use of constraint (2.37), instead of (2.36), enables us to formulate* $\mathcal{P}_{\mathrm{coh}}^{(\mathrm{robust})}(t)$ *into a SDP. Note that the robust feasible set* $\mathcal{W}_{\mathrm{coh}}(t)$ *in (2.33) is always contained in the set of robust feasible solutions of* $\mathcal{P}_{\mathrm{coh}}^{(\mathrm{robust})}(t)$.

2.3.2 Noncoherent AF Relaying

In the next theorem, we formulate the robust counterparts of the $2L$ subproblems in Lemma 3 with uncertainties associated with $\boldsymbol{A}$ and $\boldsymbol{c}$.

Theorem 2. *The robust noncoherent AF relay power allocation problem can be approximately decomposed into $2L$ subproblems. Under sidewise independent ellipsoidal uncertainty sets $\mathcal{U}_{\rm R}$ and $\mathcal{U}_{\rm L}$ given by*

$$\mathcal{U}_{\rm R} = \left\{ \boldsymbol{A} = \boldsymbol{A}_0 + \sum_{j\in N_A} z_j \boldsymbol{A}_j : \|\boldsymbol{z}\| \le \rho_1 \right\} \tag{2.49}$$

$$\mathcal{U}_{\rm L} = \left\{ \boldsymbol{c} = \boldsymbol{c}_0 + \sum_{j\in N_c} u_j \boldsymbol{c}_j : \|\boldsymbol{u}\| \le \rho_2 \right\}, \tag{2.50}$$

with each subproblem can be solved efficiently using the bisection method, except that the convex feasibility program is now replaced with its approximate robust counterpart in the form of an SDP:

$$\begin{aligned} \mathcal{P}^{(\rm robust)}_{\rm noncoh}(t,l): \mathit{find} \quad & (\boldsymbol{\zeta}_l, \tau, \mu) \\ \mathit{s.t.} \quad & (\boldsymbol{\zeta}_l, \tau, \mu) \in \mathcal{W}_{\rm noncoh}(t,l), \end{aligned} \tag{2.51}$$

such that each $l \in \mathcal{L}$, $(\boldsymbol{\zeta}, \tau, \mu) \in \mathbb{R}_+^{N_{\rm r}} \times \mathbb{R}_+ \times \mathbb{R}_+$, and the set $\mathcal{W}_{\rm noncoh}(t,l)$ is given by

$$\begin{aligned} &\mathcal{W}_{\rm noncoh}(t,l) \\ &= \Bigg\{ \boldsymbol{\zeta}_l \in \mathbb{R}_+^{N_{\rm r}} : \begin{bmatrix} \mu \boldsymbol{I}_{N_A} & \boldsymbol{0}_{N_A} & \breve{\boldsymbol{A}}_l^T \\ \boldsymbol{0}_{N_A}^T & \lambda - \mu\rho_1^2 & \boldsymbol{\zeta}_l^T \boldsymbol{A}_0^T \\ \breve{\boldsymbol{A}}_l & \boldsymbol{A}_0 \boldsymbol{\zeta}_l & \lambda \boldsymbol{I}_{N_{\rm r}} \end{bmatrix} \succeq 0, \quad \begin{bmatrix} \frac{M(l)}{\rho_2} \boldsymbol{I}_{N_c} & \breve{\boldsymbol{c}}_l \\ \breve{\boldsymbol{c}}_l^T & \frac{M(l)}{\rho_2} \end{bmatrix} \succeq 0, \\ &\qquad \begin{bmatrix} \frac{\left[\mathfrak{Re}\{\boldsymbol{c}_0^T \boldsymbol{\zeta}_l\} \cos(l\pi/L) + \mathfrak{Im}\{\boldsymbol{c}_0^T \boldsymbol{\zeta}_l\} \sin(l\pi/L)\right]}{\rho_2} \boldsymbol{I}_{N_c} & \breve{\boldsymbol{c}}_l \\ \breve{\boldsymbol{c}}_l^T & \frac{\left[\mathfrak{Re}\{\boldsymbol{c}_0^T \boldsymbol{\zeta}_l\} \cos(l\pi/L) + \mathfrak{Im}\{\boldsymbol{c}_0^T \boldsymbol{\zeta}_l\} \sin(l\pi/L)\right]}{\rho_2} \end{bmatrix} \succeq 0, \\ &\qquad \begin{bmatrix} \frac{\eta_{\rm p}+1}{2} \boldsymbol{I}_2 & \begin{pmatrix} \boldsymbol{\zeta}_l^T \boldsymbol{e}_k \\ \frac{\eta_{\rm p}-1}{2} \end{pmatrix} \\ \begin{pmatrix} \boldsymbol{\zeta}_l^T \boldsymbol{e}_k \\ \frac{\eta_{\rm p}-1}{2} \end{pmatrix}^T & \frac{\eta_{\rm p}+1}{2} \end{bmatrix} \succeq 0, \begin{bmatrix} \boldsymbol{I}_{N_{\rm r}} & \boldsymbol{\zeta}_l \\ \boldsymbol{\zeta}_l^T & 1 \end{bmatrix} \succeq 0, \begin{bmatrix} \tau & \sqrt{\frac{t\sigma_{\rm D}^2}{P_{\rm S}}} \\ \sqrt{\frac{t\sigma_{\rm D}^2}{P_{\rm S}}} & \tau \end{bmatrix} \succeq 0, \quad \forall k \in \mathcal{N}_{\rm r} \Bigg\}, \end{aligned}$$

where $\lambda = \tau\sqrt{P_{\mathrm{S}}/t\sigma_{\mathrm{D}}^2} - 1$,

$$\begin{aligned}
\breve{\boldsymbol{c}}_l &= \begin{bmatrix} \mathfrak{Re}\left\{\boldsymbol{c}_1^T\boldsymbol{\zeta}_l\right\}\cos(l\pi/L) + \mathfrak{Im}\left\{\boldsymbol{c}_1^T\boldsymbol{\zeta}_l\right\}\sin(l\pi/L) \\ \mathfrak{Re}\left\{\boldsymbol{c}_2^T\boldsymbol{\zeta}_l\right\}\cos(l\pi/L) + \mathfrak{Im}\left\{\boldsymbol{c}_2^T\boldsymbol{\zeta}_l\right\}\sin(l\pi/L) \\ \vdots \\ \mathfrak{Re}\left\{\boldsymbol{c}_{N_c}^T\boldsymbol{\zeta}_l\right\}\cos(l\pi/L) + \mathfrak{Im}\left\{\boldsymbol{c}_{N_c}^T\boldsymbol{\zeta}_l\right\}\sin(l\pi/L) \end{bmatrix} \\
M(l) &= \left[\mathfrak{Re}\left\{\boldsymbol{c}_0^T\boldsymbol{\zeta}_l\right\}\cos(l\pi/L) + \mathfrak{Im}\left\{\boldsymbol{c}_0^T\boldsymbol{\zeta}_l\right\}\sin(l\pi/L)\right] - \tau \\
\breve{\boldsymbol{A}}_l &= \left[\boldsymbol{A}_1\boldsymbol{\zeta}_l, \boldsymbol{A}_2\boldsymbol{\zeta}_l, \ldots, \boldsymbol{A}_{N_A}\boldsymbol{\zeta}_l\right].
\end{aligned}$$

Proof. The results follow straightforwardly from Lemma 3 and using similar steps leading to Theorem 1. □

2.4 Numerical Results

In this section, we illustrate the effectiveness of our power allocation algorithms for coherent and noncoherent AF relay networks using numerical examples. We determine the RPAs using our proposed algorithms with $\varepsilon = 0.001$ in Chapters 2.3 and 2.4.[10] We consider $\boldsymbol{h}_{\mathrm{B}}$ and $\boldsymbol{h}_{\mathrm{F}}$ to be mutually independent random vectors with independent and identically distributed elements which are circularly symmetric complex Gaussian r.v.'s, i.e., $h_{\mathrm{B},k} \sim \tilde{\mathcal{N}}(0,1)$ and $h_{\mathrm{F},k} \sim \tilde{\mathcal{N}}(0,1)$ for all k. The noise variances are normalized, such that $\sigma_{\mathrm{R},k}^2 = 1$ and $\sigma_{\mathrm{D}}^2 = 1$. For numerical illustrations, we use the outage probability, defined as $\mathbb{P}\{\mathsf{SNR}(\boldsymbol{p}) < \gamma_{\mathrm{th}}\}$, as the performance measure, where γ_{th} is the value of the target receive SNR and it is set at $\gamma_{\mathrm{th}} = 10$ dB. The uncertainty sets in Theorems 1 and 2 are chosen such that $N_A = 1$, $N_c = 1$, $\boldsymbol{A}_1 = \boldsymbol{A}_0$, and $\boldsymbol{c}_1 = \boldsymbol{c}_0$. We consider $\rho_1 = \rho_2 = \rho$, where $\rho = 0$ corresponds to perfect knowledge of the global CSI and $\rho = 1$ corresponds to an uncertainty that can be as large as the size of the estimated global CSI, i.e., $\boldsymbol{A}_0$ and $\boldsymbol{c}_0$.

Figure 2-2 shows the outage probability as a function of $P_{\mathrm{S}}/\sigma_{\mathrm{D}}^2$ for the coherent AF

[10] Our proposed optimal and robust power allocation algorithms, respectively, require solutions of convex feasibility programs in the form of SOCP and SDP. We use the SeDuMi convex optimization package to obtain such numerical solutions [120].

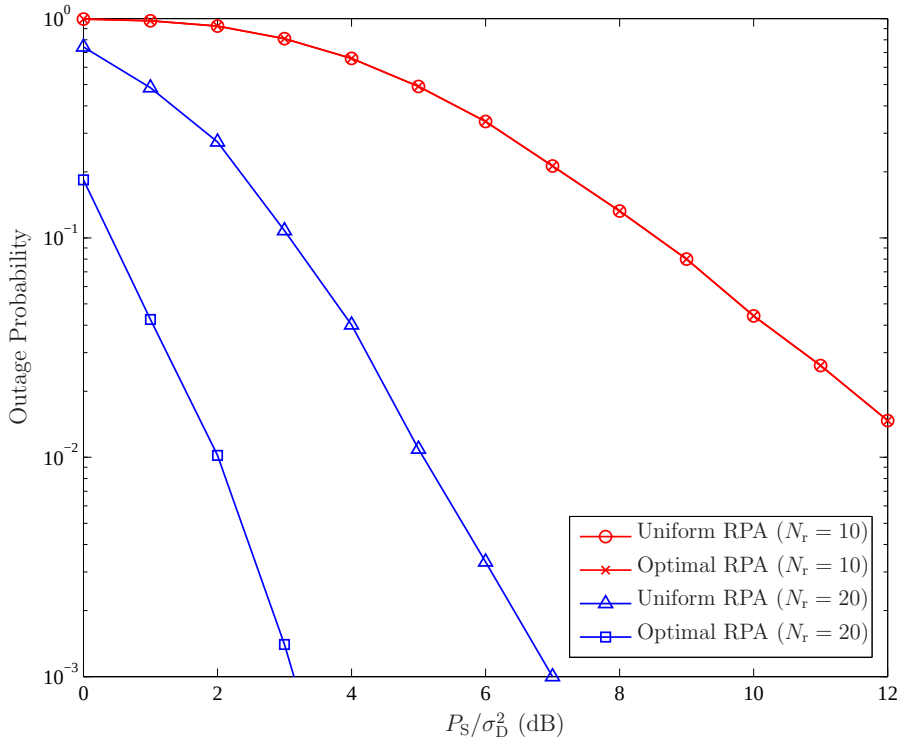

Figure 2-2: Outage probability as a function of P_S/σ_D^2 for the coherent AF relay network with $\eta_p = 0.1$.

relay network with $\eta_p = 0.1$. We consider relay networks with $N_r = 10$ and $N_r = 20$, and compare the performance of uniform and optimal RPAs. When $N_r = 10$, both the uniform and optimal power allocations result in the same performance. This can be explained by the fact that it is optimal for each relay node to transmit at the maximum transmission power P when $\eta_p = P/P_R = 0.1$. When $N_r = 20$, we first observe that lower outage probabilities can be achieved for both power allocations compared to the case with $N_r = 10$, due to the presence of diversity gains in coherent AF relay network. In addition, significant performance improvements with optimal RPA compared to uniform RPA can be observed since optimal RPA can exploit the channel variation more effectively for larger N_r to enhance the effective SNR at the destination node.

Similar to Fig. 2-2, we show the outage probability as a function of P_S/σ_D^2 for the noncoherent AF relay network with $\eta_p = 0.1$ in Fig. 2-3. Under uniform RPA, we

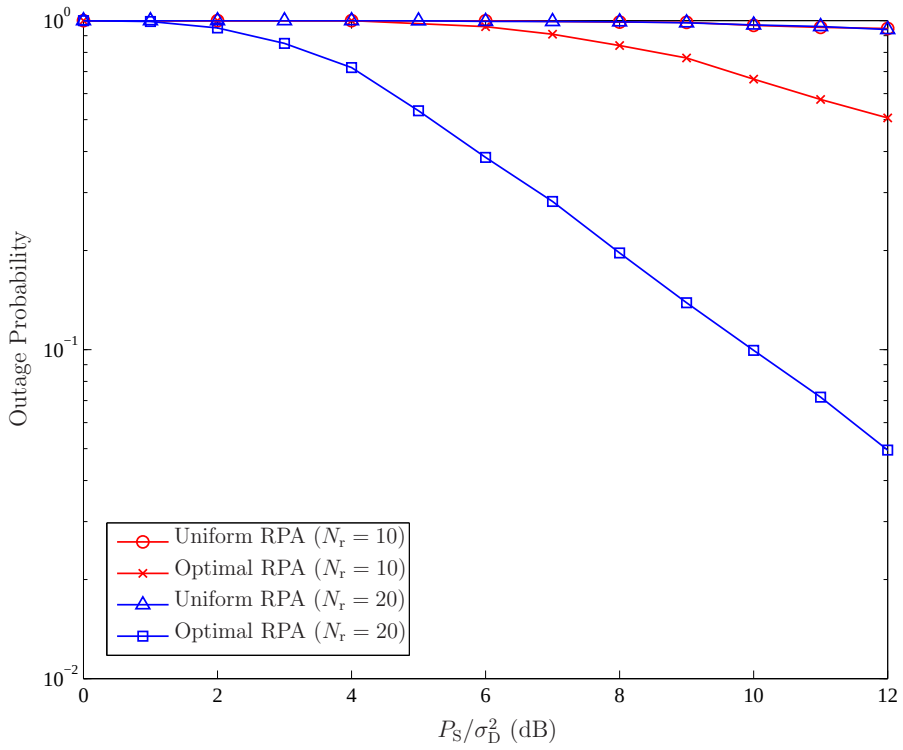

Figure 2-3: Outage probability as a function of P_S/σ_D^2 for the noncoherent AF relay network with $\eta_p = 0.1$.

observe that the increase in the number of relay nodes do not yield any performance gain. This behavior of noncoherent AF relay network is consistent with the results of [28], and can be attributed to the lack of locally-bidirectional CSIs at the relay nodes, making coherent combining at the destination node impossible. However, we can see that performance improves with optimal RPA compared to uniform RPA, and this improvement increases with N_r. Comparing Figs. 2-2 and 2-3, even with optimal RPA, the noncoherent AF relay network performs much worse than the coherent AF case, since optimal RPA is unable to fully reap the performance gain promised by coherent AF case due to the lack of distributed beamforming gain.

Figures 2-4 and 2-5 show the effect of uncertainties associated with the global CSI on the outage probabilities of coherent and noncoherent AF networks using non-robust RPAs when $N_r = 20$ and $\eta_p = 0.1$. By non-robust algorithms, we refer to optimization algorithms in Chapter 2.3 that optimize RPAs based only on $\boldsymbol{A}_0$ and

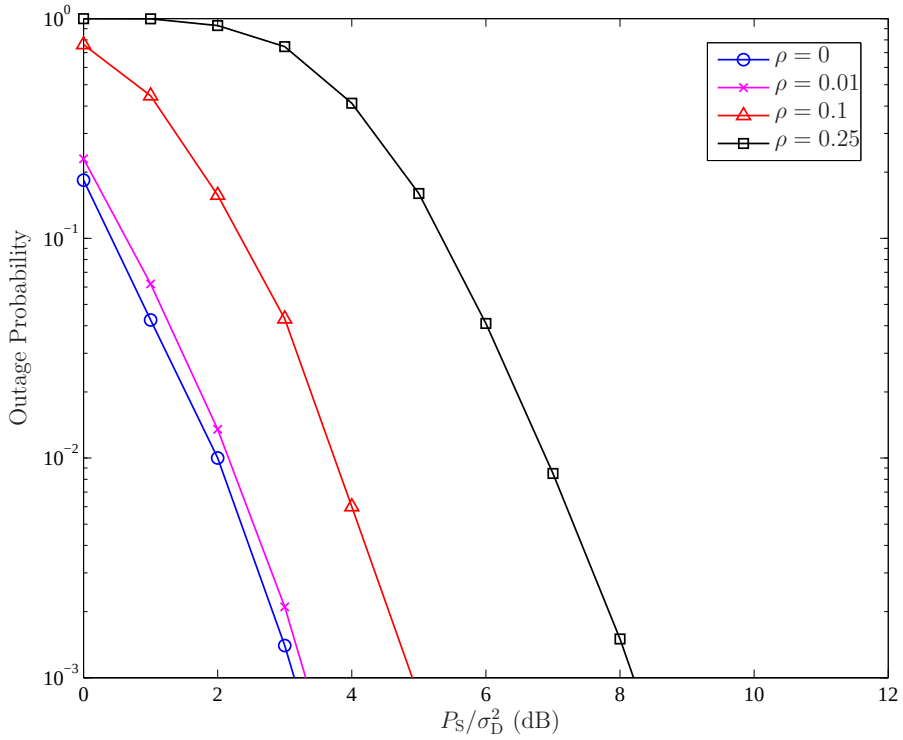

Figure 2-4: Effect of uncertain global CSI on the outage probability of the coherent AF relay network using non-robust algorithm for $\eta_p = 0.1$ and $N_r = 20$.

$\boldsymbol{c}_0$ instead of the true global CSI $\boldsymbol{A}$ and $\boldsymbol{c}$, where $\boldsymbol{A} = \boldsymbol{A}_0 + z\boldsymbol{A}_1$ and $\boldsymbol{c} = \boldsymbol{c}_0 + u\boldsymbol{c}_1$.[11] Clearly, we see that ignoring CSI uncertainties in our designs can lead to drastic performance degradation when the uncertainty size ρ becomes large. In these figures, we can see that when ρ is less than 0.01, we may ignore CSI uncertainties since the performance degradation is negligible. However, performance deteriorates rapidly as ρ increases. For example, to maintain at an outage probability of 10^{-2} in coherent AF relay network, P_S/σ_D^2 needs to increase by an additional of about 5 dB when $\rho = 0.25$. For the noncoherent AF case, a larger increase in P_S/σ_D^2 is required to maintain a target outage probability when $\rho = 0.25$. These results show that RPA is sensitive with respect to uncertainties in global CSI, and motivates the need for RPAs that are robust to global CSI uncertainties.

Figures 2-6 and 2-7 show the outage probabilities of coherent and noncoherent

[11] These results are generated based on the worst case scenario, where $z = \rho$ and $u = -\rho$.

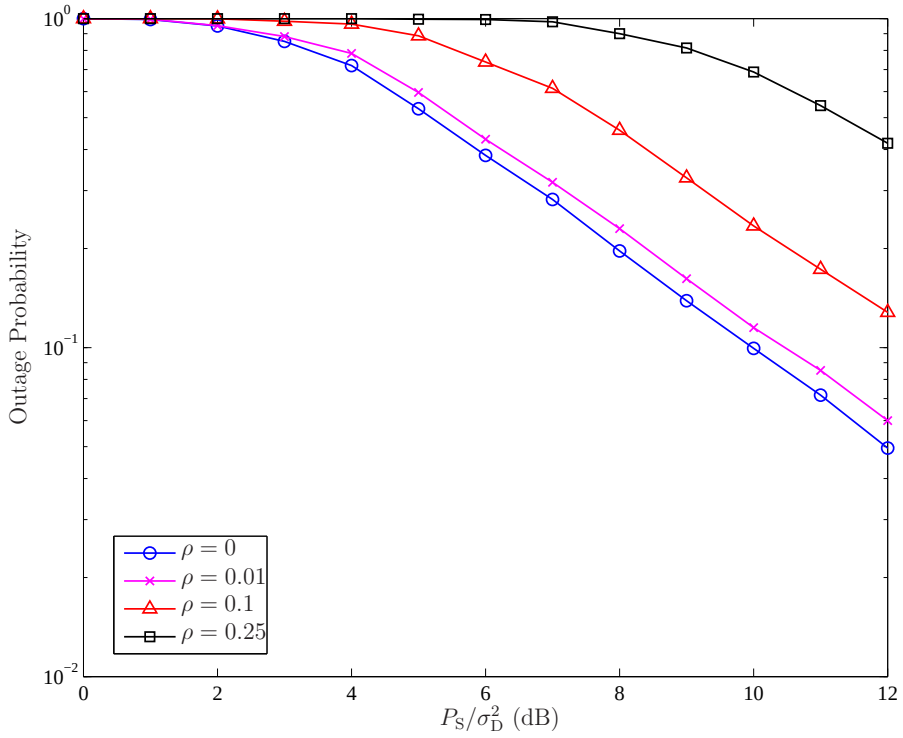

Figure 2-5: Effect of uncertain global CSI on the outage probability of the noncoherent AF relay network using non-robust algorithm for $\eta_p = 0.1$ and $N_r = 20$.

AF relay networks as a function of the size of the uncertainty set ρ using robust RPAs when $N_r = 20$ and $\eta_p = 0.1$. For comparison, we also plot the performance of uniform and non-robust RPAs in these plots. We observe that non-robust RPAs still offer some performance improvements over uniform RPAs as long as ρ is not large. When ρ is large, the effectiveness of non-robust RPA algorithms is significantly reduced. On the other hand, we see that robust RPAs provide significant performance gain over non-robust RPAs over a wide range of ρ, showing the effectiveness of our robust algorithms in the presence of global CSI uncertainty.

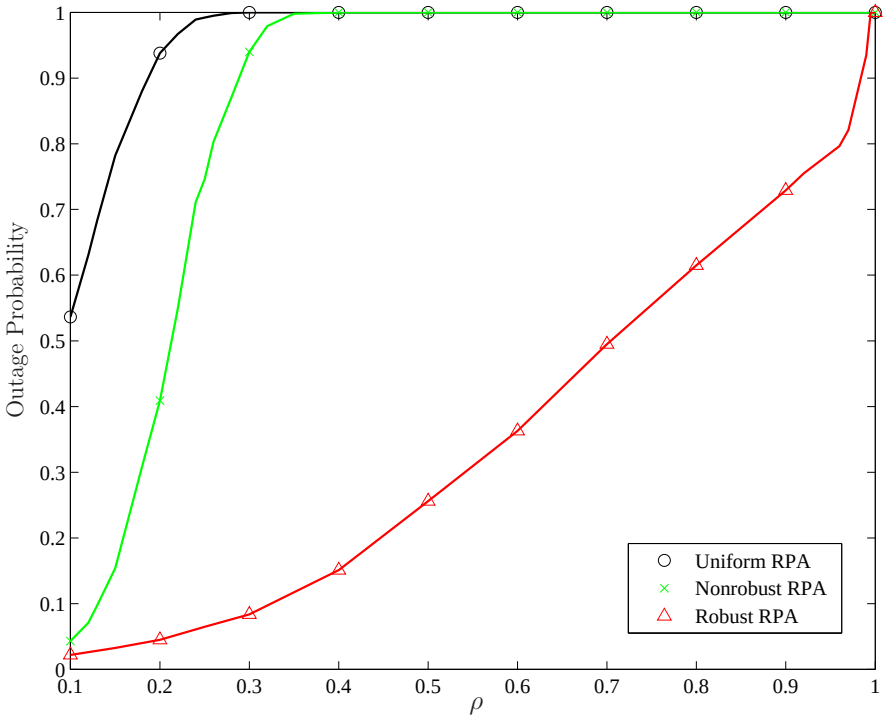

Figure 2-6: Outage probability as a function of size of uncertainty set ρ for the coherent AF relay network with $P_{\mathrm{S}}/\sigma_{\mathrm{D}}^2 = 3$ dB, $\eta_{\mathrm{p}} = 0.1$, and $N_{\mathrm{r}} = 20$.

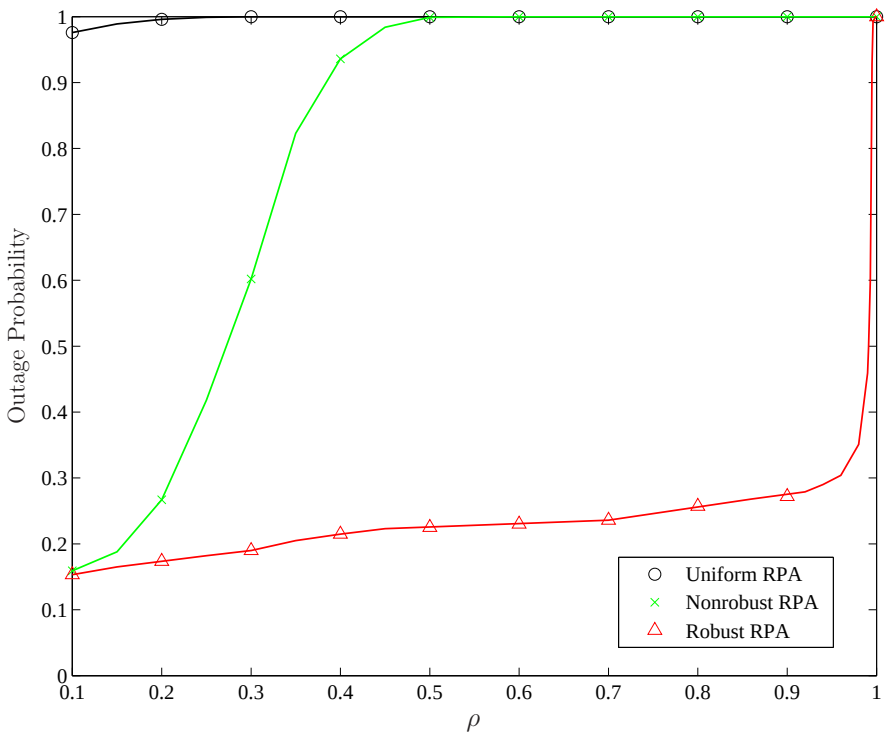

Figure 2-7: Outage probability as a function of size of uncertainty set ρ for the noncoherent AF relay network with $P_{\mathrm{S}}/\sigma_{\mathrm{D}}^2 = 12$ dB, $\eta_{\mathrm{p}} = 0.1$, and $N_{\mathrm{r}} = 20$.

Chapter 3

Robust Wireless Relay Networks: Slow Power Allocation with Guaranteed QoS

In this chapter, we formulate RPA problem as the total relay transmission power minimization problem subject to a QoS constraint.[1] Our algorithms track only the large-scale fading and thereby lead to practical implementations. We show that our optimization problems for coherent and noncoherent AF relay networks can be cast as an SOCP and an LP, respectively, under perfect knowledge of large-scale fading. Under ellipsoidal uncertainty sets, the robust counterparts of the power minimization problems for coherent and noncoherent AF relay channels can be formulated as an SDP and an SOCP, respectively.

3.1 Problem Formulation

Adopting the same network model as in Chapter 2.1, we consider a wireless relay network with one source-destination node pair and N_{r} relay nodes. In general, we can decompose each instantaneous element in $\boldsymbol{h}_{\mathrm{B}}$ and $\boldsymbol{h}_{\mathrm{F}}$ in (2.1) and (2.2) into the

[1]The required QoS is considered to be satisfied when the output SNR at the destination node exceeds a given target value.

product of two different fading effects with different timescales [121]. Specifically, we can write

$$h_{\mathrm{B},k} = \alpha_{\mathrm{B},k}\sqrt{S_{\mathrm{B},k}}, \tag{3.1}$$

$$h_{\mathrm{F},k} = \alpha_{\mathrm{F},k}\sqrt{S_{\mathrm{F},k}}, \tag{3.2}$$

where $\alpha_{\mathrm{B},k} \in \mathbb{C}$ and $\alpha_{\mathrm{F},k} \in \mathbb{C}$ reflect the channel gain associated with small-scale fading from the source to the kth relay and the kth relay to the destination, respectively. Such small-scale fading is typically due to local scattering of the environment and varies with a timescale on the order of milliseconds, and we can model $\alpha_{\mathrm{B},k} \sim \tilde{\mathcal{N}}(0,1)$ and $\alpha_{\mathrm{F},k} \sim \tilde{\mathcal{N}}(0,1)$ for all k. Each is assumed to be independent across all the relay nodes.[2] On the other hand, $S_{\mathrm{B},k} \in \mathbb{R}_+$ and $S_{\mathrm{F},k} \in \mathbb{R}_+$ capture the large-scale fading effects that are caused by shadowing. Large-scale fading varies with a timescale on the order of seconds. Usually, we can model $S_{\mathrm{B},k}$ and $S_{\mathrm{F},k}$ as [121]

$$S_{\mathrm{B},k} = \frac{10^{\sigma_{\mathrm{dB}}N/10}}{d_{\mathrm{B},k}^{\varepsilon}}, \tag{3.3}$$

$$S_{\mathrm{F},k} = \frac{10^{\sigma_{\mathrm{dB}}N/10}}{d_{\mathrm{F},k}^{\varepsilon}}, \tag{3.4}$$

where $d_{\mathrm{B},k}$ and $d_{\mathrm{F},k}$ are the normalized distances from the kth relay to the source and destination, respectively, ε is the path-loss exponent which corresponds to a decay in power, σ_{dB} is the standard deviation of the log-normal shadowing in dB, and N is a real Gaussian r.v. such that $N \sim \mathcal{N}(0,1)$.[3]

As in Chapter 2, we impose an individual source power constraint P_{S} and an individual relay power constraint P on the transmit power of the kth relay, p_k, where $p_k \leq P$. Our goal is to employ power allocation intelligently so as to minimize the

[2]The independence assumption arises due to the presence of different propagation paths and scatterers for each relay node.

[3]The parameter ε is environment-dependent and can approximately range from 1.6 (e.g., hallways inside buildings) to 8 (e.g., dense urban environments), where $\varepsilon = 2$ corresponds to the free space propagation [122]. On the other hand, the typical values of σ_{dB} range from 4 to 13 dB for outdoor channels [122]. For ease of exposition, we have assumed that the attenuations due to shadowing are independent and identically distributed (i.i.d.).

total relay transmission power of the relay nodes while satisfying the system QoS requirement. Likewise in Chapter 2, the kth diagonal element of $\boldsymbol{G}$ for noncoherent AF relaying is given by

$$g_{\text{noncoh}}^{(k)} = \sqrt{\beta_k p_k}, \tag{3.5}$$

where $\beta_k = 1/(P_{\text{S}} f_{\text{B},k}^2 + \sigma_{\text{R},k}^2)$. Comparing (3.5) with (2.6), the amplification factor β_k in (3.5) only requires knowledge of the large-scale fading gain, $f_{\text{B},k}$, which is easier to track considering the timescale over which large-scale fading varies [109, 123]. On the other hand, when each relay node can track the phase information of the small-scale fading for both backward and forward channels, it can perform distributed beamforming. This is referred to as coherent AF relaying, and the kth diagonal element of $\boldsymbol{G}$ is given by

$$g_{\text{coh}}^{(k)} = \sqrt{\beta_k p_k} \frac{\alpha_{\text{B},k}^*}{|\alpha_{\text{B},k}|} \frac{\alpha_{\text{F},k}^*}{|\alpha_{\text{F},k}|}. \tag{3.6}$$

The instantaneous SNR at the destination node conditioned on $\boldsymbol{h}_{\text{B}}$ and $\boldsymbol{h}_{\text{F}}$ is given in (2.8). Note that $\boldsymbol{p} = [p_1, p_2, \ldots, p_{N_{\text{r}}}]^T$ denotes the vector of transmitted powers of the relay nodes.

Given instantaneous $\boldsymbol{h}_{\text{B}}$ and $\boldsymbol{h}_{\text{F}}$ at the destination node, we formulate the RPA problem for minimizing the total relay transmission power subject to the constraint on SNR at the destination node. This constraint is equivalent to a certain QoS requirement such as the bit error rate or outage probability, where QoS is satisfied when the SNR at the destination node exceeds a given target value γ_{th}. With this QoS constraint, we can mathematically formulate the optimization problem as

$$\begin{aligned} \mathcal{P}_{\mathsf{SNR}}(\gamma_{\text{th}}) : \min_{\boldsymbol{p}} \quad & \text{tr}\left(\boldsymbol{Q}_{\text{R}}\right) \\ \text{s.t.} \quad & \gamma_{\text{th}} \leq \mathsf{SNR}\left(\boldsymbol{p}\right), \\ & 0 \leq [\boldsymbol{Q}_{\text{R}}]_{k,k} \leq P, \quad \forall k \in \mathcal{N}_{\text{r}}, \end{aligned} \tag{3.7}$$

where $\mathcal{N}_{\text{r}} = \{1, 2, \ldots, N_{\text{r}}\}$ and the last constraint in (3.7) captures the fact that

relay transmission power in practical systems cannot be arbitrarily large.[4] Note that solving the program $\mathcal{P}_{\mathsf{SNR}}(\gamma_{\mathrm{th}})$ in (3.7) requires the instantaneous values of $\boldsymbol{h}_{\mathrm{B}}$ and $\boldsymbol{h}_{\mathrm{F}}$.

Due to the timescale associated with small-scale fading, frequent communication between the relay nodes and the central unit is required to determine new power allocations. This motivates practical algorithms that track only large-scale fading. One possible approach is to adopt the certainty-equivalent (CE) formulation, which was developed in the context of power control for cellular networks [124, 125]. In our context, the CE output SNR for noncoherent AF relaying can be written as

$$\mathsf{SNR}_{\mathrm{noncoh}}^{\mathrm{CE}}(\boldsymbol{p}) = \frac{P_{\mathrm{S}} \sum_{k=1}^{N_{\mathrm{r}}} \beta_k S_{\mathrm{B},k} S_{\mathrm{F},k} p_k}{\sum_{k=1}^{N_{\mathrm{r}}} \beta_k S_{\mathrm{F},k} \sigma_{\mathrm{R},k}^2 p_k + \sigma_{\mathrm{D}}^2}, \tag{3.8}$$

where we have replaced all r.v.'s associated with $\{\alpha_{\mathrm{F},k}\}_{k=1}^{N_{\mathrm{r}}}$ and $\{\alpha_{\mathrm{B},k}\}_{k=1}^{N_{\mathrm{r}}}$ in (2.8) with their expected values. For coherent AF relaying, we approximate the CE output SNR as

$$\mathsf{SNR}_{\mathrm{coh}}^{\mathrm{CE}}(\boldsymbol{p}) \approx \frac{P_{\mathrm{S}} \left(\sum_{k=1}^{N_{\mathrm{r}}} \sqrt{\beta_k S_{\mathrm{B},k} S_{\mathrm{F},k} p_k} \right)^2}{\sum_{k=1}^{N_{\mathrm{r}}} \beta_k S_{\mathrm{F},k} \sigma_{\mathrm{R},k}^2 p_k + \sigma_{\mathrm{D}}^2}. \tag{3.9}$$

Indeed, (3.9) is an upper bound of the actual CE output SNR. We choose to use this expression in (3.9) since it allows efficient formulation for the optimization problem. Substituting (3.8) and (3.9) into (3.7), we can now design power allocation algorithms that track only large-scale fading. However, these slow power allocations may lead to undesirably high outage probability, i.e., $\mathbb{P}\{\mathsf{SNR}(\boldsymbol{p}) < \gamma_{\mathrm{th}}\}$, due to the random fluctuations caused by small-scale fading. This can be alleviated by using a larger SNR target value to allow for fade margins [125–127].[5] In our case, this corresponds to using a target value $\gamma_{\mathrm{th}}^{\mathrm{CE}} = \kappa \gamma_{\mathrm{th}}$ with $\kappa > 1$, where we refer to $\gamma_{\mathrm{th}}^{\mathrm{CE}}$ as the CE SNR target value.[6]

[4] Note that in conventional QoS formulation, the last constraint in (3.7) is omitted, hence it is guaranteed to be feasible in the absence of CSI uncertainties.

[5] Note that this also compensates for the use of approximation in (3.9).

[6] Clearly, κ depends on the types of relaying scheme. For convenience, we use the same notation κ for both noncoherent and coherent AF relay networks.

3.2 Optimal Relay Power Allocation

In this section, we consider the power optimization problems subject to CE SNR constraints for both coherent and noncoherent AF relay networks.

3.2.1 Coherent AF Relaying

Let $\boldsymbol{A} = \mathrm{diag}(a_1, a_2, \ldots, a_{N_\mathrm{r}}) \in \mathbb{R}_+^{N_\mathrm{r}\times N_\mathrm{r}}$ and $\boldsymbol{c} = [c_1, c_2, \ldots, c_{N_\mathrm{r}}]^T \in \mathbb{R}_+^{N_\mathrm{r}}$ where

$$a_k = \frac{\sigma_{\mathrm{R},k}}{\sigma_\mathrm{D}}\sqrt{\beta_k S_{\mathrm{F},k}}, \tag{3.10}$$

$$c_k = \sqrt{\beta_k S_{\mathrm{F},k} S_{\mathrm{B},k}}. \tag{3.11}$$

The CE power optimization problem for the coherent AF relay network can be formulated as

$$\begin{aligned} \mathcal{P}_{\mathrm{coh}}^{\mathrm{CE}}(\gamma_{\mathrm{th}}^{\mathrm{CE}}) : \min_{\boldsymbol{\zeta}} \quad & \textstyle\sum_{k=1}^{N_\mathrm{r}} \zeta_k^2 \\ \text{s.t.} \quad & \gamma_{\mathrm{th}}^{\mathrm{CE}} \le \frac{P_\mathrm{S}}{\sigma_\mathrm{D}^2}\frac{(\boldsymbol{c}^T\boldsymbol{\zeta})^2}{\|\boldsymbol{A}\boldsymbol{\zeta}\|^2+1}, \\ & \boldsymbol{\zeta} \in \mathcal{X}_\zeta, \end{aligned} \tag{3.12}$$

where $\zeta_k = \sqrt{p_k}$ and $\mathcal{X}_\zeta = \{\boldsymbol{\zeta} \in \mathbb{R}^{N_\mathrm{r}} : 0 \le \zeta_k \le \sqrt{P}, \forall k \in \mathcal{N}_\mathrm{r}\}$.[7]

Theorem 3. *The program $\mathcal{P}_{\mathrm{coh}}^{\mathrm{CE}}(\gamma_{\mathrm{th}}^{\mathrm{CE}})$ is a strictly convex optimization program with a compact feasible set. When the problem is feasible, there exists a unique optimal solution $\boldsymbol{\zeta}_{\mathrm{opt}}$. We can equivalently formulate $\mathcal{P}_{\mathrm{coh}}^{\mathrm{CE}}(\gamma_{\mathrm{th}}^{\mathrm{CE}})$ in SOCP form as*[8]

$$\begin{aligned} \mathit{min}_{\boldsymbol{\zeta},t} \quad & t \\ \mathit{s.t.} \quad & \begin{bmatrix} \boldsymbol{c}^T\boldsymbol{\zeta}\sqrt{\frac{P_\mathrm{S}}{\gamma_{\mathrm{th}}^{\mathrm{CE}}\sigma_\mathrm{D}^2}} \\ \begin{pmatrix} 1 \\ \boldsymbol{A}\boldsymbol{\zeta} \end{pmatrix} \end{bmatrix} \succeq_{\mathcal{K}} 0, \quad \begin{bmatrix} \frac{t+1}{2} \\ \begin{pmatrix} \boldsymbol{\zeta} \\ \frac{t-1}{2} \end{pmatrix} \end{bmatrix} \succeq_{\mathcal{K}} 0, \\ & \boldsymbol{\zeta} \in \mathcal{X}_\zeta. \end{aligned} \tag{3.13}$$

[7] Similarly, the above program only requires the perfect knowledge of large-scale fading.
[8] The SOCP form can be solved efficiently [114].

Proof. Clearly, the objective function $\|\boldsymbol{\zeta}\|^2$ is a strictly convex function since the Hessian matrix of the objective function is positive definite [110, 111]. To show that the feasible set is convex, we cast the first constraint in (3.12) in standard form as follows:

$$\boldsymbol{c}^T\boldsymbol{\zeta}\sqrt{\frac{P_{\mathrm{S}}}{\gamma_{\mathrm{th}}^{\mathrm{CE}}\sigma_{\mathrm{D}}^2}} \geq \left\| \begin{pmatrix} 1 \\ \boldsymbol{A}\boldsymbol{\zeta} \end{pmatrix} \right\|, \tag{3.14}$$

which can be rewritten in the form of an SOC constraint as

$$\begin{bmatrix} \boldsymbol{c}^T\boldsymbol{\zeta}\sqrt{\frac{P_{\mathrm{S}}}{\gamma_{\mathrm{th}}^{\mathrm{CE}}\sigma_{\mathrm{D}}^2}} \\ \begin{pmatrix} 1 \\ \boldsymbol{A}\boldsymbol{\zeta} \end{pmatrix} \end{bmatrix} \succeq_{\mathcal{K}} 0. \tag{3.15}$$

Therefore, the feasible set in (3.12) is convex since it is the intersection of a hypercube and an SOC, which are both convex sets [110, 111]. As a result, $\mathcal{P}_{\mathrm{coh}}^{\mathrm{CE}}(\gamma_{\mathrm{th}}^{\mathrm{CE}})$ is a strictly convex optimization program. Moreover, the feasible set is bounded since it is contained in a hypercube. It is also closed since it consists of the intersection of an SOC and a hypercube, which are both closed sets [110, 111]. Therefore, it follows that the feasible set is compact. By the Weierstrass theorem, it follows that there exists at least one optimal solution for program $\mathcal{P}_{\mathrm{coh}}^{\mathrm{CE}}(\gamma_{\mathrm{th}}^{\mathrm{CE}})$ [110, 111]. Furthermore, given the strict convexity of $\|\boldsymbol{\zeta}\|^2$, there is a unique optimal solution $\boldsymbol{\zeta}_{\mathrm{opt}}$.

To cast $\mathcal{P}_{\mathrm{coh}}^{\mathrm{CE}}(\gamma_{\mathrm{th}}^{\mathrm{CE}})$ into an SOCP, we use a slack variable $t \in \mathbb{R}_+$. The program can be equivalently written as[9]

$$\begin{aligned} \min\nolimits_{\boldsymbol{\zeta},t} \quad & t \\ \text{s.t.} \quad & \begin{bmatrix} \boldsymbol{c}^T\boldsymbol{\zeta}\sqrt{\frac{P_{\mathrm{S}}}{\gamma_{\mathrm{th}}^{\mathrm{CE}}\sigma_{\mathrm{D}}^2}} \\ \begin{pmatrix} 1 \\ \boldsymbol{A}\boldsymbol{\zeta} \end{pmatrix} \end{bmatrix} \succeq_{\mathcal{K}} 0, \\ & \textstyle\sum_{k=1}^{N_{\mathrm{r}}} \zeta_k^2 \leq t, \\ & \boldsymbol{\zeta} \in \mathcal{X}_{\zeta}. \end{aligned} \tag{3.16}$$

[9]Note that there is no loss of optimality by introducing such a slack variable [110, 111].

From [114], we can easily express the second constraint in (3.16) as

$$\begin{bmatrix} \frac{t+1}{2} \\ \begin{pmatrix} \boldsymbol{\zeta} \\ \frac{t-1}{2} \end{pmatrix} \end{bmatrix} \succeq_{\mathcal{K}} 0. \tag{3.17}$$

Substituting (3.17) into (3.16), we obtain the program (3.13) in SOCP form. □

Remark 7. *Since we can represent the program (3.12) in SOCP from Theorem 3, we can numerically solve the problem and verify its feasibility using standard optimization packages like SeDuMi [120]. Nevertheless, it is still important to devise analytical methodology to verify the consistency of the problem.*

Proposition 3 (Feasibility)**.** *A necessary and sufficient condition for* $\mathcal{P}_{\mathrm{coh}}^{\mathrm{CE}}(\gamma_{\mathrm{th}}^{\mathrm{CE}})$ *to be feasible is given by*

$$\frac{\gamma_{\mathrm{th}}^{\mathrm{CE}}\sigma_{\mathrm{D}}^2}{P_{\mathrm{S}}} \leq \Upsilon_{\mathrm{opt}}, \tag{3.18}$$

where Υ_{opt} *is the optimal objective value of the following maximization problem :*

$$\begin{array}{ll} \max_{\boldsymbol{\zeta}} & \frac{(\boldsymbol{c}^T\boldsymbol{\zeta})^2}{\|\boldsymbol{A}\boldsymbol{\zeta}\|^2+1} \\ s.t. & \boldsymbol{\zeta} \in \mathcal{X}_{\zeta}. \end{array} \tag{3.19}$$

Furthermore, we can derive a necessary condition given by

$$\gamma_{\mathrm{th}}^{\mathrm{CE}} < \frac{P_{\mathrm{S}}\|\boldsymbol{c}\|^2}{\sigma_{\mathrm{D}}^2\tau_{\min}(\boldsymbol{A}^T\boldsymbol{A})}, \tag{3.20}$$

where $\tau_{\min}(\boldsymbol{A}^T\boldsymbol{A})$ *denotes the smallest eigenvalue of* $\boldsymbol{A}^T\boldsymbol{A}$*, and* $\tau_{\min}(\boldsymbol{A}^T\boldsymbol{A}) = \min_{k\in\mathcal{N}_{\mathrm{r}}} a_k^2$.

Proof. The necessary and sufficient condition for $\mathcal{P}_{\mathrm{coh}}^{\mathrm{CE}}(\gamma_{\mathrm{th}}^{\mathrm{CE}})$ to be feasible can be immediately obtained by maximizing the right-hand side of the CE SNR constraint in (3.12) with respect to all possible $\boldsymbol{\zeta}$. This maximization can be formulated as an optimization problem in Chapter 2.2, which is shown to be quasiconvex with a

non-empty feasible set since $\eta_{\mathrm{P}} > 0$. To derive (3.20), we first note that

$$\frac{\gamma_{\mathrm{th}}^{\mathrm{CE}}\sigma_{\mathrm{D}}^2}{P_{\mathrm{S}}} < \max_{\boldsymbol{\zeta}\in\mathcal{X}_\zeta}\left(\frac{(\boldsymbol{c}^T\boldsymbol{\zeta})^2}{\|\boldsymbol{A}\boldsymbol{\zeta}\|^2}\right), \tag{3.21}$$

since the right-hand side of (3.21) is strictly greater than the right-hand side of (3.18). The right-hand side of (3.21) can be further bounded by

$$\max_{\boldsymbol{\zeta}\in\mathcal{X}_\zeta}\left(\frac{(\boldsymbol{c}^T\boldsymbol{\zeta})^2}{\|\boldsymbol{A}\boldsymbol{\zeta}\|^2}\right) \leq \frac{\|\boldsymbol{c}\|^2}{\min_{\boldsymbol{\zeta}\in\mathcal{X}_\zeta}\frac{\|\boldsymbol{A}\boldsymbol{\zeta}\|^2}{\|\boldsymbol{\zeta}\|^2}}. \tag{3.22}$$

where we have applied the Cauchy-Schwartz inequality to the vectors $\boldsymbol{c}$ and $\boldsymbol{\zeta}$. From (3.22), we apply the Rayleigh-Ritz theorem to obtain the desired result [128, p. 176]. □

Remark 8. *Proposition 3 provides us with useful conditions not only for verifying the feasibility of $\mathcal{P}_{\mathrm{coh}}^{\mathrm{CE}}(\gamma_{\mathrm{th}}^{\mathrm{CE}})$, but also for designing system parameters such as P_{S}, $\gamma_{\mathrm{th}}^{\mathrm{CE}}$, and K. For example, we could use the simple condition in (3.20) to check if $\mathcal{P}_{\mathrm{coh}}^{\mathrm{CE}}(\gamma_{\mathrm{th}}^{\mathrm{CE}})$ is infeasible. We check the condition in (3.18) only when (3.20) is satisfied. When (3.18) or (3.20) fails, we adjust the system parameters to ensure that both (3.18) and (3.20) are satisfied. This process effectively converts an infeasible program into a feasible one.*

Next, we formulate the dual problem of (3.12) and derive its Karush-Kuhn-Tucker (KKT) conditions in the following theorem.

Theorem 4 (Duality)**.** *The dual problem of $\mathcal{P}_{\mathrm{coh}}^{\mathrm{CE}}(\gamma_{\mathrm{th}}^{\mathrm{CE}})$ is given by*

$$\begin{aligned} \mathcal{DP}_{\mathrm{coh}}^{\mathrm{CE}}(\gamma_{\mathrm{th}}^{\mathrm{CE}}): \; max_{\mu,\boldsymbol{\lambda},\boldsymbol{\nu}} \quad & g(\mu,\boldsymbol{\lambda},\boldsymbol{\nu}) \\ s.t. \quad & \boldsymbol{I}_{N_{\mathrm{r}}} + \mu\boldsymbol{Q} \succ 0, \end{aligned} \tag{3.23}$$

with

$$\begin{aligned} g(\mu,\boldsymbol{\lambda},\boldsymbol{\nu}) &= \frac{\mu\gamma_{\mathrm{th}}^{\mathrm{CE}}\sigma_{\mathrm{D}}^2}{P_{\mathrm{S}}} - \mathrm{tr}\,(\boldsymbol{\Lambda}) - \frac{1}{4}(\boldsymbol{\lambda}-\boldsymbol{\nu})^T(\boldsymbol{I}_{N_{\mathrm{r}}}+\mu\boldsymbol{Q})^{-1}(\boldsymbol{\lambda}-\boldsymbol{\nu}) \\ \boldsymbol{Q} &= \frac{\gamma_{\mathrm{th}}^{\mathrm{CE}}\sigma_{\mathrm{D}}^2}{P_{\mathrm{S}}}\boldsymbol{A}^T\boldsymbol{A} - \boldsymbol{c}\boldsymbol{c}^T, \end{aligned}$$

$$\boldsymbol{\Lambda} = \sqrt{P}\mathrm{diag}(\lambda_1, \lambda_2, \ldots, \lambda_{N_\mathrm{r}}),$$

where $\mu \in \mathbb{R}_+$, $\boldsymbol{\lambda} \in \mathbb{R}_+^{N_\mathrm{r}}$ *and* $\boldsymbol{\nu} \in \mathbb{R}_+^{N_\mathrm{r}}$ *are the dual feasible variables. If the primal problem is strictly feasible, strong duality holds and there exists* $\mu > 0$ *such that*

$$\mu > -\frac{1}{\tau_{\min}(\boldsymbol{Q})}. \tag{3.24}$$

Moreover, the optimal primal solution $\boldsymbol{\zeta}_{\mathrm{opt}}$ *is of the form*

$$\boldsymbol{\zeta}_{\mathrm{opt}} = -\frac{1}{2}\left(\boldsymbol{I}_{N_\mathrm{r}} + \mu_{\mathrm{opt}}\boldsymbol{Q}\right)^{-1}(\boldsymbol{\lambda}_{\mathrm{opt}} - \boldsymbol{\nu}_{\mathrm{opt}}), \tag{3.25}$$

where $(\mu_{\mathrm{opt}}, \boldsymbol{\lambda}_{\mathrm{opt}}, \boldsymbol{\nu}_{\mathrm{opt}})$ *is the optimal dual solution and* μ_{opt} *satisfies the condition in (3.24).*

Proof. First, we set up the Lagrangian function $L : \mathbb{R}^{N_\mathrm{r}} \times \mathbb{R} \times \mathbb{R}^{N_\mathrm{r}} \times \mathbb{R}^{N_\mathrm{r}}$ associated with the primal problem (3.12) as

$$L(\boldsymbol{\zeta}, \mu, \boldsymbol{\lambda}, \boldsymbol{\nu}) = \frac{\mu\gamma_{\mathrm{th}}^{\mathrm{CE}}\sigma_{\mathrm{D}}^2}{P_{\mathrm{S}}} - \mathrm{tr}\left(\boldsymbol{\Lambda}\right) + \boldsymbol{\zeta}^T(\boldsymbol{I}_{N_\mathrm{r}} + \mu\boldsymbol{Q})\,\boldsymbol{\zeta} + \boldsymbol{\zeta}^T(\boldsymbol{\lambda} - \boldsymbol{\nu}), \tag{3.26}$$

where μ, $\boldsymbol{\lambda}$, and $\boldsymbol{\nu}$ are the Lagrange multipliers corresponding to the CE SNR constraint and power constraints in (3.12), respectively. The dual problem $\mathcal{DP}_{\mathrm{coh}}^{\mathrm{CE}}(\gamma_{\mathrm{th}}^{\mathrm{CE}})$ is given by

$$\begin{array}{ll} \max_{\mu,\boldsymbol{\lambda},\boldsymbol{\nu}} & g(\mu, \boldsymbol{\lambda}, \boldsymbol{\nu}) \\ \text{s.t.} & \boldsymbol{I}_{N_\mathrm{r}} + \mu\boldsymbol{Q} \succ 0, \end{array} \tag{3.27}$$

where the dual feasible variables are $\mu \in \mathbb{R}_+$, $\boldsymbol{\lambda} \in \mathbb{R}_+^{N_\mathrm{r}}$, and $\boldsymbol{\nu} \in \mathbb{R}_+^{N_\mathrm{r}}$. Under some constraint qualifications, strong duality holds.[10] In this case, the KKT optimality conditions are both necessary and sufficient, and the optimal solutions of the primal and dual problems, $\boldsymbol{\zeta}_{\mathrm{opt}} \in \mathbb{R}_+^{N_\mathrm{r}}$ and $(\mu_{\mathrm{opt}}, \boldsymbol{\lambda}_{\mathrm{opt}}, \boldsymbol{\nu}_{\mathrm{opt}}) \in \mathbb{R}_+ \times \mathbb{R}_+^{N_\mathrm{r}} \times \mathbb{R}_+^{N_\mathrm{r}}$, must satisfy the following three conditions.

[10] One simple version of the constraint qualifications is Slater's condition [111].

Feasibility conditions :

$$\begin{aligned}\frac{\gamma_{\mathrm{th}}^{\mathrm{CE}}\sigma_{\mathrm{D}}^2}{P_{\mathrm{S}}}+\boldsymbol{\zeta}_{\mathrm{opt}}^T\boldsymbol{Q}\boldsymbol{\zeta}_{\mathrm{opt}} &\leq 0,\\ \zeta_{k,\mathrm{opt}}-\sqrt{P} &\leq 0, \quad k\in\mathcal{N}_{\mathrm{r}}\\ -\zeta_{k,\mathrm{opt}} &\leq 0, \quad k\in\mathcal{N}_{\mathrm{r}},\end{aligned}$$

Complementary slackness conditions :

$$\begin{aligned}\mu_{\mathrm{opt}}\left(\frac{\gamma_{\mathrm{th}}^{\mathrm{CE}}\sigma_{\mathrm{D}}^2}{P_{\mathrm{S}}}+\boldsymbol{\zeta}_{\mathrm{opt}}^T\boldsymbol{Q}\boldsymbol{\zeta}_{\mathrm{opt}}\right) &= 0,\\ \lambda_{k,\mathrm{opt}}\left(\zeta_{k,\mathrm{opt}}-\sqrt{P}\right) &= 0, \quad k\in\mathcal{N}_{\mathrm{r}}\\ -\nu_{k,\mathrm{opt}}\zeta_{k,\mathrm{opt}} &= 0, \quad k\in\mathcal{N}_{\mathrm{r}},\end{aligned}$$

Stationarity condition :

$$\nabla_{\boldsymbol{\zeta}}L(\boldsymbol{\zeta}_{\mathrm{opt}},\mu_{\mathrm{opt}},\boldsymbol{\lambda}_{\mathrm{opt}},\boldsymbol{\nu}_{\mathrm{opt}})=0.$$

Using (3.26), we can evaluate the stationarity condition to obtain

$$\boldsymbol{\zeta}_{\mathrm{opt}}=-\frac{1}{2}\left(\boldsymbol{I}_{N_{\mathrm{r}}}+\mu_{\mathrm{opt}}\boldsymbol{Q}\right)^{-1}\left(\boldsymbol{\lambda}_{\mathrm{opt}}-\boldsymbol{\nu}_{\mathrm{opt}}\right), \tag{3.28}$$

where (3.28) has a unique $\boldsymbol{\zeta}_{\mathrm{opt}}$ since the matrix $(\boldsymbol{I}_{N_{\mathrm{r}}}+\mu_{\mathrm{opt}}\boldsymbol{Q})$ is positive definite. Furthermore, using the complementary slackness condition, we have $\mu_{\mathrm{opt}}>0$ since $\boldsymbol{\zeta}_{\mathrm{opt}}$ must satisfy the CE SNR constraint with equality when the primal problem is feasible [129]. Combining the above results, we obtain

$$\mu_{\mathrm{opt}}>-\frac{1}{\tau_{\min}\left(\boldsymbol{Q}\right)}, \tag{3.29}$$

where we have used the fact that the eigenvalues of a positive definite matrix are strictly positive and $\tau_{\min}\left(\boldsymbol{I}_{N_{\mathrm{r}}}+\mu\boldsymbol{Q}\right)=1+\mu\tau_{\min}\left(\boldsymbol{Q}\right)$. □

3.2.2 Noncoherent AF Relaying

Let $\boldsymbol{d} = [d_1, d_2, \ldots, d_{N_\mathrm{r}}]^T \in \mathbb{R}_+^{N_\mathrm{r}}$ and $\boldsymbol{e} = [e_1, e_2, \ldots, e_{N_\mathrm{r}}]^T \in \mathbb{R}_+^{N_\mathrm{r}}$ where

$$d_k = \frac{\sigma_{\mathrm{R},k}^2}{\sigma_\mathrm{D}^2}\beta_k S_{\mathrm{F},k}, \tag{3.30}$$

$$e_k = \beta_k S_{\mathrm{F},k} S_{\mathrm{B},k}. \tag{3.31}$$

The CE power optimization problem for the noncoherent AF relay network can be formulated as

$$\begin{aligned} \mathcal{P}_{\mathrm{noncoh}}^{\mathrm{CE}}(\gamma_{\mathrm{th}}^{\mathrm{CE}}) : \min_{\boldsymbol{p}} \quad & \textstyle\sum_{k=1}^{N_\mathrm{r}} p_k \\ \text{s.t.} \quad & \gamma_{\mathrm{th}}^{\mathrm{CE}} \leq \frac{P_\mathrm{S}}{\sigma_\mathrm{D}^2}\frac{\boldsymbol{e}^T\boldsymbol{p}}{\boldsymbol{d}^T\boldsymbol{p}+1}, \\ & \boldsymbol{p} \in \mathcal{X}_p, \end{aligned} \tag{3.32}$$

where $\mathcal{X}_p = \{\boldsymbol{p} \in \mathbb{R}^{N_\mathrm{r}} : 0 \leq p_k \leq P, \forall k \in \mathcal{N}_\mathrm{r}\}$. Note that the above program only requires perfect knowledge of large-scale fading.

Theorem 5. *The program $\mathcal{P}_{\mathrm{noncoh}}^{\mathrm{CE}}(\gamma_{\mathrm{th}}^{\mathrm{CE}})$ is a linear program given by*

$$\begin{aligned} \mathit{min}_{\boldsymbol{p}} \quad & \mathbf{1}^T\boldsymbol{p} \\ \mathit{s.t.} \quad & \boldsymbol{m} \geq \boldsymbol{B}\boldsymbol{p}, \end{aligned} \tag{3.33}$$

where $\boldsymbol{B} \in \mathbb{R}^{(2N_\mathrm{r}+1)\times N_\mathrm{r}}$ and $\boldsymbol{m} \in \mathbb{R}^{2N_\mathrm{r}+1}$ are given by

$$\boldsymbol{B} = \begin{bmatrix} \boldsymbol{d}^T - \frac{P_\mathrm{S}}{\gamma_{\mathrm{th}}^{\mathrm{CE}}\sigma_\mathrm{D}^2}\boldsymbol{e}^T \\ \boldsymbol{I}_{N_\mathrm{r}} \\ -\boldsymbol{I}_{N_\mathrm{r}} \end{bmatrix}, \qquad \boldsymbol{m} = \begin{bmatrix} -1 \\ P\mathbf{1} \\ \mathbf{0} \end{bmatrix}. \tag{3.34}$$

When the problem is feasible, there exists a set of optimal solutions $\{\boldsymbol{p}_{\mathrm{opt}}\}$ when $-\mathbf{1} \| \boldsymbol{b}_1$, and a unique optimal solution $\boldsymbol{p}_{\mathrm{opt}}$ when $-\mathbf{1} \nparallel \boldsymbol{b}_1$, such that $\boldsymbol{b}_1 = \boldsymbol{d} - \frac{P_\mathrm{S}}{\gamma_{\mathrm{th}}^{\mathrm{CE}}\sigma_\mathrm{D}^2}\boldsymbol{e}$.

Proof. To show that $\mathcal{P}_{\mathrm{noncoh}}^{\mathrm{CE}}(\gamma_{\mathrm{th}}^{\mathrm{CE}})$ is an LP, we simply express the CE SNR constraint and the power constraints in the form of $\boldsymbol{b}_k^T\boldsymbol{p} \leq m_k$, where $\boldsymbol{b}_k^T$ is the kth row vector of the matrix $\boldsymbol{B}$ and m_k is the kth element of the vector $\boldsymbol{m}$ defined in (3.34). Since the

objective function is linear in $\boldsymbol{p}$ and the feasible set is a polyhedron, it follows that we have an LP, as shown in (3.33). When the problem is feasible, the polyhedron is non-empty and the optimal objective value is finite. Furthermore, the polyhedron is bounded since it is contained in a hypercube. From [130, Corollary 2.2], it follows that there is at least one extreme point in the polyhedron. Therefore, there exists at least one optimal solution for program $\mathcal{P}^{\mathrm{CE}}_{\mathrm{noncoh}}(\gamma^{\mathrm{CE}}_{\mathrm{th}})$ [130, Theorem 2.8]. Note that the uniqueness of the optimal solution depends on the direction of $\boldsymbol{b}_1$. Since the objective function is to minimize $\mathbf{1}^T\boldsymbol{p}$, the optimal solution is to travel as far as possible in the $-\mathbf{1}$ direction. However, when $-\mathbf{1}\|\boldsymbol{b}_1$, the set of optimal solutions lies along the hyperplane $\boldsymbol{b}_1^T\boldsymbol{p} = m_1$ as this is the boundary of the feasible set. On the other hand, when $-\mathbf{1} \nparallel \boldsymbol{b}_1$, there is a unique optimal solution that can be found by moving in the $-\mathbf{1}$ direction. □

Remark 9. *To verify the feasibility of $\mathcal{P}^{\mathrm{CE}}_{\mathrm{noncoh}}(\gamma^{\mathrm{CE}}_{\mathrm{th}})$, we consider the following simple LP :*

$$\begin{aligned} &min_{\boldsymbol{p},t} && t \\ &s.t. && \boldsymbol{m} + t\mathbf{1} \geq \boldsymbol{B}\boldsymbol{p}, \end{aligned} \tag{3.35}$$

where $t \in \mathbb{R}$. It is clear that the program $\mathcal{P}^{\mathrm{CE}}_{\mathrm{noncoh}}(\gamma^{\mathrm{CE}}_{\mathrm{th}})$ is feasible when $t_{\mathrm{opt}} \leq 0$, where t_{opt} is the optimal solution to the LP in (3.35). Since LP can be solved very easily with simplex algorithm, we can also use (3.35) to determine $\gamma^{\mathrm{CE}}_{\mathrm{th}}$ that corresponds to $t_{\mathrm{opt}} \leq 0$. Such $\gamma^{\mathrm{CE}}_{\mathrm{th}}$ will result in feasible program $\mathcal{P}^{\mathrm{CE}}_{\mathrm{noncoh}}(\gamma^{\mathrm{CE}}_{\mathrm{th}})$.

As for the case of the coherent AF relay network, we formulate the dual problem of (3.32) in the following theorem.

Theorem 6 (Duality)**.** *The dual problem of $\mathcal{P}^{\mathrm{CE}}_{\mathrm{noncoh}}(\gamma^{\mathrm{CE}}_{\mathrm{th}})$ is given by*

$$\begin{aligned} \mathcal{DP}^{\mathrm{CE}}_{\mathrm{noncoh}}(\gamma^{\mathrm{CE}}_{\mathrm{th}}) : max_{\boldsymbol{\nu}} \quad & -\boldsymbol{m}^T\boldsymbol{\nu} \\ s.t. \quad & \boldsymbol{B}^T\boldsymbol{\nu} + \mathbf{1} = \mathbf{0}, \end{aligned} \tag{3.36}$$

where $\boldsymbol{\nu} \in \mathbb{R}_+^{2N_{\mathrm{r}}+1}$ is the dual feasible variable. Since strong duality holds when either the primal or dual problems is feasible, there exists an optimal $\boldsymbol{\nu}_{\mathrm{opt}} \in \mathbb{R}_+^{2N_{\mathrm{r}}+1}$ such

that

$$\begin{aligned} \mathbf{1}^T \boldsymbol{p}_{\text{opt}} + \boldsymbol{m}^T \boldsymbol{\nu}_{\text{opt}} &= 0 \\ \boldsymbol{B}^T \boldsymbol{\nu}_{\text{opt}} + \mathbf{1} &= \mathbf{0}. \end{aligned} \tag{3.37}$$

Proof. First, we set up the Lagrangian function $L : \mathbb{R}^{N_{\text{r}}} \times \mathbb{R}^{2N_{\text{r}}+1}$ associated with the primal problem (3.36) as

$$L(\boldsymbol{p}, \boldsymbol{\nu}) = -\boldsymbol{m}^T \boldsymbol{\nu} + \left(\boldsymbol{B}^T \boldsymbol{\nu} + \mathbf{1}\right)^T \boldsymbol{p}, \tag{3.38}$$

where $\boldsymbol{\nu}$ is the Lagrange multipliers corresponding to the linear constraints in (3.36). The dual problem $\mathcal{DP}^{\text{CE}}_{\text{noncoh}}(\gamma^{\text{CE}}_{\text{th}})$ is given by

$$\begin{aligned} \max\nolimits_{\boldsymbol{\nu}} \quad & -\boldsymbol{m}^T \boldsymbol{\nu} \\ \text{s.t.} \quad & \boldsymbol{B}^T \boldsymbol{\nu} + \mathbf{1} = \mathbf{0}, \\ & \boldsymbol{\nu} \succeq \mathbf{0}. \end{aligned} \tag{3.39}$$

For LP, strong duality holds when either one of the primal or dual problems is feasible [111, 130]. Thus, $(\boldsymbol{p}_{\text{opt}}, \boldsymbol{\nu}_{\text{opt}})$ are optimal if and only if they satisfy the following three conditions.

Feasibility condition of the primal problem :

$$\boldsymbol{B}\boldsymbol{p}_{\text{opt}} \leq \boldsymbol{m},$$

Feasibility conditions of the dual problem :

$$\begin{aligned} \boldsymbol{B}^T \boldsymbol{\nu}_{\text{opt}} + \mathbf{1} &= \mathbf{0}, \\ \nu_{k,\text{opt}} &\geq 0, \quad k \in \mathcal{N}_{\text{r}} \end{aligned}$$

Zero duality gap condition :

$$\mathbf{1}^T \boldsymbol{p}_{\text{opt}} + \boldsymbol{m}^T \boldsymbol{\nu}_{\text{opt}} = 0.$$

□

3.3 Robust Relay Power Allocation

To account for CSI uncertainties, we adopt the robust optimization methodology introduced in Chapter 2. As in [7, 8], we consider an ellipsoidal uncertainty set for simplicity.

3.3.1 Coherent AF Relaying

In the following, we formulate the robust counterpart of $\mathcal{P}_{\text{coh}}^{\text{CE}}(\gamma_{\text{th}}^{\text{CE}})$ by incorporating uncertainties in $\boldsymbol{A}$ and $\boldsymbol{c}$ in the following theorem. Since $(\boldsymbol{A}, \boldsymbol{c})$ appears only in the first constraint of (3.12), we need to simply focus on this constraint and build its robust counterpart given by

$$\boldsymbol{c}^T\boldsymbol{\zeta} \geq \sqrt{\frac{\gamma_{\text{th}}^{\text{CE}}\sigma_{\text{D}}^2}{P_{\text{S}}}\left(1 + \|\boldsymbol{A}\boldsymbol{\zeta}\|^2\right)}, \qquad \forall (\boldsymbol{A}, \boldsymbol{c}) \in \mathcal{U}. \tag{3.40}$$

In the following, we adopt the conservative approach which assumes that $\mathcal{U}$ affecting (3.40) is sidewise as described in Chapter 2.3.

Theorem 7. *Let $\mathcal{U}_{\text{R}}$ and $\mathcal{U}_{\text{L}}$ be sidewise independent ellipsoidal uncertainty sets given by*

$$\mathcal{U}_{\text{R}} = \left\{ \boldsymbol{A} = \boldsymbol{A}_0 + \sum_{j \in \mathcal{N}_A} u_j \boldsymbol{A}_j : \|\boldsymbol{u}\| \leq \rho_1 \right\} \tag{3.41}$$

$$\mathcal{U}_{\text{L}} = \left\{ \boldsymbol{c} = \boldsymbol{c}_0 + \sum_{j \in \mathcal{N}_c} v_j \boldsymbol{c}_j : \|\boldsymbol{v}\| \leq \rho_2 \right\}, \tag{3.42}$$

where $\mathcal{N}_A = \{1, 2, \ldots, N_A\}$, $\mathcal{N}_c = \{1, 2, \ldots, N_c\}$, and N_A and N_c are the dimensions of $\boldsymbol{u}$ and $\boldsymbol{v}$, respectively. The approximate robust counterpart of $\mathcal{P}_{\text{coh}}^{\text{CE}}(\gamma_{\text{th}}^{\text{CE}})$ with

uncertainty sets $\mathcal{U}_{\rm R}$ *and* $\mathcal{U}_{\rm L}$ *can be written in SDP form:*

$$\begin{aligned} \mathcal{RP}^{\rm CE}_{\rm coh}(\gamma^{\rm CE}_{\rm th}): \; min_{\boldsymbol{\zeta},t,\tau,\mu} \quad & t \\ s.t. \quad & (\boldsymbol{\zeta},t,\tau,\mu) \in \mathcal{S}_{\rm coh}(\gamma^{\rm CE}_{\rm th}), \end{aligned} \tag{3.43}$$

where $(\boldsymbol{\zeta},t,\tau,\mu) \in \mathbb{R}^{N_{\rm r}}_{+} \times \mathbb{R}_{+} \times \mathbb{R}_{+} \times \mathbb{R}_{+}$ *and the feasible set* $\mathcal{S}_{\rm coh}(\gamma^{\rm CE}_{\rm th})$ *is given by*

$$\begin{aligned} \mathcal{S}_{\rm coh}(\gamma^{\rm CE}_{\rm th}) = \Bigg\{ \boldsymbol{\zeta} \in \mathbb{R}^{N_{\rm r}}_{+}: & \begin{bmatrix} \mu \boldsymbol{I}_{N_A} & \boldsymbol{0}_{N_A} & \breve{\boldsymbol{A}}^T \\ \boldsymbol{0}^T_{N_A} & \tau\sqrt{\frac{P_{\rm S}}{\gamma^{\rm CE}_{\rm th}\sigma^2_{\rm D}}} - 1 - \mu\rho_1^2 & \boldsymbol{\zeta}^T\boldsymbol{A}_0^T \\ \breve{\boldsymbol{A}} & \boldsymbol{A}_0\boldsymbol{\zeta} & \left(\tau\sqrt{\frac{P_{\rm S}}{\gamma^{\rm CE}_{\rm th}\sigma^2_{\rm D}}} - 1\right)\boldsymbol{I}_{N_{\rm r}} \end{bmatrix} \succeq 0, \\ & \begin{bmatrix} \frac{\boldsymbol{c}_0^T\boldsymbol{\zeta}-\tau}{\rho_2}\boldsymbol{I}_{N_c} & \breve{\boldsymbol{c}} \\ \breve{\boldsymbol{c}}^T & \frac{\boldsymbol{c}_0^T\boldsymbol{\zeta}-\tau}{\rho_2} \end{bmatrix} \succeq 0, \\ & \begin{bmatrix} \left(\frac{t+1}{2}\right)\boldsymbol{I}_{N_{\rm r}+1} & \begin{pmatrix} \boldsymbol{\zeta} \\ \frac{t-1}{2} \end{pmatrix} \\ \left(\boldsymbol{\zeta}^T \;\; \frac{t-1}{2}\right) & \frac{t+1}{2} \end{bmatrix} \succeq 0, \\ & \begin{bmatrix} \left(\frac{P+1}{2}\right)\boldsymbol{I}_2 & \begin{pmatrix} \zeta_k \\ \frac{P-1}{2} \end{pmatrix} \\ \left(\zeta_k \;\; \frac{P-1}{2}\right) & \frac{P+1}{2} \end{bmatrix} \succeq 0, \\ & \begin{bmatrix} \tau & \sqrt{\frac{\gamma^{\rm CE}_{\rm th}\sigma^2_{\rm D}}{P_{\rm S}}} \\ \sqrt{\frac{\gamma^{\rm CE}_{\rm th}\sigma^2_{\rm D}}{P_{\rm S}}} & \tau \end{bmatrix} \succeq 0, \forall k \in \mathcal{N}_{\rm r} \Bigg\}, \end{aligned} \tag{3.44}$$

where $\breve{\boldsymbol{A}} = [\boldsymbol{A}_1\boldsymbol{\zeta}, \boldsymbol{A}_2\boldsymbol{\zeta}, \ldots, \boldsymbol{A}_{N_A}\boldsymbol{\zeta}]$*, and* $\breve{\boldsymbol{c}} = \left[\boldsymbol{c}_1^T\boldsymbol{\zeta}, \boldsymbol{c}_2^T\boldsymbol{\zeta}, \ldots, \boldsymbol{c}_{N_c}^T\boldsymbol{\zeta}\right]^T$.

Proof. Due to the sidewise independence assumption, $\boldsymbol{\zeta}$ is robust feasible if there exists $\tau \in \mathbb{R}_{+}$ such that [118, 119]

$$\sqrt{\frac{\gamma^{\rm CE}_{\rm th}\sigma^2_{\rm D}}{P_{\rm S}}\left(1 + \|\boldsymbol{A}\boldsymbol{\zeta}\|^2\right)} \leq \tau, \qquad \forall \boldsymbol{A} \in \mathcal{U}_{\rm R} \tag{3.45}$$

$$\tau \leq \boldsymbol{c}^T\boldsymbol{\zeta}, \qquad \forall \boldsymbol{c} \in \mathcal{U}_{\rm L}. \tag{3.46}$$

First, we consider (3.45) by rewriting it as follows:

$$\left\| \begin{pmatrix} 1 \\ \boldsymbol{A}\boldsymbol{\zeta} \end{pmatrix} \right\| \leq \tau \sqrt{\frac{P_{\mathrm{S}}}{\gamma_{\mathrm{th}}^{\mathrm{CE}} \sigma_{\mathrm{D}}^2}}, \qquad \forall \boldsymbol{A} \in \mathcal{U}_{\mathrm{R}}. \tag{3.47}$$

We now replace (3.47) by[11]

$$\begin{aligned} 0 &\leq \lambda, \\ \left\| \boldsymbol{A}_0 \boldsymbol{\zeta} + \breve{\boldsymbol{A}} \boldsymbol{u} \right\| &\leq \lambda, \quad \forall \boldsymbol{u} \in \{\boldsymbol{u} : \|\boldsymbol{u}\| \leq \rho_1\}, \end{aligned} \tag{3.48}$$

where $\lambda = \tau \sqrt{P_{\mathrm{S}}/\gamma_{\mathrm{th}}^{\mathrm{CE}} \sigma_{\mathrm{D}}^2} - 1$ and we have substituted $\boldsymbol{A}$ defined by the uncertainty set $\mathcal{U}_{\mathrm{R}}$ in (3.41). Now, by expanding (3.48) in terms of a quadratic form of $\boldsymbol{u}$, we have

$$\begin{aligned} 0 &\leq \lambda, \\ 0 &\leq q_0(\boldsymbol{u}), \quad \forall \boldsymbol{u} \in \{\boldsymbol{u} : 0 \leq q_1(\boldsymbol{u})\}, \end{aligned} \tag{3.49}$$

where

$$\begin{aligned} q_0(\boldsymbol{u}) &= -\boldsymbol{u}^T \breve{\boldsymbol{A}}^T \breve{\boldsymbol{A}} \boldsymbol{u} - 2 \left(\breve{\boldsymbol{A}}^T \boldsymbol{A}_0 \boldsymbol{\zeta} \right)^T \boldsymbol{u} - \boldsymbol{\zeta}^T \boldsymbol{A}_0^T \boldsymbol{A}_0 \boldsymbol{\zeta} + \lambda^2 \\ q_1(\boldsymbol{u}) &= \rho_1^2 - \boldsymbol{u}^T \boldsymbol{u}. \end{aligned} \tag{3.50}$$

From Lemma 4, it follows that (3.49) is satisfied if and only if there exists $\alpha \in \mathbb{R}_+$ such that

$$\begin{bmatrix} -\breve{\boldsymbol{A}}^T \breve{\boldsymbol{A}} & -\breve{\boldsymbol{A}}^T \boldsymbol{A}_0 \boldsymbol{\zeta} \\ \left(-\breve{\boldsymbol{A}}^T \boldsymbol{A}_0 \boldsymbol{\zeta} \right)^T & \lambda^2 - \boldsymbol{\zeta}^T \boldsymbol{A}_0^T \boldsymbol{A}_0 \boldsymbol{\zeta} \end{bmatrix} - \alpha \begin{bmatrix} -\boldsymbol{I}_{N_A} & \boldsymbol{0}_{N_A} \\ \boldsymbol{0}_{N_A}^T & \rho_1^2 \end{bmatrix} \succeq 0. \tag{3.51}$$

To convert the above quadratic matrix inequality into an LMI, we first let $\alpha = \lambda \mu$

[11] It follows from the triangle inequality that if (3.48) is satisfied, then (3.47) is always satisfied. Note that with the use of constraint (3.48), instead of (3.47), we have converted $\mathcal{RP}_{\mathrm{coh}}^{\mathrm{CE}}(\gamma_{\mathrm{th}}^{\mathrm{CE}})$ into an SDP.

for some $\mu \in \mathbb{R}_+$. Rearranging (3.51), we have[12]

$$\Delta_{\boldsymbol{E}} \triangleq \lambda \begin{bmatrix} \mu \boldsymbol{I}_{N_A} & \boldsymbol{0}_{N_A} \\ \boldsymbol{0}_{N_A}^T & \lambda - \mu\rho_1^2 \end{bmatrix} - \begin{bmatrix} \breve{\boldsymbol{A}}^T \\ \boldsymbol{\zeta}^T \boldsymbol{A}_0^T \end{bmatrix} \boldsymbol{I}_{N_\mathrm{r}} \begin{bmatrix} \breve{\boldsymbol{A}}^T \\ \boldsymbol{\zeta}^T \boldsymbol{A}_0^T \end{bmatrix}^T \succeq 0. \tag{3.52}$$

If $\lambda > 0$, it follows that $\frac{1}{\lambda}\Delta_{\boldsymbol{E}}$ in (3.52) is the Schur complement of $\lambda \boldsymbol{I}_{N_\mathrm{r}}$ in

$$\boldsymbol{M} \triangleq \begin{bmatrix} \mu \boldsymbol{I}_{N_A} & \boldsymbol{0}_{N_A} & \breve{\boldsymbol{A}}^T \\ \boldsymbol{0}_{N_A}^T & \tau\sqrt{\frac{P_\mathrm{S}}{\gamma_\mathrm{th}^\mathrm{CE}\sigma_\mathrm{D}^2}} - 1 - \mu\rho_1^2 & \boldsymbol{\zeta}^T \boldsymbol{A}_0^T \\ \breve{\boldsymbol{A}} & \boldsymbol{A}_0\boldsymbol{\zeta} & (\tau\sqrt{\frac{P_\mathrm{S}}{\gamma_\mathrm{th}^\mathrm{CE}\sigma_\mathrm{D}^2}} - 1)\boldsymbol{I}_{N_\mathrm{r}} \end{bmatrix}, \tag{3.53}$$

and by Lemma 5, $\boldsymbol{M} \succeq 0$ since $\frac{1}{\lambda}\Delta_{\boldsymbol{E}} \succeq 0$. For $\lambda = 0$, $\boldsymbol{M} \succeq 0$ holds if and only if $\mu = 0$, $\boldsymbol{A}_0\boldsymbol{\zeta} = \boldsymbol{0}$ and $\breve{\boldsymbol{A}} = \boldsymbol{0}$. Thus, we have the first LMI in (3.44). In summary, a pair $(\boldsymbol{\zeta}, \tau)$ satisfies (3.45) if there exists some $\mu \in \mathbb{R}_+$ and $\tau \geq \sqrt{\gamma_\mathrm{th}^\mathrm{CE}\sigma_\mathrm{D}^2/P_\mathrm{S}}$ such that the triple $(\boldsymbol{\zeta}, \tau, \mu)$ satisfies $\boldsymbol{M} \succeq 0$.

Next, we turn to (3.46) and substitute $\boldsymbol{c}$ defined by the uncertainty set $\mathcal{U}_\mathrm{L}$ in (3.42) into (3.46), we have equivalently

$$\breve{\boldsymbol{c}}^T \boldsymbol{v} \geq -\left(\boldsymbol{c}_0^T\boldsymbol{\zeta} - \tau\right), \qquad \forall \boldsymbol{v} \in \{\boldsymbol{v} : \|\boldsymbol{v}\| \leq \rho_2\}. \tag{3.54}$$

Following similar steps leading to (2.45), we can express the robust constraint in (3.54) as

$$\begin{bmatrix} \frac{\boldsymbol{c}_0^T\boldsymbol{\zeta} - \tau}{\rho_2} \\ \breve{\boldsymbol{c}} \end{bmatrix} \succeq_{\mathcal{K}} 0. \tag{3.55}$$

Using [114], we can represent (3.55) in the form of an LMI as

$$\begin{bmatrix} \frac{\boldsymbol{c}_0^T\boldsymbol{\zeta} - \tau}{\rho_2}\boldsymbol{I}_{N_c} & \breve{\boldsymbol{c}} \\ \breve{\boldsymbol{c}}^T & \frac{\boldsymbol{c}_0^T\boldsymbol{\zeta} - \tau}{\rho_2} \end{bmatrix} \succeq 0. \tag{3.56}$$

Therefore, we obtain the second LMI in (3.44). The other three LMIs in (3.44) are

[12] When $\lambda = 0$, we have $\mu = 0$.

easily obtained by representing the SOC constraint in terms of LMIs [114, p. 196]. □

3.3.2 Noncoherent AF Relaying

Similarly, we formulate the robust counterpart of $\mathcal{P}^{\mathrm{CE}}_{\mathrm{noncoh}}(\gamma^{\mathrm{CE}}_{\mathrm{th}})$ with uncertainties in $\boldsymbol{d}$ and $\boldsymbol{e}$.

Theorem 8. *Let $\mathcal{U}$ be an ellipsoidal uncertainty set given by*

$$\mathcal{U} = \left\{ \boldsymbol{\Delta}(\boldsymbol{d},\boldsymbol{e}) = \boldsymbol{\Delta}_0 + \sum_{j\in\mathcal{N}_\Delta} w_j \boldsymbol{\Delta}_j : \|\boldsymbol{w}\| \le \rho_0 \right\}, \tag{3.57}$$

where $\boldsymbol{\Delta}_j \triangleq \frac{P_{\mathrm{S}}}{\gamma^{\mathrm{CE}}_{\mathrm{th}}\sigma^2_{\mathrm{D}}}\boldsymbol{e}_j - \boldsymbol{d}_j \in \mathbb{R}^K$, $\mathcal{N}_\Delta = \{1,\ldots,N_\Delta\}$, and N_Δ is the dimension of $\boldsymbol{w}$. The robust counterpart of $\mathcal{P}^{\mathrm{CE}}_{\mathrm{noncoh}}(\gamma^{\mathrm{CE}}_{\mathrm{th}})$ with uncertainty set $\mathcal{U}$ is equivalent to the following SOCP:

$$\begin{aligned} \mathcal{RP}^{\mathrm{CE}}_{\mathrm{noncoh}}(\gamma^{\mathrm{CE}}_{\mathrm{th}}): \; min_{\boldsymbol{p}} \quad & \mathbf{1}^T\boldsymbol{p} \\ s.t. \quad & \boldsymbol{p} \in \mathcal{S}_{\mathrm{noncoh}}(\gamma^{\mathrm{CE}}_{\mathrm{th}}), \end{aligned} \tag{3.58}$$

where the feasible set $\mathcal{S}_{\mathrm{noncoh}}(\gamma^{\mathrm{CE}}_{\mathrm{th}})$ is given by

$$\mathcal{S}_{\mathrm{noncoh}}(\gamma^{\mathrm{CE}}_{\mathrm{th}}) = \left\{ \boldsymbol{p}\in\mathbb{R}^K : \begin{bmatrix} \frac{\boldsymbol{\Delta}_0^T\boldsymbol{p}-1}{\rho_0} \\ \breve{\boldsymbol{\Delta}} \end{bmatrix} \succeq_{\mathcal{K}} 0,\ \boldsymbol{p}\in\mathcal{X}_p \right\}, \tag{3.59}$$

and $\breve{\boldsymbol{\Delta}} = \left[\boldsymbol{\Delta}_1^T\boldsymbol{p}, \boldsymbol{\Delta}_2^T\boldsymbol{p}, \ldots, \boldsymbol{\Delta}_{N_\Delta}^T\boldsymbol{p}\right]^T$.

Proof. Since only $(\boldsymbol{d},\boldsymbol{e})$ in the first constraint of $\mathcal{P}^{\mathrm{CE}}_{\mathrm{noncoh}}(\gamma^{\mathrm{CE}}_{\mathrm{th}})$ is subject to uncertainty, we will focus on this constraint and build its robust counterpart, which is given by

$$\boldsymbol{e}^T\boldsymbol{p} \ge \frac{\gamma^{\mathrm{CE}}_{\mathrm{th}}\sigma^2_{\mathrm{D}}}{P_{\mathrm{S}}}\left(1+\boldsymbol{d}^T\boldsymbol{p}\right), \tag{3.60}$$

for all $(\boldsymbol{d},\boldsymbol{e})$ that satisfies $\boldsymbol{\Delta}(\boldsymbol{d},\boldsymbol{e}) \in \mathcal{U}$. By substituting (3.57) into (3.60), we have equivalently

$$\breve{\boldsymbol{\Delta}}^T\boldsymbol{w} \ge -\left(\boldsymbol{\Delta}_0^T\boldsymbol{p}-1\right), \qquad \forall \boldsymbol{w}\in\{\boldsymbol{w}:\|\boldsymbol{w}\|\le\rho_0\}, \tag{3.61}$$

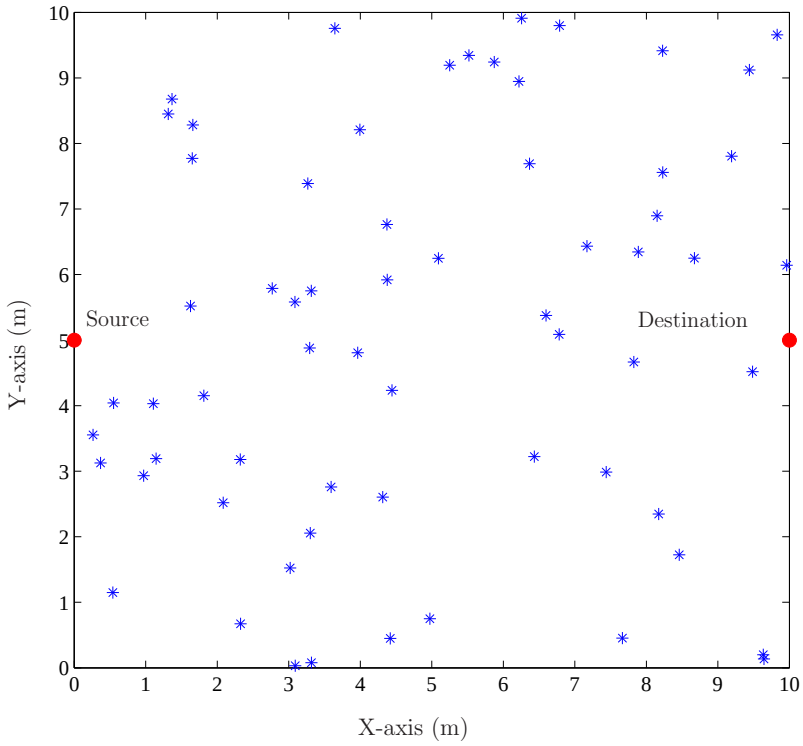

Figure 3-1: An example realization of a wireless relay network.

and the robust constraint in (3.61) is equivalent to an SOC constraint, as follows:

$$\begin{bmatrix} \frac{\boldsymbol{\Delta}_0^T \boldsymbol{p} - 1}{\rho_0} \\ \breve{\boldsymbol{\Delta}} \end{bmatrix} \succeq_{\mathcal{K}} 0. \tag{3.62}$$

Since the objective function is linear in $\boldsymbol{p}$ and the rest of the constraints in (3.59) are linear constraints, it follows that $\mathcal{RP}^{\mathrm{CE}}_{\mathrm{noncoh}}(\gamma^{\mathrm{CE}}_{\mathrm{th}})$ is an SOCP. □

3.4 Numerical Results

To illustrate the performance of our proposed algorithms, we consider networks with N_{r} relay nodes deployed randomly and independently over a 10m $\times$ 10m square. For each network, the source and destination nodes are positioned on the opposite sides of the square, i.e., the source node is fixed at $(x, y) = (0\mathrm{m}, 5\mathrm{m})$ and the destination node

is fixed at $(x, y) = (10\text{m}, 5\text{m})$. One possible realization of the network with $N_\text{r} = 64$ is shown in Fig. 3-1. For each realization of the random network topology, we generate $S_{\text{B},k}$ and $S_{\text{F},k}$ according to (3.3) and (3.4) with $\varepsilon = 4$. This procedure is repeated for 20,000 realizations. The noise variances are normalized such that $\sigma^2_{\text{R},k} = 1$ and $\sigma^2_\text{D} = 1$. The constraint on the maximum transmission power of each individual relay node is set at $P = 10$ dB. Throughout this section, we use the SeDuMi optimization package [120] to determine the RPAs according to our algorithms described in described in Chapters 3.2 and 3.3. The uncertainty sets in Theorems 7 and 8 are chosen such that $N_\Delta = 1$, $\boldsymbol{\Delta}_1 = \boldsymbol{\Delta}_0$, $N_A = 1$, $\boldsymbol{A}_1 = \boldsymbol{A}_0$, and $N_c = 1$, $\boldsymbol{c}_1 = \boldsymbol{c}_0$. We consider $\rho_0 = \rho_1 = \rho_2 = \rho$, where $\rho = 0$ corresponds to perfect knowledge of the global CSI and $\rho = 1$ corresponds to an uncertainty that is of the same size as the estimated global CSI, i.e., $\boldsymbol{d}_0, \boldsymbol{e}_0, \boldsymbol{A}_0, \boldsymbol{c}_0$.

Figures 3-2 and 3-3 show the outage probabilities (the SNR constraint in (3.7) is not satisfied) as a function of γ_th for coherent and noncoherent relay networks, respectively.[13] The power allocations used in these plots were obtained by solving $\mathcal{P}^{\text{CE}}_{\text{coh}}(\gamma^{\text{CE}}_\text{th})$ and $\mathcal{P}^{\text{CE}}_{\text{noncoh}}(\gamma^{\text{CE}}_\text{th})$ using our proposed algorithms.[14] It can be seen that the outage probabilities of the coherent and noncoherent AF relay networks decrease as the factor κ increases. This decrease shows that the CE formulation, which enables implementation of practical algorithms that track only large-scale fading, can effectively account for the random fluctuations in the actual instantaneous SNR as well as compensate for the use of approximation in (3.9). Comparing Figs. 3-2 and 3-3, we see that the CE approach is less effective in noncoherent AF relay networks, even with larger κ values, owing to the absence of phase alignment at the relay nodes.[15]

There may be some situations where $\mathcal{P}^{\text{CE}}_{\text{coh}}(\gamma^{\text{CE}}_\text{th})$ and $\mathcal{P}^{\text{CE}}_{\text{noncoh}}(\gamma^{\text{CE}}_\text{th})$ are infeasible. We denote the probabilities of such events as CE outage probabilities, i.e., probabilities that the CE SNR constraints in (3.12) and (3.32) are not satisfied. The CE outage probabilities as a function of $\gamma^{\text{CE}}_\text{th}$ are plotted for various values of P_S in Figs. 3-4 and

[13] The chosen value of σ_dB in these plots is typical for macrocellular applications [122].

[14] Recall from Chapter 3.1 that the SNR constraint in (3.7) may not be satisfied even when $\mathcal{P}^{\text{CE}}_{\text{coh}}(\gamma^{\text{CE}}_\text{th})$ and $\mathcal{P}^{\text{CE}}_{\text{noncoh}}(\gamma^{\text{CE}}_\text{th})$ are feasible.

[15] In such cases, time diversity techniques can be used [127].

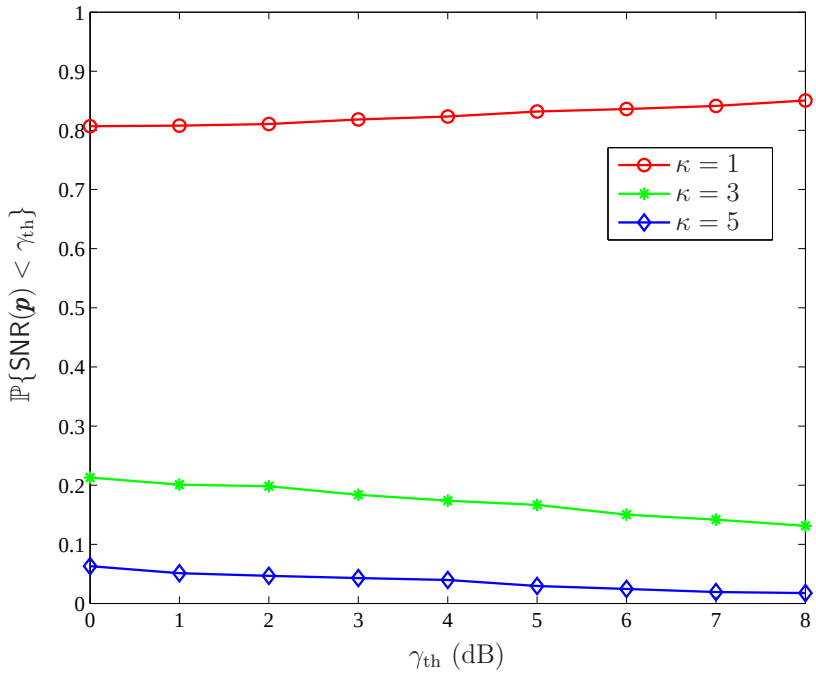

Figure 3-2: Outage probability of the coherent AF relay network with $N_{\mathrm{r}} = 64$, $P_{\mathrm{S}} = 30$ dB, and $\sigma_{\mathrm{dB}} = 8$ dB.

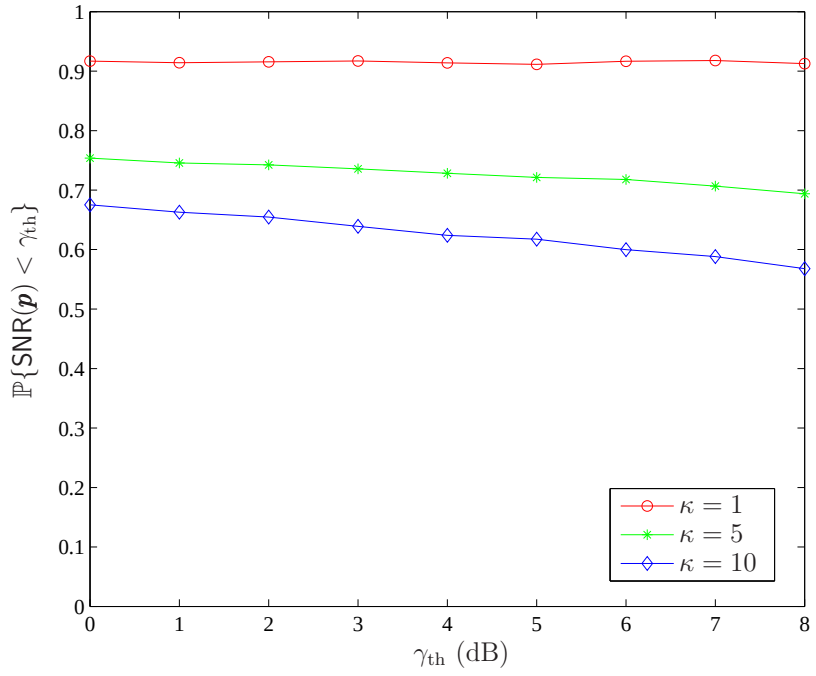

Figure 3-3: Outage probability of the noncoherent AF relay network with $N_{\mathrm{r}} = 64$, $P_{\mathrm{S}} = 30$ dB, and $\sigma_{\mathrm{dB}} = 8$ dB.

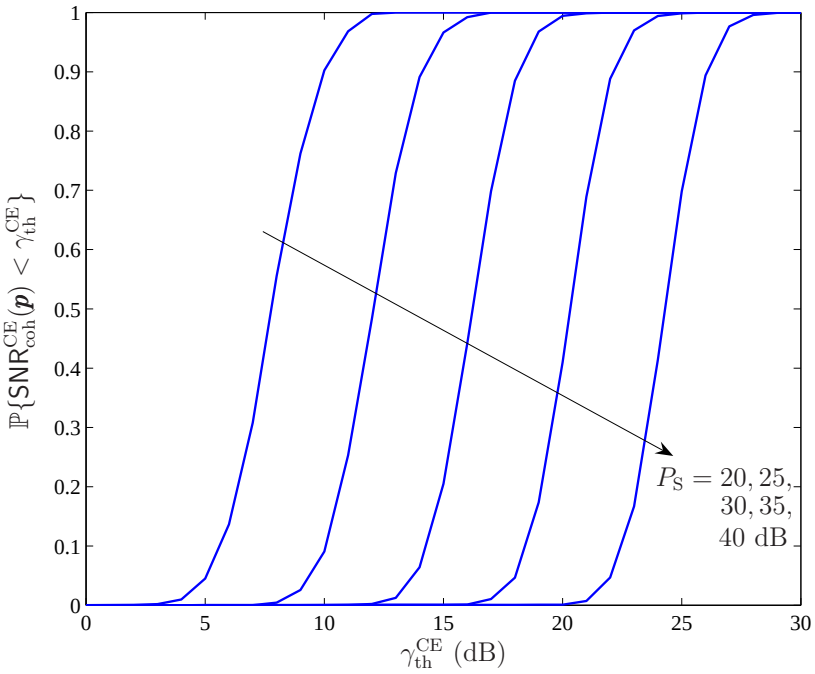

Figure 3-4: CE outage probability of the proposed power allocation algorithm for the coherent AF relay network as a function of $\gamma_{\mathrm{th}}^{\mathrm{CE}}$ with $N_{\mathrm{r}} = 64$ and $\sigma_{\mathrm{dB}} = 8$ dB.

3-5 for coherent and noncoherent AF relay networks, respectively. We see from these figures that, for a fixed CE SNR target value, an increase in source power is required to maintain a lower outage probability. This increase in required source power is more drastic in noncoherent AF relay networks compared to coherent AF relay networks.

We next compare our power allocation algorithms in terms of power-efficiency ΔP, where $\Delta P \triangleq 10\log(N_{\mathrm{r}}P/\sum_{k=1}^{N_{\mathrm{r}}} p_k)$ is defined as the ratio of the total relay transmission power based on the naive scheme and that based on our algorithm.[16] Figures 3-6 and 3-7 show the complementary cumulative distribution function (ccdf) of ΔP for coherent and noncoherent AF relay networks with different numbers of relay nodes and CE SNR target values.[17] We see that our proposed algorithms offer significant power savings in both networks. These figures indicate that ΔP increases when the number of relay nodes increases. This is because our power allocation

[16]Recall that the naive scheme is referred to one that employs maximum transmission power at each relay node.

[17]The ccdf of a r.v. X gives the probability that X is above a particular level.

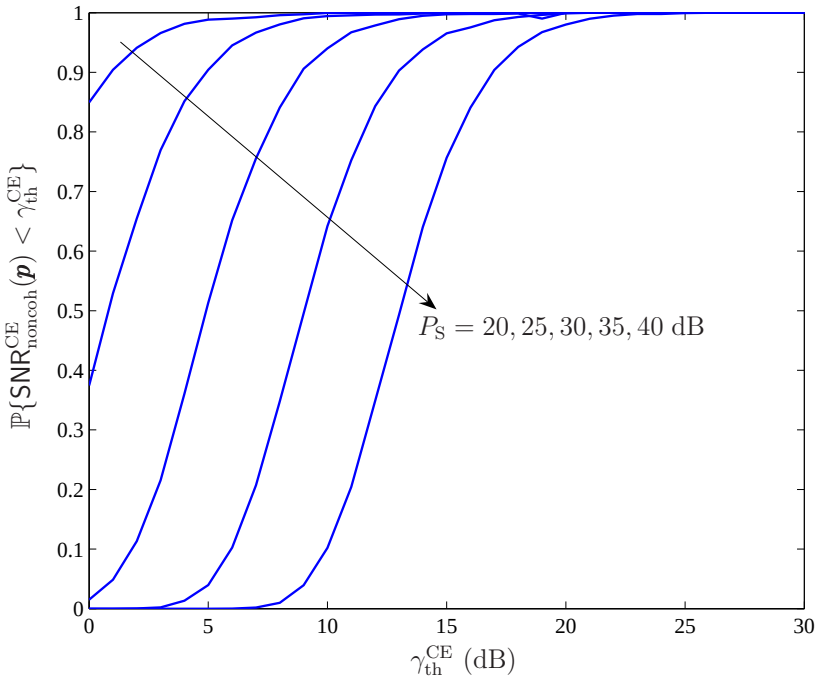

Figure 3-5: CE outage probability of the proposed power allocation algorithm for the noncoherent AF relay network as a function of $\gamma^{\mathrm{CE}}_{\mathrm{th}}$ with $N_{\mathrm{r}} = 64$ and $\sigma_{\mathrm{dB}} = 8$ dB.

algorithms exploit the channel variations in the spatial domain. When $\gamma^{\mathrm{CE}}_{\mathrm{th}}$ decreases, the efficiency increases, since less relay power expenditure is required to satisfy the CE SNR constraint. Comparing Figs. 3-6 and 3-7, we see that the increase in power-efficiency is more significant, due to a higher cooperative gain, in coherent AF relay networks compared to noncoherent AF relay networks, as observed in [95].

Figures 3-8 and 3-9 show the ccdf of ΔP for coherent and noncoherent AF relay networks with different numbers of relay nodes and σ_{dB}. These figures indicate that ΔP increases when σ_{dB} increases, implying that our proposed power allocation algorithms are more efficient for channels with large fluctuations. This increase in ΔP is more significant for large networks for the same reason noted in previous paragraph.

Figures 3-10 and 3-11 show the cumulative distribution function (cdf) of the minimum number of relay nodes that are necessary to achieve a certain percentage of the total relay transmission power in coherent and noncoherent AF relay networks, respectively. We observe that most of the total relay transmission power tends to be

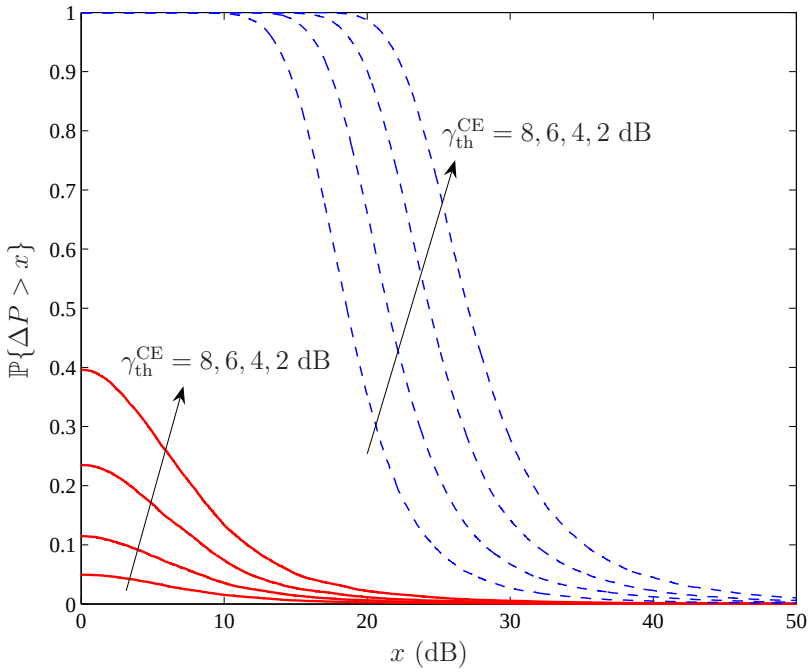

Figure 3-6: Ccdf of ΔP of the coherent AF relay network for different K and $\gamma_{\rm th}^{\rm CE}$ with $P_{\rm S} = 30$ dB and $\sigma_{\rm dB} = 8$ dB. The solid and dashed lines indicate $N_{\rm r} = 8$ and 64, respectively.

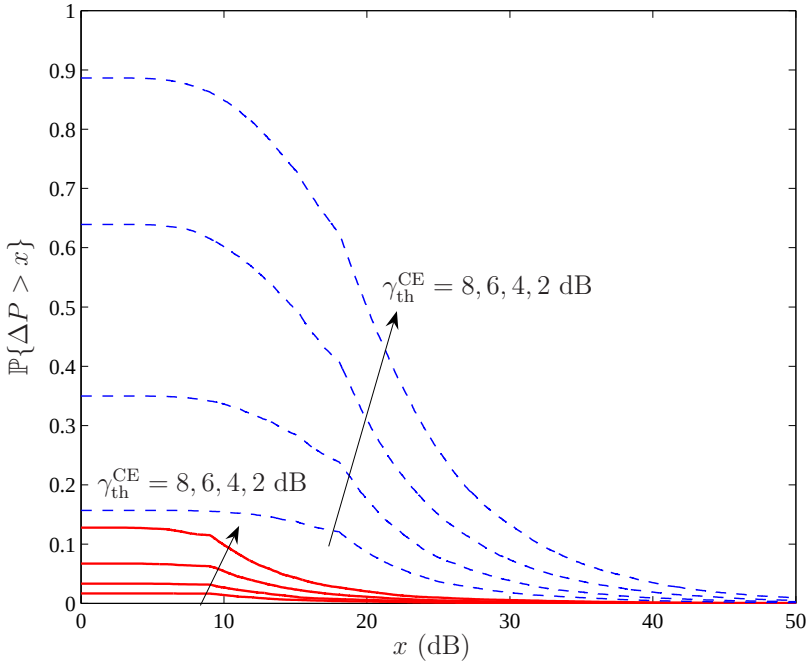

Figure 3-7: Ccdf of ΔP of the noncoherent AF relay network for different K and $\gamma_{\rm th}^{\rm CE}$ with $P_{\rm S} = 30$ dB and $\sigma_{\rm dB} = 8$ dB. The solid and dashed lines indicate $N_{\rm r} = 8$ and 64, respectively.

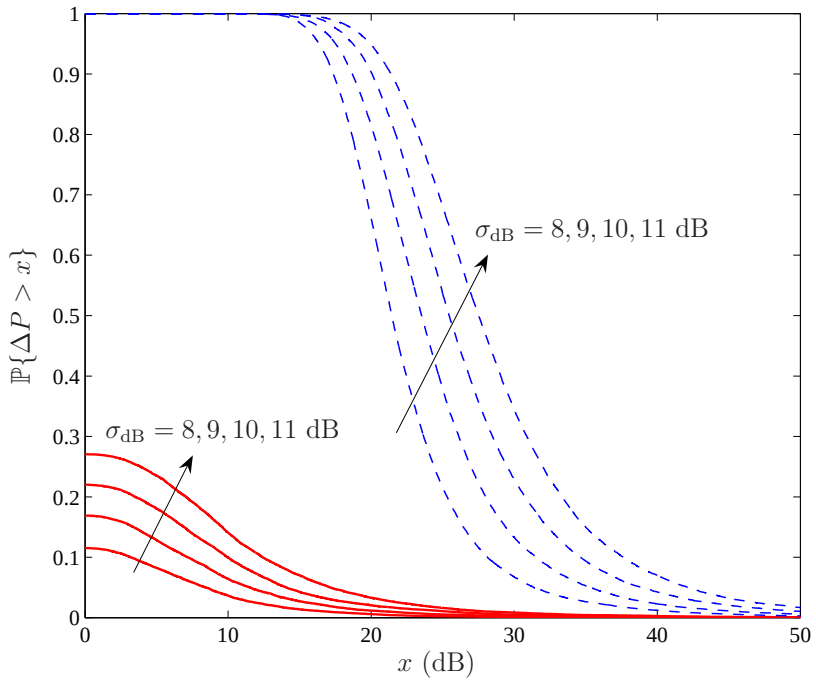

Figure 3-8: Ccdf of ΔP of the coherent AF relay network for different N_{r} and σ_{dB} with $P_{\mathrm{S}} = 30$ dB and $\gamma_{\mathrm{th}}^{\mathrm{CE}} = 6$ dB. The solid and dashed lines indicate $K = 8$ and 64, respectively.

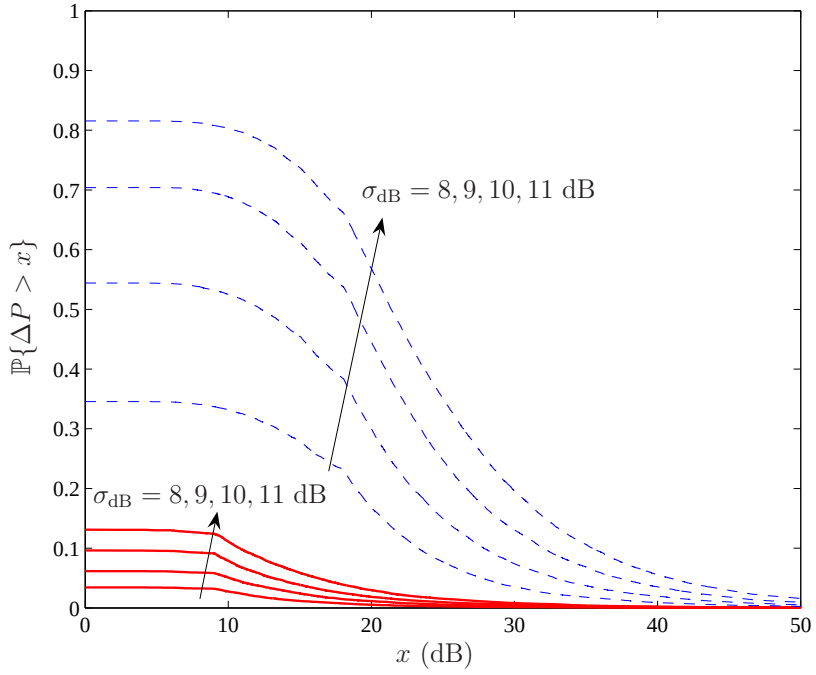

Figure 3-9: Ccdf of ΔP of the noncoherent AF relay network for different N_{r} and σ_{dB} with $P_{\mathrm{S}} = 30$ dB and $\gamma_{\mathrm{th}}^{\mathrm{CE}} = 6$ dB. The solid and dashed lines indicate $N_{\mathrm{r}} = 8$ and 64, respectively.

distributed among a smaller subset of relay nodes in the noncoherent case, compared to the coherent case. This suggests that relay selection is beneficial in noncoherent AF relay networks as observed in [12].

Lastly, we compare the robust algorithms in terms of the CE outage probabilities. Figures 3-12 and 3-13 show the CE outage probability as a function of the size of the uncertainty set ρ for coherent and noncoherent AF relay networks, respectively. We observe from these figures that adopting non-robust algorithms, i.e., simply ignoring uncertainties in the global CSI, results in a high penalty in terms of outage probability. On the other hand, we clearly see that robust algorithms provide lower outage probabilities compared to non-robust algorithms.

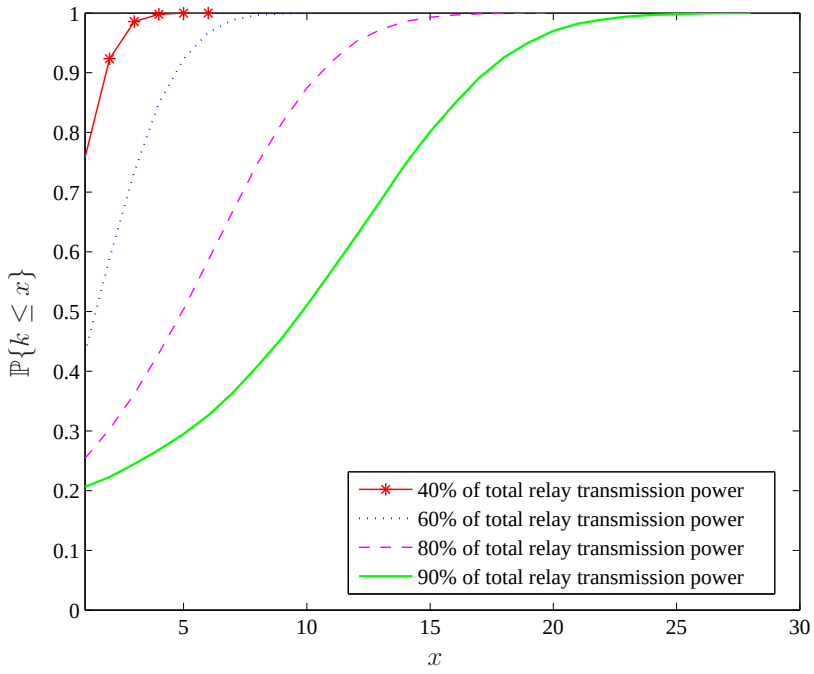

Figure 3-10: Effect of relay transmission power on cdf of the number of relay nodes for the coherent AF relay network with $N_{\mathrm{r}} = 64$, $P_{\mathrm{S}} = 30$ dB, $\sigma_{\mathrm{dB}} = 8$ dB, and $\gamma_{\mathrm{th}}^{\mathrm{CE}} = 6$ dB.

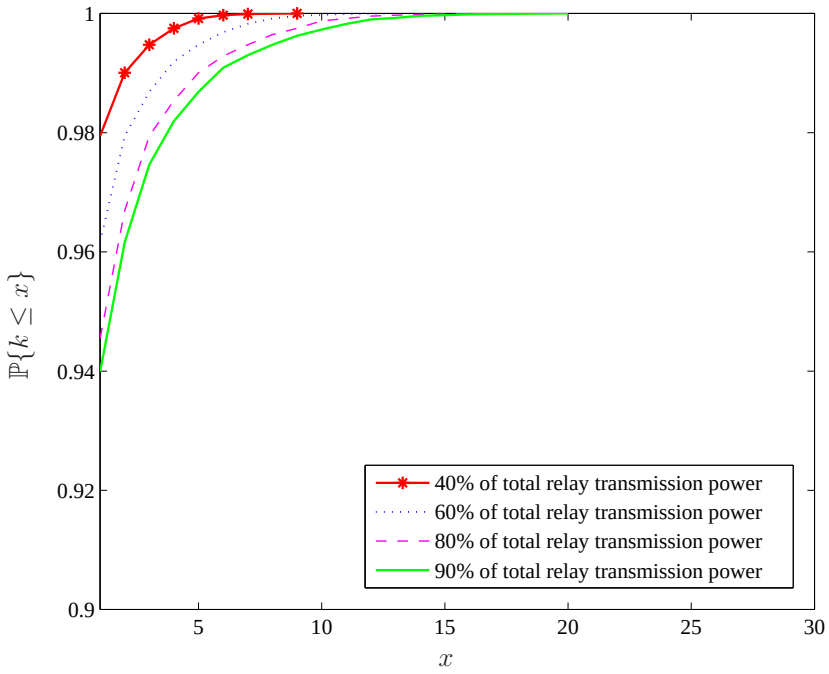

Figure 3-11: Effect of relay transmission power on cdf of the number of relay nodes for the noncoherent AF relay network with $N_{\mathrm{r}} = 64$, $P_{\mathrm{S}} = 30$ dB, $\sigma_{\mathrm{dB}} = 8$ dB, and $\gamma_{\mathrm{th}}^{\mathrm{CE}} = 6$ dB.

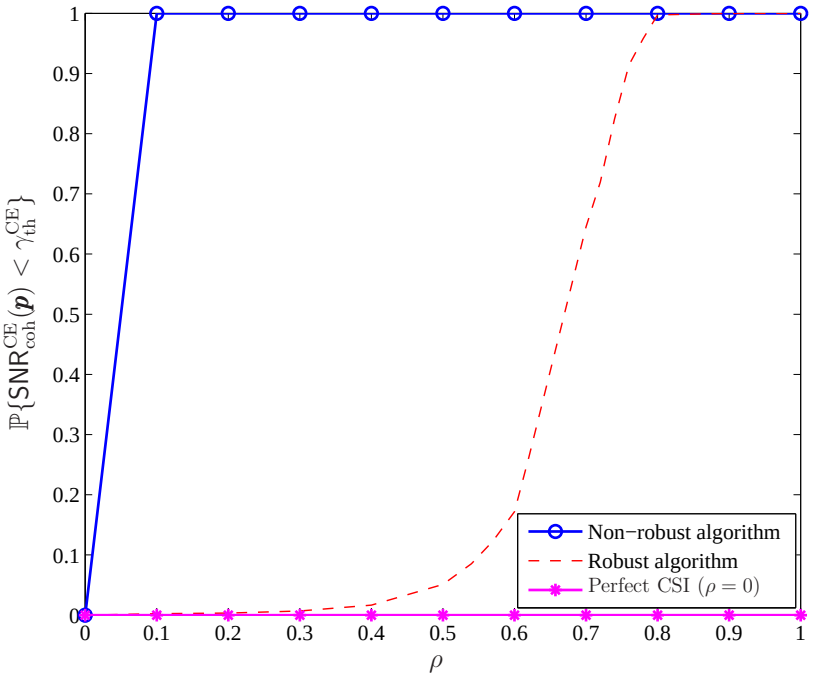

Figure 3-12: CE outage probability of robust power allocation algorithms for the coherent AF relay network with $N_{\mathrm{r}} = 64$, $P_{\mathrm{S}} = 30$ dB, $\sigma_{\mathrm{dB}} = 8$ dB, and $\gamma^{\mathrm{CE}}_{\mathrm{th}} = 6$ dB.

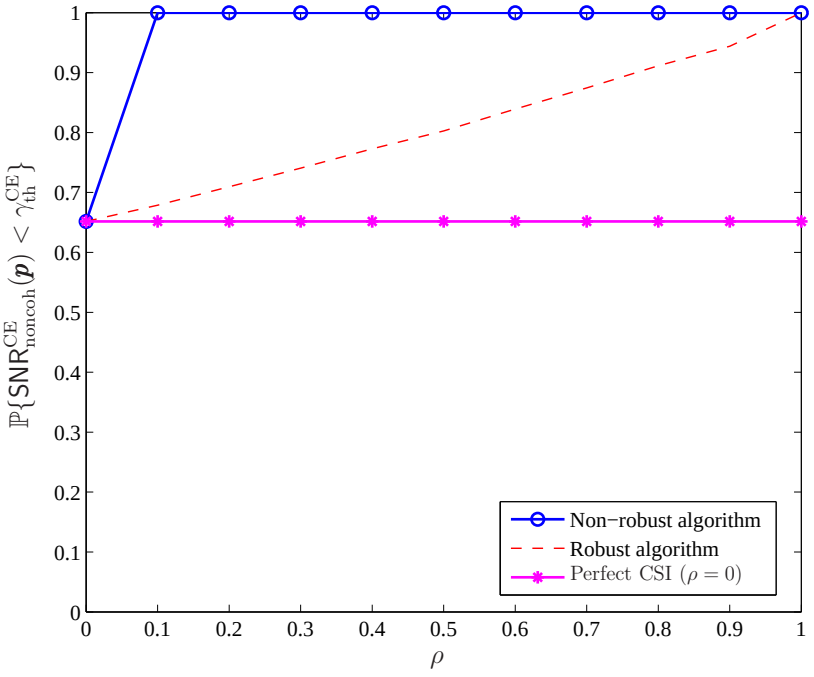

Figure 3-13: CE outage probability of robust power allocation algorithms for the noncoherent AF relay network with $N_{\mathrm{r}} = 64$, $P_{\mathrm{S}} = 30$ dB, $\sigma_{\mathrm{dB}} = 8$ dB, and $\gamma^{\mathrm{CE}}_{\mathrm{th}} = 6$ dB.

Chapter 4

Transmitted-Reference Communication Systems

In this chapter, we develop an analytical framework, based on the sampling expansion approach, to derive closed-form expressions for the BEP of TR and DTR signaling schemes in dense multipath channels. We consider receiver structures that employ AcR and modified AcR. From our results, we assess the validity of the conventional Gaussian approximation. In addition, we derive computationally simple lower bound on the BEP expression to obtain the SNR penalty associated with AcR, as compared to *All-Rake* (ARake) and *Partial-Rake* (PRake) receivers.

4.1 System and Channel Models

4.1.1 Transmitted-Reference

The transmitted signal of TR signaling for user k can be decomposed into a reference signal block $b_{\mathrm{r}}^{(k)}(t)$ and a data modulated signal block $b_{\mathrm{d}}^{(k)}(t)$ as given by

$$s_{\mathrm{TR}}^{(k)}(t) = \sum_{i} b_{\mathrm{r}}^{(k)}(t - iN_{\mathrm{s}}T_{\mathrm{f}}) + d_i^{(k)} b_{\mathrm{d}}^{(k)}(t - iN_{\mathrm{s}}T_{\mathrm{f}}), \tag{4.1}$$

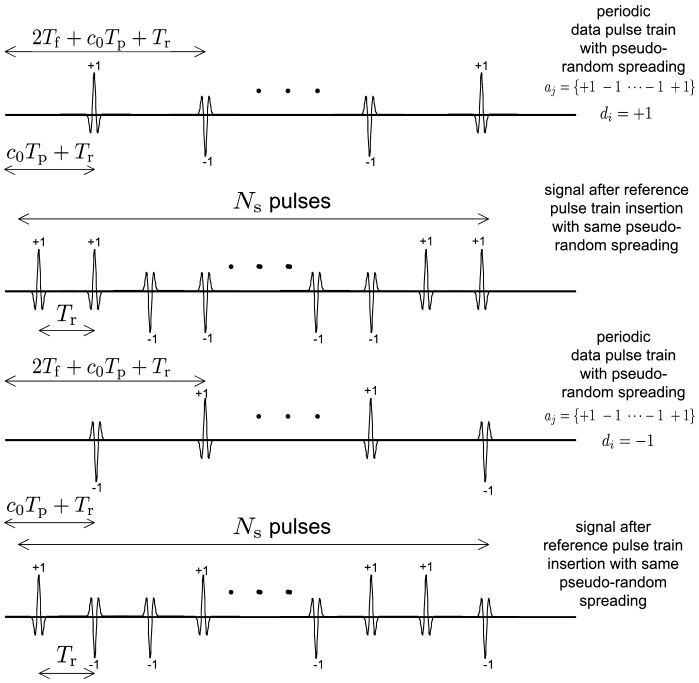

Figure 4-1: Illustration of the TR signaling scheme.

where $T_{\rm f}$ is the average pulse repetition period, $d_i^{(k)} \in \{-1, 1\}$ is the ith data symbol, and $N_{\rm s}T_{\rm f}$ is the symbol duration. The reference signal and modulated signal blocks, each consisting of $N_{\rm s}/2$ transmitted signal pulses, can be written as[1]

$$b_{\rm r}^{(k)}(t) = \sum_{j=0}^{\frac{N_{\rm s}}{2}-1} \sqrt{E_{\rm p}} a_j^{(k)} p(t - j2T_{\rm f} - c_j^{(k)} T_{\rm p}),$$
$$b_{\rm d}^{(k)}(t) = \sum_{j=0}^{\frac{N_{\rm s}}{2}-1} \sqrt{E_{\rm p}} a_j^{(k)} p(t - j2T_{\rm f} - c_j^{(k)} T_{\rm p} - T_{\rm r}), \tag{4.2}$$

where $b_{\rm d}^{(k)}(t)$ is equal to a version of $b_{\rm r}^{(k)}(t)$, delayed by $T_{\rm r}$, and $p(t)$ is a unit energy bandpass signal pulse with duration $T_{\rm p}$ and center frequency $f_{\rm c}$. The energy of the transmitted pulse is then $E_{\rm p} = E_{\rm s}/N_{\rm s}$, where $E_{\rm s}$ is the symbol energy. In our case of binary signaling, the symbol energy equals the energy per bit, $E_{\rm b}$. To enhance the robustness of TR systems against interference and to allow multiple access, DS and/or

[1]Note that other combinations of data and reference pulses are also possible [131]. For simplicity and without loss of generality, we have adopted conventional TR signaling, in which the number of reference and data pulses are equal and $N_{\rm s}$ is even [49, 52].

TH spread spectrum techniques can be used as shown in (4.2). In DS signaling, $\{a_j^{(k)}\}$ is the bipolar pseudo-random sequence of the kth user.[2] In TH signaling, $\{c_j^{(k)}\}$ is the pseudo-random sequence of the kth user, where $c_j^{(k)}$ is an integer in the range $0 \leq c_j^{(k)} < N_{\rm h}$, and $N_{\rm h}$ is the maximum allowable integer shift. A simplified example that illustrates TR signaling is shown in Fig. 4-1. The duration of the received UWB pulse is $T_{\rm g} = T_{\rm p} + T_{\rm d}$, where $T_{\rm d}$ is the maximum excess delay of the channel. To preclude inter-symbol interference (ISI) and intra-symbol interference (isi)[3], we assume that $T_{\rm r} \geq T_{\rm g}$ and $(N_{\rm h}-1)T_{\rm p} + T_{\rm r} + T_{\rm g} \leq 2T_{\rm f}$, where $T_{\rm r}$ is the time separation between each pair of data and reference pulses. If the symbol interval is less than the channel coherence time, all these pairs of separated signals will experience the same channel.[4] Note that $T_{\rm r}$ is constant for our case, as shown in Fig. 4-1, in contrast to [48], where the inter-pulse delays vary for different pairs of data-modulated and reference pulses.

4.1.2 Differential Transmitted-Reference

The transmitted signal of DTR signaling for user k is given by

$$s_{\rm DTR}^{(k)}(t) = \sum_i e_i^{(k)} b^{(k)}(t - iN_{\rm s}T_{\rm f}), \tag{4.3}$$

where $b^{(k)}(t)$ is the kth user's block-modulated signal with symbol interval $N_{\rm s}T_{\rm f}$, and $N_{\rm s}$ is the number of transmitted signal pulses in each block. The data symbol $d_i^{(k)}$ is now differentially encoded such that $e_i^{(k)} = e_{i-1}^{(k)} d_i^{(k)}$, where $d_i^{(k)} \in \{-1, 1\}$. The $b^{(k)}(t)$-shaped signal block can be written as

$$b^{(k)}(t) = \sum_{j=0}^{N_{\rm s}-1} \sqrt{E_{\rm p}} a_j^{(k)} p(t - jT_{\rm f} - c_j^{(k)} T_{\rm p}), \tag{4.4}$$

[2]Walsh-Hadamard sequences are used in [131].

[3]ISI and isi may not always be negligible due to constraints on $T_{\rm f}$ and data-rate requirements. In this case, our results will serve as a lower bound.

[4]For TR signaling with an AcR, only adjacent data and reference pulses need to be within the channel coherence time. The condition that all pulses within a symbol experience the same channel, however, will enable us to extend our analysis to TR signaling with a modified AcR, where the channel is assumed to be constant over two symbols.

where $\{a_j^{(k)}\}$ and $\{c_j^{(k)}\}$ are the DS and TH sequences that provide robustness to interference and multiple-access capability for DTR systems. Note that a DTR signal looks similar to a short-code CDMA signal, except that pulses are separated by at least $T_{\rm g}$ and TH is also present. The TH sequence is pseudo-random with the range $0 \le c_j^{(k)} < N_{\rm h}$, where $N_{\rm h}$ satisfies $(N_{\rm h}-1)T_{\rm p} + T_{\rm g} \le T_{\rm f}$ to preclude ISI and isi. The channel must be constant over two symbols in order to use differential encoding over two adjacent symbols.

4.1.3 Channel Model

The received signal can be written as

$$r_{\rm TR}(t) = \int_{-\infty}^{+\infty} h(\tau) s_{\rm TR}(t-\tau) d\tau + n(t), \tag{4.5}$$

where $h(t)$ is the impulse response of the channel and $n(t)$ is zero-mean, white Gaussian noise with two-sided power spectral density $N_0/2$. Note that a similar equation also applies to DTR signaling by replacing $s_{\rm TR}(t)$ with $s_{\rm DTR}(t)$. The channel impulse response, modeled as linear time-invariant, can be written as $h(t) = \sum_{l=1}^{L} \alpha_l \delta(t-\tau_l)$, where L is the number of resolvable multipath components, and α_l and τ_l respectively denote the attenuation and delay of lth path. We can express $\alpha_l = |\alpha_l| \exp(j\phi_l)$, where $\phi_l = 0$ or π with equal probability. As in [37, 38], we consider the resolvable dense multipath channel,[5] i.e., $|\tau_l - \tau_j| \ge T_{\rm p}, \forall l \ne j$, where $\tau_l = \tau_1 + (l-1)T_{\rm p}$, and $\{\alpha_l\}$ are assumed to be statistically independent r.v.'s.

4.2 Receiver Models

In the following, we suppress the index k since we are considering single user system. Without loss of generality, we consider the detection of the data symbol at $i = 0$. We

[5]Such an assumption may not be always true [132, 133]. However, the dense resolvable multipath channel serves as a reasonable approximation to realistic UWB channels. Therefore, our BEP analysis still provides insight into the performance of TR signaling.

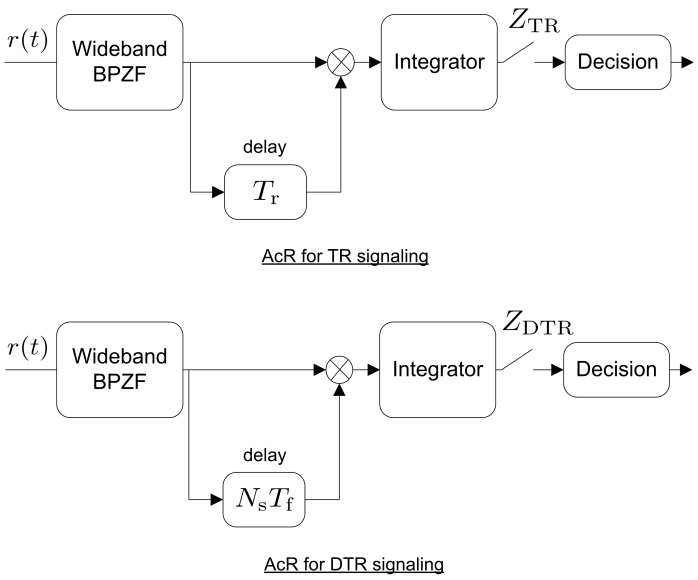

Figure 4-2: AcR for TR and DTR signaling schemes.

assume perfect synchronization at the receiver.[6]

4.2.1 Autocorrelation Receiver

As shown in Fig. 4-2, the AcR first passes the received signal through an ideal bandpass zonal filter (BPZF) with center frequency f_{c} to eliminate out-of-band noise. If the bandwidth W of the BPZF is large enough, then the signal spectrum will pass through undistorted. Consequently, the ISI and isi caused by filtering will be negligible. In this case, the output of the BPZF for TR and DTR signaling can be expressed respectively as

$$\begin{aligned}\widetilde{r}_{\mathrm{TR}}(t) = \sum_{i}\sum_{j=0}^{\frac{N_{\mathrm{s}}}{2}-1}\sum_{l=1}^{L}\Big[&\sqrt{E_{\mathrm{p}}}\alpha_l a_j p(t - iN_{\mathrm{s}}T_{\mathrm{f}} - j2T_{\mathrm{f}} - c_jT_{\mathrm{p}} - \tau_l) \\ &+ \sqrt{E_{\mathrm{p}}}\alpha_l a_j d_i p(t - iN_{\mathrm{s}}T_{\mathrm{f}} - j2T_{\mathrm{f}} - c_jT_{\mathrm{p}} - T_{\mathrm{r}} - \tau_l)\Big] \\ &+ \widetilde{n}(t), \end{aligned} \tag{4.6}$$

[6]It has been shown that we can relax the assumption of perfect synchronization in TR signaling due to its robustness against synchronization errors [134, 135]. However, exactly how this synchronization is achieved [134, 136] and the sensitivity analysis of synchronization errors [135] are beyond the scope of this dissertation.

and

$$\widetilde{r}_{\mathrm{DTR}}(t) = \sum_{i} \sum_{j=0}^{N_{\mathrm{s}}-1} \sum_{l=1}^{L} \sqrt{E_{\mathrm{p}}} \alpha_l a_j e_i p(t - iN_{\mathrm{s}}T_{\mathrm{f}} - jT_{\mathrm{f}} - c_j T_{\mathrm{p}} - \tau_l) + \widetilde{n}(t), \quad (4.7)$$

where $\widetilde{n}(t)$ is a zero-mean, Gaussian random process with autocorrelation function

$$R_{\widetilde{n}}(\tau) = WN_0 \,\mathrm{sinc}(W\tau) \cos(2\pi f_{\mathrm{c}} \tau). \quad (4.8)$$

Note that when $W \gg 1/T_{\mathrm{g}}$, $R_{\widetilde{n}}(\tau)$ in (4.8) is approximately equal to zero for $|\tau| \geq T_{\mathrm{g}}$. This implies that the noise samples separated by more than T_{g} or at a multiple of $1/W$ are statistically independent.

The filtered received signal is passed through a correlator with integration interval T ($T_{\mathrm{p}} \leq T \leq T_{\mathrm{g}}$), as shown in Fig. 4-2, to collect the received signal energy. The integration interval T determines the number of multipath components (or equivalently, the amount of energy) captured by the receiver, as well as the amount of noise and interference accumulation. As will be shown in later sections, the optimum T depends on various channel conditions, such as the decay factor of the channel power dispersion profile (PDP), and on the signal-to-interference ratio (SIR). The decision statistics generated at the integrator output of the AcR can be written respectively as

$$Z_{\mathrm{TR}} = \sum_{j=0}^{\frac{N_{\mathrm{s}}}{2}-1} \int_{j2T_{\mathrm{f}}+T_{\mathrm{r}}+c_j T_{\mathrm{p}}}^{j2T_{\mathrm{f}}+T_{\mathrm{r}}+c_j T_{\mathrm{p}}+T} \widetilde{r}_{\mathrm{TR}}(t)\, \widetilde{r}_{\mathrm{TR}}(t - T_{\mathrm{r}}) dt, \quad (4.9)$$

and

$$Z_{\mathrm{DTR}} = \sum_{j=0}^{N_{\mathrm{s}}-1} \int_{jT_{\mathrm{f}}+c_j T_{\mathrm{p}}}^{jT_{\mathrm{f}}+c_j T_{\mathrm{p}}+T} \widetilde{r}_{\mathrm{DTR}}(t)\, \widetilde{r}_{\mathrm{DTR}}(t - N_{\mathrm{s}}T_{\mathrm{f}}) dt, \quad (4.10)$$

for TR and DTR signaling.

4.2.2 Modified Autocorrelation Receiver

The AcR performance for both TR and DTR signaling can be improved by averaging respectively over $N_{\rm s}/2$ and $N_{\rm s}$ received reference pulses from the previous symbol [49].[7] This, however, requires the channel to remain constant over two symbols. The decision statistics of this modified AcR for TR and DTR signaling are given respectively by

$$Z_{\rm ATR} = \sum_{j=0}^{\frac{N_{\rm s}}{2}-1} a_j \int_{j2T_{\rm f}+T_{\rm r}+c_jT_{\rm p}}^{j2T_{\rm f}+T_{\rm r}+c_jT_{\rm p}+T} \widetilde{r}_{\rm TR}(t) \times \left[\frac{2}{N_{\rm s}} \sum_{k=-j}^{\frac{N_{\rm s}}{2}-1-j} a_{j+k}\widetilde{r}_{\rm TR}\Big(t-(N_{\rm s}-2k)T_{\rm f}-(c_j-c_{j+k})T_{\rm p}-T_{\rm r}\Big)\right] dt, \tag{4.11}$$

and

$$Z_{\rm ADTR} = \sum_{j=0}^{N_{\rm s}-1} a_j \int_{jT_{\rm f}+c_jT_{\rm p}}^{jT_{\rm f}+c_jT_{\rm p}+T} \widetilde{r}_{\rm DTR}(t) \times \left[\frac{1}{N_{\rm s}} \sum_{k=-j}^{N_{\rm s}-1-j} a_{j+k}\widetilde{r}_{\rm DTR}\Big(t-(N_{\rm s}-k)T_{\rm f}-(c_j-c_{j+k})T_{\rm p}\Big)\right] dt. \tag{4.12}$$

Note that the modified AcR generally has a higher receiver complexity than AcR since it requires additional memory to store previous received samples and averaging them to obtain the decision statistics in (4.11) and (4.12).

4.3 Performance Analysis

Next, we first derive the BEP of TR signaling with AcR in dense multipath channels using the Gaussian approximation approach and point out the limitations of such an approach. To alleviate such limitations, we develop an analytical framework based

[7] This averaging can be thought of as forming an estimate of the channel. In fact, when the observation noise is Gaussian, this is equivalent to forming a maximum likelihood estimate of the channel [29].

on sampling expansion approach to derive the BEP expressions for TR and DTR signaling schemes when AcR and modified AcR are used.

4.3.1 Gaussian Approximation Approach

First, by representing the output of AcR in (4.9) in terms of four components, Z_1, Z_2, Z_3, and Z_4, where each of these terms is defined and derived in Appendix B.1. The conventional approach to analyze the performance of TR signaling is to assume that the distributions of the noise components Z_2, Z_3, and Z_4 are conditionally Gaussian and mutually uncorrelated when conditioned on $\{\alpha_l\}_{l=1}^{L}$ [48–50]. This assumption is valid when the time-bandwidth product or N_s is large. When the time-bandwidth product is large, (4.9) can be approximated by a conditional Gaussian r.v. by invoking the Central-Limit Theorem [49,50]. When N_s is large, Z_4 in (B.4) can also be approximated as Gaussian by the Central-Limit Theorem [49]. The mutually uncorrelated assumption is valid when $W \gg 1/T_\mathrm{g}$ [49, 50]. Only when all the above assumptions are valid, can we invoke the Gaussian approximation to derive the conditional BEP for TR signaling with AcR as[8]

$$\mathbb{P}\left\{e|\gamma_\mathrm{TR}\right\} = Q\left(\sqrt{\frac{\mathbb{E}\left\{Z_\mathrm{TR}|\{\alpha_l\}_{l=1}^{L_\mathrm{CAP}}, d_0=+1\right\}^2}{\mathbb{V}\left\{Z_\mathrm{TR}|\{\alpha_l\}_{l=1}^{L_\mathrm{CAP}}\right\}}}\right), \tag{4.13}$$

where $Q(\cdot)$ is the Gaussian Q-function, $\gamma_\mathrm{TR} = \frac{E_\mathrm{s}}{2N_0}\sum_{l=1}^{L_\mathrm{CAP}}\alpha_l^2$ denotes the instantaneous received SNR of TR signaling with AcR, $L_\mathrm{CAP} \triangleq \lceil \min\{WT, WT_\mathrm{g}\}\rceil$ denotes the actual number of multipath components captured by the AcR.

Under the Gaussian approximation, the derivation of the conditional BEP in (4.13) is reduced to the derivation of the conditional mean and variance. The conditional mean is given by

$$\mathbb{E}\left\{Z_\mathrm{TR}|\{\alpha_l\}_{l=1}^{L_\mathrm{CAP}}, d_0=+1\right\} = \frac{E_\mathrm{s}}{2}\sum_{l=1}^{L_\mathrm{CAP}}\alpha_l^2, \tag{4.14}$$

[8]Note that we have exploited symmetry about d_0 to obtain (4.13).

and the derivation can be found in Appendix B.1. The mutual independence assumption of Z_2, Z_3, and Z_4 leads to the following result (see Appendix B.2)

$$\begin{aligned}\mathbb{V}\left\{Z_{\mathrm{TR}}|\{\alpha_l\}_{l=1}^{L_{\mathrm{CAP}}}\right\} &= \mathbb{V}\left\{Z_2|\{\alpha_l\}_{l=1}^{L_{\mathrm{CAP}}}\right\} + \mathbb{V}\left\{Z_3|\{\alpha_l\}_{l=1}^{L_{\mathrm{CAP}}}\right\} + \mathbb{V}\left\{Z_4|\{\alpha_l\}_{l=1}^{L_{\mathrm{CAP}}}\right\} \\ &\approx \frac{N_0 E_{\mathrm{s}}}{2}\sum_{l=1}^{L_{\mathrm{CAP}}}\alpha_l^2 + \frac{N_{\mathrm{s}}}{4}N_0^2 WT. \end{aligned} \tag{4.15}$$

Using (4.13)-(4.15), we can rewrite the conditional BEP for TR signaling with AcR in (4.13) as

$$\mathbb{P}\left\{e|\gamma_{\mathrm{TR}}\right\} = Q\left(\frac{\gamma_{\mathrm{TR}}}{\sqrt{\gamma_{\mathrm{TR}} + \frac{N_{\mathrm{s}}}{4}WT}}\right). \tag{4.16}$$

From (4.16), we can see that the amount of received energy captured by the AcR depends on WT. Under the resolvable multipath assumption, L_{CAP} increases with WT until $L_{\mathrm{CAP}} = L$. Increasing WT beyond this point will only accumulate more noise energy in the receiver as seen in the denominator of (4.16). The BEP of TR signaling can then be obtained by averaging the conditional BEP in (4.16) as

$$P_{\mathrm{e,TR}} = \int_0^\infty \mathbb{P}\left\{e|x\right\} f_{\gamma_{\mathrm{TR}}}(x)dx, \tag{4.17}$$

where $f_{\gamma_{\mathrm{TR}}}(\cdot)$ is the pdf of γ_{TR}. The direct approach to evaluate (4.17) seems intractable since $\mathbb{P}\{e|x\}$ is written in terms of a definite integral (i.e., Gaussian Q-function) whose limit is a r.v. to be averaged. A common approach to alleviate this problem is to use the alternative expression for the Gaussian Q-function which has previously enabled numerous analysis of wireless scenarios involving fading channels [137]. Even with this approach, the evaluation of (4.17) is very difficult, if at all possible, since γ_{TR} appears in both the numerator and denominator of the argument to the Q-function. At this point, one may resort to numerically averaging (4.17) via a quasi analytical/experimental approach [49, 53] as suggested originally in [37] or a quasi-analytical/simulation approach [50]. Hence, this motivates us to develop an alternative approach to derive closed-form BEP expressions of TR signaling schemes

for a broad class of fading channels.

4.3.2 Sampling Expansion Approach

To enable the BEP analysis of TR signaling schemes, we can use the sampling functions as the set of orthonormal functions to project the received waveform onto the subspace of band-limited functions with approximate dimensionality $2WT$. Further details regarding this sampling expansion approach can be found in Appendix B.3.

Transmitted-Reference

The conditional BEP for TR signaling with AcR can be found by evaluating

$$\mathbb{P}\left\{e|\gamma_{\mathrm{TR}}\right\} = \frac{1}{2}\,\mathbb{P}\left\{Z_{\mathrm{TR}} < 0 | d_0 = +1\right\} + \frac{1}{2}\,\mathbb{P}\left\{Z_{\mathrm{TR}} > 0 | d_0 = -1\right\}. \tag{4.18}$$

To derive the conditional BEP in (4.18), we rewrite Z_{TR} in (4.9) as follows:

$$\begin{aligned} Z_{\mathrm{TR}} = \sum_{j=0}^{\frac{N_{\mathrm{s}}}{2}-1} \int_0^T & \Big[\breve{b}_{\mathrm{r}}(t + j2T_{\mathrm{f}} + c_j T_{\mathrm{p}}) + \widetilde{n}(t + j2T_{\mathrm{f}} + c_j T_{\mathrm{p}})\Big] \\ & \times \Big[d_0 \breve{b}_{\mathrm{d}}(t + j2T_{\mathrm{f}} + c_j T_{\mathrm{p}} + T_{\mathrm{r}}) + \widetilde{n}(t + j2T_{\mathrm{f}} + c_j T_{\mathrm{p}} + T_{\mathrm{r}})\Big] dt, \end{aligned} \tag{4.19}$$

where $\breve{b}_{\mathrm{r}}(t) \triangleq (b_{\mathrm{r}} * h * h_{\mathrm{ZF}})(t)$, $\breve{b}_{\mathrm{d}}(t) \triangleq (b_{\mathrm{d}} * h * h_{\mathrm{ZF}})(t)$, and $h_{\mathrm{ZF}}(t)$ is the impulse response of the BPZF. Note that if the symbol interval is less than the coherence time, all pairs of separated pulses will experience the same channel; hence $\breve{b}_{\mathrm{r}}(t + j2T_{\mathrm{f}} + c_j T_{\mathrm{p}}) = \breve{b}_{\mathrm{d}}(t + j2T_{\mathrm{f}} + c_j T_{\mathrm{p}} + T_{\mathrm{r}})$ for all $t \in (0, T)$ and j. In this case, we can significantly simplify the expression in (4.19) as follows:

$$\begin{aligned} Z_{\mathrm{TR}} &= \sum_{j=0}^{\frac{N_{\mathrm{s}}}{2}-1} \int_0^T \Big[w_j(t) + \eta_{1,j}(t)\Big]\Big[d_0 w_j(t) + \eta_{2,j}(t)\Big] dt \\ &= \sum_{j=0}^{\frac{N_{\mathrm{s}}}{2}-1} U_j, \end{aligned} \tag{4.20}$$

where we have used $w_j(t) \triangleq \breve{b}_{\rm r}(t + j2T_{\rm f} + c_j T_{\rm p}) = \sqrt{E_{\rm p}} a_j \sum_{l=1}^{L} \alpha_l p(t - \tau_l)$, $\eta_{1,j}(t) \triangleq \widetilde{n}(t + j2T_{\rm f} + c_j T_{\rm p})$, and $\eta_{2,j}(t) \triangleq \widetilde{n}(t + j2T_{\rm f} + c_j T_{\rm p} + T_{\rm r})$, all defined over the interval $[0, T]$. Note that because the noise samples are taken at least $T_{\rm g}$ apart, they are essentially independent, regardless of c_j.[9] We further observe that U_j is simply the integrator output corresponding to the jth received modulated monocycle. Applying the sampling expansion approach developed in Appendix B.3, we can represent U_j as

$$U_j = \frac{1}{2W} \sum_{m=1}^{2WT} \left(d_0 w_{j,m}^2 + w_{j,m}\eta_{2,j,m} + d_0 w_{j,m}\eta_{1,j,m} + \eta_{1,j,m}\eta_{2,j,m} \right), \tag{4.21}$$

where $w_{j,m}$, $\eta_{1,j,m}$, and $\eta_{2,j,m}$, for odd m (even m) are the real (imaginary) parts of the samples of the equivalent low-pass version of $w_j(t)$, $\eta_{1,j}(t)$, and $\eta_{2,j}(t)$ respectively, sampled at Nyquist rate W over the interval $[0, T]$. Conditioned on d_0 and $a_j = +1$, we can express (4.21) in the form of a summation of squares:

$$U_{j|d_0=+1} = \sum_{m=1}^{2WT} \left[\left(\frac{1}{\sqrt{2W}} w_{j,m} + \beta_{1,j,m} \right)^2 - \beta_{2,j,m}^2 \right], \tag{4.22}$$

$$U_{j|d_0=-1} = \sum_{m=1}^{2WT} \left[-\left(\frac{1}{\sqrt{2W}} w_{j,m} - \beta_{2,j,m} \right)^2 + \beta_{1,j,m}^2 \right], \tag{4.23}$$

where $\beta_{1,j,m} = \frac{1}{2\sqrt{2W}}(\eta_{2,j,m} + \eta_{1,j,m})$ and $\beta_{2,j,m} = \frac{1}{2\sqrt{2W}}(\eta_{2,j,m} - \eta_{1,j,m})$ are statistically independent Gaussian r.v.'s with variance $\sigma_{\rm TR}^2 = \frac{N_0}{4}$. Due to the statistical symmetry of U_j with respect to d_0, we simply need to calculate the BEP conditioned on $d_0 = +1$. For notational simplicity, we define the normalized r.v.'s Y_1, Y_2, Y_3, and Y_4 as

$$Y_1 \triangleq \frac{1}{2\sigma_{\rm TR}^2} \sum_{j=0}^{\frac{N_{\rm s}}{2}-1} \sum_{m=1}^{2WT} \left(\frac{1}{\sqrt{2W}} w_{j,m} + \beta_{1,j,m} \right)^2,$$

$$Y_2 \triangleq \frac{1}{2\sigma_{\rm TR}^2} \sum_{j=0}^{\frac{N_{\rm s}}{2}-1} \sum_{m=1}^{2WT} \beta_{2,j,m}^2,$$

$$Y_3 \triangleq \frac{1}{2\sigma_{\rm TR}^2} \sum_{j=0}^{\frac{N_{\rm s}}{2}-1} \sum_{m=1}^{2WT} \left(\frac{1}{\sqrt{2W}} w_{j,m} - \beta_{2,j,m} \right)^2,$$

[9] As a result, no assumption on c_j is required since the above analysis is independent of $\{c_j\}$.

$$Y_4 \triangleq \frac{1}{2\sigma_{\mathrm{TR}}^2} \sum_{j=0}^{\frac{N_\mathrm{s}}{2}-1} \sum_{m=1}^{2WT} \beta_{1,j,m}^2. \tag{4.24}$$

Conditioned on the channel, Y_1 and Y_3 are noncentral chi-squared r.v.'s, whereas Y_2 and Y_4 are central chi-squared r.v.'s each having $N_\mathrm{s}WT$ degrees of freedom. Both Y_1 and Y_3 have the same non-centrality parameter, given by

$$\mu_{\mathrm{TR}} = \frac{1}{2\sigma_{\mathrm{TR}}^2} \sum_{j=0}^{\frac{N_\mathrm{s}}{2}-1} \int_0^T w_j^2(t)dt = \frac{E_\mathrm{s}}{N_0} \sum_{l=1}^{L_{\mathrm{CAP}}} \alpha_l^2. \tag{4.25}$$

The probability density functions (pdfs) of Y_1 and Y_2 conditioned on μ_{TR} are then given by

$$f_{Y_1|\mu_{\mathrm{TR}}}(y_1) = f_{\mathrm{NC}}(y_1, \mu_{\mathrm{TR}}, q_{\mathrm{TR}}), \tag{4.26}$$

$$f_{Y_2|\mu_{\mathrm{TR}}}(y_2) = f_{\mathrm{C}}(y_2, q_{\mathrm{TR}}), \tag{4.27}$$

where $q_{\mathrm{TR}} = \frac{N_\mathrm{s}WT}{2}$. We have defined the following pdfs for notational convenience

$$f_{\mathrm{NC}}(y, \mu, n) \triangleq e^{-(y+\mu)} \left(\frac{y}{\mu}\right)^{\frac{(n-1)}{2}} I_{n-1}\left(2\sqrt{y\mu}\right), \quad y \geq 0$$

$$f_{\mathrm{C}}(y, n) \triangleq \frac{y^{(n-1)}}{(n-1)!} \exp\left(-y\right), \qquad y \geq 0$$

where $I_{n-1}(\cdot)$ is the $(n-1)$th order modified Bessel function of the first kind. The functions $f_{\mathrm{NC}}(y, \mu, n)$ and $f_{\mathrm{C}}(y, n)$ respectively are the pdfs of the noncentral and central chi-squared r.v.'s with $2n$ degrees of freedom and non-centrality parameter μ [137]. Using (4.26) and (4.27) and the fact that $\gamma_{\mathrm{TR}} = \mu_{\mathrm{TR}}/2$, the conditional BEP in (4.18) becomes

$$\begin{aligned} \mathbb{P}\left\{e|\gamma_{\mathrm{TR}}\right\} &= \mathbb{P}\left\{Y_1 < Y_2 | d_0 = +1\right\} \\ &= \frac{e^{-\mu_{\mathrm{TR}}/2}}{2^{q_{\mathrm{TR}}}} \sum_{n=0}^{q_{\mathrm{TR}}-1} \frac{(\mu_{\mathrm{TR}}/2)^n}{n!} \sum_{k=n}^{q_{\mathrm{TR}}-1} \frac{1}{2^k} \frac{(k+q_{\mathrm{TR}}-1)!}{(k-n)!(q_{\mathrm{TR}}+n-1)!}, \end{aligned} \tag{4.28}$$

where the detailed derivation of (4.28) can be found in Appendix B.4. Recall that the conditional BEP in (4.16), obtained by the Gaussian approximation, has the γ_{TR} appearing in both the numerator and denominator of the Gaussian Q-function, which makes the BEP analysis in fading channels intractable. In contrast, the form in (4.28) is desirable as it enables the averaging of $\mathbb{P}\{e|\gamma_{\mathrm{TR}}\}$ with respect to γ_{TR} as follows:

$$\begin{aligned} P_{\mathrm{e,TR}} &= \mathbb{E}_{\gamma_{\mathrm{TR}}}\Big\{\mathbb{P}\left\{e|\gamma_{\mathrm{TR}}\right\}\Big\} \\ &= \frac{1}{2^{q_{\mathrm{TR}}}}\sum_{n=0}^{q_{\mathrm{TR}}-1}\frac{\mathbb{E}_{\mu_{\mathrm{TR}}}\left\{(\mu_{\mathrm{TR}}/2)^n e^{-\mu_{\mathrm{TR}}/2}\right\}}{n!}\sum_{k=n}^{q_{\mathrm{TR}}-1}\frac{1}{2^k}\frac{(k+q_{\mathrm{TR}}-1)!}{(k-n)!(q_{\mathrm{TR}}+n-1)!} \\ &= \frac{1}{2^{q_{\mathrm{TR}}}}\left[\sum_{n=0}^{q_{\mathrm{TR}}-1}\frac{(-j)^n}{n!}\frac{d^n}{dv^n}\psi_{\mu_{\mathrm{TR}}}(jv/2)\Big|_{jv=-1}\sum_{k=n}^{q_{\mathrm{TR}}-1}\frac{1}{2^k}\frac{(k+q_{\mathrm{TR}}-1)!}{(k-n)!(q_{\mathrm{TR}}+n-1)!}\right] \\ &\triangleq P_{\mathrm{e}}(\psi_{\mu_{\mathrm{TR}}}(jv),\, q_{\mathrm{TR}}), \end{aligned} \tag{4.29}$$

where $\psi_{\mu_{\mathrm{TR}}}(jv) \triangleq \mathbb{E}\left\{\exp(jv\mu_{\mathrm{TR}})\right\}$ is the characteristic function (CF) of μ_{TR}. When the channel is resolvable and multipath components are statistically independent, $\psi_{\mu_{\mathrm{TR}}}(jv) = \prod_{l=1}^{L_{\mathrm{CAP}}}\psi_l(\frac{jvE_{\mathrm{s}}}{N_0})$, where $\psi_l(jv)$ is the CF of α_l^2 whose closed-form expression is known for a broad class of channel fading statistics [137]. Therefore, (4.29) gives us a closed-form expression for the BEP of TR signaling with AcR.

Next, we extend the above analysis to derive the BEP of TR signaling with modified AcR. In this case, the variance of $\eta_{1,j,m}/\sqrt{2W}$ is now reduced to N_0/N_{s} due to the noise averaging effect in (4.10). As a result, the variance σ^2_{ATR} of $\beta_{1,j,m}$ and $\beta_{2,j,m}$ becomes

$$\sigma^2_{\mathrm{ATR}} = \frac{\mathbb{V}\left\{\eta_{2,j,m}\right\} + \mathbb{V}\left\{\eta_{1,j,m}\right\}}{8W} = \frac{N_0(N_{\mathrm{s}}+2)}{8N_{\mathrm{s}}}, \tag{4.30}$$

and the non-centrality parameter of Y_1 in (4.24) becomes

$$\mu_{\mathrm{ATR}} \triangleq \frac{1}{2\sigma^2_{\mathrm{ATR}}}\sum_{j=0}^{\frac{N_{\mathrm{s}}}{2}-1}\int_0^T w_j^2(t)dt = \frac{2N_{\mathrm{s}}}{N_{\mathrm{s}}+2}\left(\frac{E_{\mathrm{s}}}{N_0}\sum_{l=1}^{L_{\mathrm{CAP}}}\alpha_l^2\right). \tag{4.31}$$

Note that the non-centrality parameter of a modified AcR is at most two times larger

than that of AcR from Table 4.1. Using (4.29), the BEP of TR signaling with a modified AcR can be written as

$$P_{\mathrm{e,ATR}} = P_{\mathrm{e}}(\psi_{\mu_{\mathrm{ATR}}}(jv), q_{\mathrm{TR}}), \tag{4.32}$$

where $\psi_{\mu_{\mathrm{ATR}}}(jv) \triangleq \mathbb{E}\left\{\exp(jv\mu_{\mathrm{ATR}})\right\}$ is the CF of μ_{ATR}.

Differential Transmitted-Reference

Using the sampling approach, we can represent U_j as

$$U_j = \frac{1}{2W}\sum_{m=1}^{2WT}\left(d_0 w_{j,m}^2 + e_{-1}w_{j,m}\eta_{2,j,m} + e_0 w_{j,m}\eta_{1,j,m} + \eta_{1,j,m}\eta_{2,j,m}\right), \tag{4.33}$$

where $w_{j,m}$, $\eta_{1,j,m}$, and $\eta_{2,j,m}$, for odd m (even m) are the real (imaginary) parts of the samples of the equivalent low-pass version of $w_j(t) \triangleq (b*h*h_{\mathrm{ZF}})(t+jT_{\mathrm{f}}+c_jT_{\mathrm{p}}) = \sqrt{E_{\mathrm{p}}}a_j\sum_{l=1}^{L}\alpha_l p(t-\tau_l)$, $\eta_{1,j}(t) \triangleq \widetilde{n}(t+jT_{\mathrm{f}}+c_jT_{\mathrm{p}}-N_{\mathrm{s}}T_{\mathrm{f}})$, and $\eta_{2,j}(t) \triangleq \widetilde{n}(t+jT_{\mathrm{f}}+c_jT_{\mathrm{p}})$, respectively, sampled at Nyquist rate W over the interval $[0,T]$. Similar to TR signaling, our following analysis requires no assumption on $\{c_j\}$, and we exploit statistical symmetry of U_j with respect to d_0 and $\{a_j\}$. Conditioned on $d_0=+1$, we can express (4.33) in the form of (4.22),[10] where in this case $\beta_{1,j,m} = \frac{1}{2\sqrt{2W}}(e_{-1}\eta_{2,j,m}+e_0\eta_{1,j,m})$ and $\beta_{2,j,m} = \frac{1}{2\sqrt{2W}}(e_{-1}\eta_{2,j,m}-e_0\eta_{1,j,m})$ are statistically independent Gaussian r.v.'s. with variance $\sigma_{\mathrm{DTR}}^2 = \frac{N_0}{4}$. Due to symmetry, we only need to consider Y_1 and Y_2 in (4.24), where the non-centrality parameter of Y_1 is now given by

$$\mu_{\mathrm{DTR}} \triangleq \frac{1}{2\sigma_{\mathrm{DTR}}^2}\sum_{j=0}^{N_{\mathrm{s}}-1}\int_0^T w_j^2(t)dt = \frac{2E_{\mathrm{s}}}{N_0}\sum_{l=1}^{L_{\mathrm{CAP}}}\alpha_l^2, \tag{4.34}$$

and the pdfs of Y_1 and Y_2 conditioned on μ_{DTR} are given by

$$f_{Y_1|\mu_{\mathrm{DTR}}}(y_1) = f_{\mathrm{NC}}(y_1, \mu_{\mathrm{DTR}}, q_{\mathrm{DTR}}), \tag{4.35}$$

$$f_{Y_2|\mu_{\mathrm{DTR}}}(y_2) = f_{\mathrm{C}}(y_2, q_{\mathrm{DTR}}), \tag{4.36}$$

[10] When $d_0 = +1$, the pairs of differentially encoded bits are either $(e_{-1}, e_0) = (+1,+1)$ or $(e_{-1}, e_0) = (-1,-1)$ with probability $\frac{1}{2}$ each. By symmetry, we only need to consider $(e_{-1}, e_0) = (+1,+1)$.

Table 4.1: TR Signaling schemes

Signaling	Non-centrality parameter of Y_1	Variance of $\beta_{1,j,m}$	Degrees of freedom of Y_1
TR	$\frac{E_\mathrm{s}}{N_0}\sum_{l=1}^{L_\mathrm{CAP}}\alpha_l^2$	$\frac{N_0}{4}$	$\frac{N_\mathrm{s}WT}{2}$
ATR	$\frac{2N_\mathrm{s}}{(N_\mathrm{s}+2)}\left(\frac{E_\mathrm{s}}{N_0}\sum_{l=1}^{L_\mathrm{CAP}}\alpha_l^2\right)$	$\frac{N_0(N_\mathrm{s}+2)}{8N_\mathrm{s}}$	$\frac{N_\mathrm{s}WT}{2}$
DTR	$\frac{2E_\mathrm{s}}{N_0}\sum_{l=1}^{L_\mathrm{CAP}}\alpha_l^2$	$\frac{N_0}{4}$	$N_\mathrm{s}WT$
ADTR	$\frac{4N_\mathrm{s}}{(N_\mathrm{s}+1)}\left(\frac{E_\mathrm{s}}{N_0}\sum_{l=1}^{L_\mathrm{CAP}}\alpha_l^2\right)$	$\frac{N_0(N_\mathrm{s}+1)}{8N_\mathrm{s}}$	$N_\mathrm{s}WT$

where $q_\mathrm{DTR} = N_\mathrm{s}WT$. As shown in Table 4.1, we can observe that the basic difference between TR and DTR signaling lies not only in a doubled non-centrality parameter, but also in double the degrees of freedom. The non-centrality parameter reflects the amount of useful energy captured by the correlator at the receiver, hence, larger values result in better performance. On the contrary, the degrees of freedom of Y_1 account for the noise accumulation in the integration interval; thus, larger values result in poorer performance. Following the derivation leading to (4.29), the BEP of DTR signaling with AcR can be written as

$$P_{\mathrm{e,DTR}} = P_\mathrm{e}(\psi_{\mu_\mathrm{DTR}}(jv), q_\mathrm{DTR}), \tag{4.37}$$

where $\psi_{\mu_\mathrm{DTR}}(jv) \triangleq \mathbb{E}\left\{\exp(jv\mu_\mathrm{DTR})\right\}$ is the CF of μ_DTR.

For DTR signaling with a modified AcR, the non-centrality parameter of Y_1 in (4.24) becomes

$$\mu_\mathrm{ADTR} \triangleq \frac{1}{2\sigma^2_\mathrm{ADTR}}\sum_{j=0}^{N_\mathrm{s}-1}\int_0^T w_j^2(t)dt = \frac{4N_\mathrm{s}}{(N_\mathrm{s}+1)}\left(\frac{E_\mathrm{s}}{N_0}\sum_{l=1}^{L_\mathrm{CAP}}\alpha_l^2\right), \tag{4.38}$$

where the variance σ^2_{ADTR} of $\beta_{1,j,m}$ and $\beta_{2,j,m}$ is

$$\sigma^2_{\mathrm{ADTR}} = \frac{\mathbb{V}\left\{e_{i-1}\eta_{2,j,m}\right\} + \mathbb{V}\left\{e_i\eta_{1,j,m}\right\}}{8W} = \frac{N_0(N_\mathrm{s}+1)}{8N_\mathrm{s}}. \tag{4.39}$$

The pdfs of Y_1 and Y_2 conditioned on μ_{ADTR} are now given by

$$f_{Y_1|\mu_{\mathrm{ADTR}}}(y_1) = f_{\mathrm{NC}}(y_1, \mu_{\mathrm{ADTR}}, q_{\mathrm{DTR}}), \tag{4.40}$$

$$f_{Y_2|\mu_{\mathrm{ADTR}}}(y_2) = f_{\mathrm{C}}(y_2, q_{\mathrm{DTR}}). \tag{4.41}$$

Following the derivation leading to (4.29), the BEP of DTR signaling with a modified AcR is given by

$$P_{\mathrm{e,ADTR}} = P_{\mathrm{e}}(\psi_{\mu_{\mathrm{ADTR}}}(jv), q_{\mathrm{DTR}}). \tag{4.42}$$

where $\psi_{\mu_{\mathrm{ADTR}}}(jv) \triangleq \mathbb{E}\left\{\exp(jv\mu_{\mathrm{ADTR}})\right\}$ is the CF of μ_{ADTR}.

4.3.3 SNR Penalty

With the closed-form expression in (4.29), one can now answer the following question: What is the SNR penalty associated with TR signaling with AcR when compared to ARake and PRake receivers? In the following, we provide some numerical results and a computationally simple lower bound on (4.29) to quantify the SNR penalty associated with TR signaling with AcR.

The ideal Rake receiver with full diversity is known as the ARake receiver [138], whereas the PRake receiver refers to a lower complexity Rake receiver that combines only the first incoming L_p multipath components [139]. Note that both receivers assume perfect channel estimation. By using the alternative expression for Gaussian Q-function [137], the BEP of BPSK for a PRake receiver in independent Nakagami channels with uniform PDP, is given by [137]

$$P_{\mathrm{e,PRake}} = \frac{1}{\pi}\int_0^{\frac{\pi}{2}} \left(1 + \frac{\bar{\gamma}}{m\sin^2\theta}\right)^{-mL_\mathrm{p}} d\theta, \tag{4.43}$$

where $\bar{\gamma} = \frac{E_s}{LN_0}$. When $L_p = L$, (4.43) simply becomes the BEP of BPSK for the ARake receiver. From (4.28), we can derive a simple lower bound on the BEP of TR signaling with AcR by using a first order Taylor series approximation of (4.28) about $\mathbb{E}\{\mu_{TR}\}$ to obtain

$$P_{e,TR} \geq \frac{\exp\left(-\mathbb{E}\{\mu_{TR}\}/2\right)}{2^{q_{TR}}} \sum_{i=0}^{q_{TR}-1} \frac{\left(\mathbb{E}\{\mu_{TR}\}/2\right)^i}{i!} \sum_{k=i}^{q_{TR}-1} \frac{1}{2^k} \frac{(k+q_{TR}-1)!}{(k-i)!(q_{TR}+i-1)!}, \tag{4.44}$$

where $\mathbb{E}\{\mu_{TR}\} = E_s/N_0$. Note that the right-hand-side of (4.44) becomes a lower bound on $P_{e,TR}$ since the remaining terms in the Taylor series expansion of (4.28) about $\mathbb{E}\{\mu_{TR}\}$ are all positive.

4.4 Numerical Results

In this section, we evaluate the performance of TR and DTR signaling schemes based on our derived BEP expressions in previous sections. For UWB channels, it has been verified experimentally that the multipath gains can be modeled as Nakagami-m r.v.'s [38]. As a result, we consider a dense resolvable multipath channel, where each multipath gain is Nakagami distributed with fading severity index m and uniform PDP with $L = 40$. Figures 4-3 and 4-4 show the BEP performance of TR signaling with AcR with $N_s = 2$ and $N_s = 16$ respectively. Both figures show that the performance of TR signaling with AcR generally improves as WT increases. This is expected since more multipath components are captured by the receiver, resulting in an increase in diversity order as well as energy capture. It can also be seen that results based on the Gaussian approximation can differ from our closed-form BEP expression in (4.29). Furthermore, the accuracy of the Gaussian approximation improves as WT and N_s increase as explained in Section 4.3.1.

The effect of WT on the BEP performance of TR signaling with $N_s = 16$ is shown in Fig. 4-5. It can be observed that the BEP decreases with WT until it reaches the

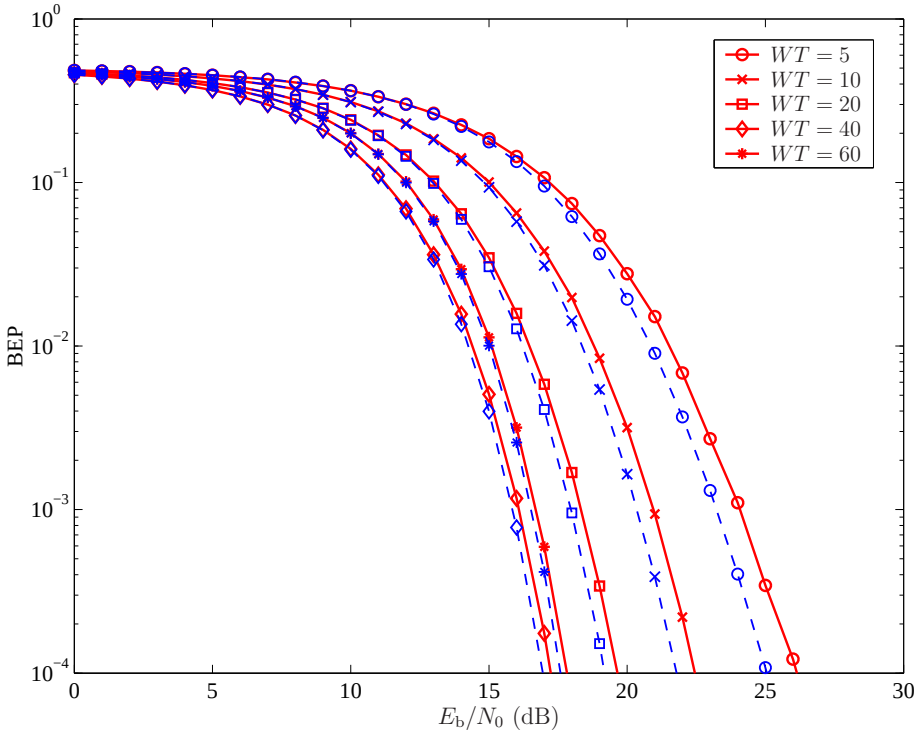

Figure 4-3: BEP performance of TR signaling with AcR with $m = 2.0$ and $N_s = 2$. The solid and dashed lines denote the Gaussian approximation and sampling expansion, respectively.

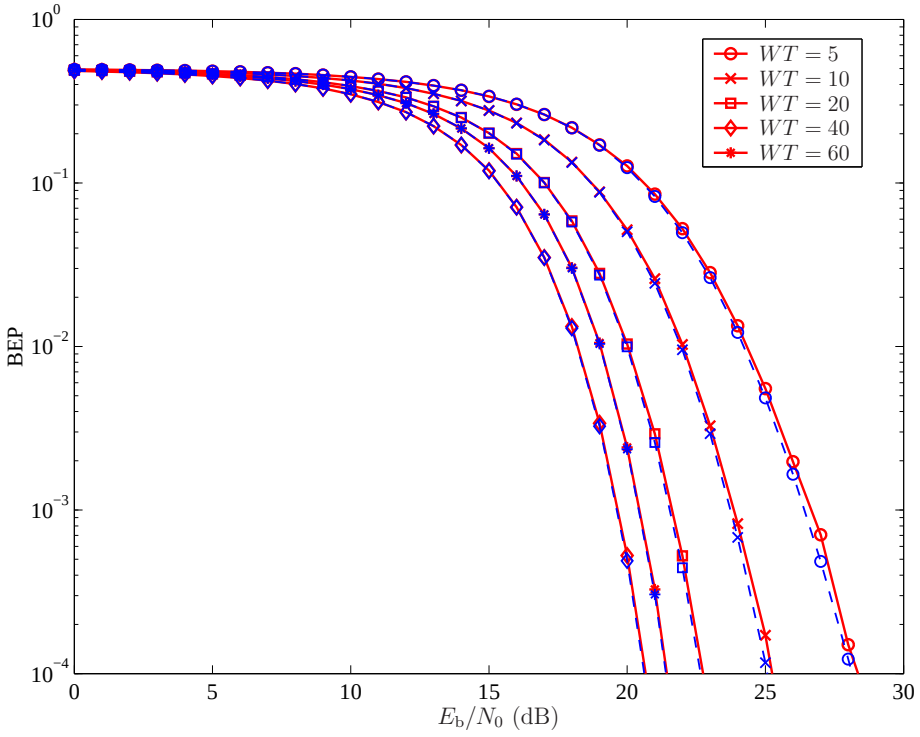

Figure 4-4: BEP performance of TR signaling with AcR with $m = 2.0$ and $N_s = 16$. The solid and dashed lines denote the Gaussian approximation and sampling expansion, respectively.

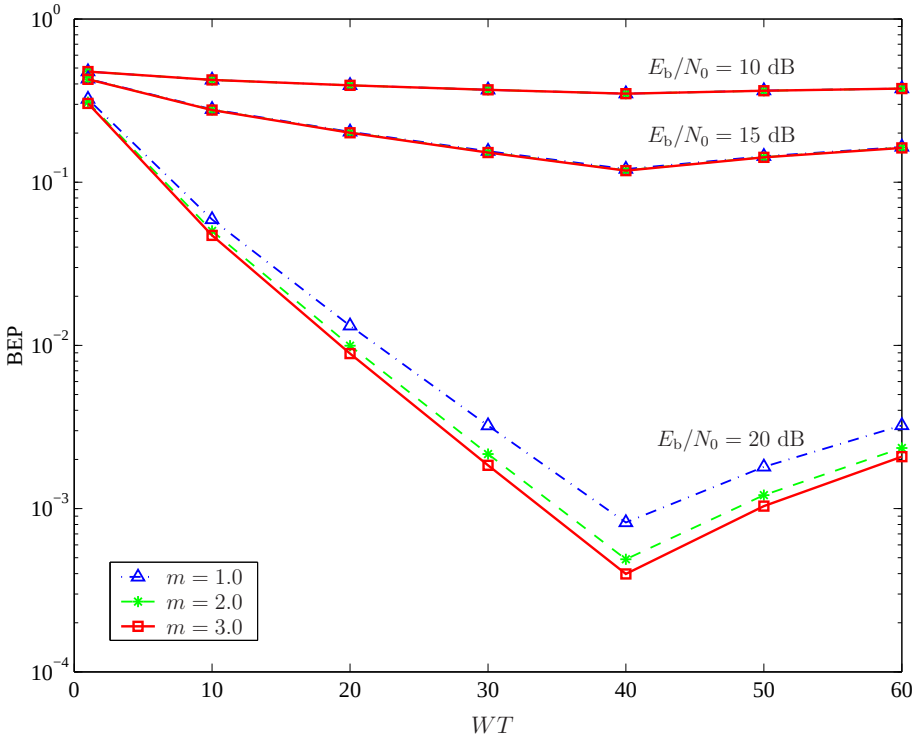

Figure 4-5: Effect of integration interval T of AcR on the performance of TR signaling.

optimum value of 40, which is equal to L.[11] This behavior, which is more pronounced at high E_b/N_0, can be explained by the fact that the loss due to noise accumulation is less than the gain of capturing more multipath energy as WT increases. However, increasing WT beyond the optimum value will only accumulate more noise energy, as reflected in the increase of BEP after $WT = 40$. In addition, we can also see that the diversity gain is larger for the higher fading severity index m, especially for large values of E_b/N_0.

In Fig. 4-6, the effect of N_s on the BEP performance of TR signaling with AcR is plotted using (4.29) with $WT = L$. For a fixed E_b/N_0, increasing N_s is equivalent to increasing the degrees of freedom of q_{TR} in (4.28), which leads to more noise energy accumulation. This can be seen as the gradual performance degradation as N_s increases in Fig. 4-6. In order to improve the performance of TR signaling with AcR, the modified AcR can be used and the BEP performance comparison is shown in Fig.

[11] Note that the optimum integration interval of AcR is not always equal to L, and depends on the PDP of the channel.

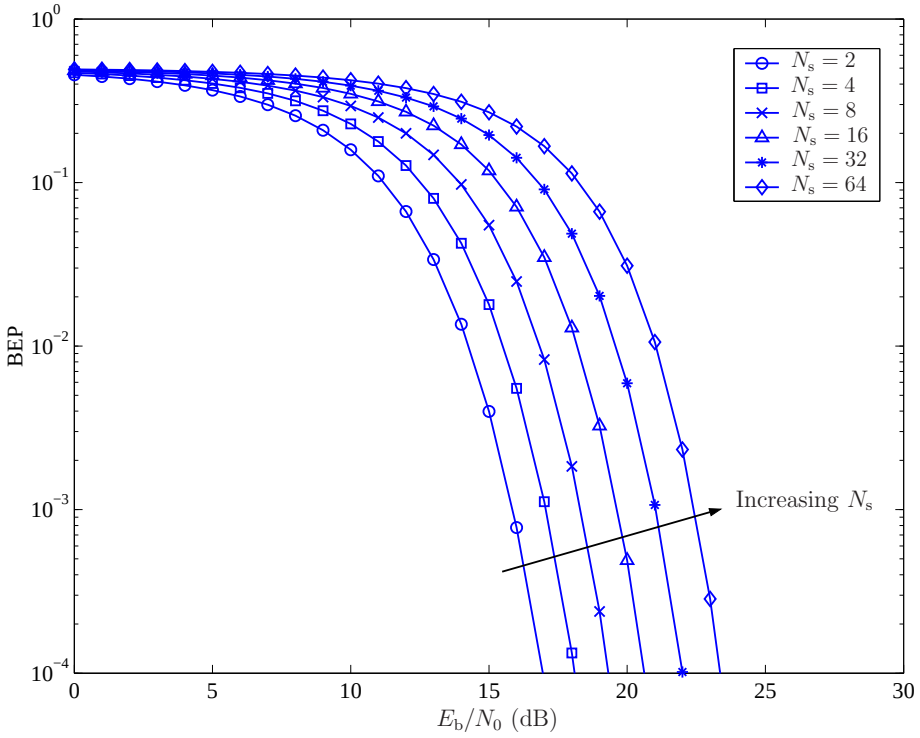

Figure 4-6: Effect of N_s on the performance of TR signaling with AcR with $m = 2.0$ and $WT = L$.

4-7 using (4.29) and (4.32). In Fig. 4-7, we compares the BEP performance of TR and DTR signaling schemes when $WT = L$. The difference between TR and DTR signaling is about 2 dB, slightly less than the 3 dB expected from the doubling of the non-centrality parameter shown in Table 4.1. This loss of 1 dB can be attributed to more noise accumulation as $q_{\text{DTR}} = 2q_{\text{TR}}$. Note that the optimum WT is L for uniform PDP as shown in Fig. 4-5. By comparing the performance between an AcR and a modified AcR, it can be observed in Fig. 4-7 that the modified AcR performs better than the AcR by about 3 dB for both signaling schemes. This accounts for the increase of about a factor of two in the instantaneous received SNR through the non-centrality parameter when a modified AcR is used, as indicated in Table 4.1.

Lastly, in Fig. 4-8, the lower bound in (4.44) is plotted against the exact BEP in (4.30) when $WT = L$.[12] In addition, the BEP performance curves of the ARake and PRake receivers using (4.43) are included to obtain the SNR penalty associated

[12]Fig.8 shows the BEP as low as 10^{-6} only to illustrate the behavior of the lower bound; these extremely low BEP's are not practical, especially for wireless mobile communications.

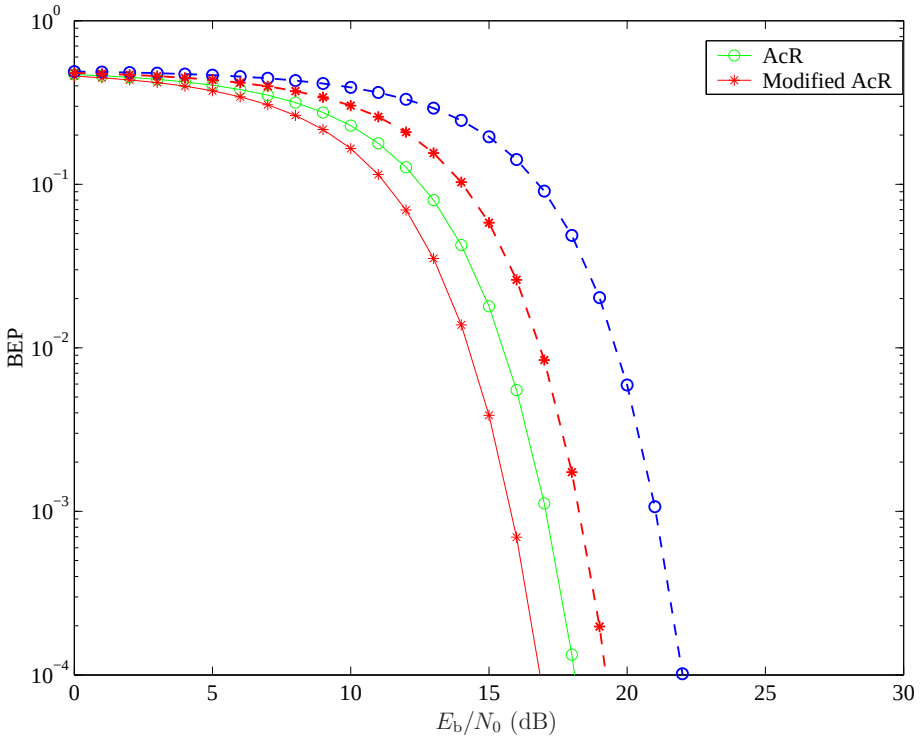

Figure 4-7: BEP performance of TR and DTR signaling schemes with $m = 2.0$ and $WT = L$. The solid and dashed lines indicate the TR and DTR signaling, respectively.

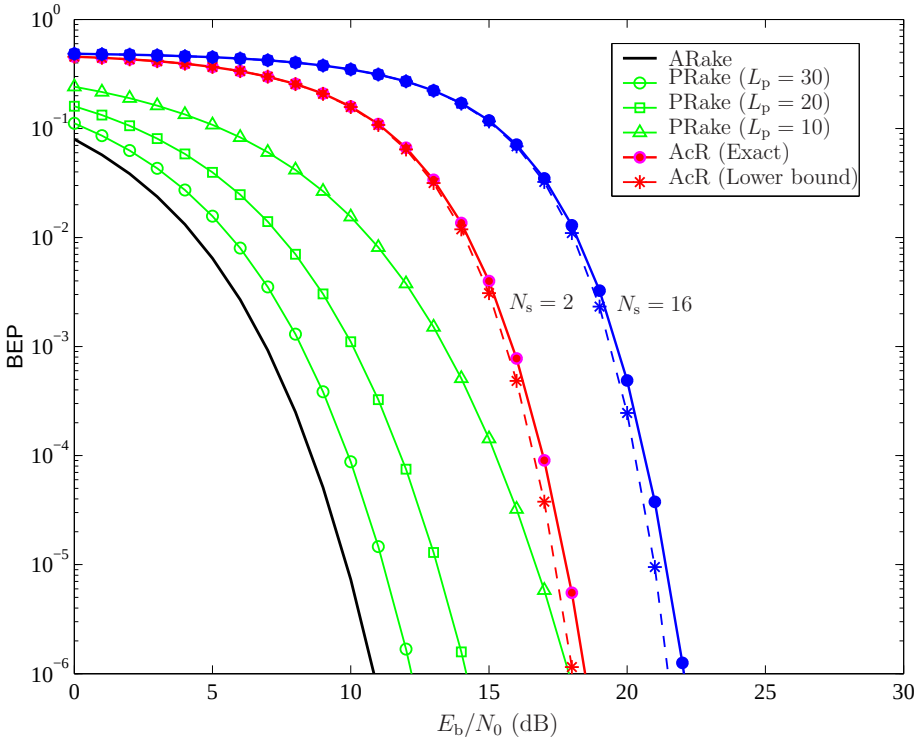

Figure 4-8: BEP performance comparison between TR signaling with AcR, PRake and ARake receivers with $m = 2.0$ and $WT = L$. The dashed lines indicate the lower bound in (4.44).

with AcR. It can be observed that the lower bound in (4.44) is quite close to the exact expression in (4.29) for the BEP range of interest. Hence, this computationally simple lower bound can be used for assessing the SNR penalty associated with an AcR, as compared to ARake and PRake receivers. For example, it can be seen in Fig. 4-8 that the AcR suffers a SNR penalty of about 8.8 dB and 12.6 dB respectively at BEP $= 10^{-3}$ for $N_{\rm s} = 2$ and $N_{\rm s} = 16$ with respect to ARake receiver. Observe that TR system performs more than 6 dB worse than the ideal system. The reasons due to this SNR gap can be accounted by the 3 dB loss due to reference energy, 3 dB loss due to noncoherent-based detection, and the remaining SNR loss due to noise accumulation in the presence of multipath channels. From (4.16), we see that this effect is captured by the term $N_{\rm s}WT/4$ in the denominator. In addition, the SNR penalty decreases with respect to PRake receiver when $L_{\rm p}$ decreases. At BEP $= 10^{-3}$, the SNR penalty associated with AcR, as compared to PRake receiver with $L_{\rm p} = 10$ is about 2.1 dB and 5.9 dB respectively for $N_{\rm s} = 2$ and $N_{\rm s} = 16$.

Chapter 5

Transmitted-Reference Schemes in the Presence of Narrowband Interference

In this chapter, we analyze the performance of TR and DTR signaling schemes in the presence of NBI. We adopt the sampling expansion approach developed in Chapter 4 to analyze the BEP performance in the presence of NBI. We develop a quasi-analytical method as well as an approximate analytical method to evaluate the BEP of TR and DTR signaling in the presence of NBI and show that the approximate analytical method is particularly useful in obtaining BEP expressions that provide insight into the effect of NBI.

5.1 Narrowband Interference Analysis

In the presence of NBI, the received signal can be written as $r(t) = (h * s)(t) + J(t) + n(t)$, where $J(t)$ denotes the NBI and $s(t)$ denotes the signal transmitted via TR or DTR signaling. The autocorrelation function of the superposition of the two independent noise processes, $n_{\mathrm{T}}(t) \triangleq J(t)+n(t)$, is given by $R_{n_{\mathrm{T}}}(\tau) = R_{\mathrm{J}}(\tau)+\frac{N_0}{2}\delta(\tau)$, where $R_{\mathrm{J}}(\tau) = \mathbb{E}\{J(t)J(t+\tau)\}$. Since the bandwidth of typical NBI is smaller than that of the transmitted pulse, the autocorrelation function of $\widetilde{n}_{\mathrm{T}}(t)$, the bandpass

filtered version of $n_{\mathrm{T}}(t)$, is given by

$$R_{\widetilde{n}_{\mathrm{T}}}(\tau) = R_{\mathrm{J}}(\tau) + WN_0 \operatorname{sinc}(W\tau)\cos(2\pi f_{\mathrm{c}}\tau). \tag{5.1}$$

As in [64], we model the NBI as a single-tone continuous-wave signal given by[1]

$$J(t) = \alpha_{\mathrm{J}}\sqrt{2J_0}\cos(2\pi f_{\mathrm{J}}t + \theta), \tag{5.2}$$

where J_0 is the average NBI power, α_{J} is a slowly-varying Rayleigh distributed r.v. with $\mathbb{E}\{\alpha_{\mathrm{J}}^2\} = 1$, f_{J} is the NBI carrier frequency, and θ is the random phase, uniformly distributed over $[0, 2\pi)$.[2] Thus, $R_{\mathrm{J}}(\tau) = J_0\cos(2\pi f_{\mathrm{J}}\tau)$, which means that $\widetilde{n}_{\mathrm{T}}(t)$ is colored, and the samples of $\widetilde{n}_{\mathrm{T}}(t)$ taken at an interval of $1/W$ are correlated. In the following, we derive the BEP of TR and DTR signaling with an AcR in the presence of NBI, where we define $\mathsf{SIR} \triangleq E_{\mathrm{s}}/(N_{\mathrm{s}}T_{\mathrm{f}}J_0)$. The extension to modified AcR is straightforward and omitted for brevity.

5.1.1 Transmitted-Reference

By incorporating the NBI given in (5.2) and using the sampling expansion approach proposed in Chapter 4.3.2, we can rewrite U_j in (4.21) as

$$U_j = \frac{1}{2W}\sum_{m=1}^{2WT}\Big[d_0 w_{j,m}^2 + w_{j,m}(\xi_{2,j,m} + \eta_{2,j,m}) + d_0 w_{j,m}(\xi_{1,j,m} + \eta_{1,j,m}) + (\xi_{1,j,m} + \eta_{1,j,m})(\xi_{2,j,m} + \eta_{2,j,m})\Big], \tag{5.3}$$

where $\xi_{1,j,m}$ and $\xi_{2,j,m}$, for odd m (even m) respectively are the real (imaginary) parts of the samples of the equivalent low-pass version of $\xi_{1,j}(t)$ and $\xi_{2,j}(t)$, given by

$$\xi_{1,j}(t) = \alpha_{\mathrm{J}}\sqrt{2J_0}\cos\left[2\pi f_{\mathrm{J}}\left(t + j2T_{\mathrm{f}} + c_j T_{\mathrm{p}}\right) + \theta\right],$$

[1] Results in [64] show that NBI can be reasonably well approximated by a tone interferer, where the interfering node is located at a fixed distance from the receiver.

[2] Unlike UWB signals, NBI experiences frequency flat fading and the amplitude α_{J} is assumed to be constant over at least two symbols of TR signaling.

$$\xi_{2,j}(t) = \alpha_{\rm J}\sqrt{2J_0}\cos\left[2\pi f_{\rm J}\left(t + j2T_{\rm f} + c_jT_{\rm p} + T_{\rm r}\right) + \theta\right]. \tag{5.4}$$

The rest of the terms in (5.3) are defined similarly to those in (4.21). By conditioning on d_0, we can rewrite (5.3) in the form of (4.22) and (4.23), where $\beta_{1,j,m} \triangleq \frac{1}{2\sqrt{2W}}(\eta_{2,j,m} + \xi_{2,j,m} + \eta_{1,j,m} + \xi_{1,j,m})$ and $\beta_{2,j,m} \triangleq \frac{1}{2\sqrt{2W}}(\eta_{2,j,m} + \xi_{2,j,m} - \eta_{1,j,m} - \xi_{1,j,m})$. Further conditioning on θ, $\alpha_{\rm J}$, and $\{c_j\}$, the quantities $\xi_{1,j,m}$ and $\xi_{2,j,m}$ in (5.4) are deterministic, and the conditional variance $\sigma^2_{\rm TR}$ of $\beta_{1,j,m}$ and $\beta_{2,j,m}$ is simply $\frac{N_0}{4}$. Thus, the statistical characterization of U_j when conditioned on θ, $\alpha_{\rm J}$, $\{c_j\}$, $\{a_j\}$, and $\{\alpha_l\}$ is no longer symmetric with respect to d_0 due to the presence of the interference term. Note that $U_{j|d_0=+1}$ is simply the difference of two noncentral chi-squared r.v.'s with the same degrees of freedom, but different non-centrality parameters. As a result, we need to separately calculate the conditional BEP with respect to d_0 to obtain the overall BEP.

First, we derive the non-centrality parameters of Y_1 and Y_2 when conditioned on Ψ as follows:

$$\begin{aligned}
\mu^{\rm (NBI)}_{{\rm TR},Y_1} &\triangleq \frac{1}{2\sigma^2_{\rm TR}}\sum_{j=0}^{\frac{N_{\rm s}}{2}-1}\int_0^T\left[w_j(t) + \frac{\xi_{1,j}(t)+\xi_{2,j}(t)}{2}\right]^2 dt \\
&\approx \frac{E_{\rm s}}{N_0}\sum_{l=1}^{L_{\rm CAP}}\alpha_l^2 + \frac{\alpha_{\rm J}^2N_{\rm s}J_0T}{2N_0} + \frac{\alpha_{\rm J}^2N_{\rm s}J_0T}{2N_0}\cos(2\pi f_{\rm J}T_{\rm r}) \\
&\quad + \frac{4\alpha_{\rm J}|\widehat{P}(f_{\rm J})|\sqrt{2E_{\rm p}J_0}\cos\left(\pi f_{\rm J}T_{\rm r}\right)}{N_0}\sum_{j=0}^{\frac{N_{\rm s}}{2}-1}a_j \\
&\quad \times \sum_{l=1}^{L_{\rm CAP}}\alpha_l\cos\left(2\pi f_{\rm J}\left(\tau_l + j2T_{\rm f} + c_jT_{\rm p} + T_{\rm r}/2\right) + \varphi\right), \qquad (5.5) \\
\mu^{\rm (NBI)}_{{\rm TR},Y_2} &\triangleq \frac{1}{8\sigma^2_{\rm TR}}\sum_{j=0}^{\frac{N_{\rm s}}{2}-1}\int_0^T(\xi_{2,j}(t) - \xi_{1,j}(t))^2dt \\
&\approx \frac{\alpha_{\rm J}^2N_{\rm s}J_0T}{2N_0} - \frac{\alpha_{\rm J}^2N_{\rm s}J_0T}{2N_0}\cos(2\pi f_{\rm J}T_{\rm r}), \qquad (5.6)
\end{aligned}$$

where $\Psi \triangleq \left\{\alpha_{\rm J}, \{\alpha_l\}_{l=1}^{L}, \varphi, \{c_j\}_{j=1}^{N_{\rm s}/2}, \{a_j\}_{j=1}^{N_{\rm s}/2}\right\}$. The detailed derivation and the justification of the approximations leading to (5.5) and (5.6), as well as the definition of φ

and $\widehat{P}(f_{\rm J})$ can be found in Appendix C.1. Note that Y_2 in (4.24) is now a noncentral chi-squared r.v. due to the presence of NBI. From (5.5) and (5.6), it is interesting to see that the NBI affects the performance by changing the conditional means and variances of Y_1 and Y_2.[3] Using (5.5) and (5.6), the conditional pdfs of Y_1 and Y_2 are given by

$$f_{Y_1|\Psi}(y_1) = f_{\rm NC}\left(y_1, \mu^{\rm (NBI)}_{{\rm TR},Y_1}, q_{\rm TR}\right), \tag{5.7}$$

$$f_{Y_2|\alpha_{\rm J}}(y_2) = f_{\rm NC}\left(y_2, \mu^{\rm (NBI)}_{{\rm TR},Y_2}, q_{\rm TR}\right), \tag{5.8}$$

where we have suppressed the conditioning r.v.'s $\{\alpha_l\}$, φ, $\{c_j\}$, and $\{a_j\}$ in (5.8) since (5.6) does not depend on these r.v.'s. Now, to evaluate the BEP for $Z_{\rm TR} \leq 0$ when $d_0 = +1$, we use the inversion theorem [140] to obtain

$$\begin{aligned}
&\mathbb{P}\left\{Z_{\rm TR} \leq 0 | d_0 = +1\right\} \\
&= \frac{1}{2} + \frac{1}{\pi}\int_0^\infty \left(\frac{1}{1+v^2}\right)^{q_{\rm TR}} \mathfrak{Re}\left\{\frac{\mathbb{E}_\Psi\left\{\exp\left(\frac{-jv\mu^{\rm (NBI)}_{{\rm TR},Y_1}}{1+jv}\right)\exp\left(\frac{jv\mu^{\rm (NBI)}_{{\rm TR},Y_2}}{1-jv}\right)\right\}}{jv}\right\} dv,
\end{aligned} \tag{5.9}$$

where $\mathfrak{Re}\{\cdot\}$ denotes the real part. By resorting to a quasi-analytical method, the statistical expectation in (5.9) can be calculated by numerically averaging each argument within the expectation with respect to its corresponding r.v.'s. Alternatively, we can resort to an approximate analytical method, where we consider the last term in (5.5) negligible compared to the first two terms.[4] As a result, we can further suppress the conditioning r.v.'s φ, $\{c_j\}$, and $\{a_j\}$ in (5.7), since the dependence of $\mu^{\rm (NBI)}_{{\rm TR},Y_1}$ on these r.v.'s is now negligible. The approximate BEP conditioned on $d_0 = +1$ can be rewritten as

[3]The mean and variance of a non-central chi-squared r.v. are given by $(k+\mu)$ and $2(k+2\mu)$ respectively, where k is the degrees of freedom and μ is the non-centrality parameter.

[4]The validity of this approximation will be discussed in details in Appendix C and numerical results.

$$
\begin{aligned}
&\mathbb{P}\left\{Z_{\mathrm{TR}} \leq 0 | d_0 = +1\right\} \\
&\simeq \frac{1}{2} + \frac{1}{\pi} \int_0^{\infty} \left(\frac{1}{1+v^2}\right)^{q_{\mathrm{TR}}} \mathfrak{Re}\left\{ \frac{\mathbb{E}_{\{\alpha_l\},\alpha_{\mathrm{J}}} \left\{ \exp\left(\frac{-jv\mu_{\mathrm{TR},Y_1}^{(\mathrm{NBI})}}{1+jv}\right) \exp\left(\frac{jv\mu_{\mathrm{TR},Y_2}^{(\mathrm{NBI})}}{1-jv}\right)\right\}}{jv} \right\} dv \\
&= \frac{1}{2} + \frac{1}{\pi} \int_0^{\infty} \left(\frac{1}{1+v^2}\right)^{q_{\mathrm{TR}}} \mathfrak{Re}\left\{ \frac{\psi_{\mu_{\mathrm{TR}}}\left(\frac{-jv}{1+jv}\right) \psi_{\mathrm{J}}\left(g_{\mathrm{TR},d_0=+1}(jv)\right)}{jv} \right\} dv \\
&\triangleq P_{\mathrm{e}}^{(\mathrm{NBI})}\Big(\psi_{\mu_{\mathrm{TR}}}(jv), \psi_{\mathrm{J}}\left(g_{\mathrm{TR},d_0=+1}(jv)\right), q_{\mathrm{TR}}\Big), \qquad (5.10)
\end{aligned}
$$

where $\psi_{\mu_{\mathrm{TR}}}(jv)$ is defined after (4.29). Given that $\psi_{\mathrm{J}}(jv)$ is the CF of α_{J}^2, $g_{\mathrm{TR},d_0=+1}(jv)$ in (5.10) is defined as follows:

$$
g_{\mathrm{TR},d_0=+1}(jv) \triangleq \frac{-jv}{1+jv} \cdot \frac{N_{\mathrm{s}} J_0 T}{2N_0}\Big[1 + \cos(2\pi f_{\mathrm{J}} T_{\mathrm{r}})\Big] + \frac{jv}{1-jv} \cdot \frac{N_{\mathrm{s}} J_0 T}{2N_0}\Big[1 - \cos(2\pi f_{\mathrm{J}} T_{\mathrm{r}})\Big]. \qquad (5.11)
$$

In the absence of NBI or when $J_0 = 0$, (5.10) gives us an alternative, but equivalent, expression to (4.29) for the BEP of TR signaling with an AcR.[5]

From (4.23), we can observe that $U_{j|d_0=-1}$, when conditioned on Ψ, is also the difference of two noncentral chi-squared r.v.'s with same degrees of freedom, but with different non-centrality parameters. Following the derivation from (5.5) to (5.9), we can again resort to the quasi-analytical method to evaluate $\mathbb{P}\left\{Z_{\mathrm{TR}} > 0 | d_0 = -1\right\}$. We first derive the non-centrality parameters of Y_3 and Y_4 in (4.24) conditioned on Ψ as follows:

$$
\begin{aligned}
\mu_{\mathrm{TR},Y_3}^{(\mathrm{NBI})} \approx{}& \frac{E_{\mathrm{s}}}{N_0} \sum_{l=1}^{L_{\mathrm{CAP}}} \alpha_l^2 + \frac{\alpha_{\mathrm{J}}^2 N_{\mathrm{s}} J_0 T}{2N_0} - \frac{\alpha_{\mathrm{J}}^2 N_{\mathrm{s}} J_0 T}{2N_0} \cos(2\pi f_{\mathrm{J}} T_{\mathrm{r}}) \\
&+ \frac{4\alpha_{\mathrm{J}} |\widehat{P}(f_{\mathrm{J}})| \sqrt{2E_{\mathrm{p}} J_0}\, \sin\left(\pi f_{\mathrm{J}} T_{\mathrm{r}}\right)}{N_0} \sum_{j=0}^{\frac{N_{\mathrm{s}}}{2}-1} a_j
\end{aligned}
$$

[5]Note that the difference in the expressions lies in the fact that we have used the inversion theorem [137, 140] to derive $\mathbb{P}\left\{Z_{\mathrm{TR}} \leq 0 | d_0 = +1\right\}$ in (5.10).

$$\times \sum_{l=1}^{L_{\mathrm{CAP}}} \alpha_l \sin\left(2\pi f_{\mathrm{J}}\left(\tau_l + j2T_{\mathrm{f}} + c_j T_{\mathrm{p}} + T_{\mathrm{r}}/2\right) + \varphi\right), \quad (5.12)$$

$$\mu_{\mathrm{TR},Y_4}^{(\mathrm{NBI})} \approx \frac{\alpha_{\mathrm{J}}^2 N_{\mathrm{s}} J_0 T}{2N_0} + \frac{\alpha_{\mathrm{J}}^2 N_{\mathrm{s}} J_0 T}{2N_0}\cos(2\pi f_{\mathrm{J}} T_{\mathrm{r}}), \quad (5.13)$$

where the detailed derivation and the justification of the approximations leading to (5.12) and (5.13) can be found in Appendix C.2. We then replace $\mu_{\mathrm{TR},Y_1}^{(\mathrm{NBI})}$ and $\mu_{\mathrm{TR},Y_2}^{(\mathrm{NBI})}$ in (5.9) with $\mu_{\mathrm{TR},Y_3}^{(\mathrm{NBI})}$ and $\mu_{\mathrm{TR},Y_4}^{(\mathrm{NBI})}$ to obtain $\mathbb{P}\{Z_{\mathrm{TR}} > 0 | d_0 = -1\}$. Alternatively, under the approximate analytical method leading to (5.10) and (5.11) when the dependence of $\mu_{\mathrm{TR},Y_3}^{(\mathrm{NBI})}$ on φ, $\{c_j\}$ and $\{a_j\}$ is negligible, we can ignore the last term in (5.12). The approximate BEP conditioned on $d_0 = -1$ is then given by

$$\mathbb{P}\{Z_{\mathrm{TR}} > 0 | d_0 = -1\} \simeq P_{\mathrm{e}}^{(\mathrm{NBI})}\Big(\psi_{\mu_{\mathrm{TR}}}(jv), \psi_{\mathrm{J}}\left(g_{\mathrm{TR},d_0=-1}(jv)\right), q_{\mathrm{TR}}\Big), \quad (5.14)$$

where $g_{\mathrm{TR},d_0=-1}(jv)$ in (5.14) is defined as follows:

$$g_{\mathrm{TR},d_0=-1}(jv) \triangleq \frac{-jv}{1+jv}\cdot\frac{N_{\mathrm{s}}J_0T}{2N_0}\Big[1-\cos(2\pi f_{\mathrm{J}}T_{\mathrm{r}})\Big] + \frac{jv}{1-jv}\cdot\frac{N_{\mathrm{s}}J_0T}{2N_0}\Big[1+\cos(2\pi f_{\mathrm{J}}T_{\mathrm{r}})\Big]. \quad (5.15)$$

Using (5.10) and (5.14), it follows that the approximate BEP of TR signaling with an AcR in the presence of NBI is given by

$$P_{\mathrm{e,TR}}^{(\mathrm{NBI})} \simeq \frac{1}{2}\Bigg[P_{\mathrm{e}}^{(\mathrm{NBI})}\Big(\psi_{\mu_{\mathrm{TR}}}(jv), \psi_{\mathrm{J}}\left(g_{\mathrm{TR},d_0=+1}(jv)\right), q_{\mathrm{TR}}\Big) + P_{\mathrm{e}}^{(\mathrm{NBI})}\Big(\psi_{\mu_{\mathrm{TR}}}(jv), \psi_{\mathrm{J}}\left(g_{\mathrm{TR},d_0=-1}(jv)\right), q_{\mathrm{TR}}\Big)\Bigg]. \quad (5.16)$$

Note that the fidelity of the above approximation depends on the insignificance of the last terms in both $\mu_{\mathrm{TR},Y_1}^{(\mathrm{NBI})}$ and $\mu_{\mathrm{TR},Y_3}^{(\mathrm{NBI})}$. As shown in Appendix C and the numerical results, the approximation is in good agreement with the quasi-analytical results for cases of practical interest.[6]

[6]However, in cases when this approximation fails, we can always resort to the quasi-analytical method.

5.1.2 Differential Transmitted-Reference

Following the sampling expansion approach and incorporating the NBI in (5.2), we can rewrite U_j in (4.33) as

$$U_j = \frac{1}{2W}\sum_{m=1}^{2WT}\Big[d_0 w_{j,m}^2 + e_{-1}w_{j,m}(\xi_{2,j,m}+\eta_{2,j,m}) + e_0 w_{j,m}(\xi_{1,j,m}+\eta_{1,j,m}) + (\xi_{1,j,m}+\eta_{1,j,m})(\xi_{2,j,m}+\eta_{2,j,m})\Big], \tag{5.17}$$

where $\xi_{1,j,m}$ and $\xi_{2,j,m}$, for odd m (even m) are the real (imaginary) parts of the samples of the equivalent low-pass version of $\xi_{1,j}(t) \triangleq J(t + jT_{\rm f} + c_j T_{\rm p} - N_{\rm s}T_{\rm f})$, and $\xi_{2,j}(t) \triangleq J(t + jT_{\rm f} + c_j T_{\rm p})$, respectively, in the interval $[0, T]$, and the rest of the terms in (5.17) are defined similarly as in (4.33). Conditioned on d_0, we can rewrite (5.17) in the form of (4.22) and (4.23), where $\beta_{1,j,m} = \frac{1}{2\sqrt{2W}}(e_{-1}\eta_{2,j,m} + e_{-1}\xi_{2,j,m} + e_0\eta_{1,j,m} + e_0\xi_{1,j,m})$ and $\beta_{2,j,m} = \frac{1}{2\sqrt{2W}}(e_{-1}\eta_{2,j,m} + e_{-1}\xi_{2,j,m} - e_0\eta_{1,j,m} - e_0\xi_{1,j,m})$. Further conditioning on θ, $\alpha_{\rm J}$, $\{c_j\}$, and $d_0 = +1$, the conditional variance $\sigma^2_{\rm DTR}$ of $\beta_{1,j,m}$ and $\beta_{1,j,m}$ is $\frac{N_0}{4}$.[7] Following the discussion for TR signaling, we will develop the approximate analytical method below. Under the approximation presented in Appendix C.3, the conditional non-centrality parameters of Y_1 and Y_2 in (4.24) are given by

$$\mu^{(\rm NBI)}_{{\rm DTR},Y_1} \approx \frac{2E_{\rm s}}{N_0}\sum_{l=1}^{L_{\rm CAP}}\alpha_l^2 + \frac{\alpha_{\rm J}^2 N_{\rm s}J_0 T}{N_0} + \frac{\alpha_{\rm J}^2 N_{\rm s}J_0 T}{N_0}\cos(2\pi f_{\rm J}N_{\rm s}T_{\rm f}), \tag{5.18}$$

$$\mu^{(\rm NBI)}_{{\rm DTR},Y_2} \approx \frac{\alpha_{\rm J}^2 N_{\rm s}J_0 T}{N_0} - \frac{\alpha_{\rm J}^2 N_{\rm s}J_0 T}{N_0}\cos(2\pi f_{\rm J}N_{\rm s}T_{\rm f}), \tag{5.19}$$

and the conditional non-centrality parameters of Y_3 and Y_4 in (4.24) are given by

$$\mu^{(\rm NBI)}_{{\rm DTR},Y_3} \approx \frac{2E_{\rm s}}{N_0}\sum_{l=1}^{L_{\rm CAP}}\alpha_l^2 + \frac{\alpha_{\rm J}^2 N_{\rm s}J_0 T}{N_0} - \frac{\alpha_{\rm J}^2 N_{\rm s}J_0 T}{N_0}\cos(2\pi f_{\rm J}N_{\rm s}T_{\rm f}), \tag{5.20}$$

$$\mu^{(\rm NBI)}_{{\rm DTR},Y_4} \approx \frac{\alpha_{\rm J}^2 N_{\rm s}J_0 T}{N_0} + \frac{\alpha_{\rm J}^2 N_{\rm s}J_0 T}{N_0}\cos(2\pi f_{\rm J}N_{\rm s}T_{\rm f}). \tag{5.21}$$

[7] Note that this conditional variance $\sigma^2_{\rm DTR}$ remains the same even when $d_0 = -1$.

Using (5.18) to (5.21), the approximate BEP of DTR signaling with an AcR in the presence of NBI is then given by

$$P_{\mathrm{e,DTR}}^{(\mathrm{NBI})} \simeq \frac{1}{2}\Bigg[P_{\mathrm{e}}^{(\mathrm{NBI})}\Big(\psi_{\mu_{\mathrm{DTR}}}(jv), \psi_{\mathrm{J}}\left(g_{\mathrm{DTR},d_0=+1}(jv)\right), q_{\mathrm{DTR}}\Big) + P_{\mathrm{e}}^{(\mathrm{NBI})}\Big(\psi_{\mu_{\mathrm{DTR}}}(jv), \psi_{\mathrm{J}}\left(g_{\mathrm{DTR},d_0=-1}(jv)\right), q_{\mathrm{DTR}}\Big)\Bigg], \tag{5.22}$$

where $\psi_{\mu_{\mathrm{DTR}}}(jv)$ is defined after (4.37), $g_{\mathrm{DTR},d_0=+1}(jv)$ and $g_{\mathrm{DTR},d_0=-1}(jv)$ are defined as follows:

$$g_{\mathrm{DTR},d_0=+1}(jv) \triangleq \frac{-jv}{1+jv}\cdot\frac{N_{\mathrm{s}}J_0T}{N_0}\Big[1+\cos(2\pi f_{\mathrm{J}}N_{\mathrm{s}}T_{\mathrm{f}})\Big] + \frac{jv}{1-jv}\cdot\frac{N_{\mathrm{s}}J_0T}{N_0}\Big[1-\cos(2\pi f_{\mathrm{J}}N_{\mathrm{s}}T_{\mathrm{f}})\Big], \tag{5.23}$$

$$g_{\mathrm{DTR},d_0=-1}(jv) \triangleq \frac{-jv}{1+jv}\cdot\frac{N_{\mathrm{s}}J_0T}{N_0}\Big[1-\cos(2\pi f_{\mathrm{J}}N_{\mathrm{s}}T_{\mathrm{f}})\Big] + \frac{jv}{1-jv}\cdot\frac{N_{\mathrm{s}}J_0T}{N_0}\Big[1+\cos(2\pi f_{\mathrm{J}}N_{\mathrm{s}}T_{\mathrm{f}})\Big]. \tag{5.24}$$

We remark that (5.16) and (5.22) can be evaluated for a broad class of fading channels, including Nakagami, Rice, and Rayleigh, whose CFs are known in closed-form [137].

5.2 Numerical Results

In this section, we evaluate the performance of TR and DTR signaling schemes with NBI, based on the unified analysis developed in previous sections. We consider a bandpass UWB system with pulse duration $T_{\mathrm{p}} = 0.5$ ns, average repetition period $T_{\mathrm{f}} = 100$ ns, and $N_{\mathrm{s}} = 16$. For simplicity, T_{r} is set such that there is no ISI or isi in the system, i.e., $T_{\mathrm{r}} = 2T_{\mathrm{f}} - T_{\mathrm{g}} - N_{\mathrm{h}}T_{\mathrm{p}}$. We consider a TH sequence of all ones ($c_j = 1$ for all j) and $N_{\mathrm{h}} = 2$. The NBI carrier frequency is $f_{\mathrm{J}} = 2.45$ GHz.[8] Since the NBI experiences flat Rayleigh fading, the CF of α_{J}^2 is $\psi_{\mathrm{J}}(jv) = 1/(1-jv)$. For UWB channels, it has been verified experimentally that the multipath gains can be modeled as Nakagami-m r.v.'s [38]. As a result, we consider a dense resolvable

[8]For our numerical results, we assume that the NBI is within the band of interest.

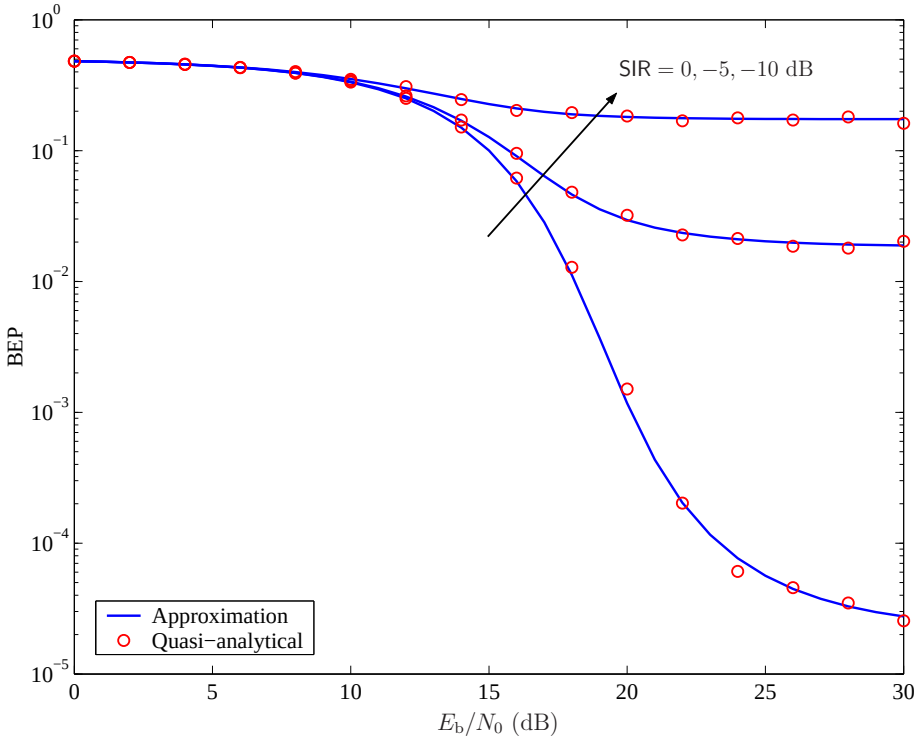

Figure 5-1: BEP performance of TR signaling with AcR in the presence of NBI for $(L, \epsilon, m) = (32, 0, 3)$ and $WT = L$.

multipath channel, where each multipath gain is Nakagami distributed with fading severity index m and average power $\mathbb{E}\{\alpha_l^2\}$, where $\mathbb{E}\{\alpha_l^2\} = \mathbb{E}\{\alpha_1^2\}\exp[-\epsilon(l-1)]$, for $l = 1, \ldots, L$, are normalized such that $\sum_{l=1}^{L}\mathbb{E}\{\alpha_l^2\} = 1$. For simplicity, the fading severity index m is assumed to be identical for all paths. The average power of the first arriving multipath component is given by $\mathbb{E}\{\alpha_1^2\}$, and ϵ is the power decay factor. With this model, we consider two sets of parameters, $(L, \epsilon, m) = (32, 0, 3)$ for uniform PDP and $(32, 0.4, 3)$ for exponential PDP.

To better understand the validity of the approximation developed in Section V, we compare the BEP performance of TR signaling with an AcR in the presence of NBI when $a_j = 1$ for all j and $|\widehat{P}(f_{\mathrm{J}})| \approx \sqrt{T_{\mathrm{p}}}$.[9] Fig. 5-1 shows the BEP performance of TR signaling for different SIR values, $(L, \epsilon, m) = (32, 0, 3)$ and $WT = L$. It can be observed that the approximate analytical results are in good agreement with the quasi-analytical results. We further investigate the effect of the NBI carrier frequency

[9]For simplicity, we have considered the case where the frequency response of $p(t)$ is flat over the bandwidth W.

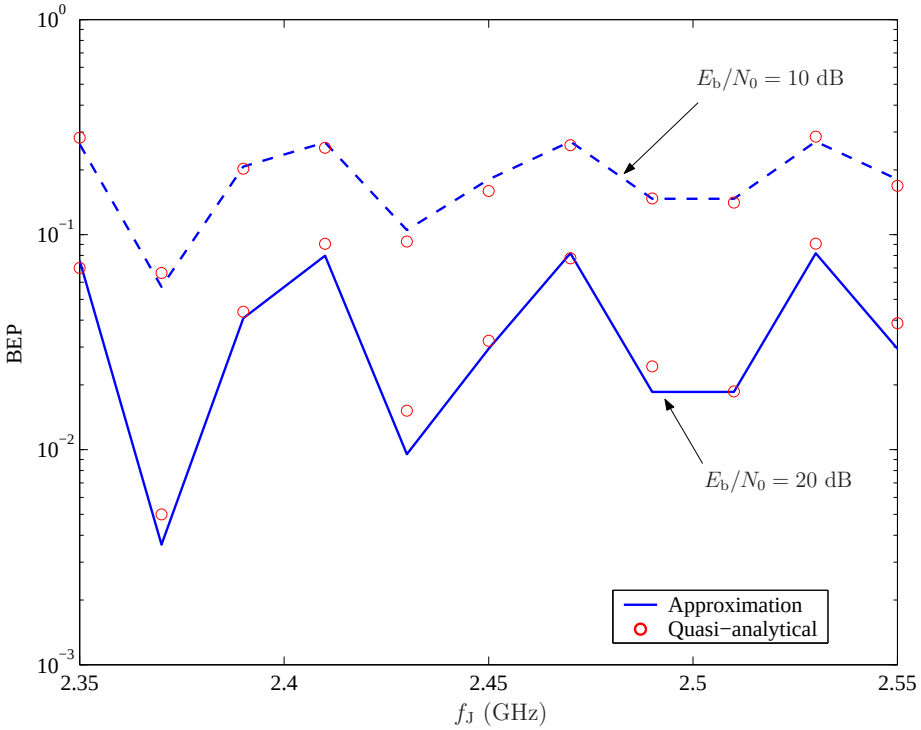

Figure 5-2: Effect of NBI carrier frequency on BEP performance of TR signaling with AcR for $(L, \epsilon, m) = (32, 0, 3)$ and $WT = L$.

on the fidelity of the approximation in Fig. 5-2 for $(L, \epsilon, m) = (32, 0, 3)$, $WT = L$, and SIR = -5 dB. Similar to the results in Fig. 5-1, the approximate analytical method is in good agreement with the quasi-analytical results, showing the usefulness of the approximation for investigating the performance of TR signaling schemes in the presence of NBI.

To understand the effect of NBI and PDP on the choice of integration interval T of an AcR, we first plot the BEP of TR signaling in Fig. 5-3 as a function of time-bandwidth product, WT, using an analytical approximation for $(L, \epsilon, m) = (32, 0, 3)$. Fig. 5-3 shows that with this PDP, the optimum T is always equal to T_g (i.e., $WT = L$), regardless of the presence of NBI. It can also be observed that the performance gain for using the optimum T is significant in the absence of NBI, especially at high E_b/N_0. This is because, in the absence of NBI, more useful energy is captured with increasing WT until optimum WT is reached for high E_b/N_0. However, in the presence of NBI, interference energy is also accumulated for every increase in WT,

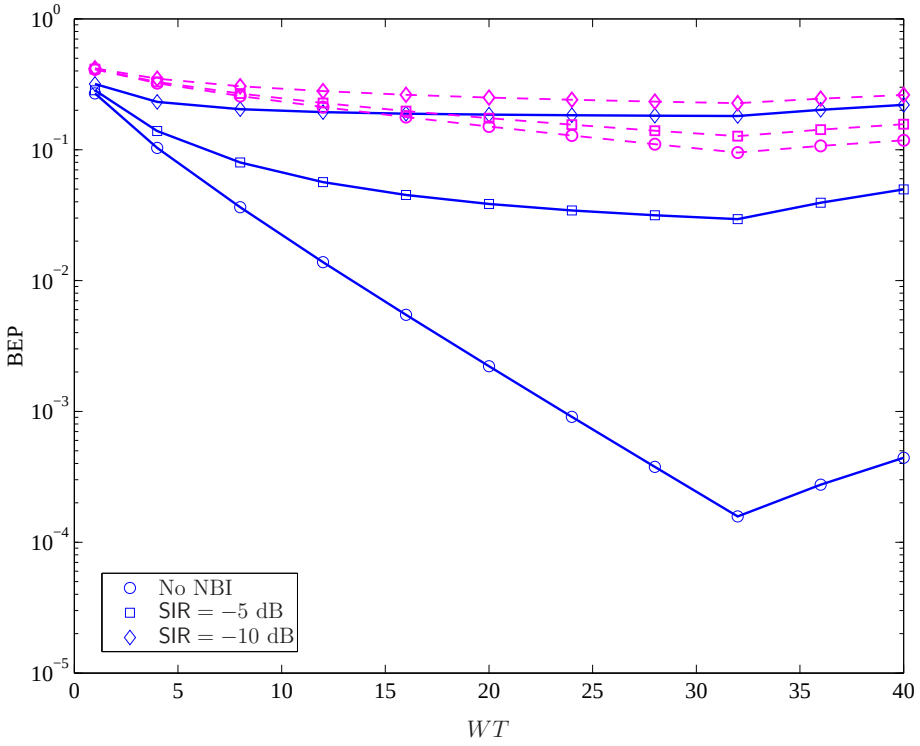

Figure 5-3: Effect of integration interval T on BEP performance of TR signaling with AcR for uniform PDP. The solid and dashed lines indicate $E_b/N_0 = 20$ dB and $E_b/N_0 = 15$ dB, respectively.

causing performance degradation. This trade-off is more subtle for channels with non-uniform PDP, as illustrated in Fig. 5-4 for $(L, \epsilon, m) = (32, 0.4, 3)$. It can be seen that the optimum T is no longer at T_g, since the gain from collecting more residual multipath energies inherent in the channel with exponential PDP is not sufficient to compensate for the noise accumulation beyond the optimum point. Moreover, we observe that the optimum T increases with E_b/N_0 and SIR, due to decreasing noise and interference accumulation. In general, the optimum T depends on the channel PDP, the operating E_b/N_0, and the SIR. Consequently, it is important that the AcR is designed with an appropriate choice of T. Some of our work in this direction is reported in [141].

The effect of NBI on TR and DTR signaling with an AcR is plotted in Fig. 5-5 for different SIR values, $(L, \epsilon, m) = (32, 0.4, 3)$, and optimum T chosen for each E_b/N_0 and SIR. First, we can observe that the error floor for large values of E_b/N_0 becomes

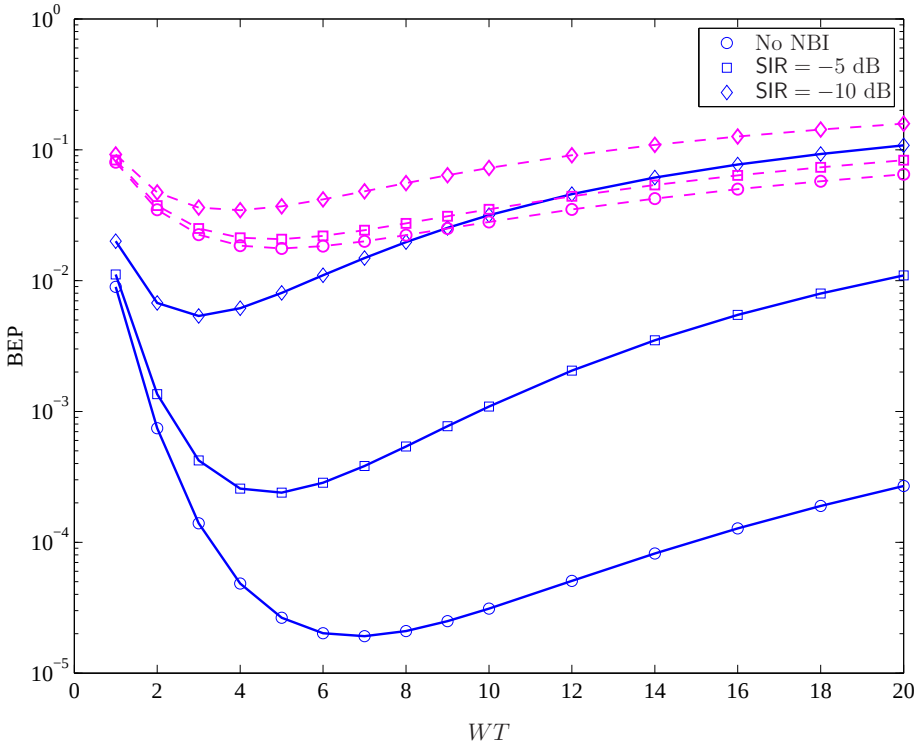

Figure 5-4: Effect of integration interval T on BEP performance of TR signaling with AcR for exponential PDP. The solid and dashed lines indicate $E_b/N_0 = 20$ dB and $E_b/N_0 = 15$ dB, respectively.

more significant as SIR decreases for both signaling schemes. In the absence of NBI, DTR signaling has a gain of about 3 dB compared to TR signaling. However, this gain diminishes as SIR decreases. After certain points (e.g, $E_b/N_0 = 20$, 16, 10 dB for SIR = -5, -10, -20 dB, respectively), DTR signaling performs worse than TR signaling, as indicated by the error floor. In the interference-limited regime, it is particularly interesting to observe that TR signaling is more robust against NBI compared to DTR signaling. This is because interference is more severe in DTR signaling due to the presence of more noise and interference terms as $q_{\mathrm{DTR}} = 2q_{\mathrm{TR}}$. Despite a doubling of the received multipath energies in DTR signaling compared to TR signaling, the presence of more interference terms essentially outweighs this gain, as indicated by the crossing of the curves in Fig. 5-5.

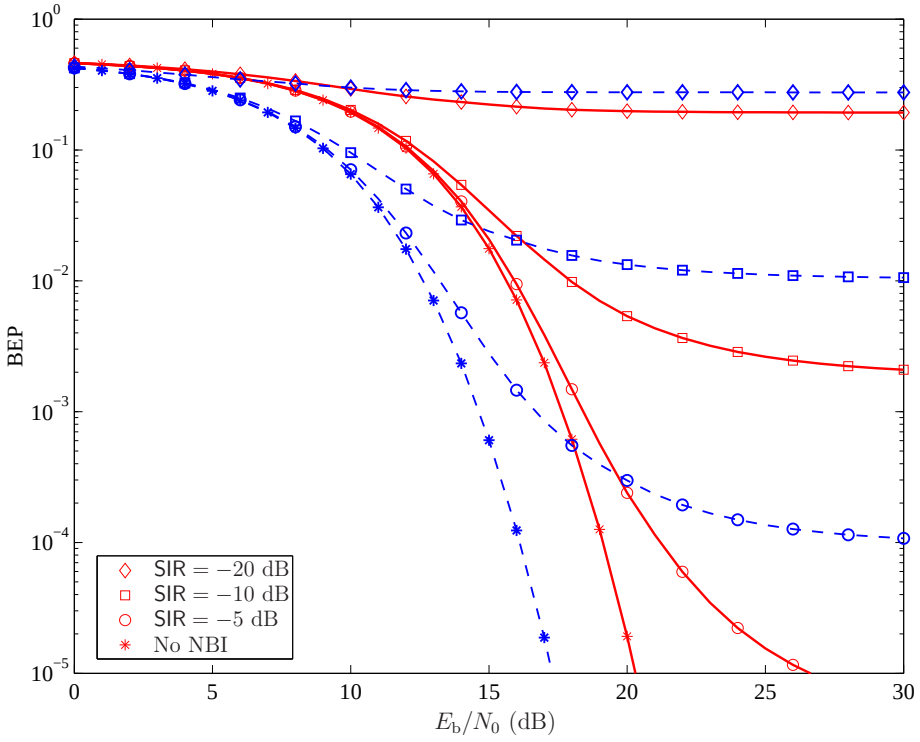

Figure 5-5: Effect of NBI on BEP performance of TR and DTR signaling with AcR for $(L, \epsilon, m) = (32, 0.4, 3)$ and optimum T chosen for each SNR and SIR. The solid and dashed lines indicate the TR and DTR signaling, respectively.

Chapter 6

Cooperation for Energy Efficiency in Wireless Sensor Networks

In this chapter, we investigate the problem of binary decentralized detection in a dense and randomly deployed WSN, whereby the communication channels between the nodes and the fusion center are bandwidth-constrained. We consider a scenario in which sensor observations, conditioned on the alternate hypothesis, are independent but not identically distributed across the sensor nodes. We compare two different fusion architectures, namely, the parallel fusion architecture (PFA) and the cooperative fusion architecture (CFA), for such bandwidth-constrained WSNs, where each sensor node is restricted to send a 1-bit information to the fusion center. For each architecture, we derive expression for the probability of decision error at the fusion center. We propose a consensus flooding protocol for CFA and analyze its average energy consumption. We analyze the effects of PoI intensity, realistic link models, consensus flooding protocol, and network connectivity on the system reliability and average energy consumption for both fusion architectures.

6.1 Sensing Model

We consider a dense WSN with a large number of identical sensor nodes deployed randomly over a wide region. Our goal is to detect or monitor a PoI in the sensor field

using these geographically dispersed nodes. First, we model the PoI as an isotropic signal source with path loss factor α_{f}. This model is general and captures PoI such as leakage of some contaminating chemical in industrial settings, a moving armored vehicle in a battlefield, or a source of a radioactive material [142–145]. The path loss factor α_{f} will depend on the type of signal considered (chemical contamination, sound, radioactive radiation, etc.). Thus, the received signal strength at a distance d away from the PoI is given by

$$P(d) = \frac{P_0}{d^{\alpha_{\mathrm{f}}}}, \tag{6.1}$$

where P_0 is the signal strength of the PoI measured at 1 meter from the location of the PoI.

The location of the sensor nodes can be a direct consequence of certain random deployment strategies. For example, sensor nodes may be air-dropped or launched via artillery in battlefields or unknown environments. Under this scenario, the spatial distribution of the nodes over the region can be modeled by a homogeneous Poisson point process with intensity ρ. The probability that there are n_{t} sensor nodes within region A of size $|A|$ is given by

$$\mathbb{P}\left\{N_{\mathrm{t}} = n_{\mathrm{t}}\right\} = \frac{\lambda_{\mathrm{t}}^{n_{\mathrm{t}}} \exp\left(-\lambda_{\mathrm{t}}\right)}{n_{\mathrm{t}}!}, \quad n_{\mathrm{t}} \geq 0 \tag{6.2}$$

where N_{t} is a Poisson r.v. with mean $\lambda_{\mathrm{t}} = \mathbb{E}\left\{N_{\mathrm{t}}\right\} = \rho|A|$. We assume that the sensor observations are independent conditioned on whether the PoI is present or absent. In particular, when conditioned on the presence of the PoI, the sensor observations are not identically distributed across the nodes, i.e., the observations at the nodes are spatially varying. In this case, the independent observation at each sensor node after appropriate sampling and processing is given by

$$y_n = \begin{cases} z_n, & \text{when PoI is absent} \\ \sqrt{P(d_n)} + z_n, & \text{when PoI is present,} \end{cases} \tag{6.3}$$

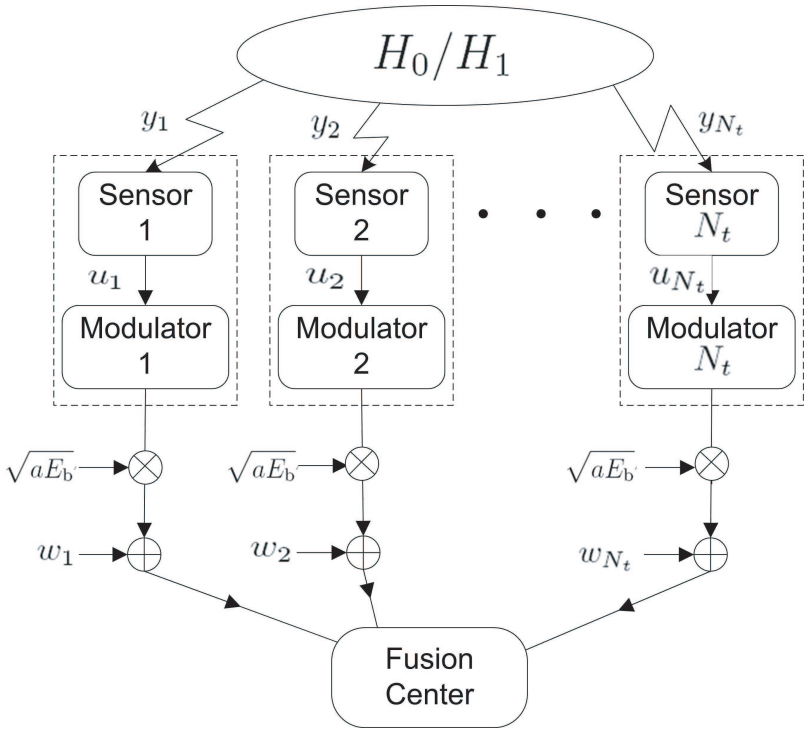

Figure 6-1: Parallel fusion architecture.

where $n = 1, \ldots, N_t$, and z_n is the independent observation noise across the nodes and is distributed according to a zero-mean Gaussian distribution with variance σ_z^2, i.e., $z_n \sim \mathcal{N}(0, \sigma_z^2)$, and $P(d_n)$ is the received signal strength at the nth node with a distance d_n away from the PoI given by (6.1).

Thus, we can formulate the above decentralized detection problem as a binary hypothesis testing problem with the following hypotheses:

$$\begin{aligned} H_0 &: \text{PoI absent} \\ H_1 &: \text{PoI present.} \end{aligned} \tag{6.4}$$

For simplicity, we assume that the PoI is located at the center of region A when conditioned on H_1.[1] The fusion center's task is to decide whether the PoI is present in the WSN based on the information collected from the sensor nodes.

[1] As a result, we can neglect the border effects.

6.2 Decentralized Detection Problem

Given the sensing model in Chapter 6.1, we want to decide whether the PoI has occurred in region A given that sensor nodes are allowed to cooperate or not to cooperate depending on the fusion architectures.

6.2.1 Parallel Fusion Architecture

In PFA, all the nodes make their local decisions independently without cooperating with one another. Since we are considering bandwidth-constrained WSNs, i.e., the communication channels between the sensor nodes and the fusion center are bandwidth-constrained, each sensor is restricted to sending a 1-bit information to the fusion center.[2] Consequently, local decisions are quantized as follows:

$$u_n = \begin{cases} -1, \text{ when } \widehat{H}(y_n) = H_0 \\ +1, \text{ when } \widehat{H}(y_n) = H_1, \end{cases} \tag{6.5}$$

and $\widehat{H}(y_n)$ is the decision made at the nth node. The detection performance of the nth node can be characterized by its corresponding probability of false-alarm and detection, denoted by $P_{\mathrm{f}}^{(n)}$ and $P_{\mathrm{d}}^{(n)}$ respectively. The probability of false-alarm is given by

$$P_{\mathrm{f}}^{(n)} = \mathbb{P}\{y_n \geq \zeta_n | H_0\} = Q\left(\frac{\zeta_n}{\sigma_z}\right), \tag{6.6}$$

where ζ_n is the local decision threshold of the nth node. The probability of detection at the nth node is then given by

$$P_{\mathrm{d}}^{(n)} = \mathbb{P}\{y_n \geq \zeta_n | H_1, P(d_n)\} = P_{\mathrm{d}}(\zeta_n, d_n), \tag{6.7}$$

[2]Note that in some applications, it is reasonable to relax the bandwidth constraint on the communication channels. In such scenarios, the nodes can be designed to send more information bits about their inference, e.g, sending quantized sensor observations or quantized local likelihood ratios.

where $P_{\mathrm{d}}(\zeta, d)$ is defined as follows:

$$P_{\mathrm{d}}(\zeta, d) \triangleq Q\left(\frac{\zeta - \sqrt{P(d)}}{\sigma_z}\right). \tag{6.8}$$

During the data-retrieval period, the fusion center will trigger the nodes within its activation range by sending a beacon signal. All the nodes that are within this activated region A then send their local decisions to the fusion center. Without loss of generality, we consider an equivalent discrete-time communication model [85,86,88].[3] As shown in Fig. 6-1, local decisions $\{u_n\}$ are transmitted over parallel channels to the fusion center.

The received signal at the fusion center from the nth sensor node is given by

$$r_n = \sqrt{aE_{\mathrm{b}}}u_n + w_n, \tag{6.9}$$

where E_{b} is the transmit energy per bit, and a accounts for the up-link path loss, which is assumed to be identical for all nodes.[4] The channel noise, w_n, is modeled as a zero-mean Gaussian r.v. with variance $N_0/2$ and it is assumed to be i.i.d. across the nodes. We can define $\mathsf{SNR} = aE_{\mathrm{b}}/N_0$ as the received SNR from each node at the fusion center. The goal of the fusion center is to make a global decision about the hypotheses based on the N_{t} received observations given by $\mathbf{r} = [r_1, \ldots, r_{N_{\mathrm{t}}}]^T$.

Given $N_{\mathrm{t}} = n_{\mathrm{t}}$, a, $\{P_{\mathrm{d}}^{(n)}\}$, and $\{P_{\mathrm{f}}^{(n)}\}$, the optimal fusion rule is given by

$$\Lambda(\mathbf{r}) = \log\left[\prod_{n=1}^{n_{\mathrm{t}}} \frac{p_{r_n|H_1}(r_n|H_1)}{p_{r_n|H_0}(r_n|H_0)}\right] \underset{H_0}{\overset{H_1}{\gtrless}} \tau. \tag{6.10}$$

As pointed out in [85,86], the above fusion rule is not easily computable at the fusion center, particularly for bandwidth-constrained WSNs, since it requires each node to send its $P_{\mathrm{d}}^{(n)}$ and $P_{\mathrm{f}}^{(n)}$ to the fusion center or the fusion center needs to know *a priori*

[3]Such a simplified assumption allows us to study in isolation the effect of cooperation between the nodes. Moreover, this model implicitly assumes that coherent detection with perfect channel state information and perfect synchronization is performed at the fusion center.

[4]When the fusion center is located at an altitude significantly higher than the radius of the sensor field, this is a reasonable assumption.

$P_{\mathrm{d}}^{(n)}$ and $P_{\mathrm{f}}^{(n)}$ for all n, which directly depends on the locations of all the nodes, the intensity of the PoI, and the local threshold ζ_n.[5] As a result, the fusion center can only rely on suboptimal fusion rule; in particular, we adopt the equal gain combining (EGC) fusion rule given by

$$\Lambda(\mathbf{r}) = \frac{1}{n_{\mathrm{t}}} \sum_{n=1}^{n_{\mathrm{t}}} r_n \underset{H_0}{\overset{H_1}{\gtrless}} \tau, \tag{6.11}$$

which has been shown to be robust for a wide range of SNR [85,86]. In the following, we consider the scenario in which all nodes use the common local threshold ζ. In this case, $P_{\mathrm{f}}^{(n)} = P_{\mathrm{f}}$ is fixed as a design parameter (generally $P_{\mathrm{f}} \ll 1$) so that the decision threshold ζ can be evaluated according to (6.6).

Now, using the spatial Poisson distribution of the nodes and (6.8), the number of nodes that can detect the PoI when conditioned on H_1, hence with local decision $u_n = +1$, is a Poisson r.v., N_{d}, with mean given by

$$\lambda_{\mathrm{d}} = \mathbb{E}\, N_{\mathrm{d}} = \rho \int_A P_{\mathrm{d}}(\zeta, \|\mathbf{x} - \mathbf{x}_{\mathrm{PoI}}\|) d\mathbf{x}, \tag{6.12}$$

where $\mathbf{x}$ and $\mathbf{x}_{\mathrm{PoI}}$ denote the locations of sensor node and PoI, respectively. Conditioned on N_{t}, the ratio $\lambda_{\mathrm{d}}/\lambda_{\mathrm{t}}$ is the average percentage of nodes in region A which successfully detects the PoI. Using $P_{\mathrm{d}}(\zeta, d)$ given by (6.8), the integral in (6.12) can be evaluated numerically. Note the expression in (6.12) is general and is applicable for general PoI and sensor measurement models, as long as $P_{\mathrm{d}}(\zeta, d)$ is well-defined.[6] On the other hand, by the spatial Poisson distribution of the nodes, the false-alarmed nodes can be obtained by thinning the original sensor nodes with thinning probability $(1 - P_{\mathrm{f}})$. Hence, the number of false-alarmed nodes, N_{f}, is also Poisson distributed

[5]Here, we do not consider the presence of an intelligent sensor manager at the fusion center that is capable of selecting only the useful information from the sensor field or know the shape of the spatial signal of PoI.

[6]For example, when the sensor noise z_n is negligible and A is large, log-normal shadowing in (6.1) leads to an analogous model adopted in [146], which admits a closed-form expression for (6.12).

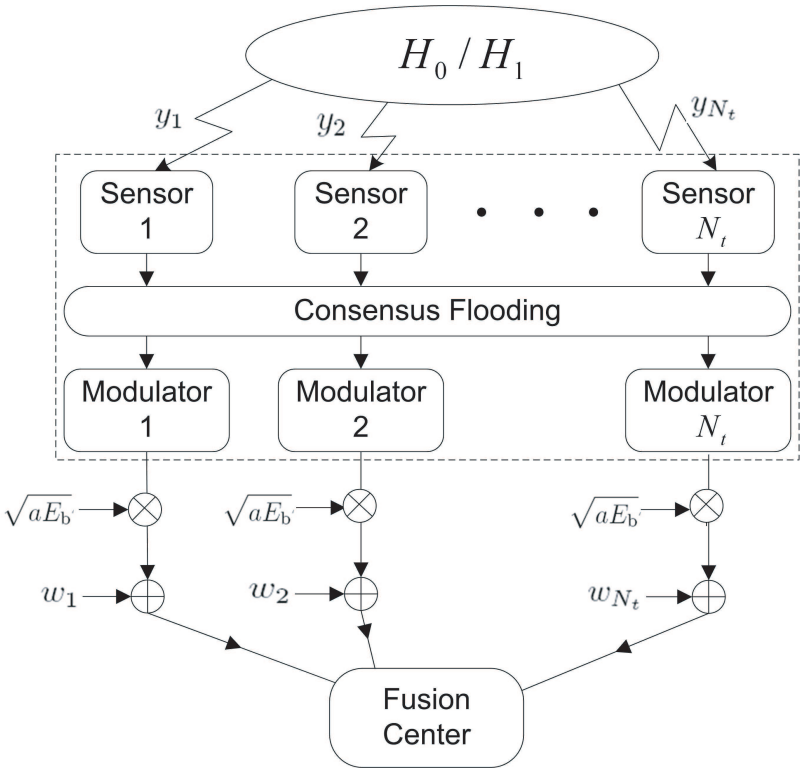

Figure 6-2: Cooperative fusion architecture.

with mean given by

$$\lambda_{\mathrm{f}} = \mathbb{E}\{N_{\mathrm{f}}\} = \lambda_{\mathrm{t}} P_{\mathrm{f}}. \tag{6.13}$$

Note that λ_{f} is generally smaller than λ_{d} for small P_{f}.

6.2.2 Cooperative Fusion Architecture

In CFA, the sensor nodes need to disseminate and agree on a common decision throughout the network via a consensus flooding protocol, before sending the agreed decision to the fusion center as shown in Fig. 6-2. Similar to (6.9), activated nodes send the agreed decision to the fusion center via parallel channels.

Consensus Flooding Protocol

When the PoI intensity is weak[7], Parley algorithm is likely to lead to consensus in the wrong decision since majority of the nodes in the WSN have rejected H_1. Although [94] attempts to relax the stringent assumptions of conventional Parley algorithm, it requires self-organizing network that is capable of exchanging enormous amount of information. This greatly limits the applicability of this algorithm in large scale networks, especially if energy constraint is enforced at each sensor node. As such, we propose a consensus flooding protocol that accounts for weak PoI intensity and reduces the possibility of false-alarm flooding. We define the deliver ratio, D_{r}, as the ratio between the number of nodes that declare $u = +1$ at the end of flooding and the total number of nodes. Specifically, we introduce a voting scheme in our flooding protocol via the use of a threshold T_{h}. Through T_{h}, we can find a good trade-off between a high D_{r} when PoI is present and a low D_{r} when PoI is absent. The latter situation can be achieved by minimizing the possibility of false-alarm flooding. The details of our consensus flooding protocol are given as follows:

S1 The consensus flooding protocol is activated by sending a beacon signal from the fusion center to the sensor field.

S2 All activated nodes make a decision based on the measured strength of the PoI intensity.

S3 Nodes that have declared $\widehat{H} = H_1$ (PoI is present) will each send a broadcast packet to neighboring nodes only once. Each node then initiates a counter with a value of one, sets a fixed assessment delay (FAD), and proceeds to S5.

S4 Nodes that have declared $\widehat{H} = H_0$ (PoI is absent) will remain silent and listen to neighboring nodes. Each node then initiates a counter with a value of zero, sets a FAD, and proceeds to S5.

S5 During FAD, the counter is incremented by one for each received broadcast packet.

[7]In the numerical results, we will show that the main advantage of CFA is achieved in such a scenario.

S6 After FAD expires, each node compares its counter with a pre-set value $T_{\rm h}$. If counter is less than $T_{\rm h}$, set $\widehat{H} = H_0$. Otherwise, set $\widehat{H} = H_1$.

S7 If the node has changed its decision and has not broadcasted before, it will proceed to S3. Else it will remain silent.

S8 The consensus flooding protocol is stopped after a certain number of iterations**,** and all activated nodes send their decisions to the fusion center.

Note that the above flooding protocol differs from the conventional broadcasting protocols. Conventional broadcasting protocols are designed to maximize the delivery ratio as well as to minimize the redundant retransmissions, regardless of the correctness of the message broadcasted [147, 148].[8] Unlike the Parley algorithm [91] or conventional broadcasting protocols [147,148], our consensus flooding protocol adopts a voting scheme to enable agreement in decisions and to control false-alarm flooding. In addition, only nodes that declare H_1 are allowed to broadcast their decisions. When time constraint is not stringent, the FAD value and the number of protocol iterations can be chosen large enough to allow the consensus flooding protocol to terminate correctly. The choice of the threshold $T_{\rm h}$ in the voting scheme essentially depends on the degree of connection, which is defined as the average number of neighbors, $\lambda_{\rm h}$, each node can hear. Thus, we can parameterize our consensus flooding protocol by $(T_{\rm h}, \lambda_{\rm h}, D_{\rm r})$, where the parameters, $T_{\rm h}$ and $\lambda_{\rm h}$, are chosen to meet a given $D_{\rm r}$ when conditioned on H_1, and to minimize the possibility of false-alarm flooding.

Inter-node Communication Model

We model our inter-node wireless links as being subjected to attenuation with both distance and log-normal shadowing [146, 149, 150]. The motivation for considering such a channel model stemmed from the fact that deterministic path-loss model often leads to inaccurate analysis due to ignorance of the stochastic nature of wireless

[8] In [147, 148], the delivery ratio is simply defined as the ratio between the number of nodes that received the broadcasted message over the total number of nodes.

channel [151–154]. For example, it has been shown by several authors that shadowing improves the connectivity properties of the wireless networks [146, 149, 150].

The received packet energy of a receiving node at a distance r away from the broadcasting node can be written as

$$E_{\text{rec}} = E_{\text{flood}} K r^{-\alpha} 10^{\frac{S_{i,j}}{10}}, \tag{6.14}$$

where E_{flood} is the energy required by each node to broadcast a packet and it generally depends on the inter-node transmitted power, bit rate, and packet length. The path loss exponent, α, of the wireless inter-node link takes values between 2 and 4, and K is a constant that depends on the antenna gain and wavelength. We consider the attenuation due to shadowing between any two nodes i and j as i.i.d. For log-normal shadowing, $S_{i,j} \sim \mathcal{N}(0, \sigma_S^2)$. Now, we consider that all nodes have the same receiver sensitivity, where $E_{\min}$ is the minimum receive energy such that packets are correctly detected with probability one if and only if E_{rec} is greater than $E_{\min}$, otherwise they are discarded. Mathematically, this is equivalent to the connection condition, whereby node i and j at a given distance r apart are connected if

$$r \leq R_{\text{c}} \triangleq a_{\text{c}} \exp\left(b_{\text{c}} S_{i,j}\right), \tag{6.15}$$

where $a_{\text{c}} = \left(\frac{K E_{\text{flood}}}{E_{\min}}\right)^{\frac{1}{\alpha}}$, $b_{\text{c}} = \frac{\ln 10}{10\alpha}$, and R_{c} can be interpreted as the connection distance, which is a r.v. due to the effect of shadowing. In the absence of shadowing (i.e., $S_{i,j} = 0$), R_{c} is a deterministic circular coverage radius.

From the spatial Poisson distribution of the nodes, given that a particular node falls within a disk of radius r_0, its location is uniformly distributed over the disk. Given this particular node, the number of nodes, N_{h}, connected to it forms a Poisson process with mean given by

$$\begin{aligned}
\lambda_{\text{h}} &= \int_0^{2\pi} \int_0^{\infty} \rho r Q\left(\frac{1}{b_{\text{c}}\sigma_{\text{S}}} \ln \frac{r}{a_{\text{c}}}\right) dr d\theta \\
&= 2\pi\rho \int_{-\infty}^{\infty} \int_0^{a_{\text{c}} \exp(b_{\text{c}}\sigma_{\text{S}} x)} \frac{r}{\sqrt{2\pi}} \exp\left(-\frac{x^2}{2}\right) dr dx
\end{aligned}$$

$$= \pi\rho a_{\mathrm{c}}^2 \int_{-\infty}^{\infty} \frac{1}{\sqrt{2\pi}} \exp\left(-\frac{x^2}{2} + 2b_{\mathrm{c}}\sigma_{\mathrm{S}}x\right) dx$$
$$= \pi\rho a_{\mathrm{c}}^2 \exp\left(2b_{\mathrm{c}}^2\sigma_S^2\right). \tag{6.16}$$

From (6.16), we can observe that the degree of connection increases with shadowing and this coincides with the results of [146, 149, 150]. Given a certain λ_{h}, we can use (6.16) to obtain the required packet energy E_{flood}, which is given by

$$\frac{E_{\mathrm{flood}}}{E_{\min}} = \frac{1}{K}\left(\frac{\lambda_{\mathrm{h}}}{\rho\pi\exp\left(2b_{\mathrm{c}}^2\sigma_S^2\right)}\right)^{\frac{\alpha}{2}}. \tag{6.17}$$

Network Connectivity Analysis

The analytical characterization of D_{r} for our consensus flooding protocol is not a trivial problem. Here, we will provide some conservative bounds through the use of network connectivity concepts [149, 150]. We will show how we can relate D_{r}, through the concept of network connectivity, to the protocol parameters λ_{h} and T_{h}. In particular, we will obtain bounds on the range of λ_{h} to satisfy a specified D_{r} under both hypothesis (PoI present and absent). In the following, we provide some notions of network connectivity which we use in our analysis.

Definition 1. *The network can be viewed as a directed graph where each node is a vertex and a directed edge exists from vertex i to j if and only if node i can directly transmit to node j. A network is said to be connected if for every pair of vertexes there exits a directed path between them.*

Definition 2. *The probability that the network is connected and each node has at least n neighbors is defined as $\mathbb{P}_{\mathrm{c}}\{n\}$.*

Since N_{h} is Poisson distributed, the probability that a node does not hear a sufficient number of neighboring nodes ($N_{\mathrm{h}} < T_{\mathrm{h}}$) is given by

$$P_{T_{\mathrm{h}}} = \mathbb{P}\{\text{hears less than } T_h \text{ nodes}\} = \sum_{i=0}^{T_{\mathrm{h}}-1} \frac{\lambda_{\mathrm{h}}^i \exp\left(-\lambda_{\mathrm{h}}\right)}{i!}, \tag{6.18}$$

and the probability that a node is isolated, i.e., it cannot hear any neighboring node

$(T_h = 1)$ is then given by

$$\mathbb{P}\left\{N_{\mathrm{h}} = 0\right\} = \exp\left(-\lambda_{\mathrm{h}}\right). \tag{6.19}$$

Given that $N_{\mathrm{t}} = n_{\mathrm{t}}$, the conditional probability that none of these nodes is isolated is approximated by [149, 150]

$$\mathbb{P}\{\text{no node isolated}|N_{\mathrm{t}} = n_{\mathrm{t}}\} \cong \left(1 - \mathbb{P}\left\{N_{\mathrm{h}} = 0\right\}\right)^{n_{\mathrm{t}}}, \tag{6.20}$$

where the approximation arises from the assumption that the events of isolated nodes are statistically independent. The validity of this approximation has been verified via simulations in [149, 150]. By the spatial Poisson distribution of the nodes, the probability that none of the nodes is isolated is given by

$$\begin{aligned}\mathbb{P}\{\text{no node isolated}\} &= \sum_{n_{\mathrm{t}}=0}^{\infty} \mathbb{P}\{\text{no node isolated}|N_{\mathrm{t}} = n_{\mathrm{t}}\} \frac{\lambda_{\mathrm{t}}^{n_{\mathrm{t}}} \exp\left(-\lambda_{\mathrm{t}}\right)}{n_{\mathrm{t}}!} \\ &= \exp(-\lambda_{\mathrm{t}} \exp(-\lambda_{\mathrm{h}})),\end{aligned} \tag{6.21}$$

and we make the approximation that $\mathbb{P}_{\mathrm{c}}\{1\} \approx \mathbb{P}\{\text{no node isolated}\}$ when the network is highly connected [149, 150].[9]

When $T_{\mathrm{h}} > 1$ (consensus flooding protocol with voting scheme enabled), the condition for a node to change its decision to $u_{\mathrm{n}} = +1$ is when it hears at least T_{h} neighbors. Similar to (6.20), the conditional probability that none of the nodes has a degree of connection less than T_{h} can be approximated by[10]

$$\mathbb{P}\{\text{no node with } N_{\mathrm{h}} < T_{\mathrm{h}}|N_{\mathrm{t}} = n_{\mathrm{t}}\} \cong \left(1 - P_{T_{\mathrm{h}}}\right)^{n_{\mathrm{t}}}, \tag{6.22}$$

which becomes (6.20) when $T_{\mathrm{h}} = 1$. Using (6.18) and (6.22), the probability that

[9] Note that the non-existence of isolated nodes is only a necessary, but not sufficient condition for a network to be connected.

[10] The approximation arises from the assumption that the events of isolated nodes are statistically independent.

none of the nodes has a degree of connection less than T_{h} is given by

$$\mathbb{P}\{\text{no node with } N_{\mathrm{h}} < T_{\mathrm{h}}\} = \exp\left(-\lambda_{\mathrm{t}} \exp(-\lambda_{\mathrm{h}}) \sum_{i=0}^{T_{\mathrm{h}}-1} \frac{\lambda_{\mathrm{h}}^{i}}{i!}\right), \tag{6.23}$$

where we can similarly make the approximation that $\mathbb{P}_{\mathrm{c}}\{T_{\mathrm{h}}\} \approx \mathbb{P}\{\text{no node with } N_{\mathrm{h}} < T_{\mathrm{h}}\}$ when the network is highly connected. The validity of our approximations in (6.21) and (6.23) will be verified via simulations in a later section. In addition, we will further verify our claim via simulations that when the network is highly connected according to our definition 2, i.e., $\mathbb{P}_{\mathrm{c}}\{T_{\mathrm{h}}\} \geq 0.9$, the delivery ratio D_{r} of the consensus flooding protocol under H_1 is also high, i.e., under H_1, $D_{\mathrm{r}} \geq \mathbb{P}_{\mathrm{c}}\{T_{\mathrm{h}}\}$. Since this is a conservative condition, we can only determine an upper bound on λ_{h} given T_{h} and D_{r} using (6.21) and (6.23).

With our consensus flooding protocol, for a given D_{r}, the number of nodes, N_{a}, that agree on the correct local decision $u = +1$ under H_1 is approximated as a Poisson r.v. with mean given by

$$\lambda_{\mathrm{a}} = \mathbb{E}\{N_{\mathrm{a}}\} = \lambda_{\mathrm{t}} D_{\mathrm{r}}. \tag{6.24}$$

On the other hand, we also need to ensure that our consensus flooding protocol minimizes the possibility of false-alarm flooding. Considering that the density of false-alarmed nodes is ρP_{f} and for a given P_{f} in (6.6), the conditional probability that all nodes hear less than T_{h} false-alarmed nodes is given by

$$\begin{aligned} &\mathbb{P}\{\text{all nodes hear less than } T_{\mathrm{h}} \text{ false-alarmed nodes} | N_{\mathrm{t}} = n_{\mathrm{t}}\} \\ &\cong \left(\exp(-P_{\mathrm{f}}\lambda_{\mathrm{h}}) \sum_{i=0}^{T_{\mathrm{h}}-1} \frac{(P_{\mathrm{f}}\lambda_{\mathrm{h}})^{i}}{i!}\right)^{n_{\mathrm{t}}}, \end{aligned} \tag{6.25}$$

and the probability that all nodes hear less than T_{h} false-alarmed nodes is then given by

$$\mathbb{P}\{\text{all nodes hear less than } T_{\mathrm{h}} \text{ false-alarmed nodes}\}$$

$$= \exp\left\{\lambda_{\mathrm{t}}\left[\left(\exp(-P_{\mathrm{f}}\lambda_{\mathrm{h}})\sum_{i=0}^{T_{\mathrm{h}}-1}\frac{(P_{\mathrm{f}}\lambda_{\mathrm{h}})^i}{i!}\right)-1\right]\right\}. \tag{6.26}$$

Note that the event that all nodes hear less than T_{h} false-alarmed nodes is only a sufficient, but not necessary condition for absence of false-alarm flooding. Since the probability that no false flooding occurs is greater than (6.26), we can ensure that our consensus flooding protocol minimizes the possibility of false-alarm flooding by satisfying $P\{\text{false-alarm flooding occurs}\} \leq P_{\mathrm{f}}$.[11]

In summary, we have developed a framework for determining the connection degree of our consensus flooding protocol with a given P_{f} and T_{h}, and high delivery ratio, i.e., $D_{\mathrm{r}} \geq 0.9$, using concept of network connectivity. Specifically, we use (6.23) and (6.26) to determine λ_{h} by fixing $D_{\mathrm{r}} \geq 0.9$ (when POI is present) and $P\{\text{false alarm flooding occurs}\} \leq P_{\mathrm{f}}$. It is interesting to note that, due to the Poisson nature of the WSN, these probabilities do not depend on the channel model details, but only on the synthetic parameter, namely the connection degree λ_{h}.

6.3 Performance Analysis

6.3.1 Probability of Error Analysis

We consider a Bayesian approach, whereby the *a priori* probabilities of the null and alternate hypotheses, $\mathbb{P}\{H_0\}$ and $\mathbb{P}\{H_1\}$, are known at the fusion center. Without loss of generality, we assume that the hypotheses are equally likely. The fusion center employs the EGC fusion rule in (6.11) with threshold $\tau = 0$.[12] Utilizing the total probability law, we can write the probability of decision error at the fusion center as

$$P_{\mathrm{e}} = \frac{1}{2}\mathbb{P}\{e|H_1\} + \frac{1}{2}\mathbb{P}\{e|H_0\}, \tag{6.27}$$

[11]The motivation for this criterion comes from the consideration that at the fusion center we do not want a catastrophic false-alarm flooding event with a probability higher than the P_{f} of each node.

[12]Note that the EGC fusion rule treats all the received observations equally, and $\tau = 0$ is a reasonable choice due to our antipodal signal structure of u_n.

Parallel Fusion Architecture

The conditional probability $\mathbb{P}\{e|H_1\}$ in (6.27) is given by

$$\begin{aligned}\mathbb{P}\{e|H_1\} &= \mathbb{E}_{N_\mathrm{t}}\left\{\mathbb{P}\left(\sum_{n=1}^{n_\mathrm{t}} r_n \leq 0 | N_\mathrm{t}=n_\mathrm{t}, H_1\right)\right\} \\ &= \mathbb{E}_{N_\mathrm{t}}\left\{\sum_{m=0}^{N_\mathrm{t}} B(m, \lambda_\mathrm{d}/\lambda_\mathrm{t}, N_\mathrm{t})\left[1-Q\left(-(2m-N_\mathrm{t})\sqrt{2\mathsf{SNR}/N_\mathrm{t}}\right)\right]\right\}.\end{aligned} \tag{6.28}$$

Similar to (6.28), we can also derive $\mathbb{P}\{e|H_0\}$ in (6.27) as follows:

$$\begin{aligned}\mathbb{P}\{e|H_0\} &= \mathbb{E}_{N_\mathrm{t}}\left\{\mathbb{P}\left(\sum_{n=1}^{n_\mathrm{t}} r_n > 0 | N_\mathrm{t}=n_\mathrm{t}, H_0\right)\right\} \\ &= \mathbb{E}_{N_\mathrm{t}}\left\{\sum_{m=0}^{N_\mathrm{t}} B(m, \lambda_\mathrm{f}/\lambda_\mathrm{t}, N_\mathrm{t}) Q\left(-(2m-N_\mathrm{t})\sqrt{2\mathsf{SNR}/N_\mathrm{t}}\right)\right\},\end{aligned} \tag{6.29}$$

By substituting (6.28) and (6.29) into (6.27), we obtain the probability of decision error for PFA at the fusion center as follows:

$$\begin{aligned}P_\mathrm{e}^{(\mathrm{PFA})} = &\frac{1}{2}\mathbb{E}_{N_\mathrm{t}}\left\{\sum_{m=0}^{N_\mathrm{t}} B(m, \lambda_\mathrm{d}/\lambda_\mathrm{t}, N_\mathrm{t})\left[1-Q\left(-(2m-N_\mathrm{t})\sqrt{2\mathsf{SNR}/N_\mathrm{t}}\right)\right]\right\} \\ &+\frac{1}{2}\mathbb{E}_{N_\mathrm{t}}\left\{\sum_{m=0}^{N_\mathrm{t}} B(m, \lambda_\mathrm{f}/\lambda_\mathrm{t}, N_\mathrm{t}) Q\left(-(2m-N_\mathrm{t})\sqrt{2\mathsf{SNR}/N_\mathrm{t}}\right)\right\},\end{aligned} \tag{6.30}$$

where $B(n, p, n_\mathrm{t})$ denotes the binomial probability distribution of a r.v. n with parameters n_t and p.

Cooperative Fusion Architecture

The conditional probability $\mathbb{P}\{e|H_1\}$ follows straightforwardly from (6.28) and is given by

$$\mathbb{P}\{e|H_1\} = \mathbb{E}_{N_\mathrm{t}}\left\{\mathbb{P}\left(\sum_{n=1}^{n_\mathrm{t}} r_n \leq 0 | N_\mathrm{t}=n_\mathrm{t}, H_1\right)\right\}$$

$$= \mathbb{E}_{N_\mathrm{t}} \left\{ \sum_{m=0}^{N_\mathrm{t}} B(m, \lambda_\mathrm{a}/\lambda_\mathrm{t}, N_\mathrm{t}) \left[1 - Q\left(-(2m - N_\mathrm{t}) \sqrt{2\mathsf{SNR}/N_\mathrm{t}} \right) \right] \right\}. \tag{6.31}$$

On the other hand, $\mathbb{P}\{e|H_0\}$ is given by

$$\begin{aligned} \mathbb{P}\{e|H_0\} &= \mathbb{E}_{N_\mathrm{t}} \left\{ \mathbb{P}\left(\sum_{n=1}^{n_\mathrm{t}} r_n > 0 | N_\mathrm{t} = n_\mathrm{t}, H_0 \right) \right\} \\ &= \mathbb{E}_{N_\mathrm{t}} \left\{ Q\left(\sqrt{2N_\mathrm{t}\mathsf{SNR}} \right) \right\}, \end{aligned} \tag{6.32}$$

where all nodes send the common correct decision $u = 0$ after the consensus flooding when P_f is small. Thus, by substituting (6.31) and (6.32) into (6.27), we obtain the probability of decision error for CFA at the fusion center as follows:

$$\begin{aligned} P_\mathrm{e}^{(\mathrm{CFA})} = &\frac{1}{2} \mathbb{E}_{N_\mathrm{t}} \left\{ \sum_{m=0}^{N_\mathrm{t}} B(m, \lambda_\mathrm{a}/\lambda_\mathrm{t}, N_\mathrm{t}) \left[1 - Q\left(-(2m - N_\mathrm{t}) \sqrt{2\mathsf{SNR}/N_\mathrm{t}} \right) \right] \right\} \\ &+ \frac{1}{2} \mathbb{E}_{N_\mathrm{t}} \left\{ Q\left(\sqrt{2N_\mathrm{t}\mathsf{SNR}} \right) \right\}. \end{aligned} \tag{6.33}$$

6.3.2 Energy Efficiency Analysis

The average energy consumed by each node in the PFA to convey a single information bit to the fusion center at a target P_e is simply given by

$$E_\mathrm{avg}^{(\mathrm{PFA})} = E_\mathrm{b}^{(\mathrm{PFA})}, \tag{6.34}$$

since the PFA does not have any cooperation overhead. To execute the consensus flooding protocol in the CFA, the average number of nodes that send a broadcast packet under H_1 is equal to $\lambda_\mathrm{a} + \lambda_\mathrm{d} \cdot P_{T_\mathrm{h}}$. Recall that λ_a is the average number of nodes which sent a broadcast packet during the flooding process and agreed on the correct decision, and $\lambda_\mathrm{d} \cdot P_{T_\mathrm{h}}$ is the average number of nodes which detected the PoI but did not participate in the flooding process since they do not hear a sufficient number of neighbors. Combining both the transmission and the flooding energy, the

average energy consumed by each node to convey a single information bit to the fusion center when conditioned on H_1 is given by

$$E_{\text{avg}|H_1}^{(\text{CFA})} = E_{\text{b}}^{(\text{CFA})} + \frac{E_{\text{flood}}}{\lambda_{\text{t}}} \left(\lambda_{\text{a}} + \lambda_{\text{d}} \cdot P_{T_{\text{h}}}\right). \tag{6.35}$$

According to our analysis in Chapter 6.2.3, our consensus flooding protocol can ensure that the probability of false-alarm flooding is lower than P_{f}. As a result, the average number of nodes that send a broadcast packet is not larger than λ_{f}, and the average energy consumed by each node to convey a single information bit to the fusion center when conditioned on H_0 is given by

$$E_{\text{avg}|H_0}^{(\text{CFA})} = E_{\text{b}}^{(\text{CFA})} + \frac{E_{\text{flood}}\lambda_{\text{f}}}{\lambda_{\text{t}}}. \tag{6.36}$$

Combining (6.35) and (6.36), the total average energy consumed by each node in the CFA to convey a single information bit to the fusion center at a target P_{e} is given by

$$\begin{aligned} E_{\text{avg}}^{(\text{CFA})} &= \mathbb{P}(H_0)\left[E_{\text{b}}^{(\text{CFA})} + \frac{E_{\text{flood}}\lambda_{\text{f}}}{\lambda_{\text{t}}}\right] + \mathbb{P}(H_1)\left[E_{\text{b}}^{(\text{CFA})} + \frac{E_{\text{flood}}}{\lambda_{\text{t}}}\left(\lambda_{\text{a}} + \lambda_{\text{d}} \cdot P_{T_{\text{h}}}\right)\right] \\ &= E_{\text{b}}^{(\text{CFA})}\left\{1 + \frac{\delta}{2\lambda_{\text{t}}}\left[\lambda_{\text{f}} + \left(\lambda_{\text{a}} + \lambda_{\text{d}} \cdot P_{T_{\text{h}}}\right)\right]\right\}, \end{aligned} \tag{6.37}$$

where $E_{\text{flood}} = \delta E_{\text{b}}$. In realistic WSNs, the choice of δ depends mainly on the relationship between the up-link path-loss and the inter-node wireless links in (6.14). In general, $\frac{E_{\text{flood}}}{2\lambda_{\text{t}}}\left[\lambda_{\text{f}} + (\lambda_{\text{a}} + \lambda_{\text{d}} \cdot P_{T_{\text{h}}})\right]$ accounts for the cooperation overhead since it represents the increase in the average energy consumption per node in order to cooperate.[13]

By using (6.34) and (6.37), we can then compute the average energy gain (in dB) due to cooperation as

$$\Delta_{\text{E}} = 10\log\left(\frac{E_{\text{avg}}^{(\text{PFA})}}{E_{\text{avg}}^{(\text{CFA})}}\right) = 10\log\left(\frac{E_{\text{b}}^{(\text{PFA})}}{E_{\text{b}}^{(\text{CFA})}\left\{1 + \frac{\delta}{2\lambda_{\text{t}}}\left[\lambda_{\text{f}} + (\lambda_{\text{a}} + \lambda_{\text{d}} \cdot P_{T_{\text{h}}})\right]\right\}}\right). \tag{6.38}$$

[13]Note that we have considered implicitly that the energy required for listening is negligible.

For a target P_{e}, $\mathrm{SNR}^{(\mathrm{PFA})}$ and $\mathrm{SNR}^{(\mathrm{CFA})}$ can be determined by simply inverting (6.30) and (6.33) respectively. Substituting these values into (6.38), we obtain

$$\Delta_{\mathrm{E}} = 10 \log \left(\frac{\mathsf{SNR}^{(\mathrm{PFA})}}{\mathsf{SNR}^{(\mathrm{CFA})} \left\{ 1 + \frac{\delta}{2\lambda_{\mathrm{t}}} \left[\lambda_{\mathrm{f}} + (\lambda_{\mathrm{a}} + \lambda_{\mathrm{d}} \cdot P_{T_{\mathrm{h}}}) \right] \right\}} \right). \tag{6.39}$$

From (6.39), we can observe that the gain from cooperation depends on how much energy is spent on local data exchange. This additional required energy explicitly depends on the connectivity of the network through $P_{T_{\mathrm{h}}}$, the delivery ratio of the consensus flooding protocol through λ_{a}, the average flooding energy through δ, and the average number of active sensor nodes through λ_{t}.

6.4 Numerical Results

In this section, we evaluate the performance of both architectures based on our analytical results developed in the previous sections. As shown, our methodology highlights dependency on a large set of parameters that reflect different aspects of the system, such as the average number of nodes in the sensor field (through λ_{t}), PoI intensity (through $\lambda_{\mathrm{d}}/\lambda_{\mathrm{t}}$), inter-node wireless link condition (through λ_{h}), target probability of decision error at the fusion center (P_{e}), probability of false-alarm (P_{f}), and the consensus flooding protocol ($T_{\mathrm{h}}, \lambda_{\mathrm{h}}, D_{\mathrm{r}}$).

Our simulation setup consists of a square of 300×300 m^2 with 500 nodes randomly and independently placed. However, only a circle of radius 75 m is considered to avoid border effects. No medium access control is considered. The inter-node communication model in (6.14) is used with $K = 40$ dB, $\alpha = 3.5$ and $\sigma_{\mathrm{S}} = 4$. In Fig. 6-3, we plot $\mathbb{P}_{\mathrm{c}}\{T_{\mathrm{h}}\}$ based on simulation and analytical expression (6.23) when $\lambda_{\mathrm{d}}/\lambda_{\mathrm{t}} = 0.5$ and PoI is present.[14] It can be seen that for large λ_{h}, $\mathbb{P}_{\mathrm{c}}\{T_{\mathrm{h}}\}$ tends to 1 for different T_{h} values, and the simulation and analytical results are in good agreement verifying that (6.23) is a good approximation for $\mathbb{P}_{\mathrm{c}}\{T_{\mathrm{h}}\}$. Moreover, we have

[14] We have also verified by simulation that the effect of the ratio $\lambda_{\mathrm{d}}/\lambda_{\mathrm{t}}$ is negligible. The results are not shown due to space constraint.

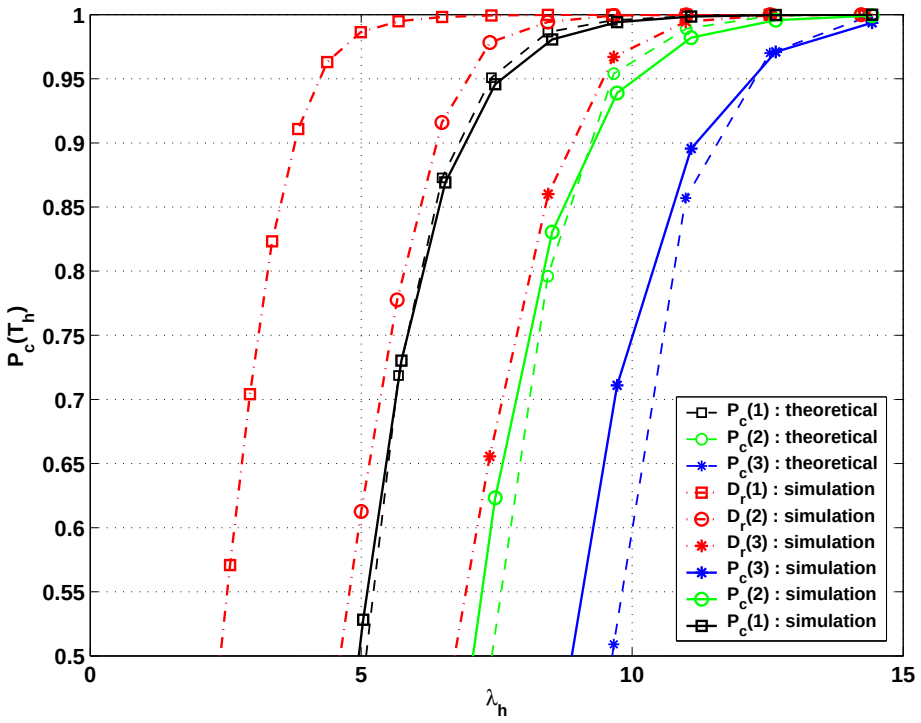

Figure 6-3: Comparison of $\mathbb{P}_{\mathrm{c}}\{T_{\mathrm{h}}\}$ using simulation and analytical results when $\lambda_{\mathrm{d}}/\lambda_{\mathrm{t}} = 0.5$. The solid and dashed lines indicate the analytical result using (6.23) and simulation result respectively.

plotted simulation results for D_{r} in Fig. 6-3, and, indeed, we can observe that $\mathbb{P}_{\mathrm{c}}\{T_{\mathrm{h}}\}$ is lower than D_{r}. As a result, we can obtain an upper bound on λ_{h} for a given T_{h} and $D_{\mathrm{r}} \geq 0.9$ from (6.23). For example, given that $T_{\mathrm{h}} = 3$, we have $\lambda_{\mathrm{h}} = 11$ and 15 for $D_{\mathrm{r}} = 0.9$ and $D_{\mathrm{r}} = 0.99$ respectively. In the following, we will consider two sets of consensus flooding protocol parameters $(T_{\mathrm{h}}, \lambda_{\mathrm{h}}, D_{\mathrm{r}}) = (3, 11, 0.9)$, and $(T_{\mathrm{h}}, \lambda_{\mathrm{h}}, D_{\mathrm{r}}) = (3, 15, 0.99)$.[15]

The performance of both architectures as a function of λ_{t} in the sensor field with different PoI intensity ($\lambda_{\mathrm{d}}/\lambda_{\mathrm{t}} = 0.1$ and $\lambda_{\mathrm{d}}/\lambda_{\mathrm{t}} = 0.8$) is plotted in Fig. 6-4. The consensus flooding protocol parameter set used is $(T_{\mathrm{h}}, \lambda_{\mathrm{h}}, D_{\mathrm{r}}) = (3, 11, 0.9)$, and SNR = -15 dB. For weak PoI intensity ($\lambda_{\mathrm{d}}/\lambda_{\mathrm{t}} = 0.1$), PFA performs poorly as expected due to small sensing coverage. For strong PoI intensity ($\lambda_{\mathrm{d}}/\lambda_{\mathrm{t}} = 0.8$), PFA performs better and the probability of error decays with increasing λ_{t}. For CFA, we can observe

[15]For these sets of consensus flooding protocol parameters, the condition that $P\{\text{false-alarm flooding occurs}\} \leq P_{\mathrm{f}}$ is also satisfied for $P_{\mathrm{f}} = 10^{-3}$ using (6.26).

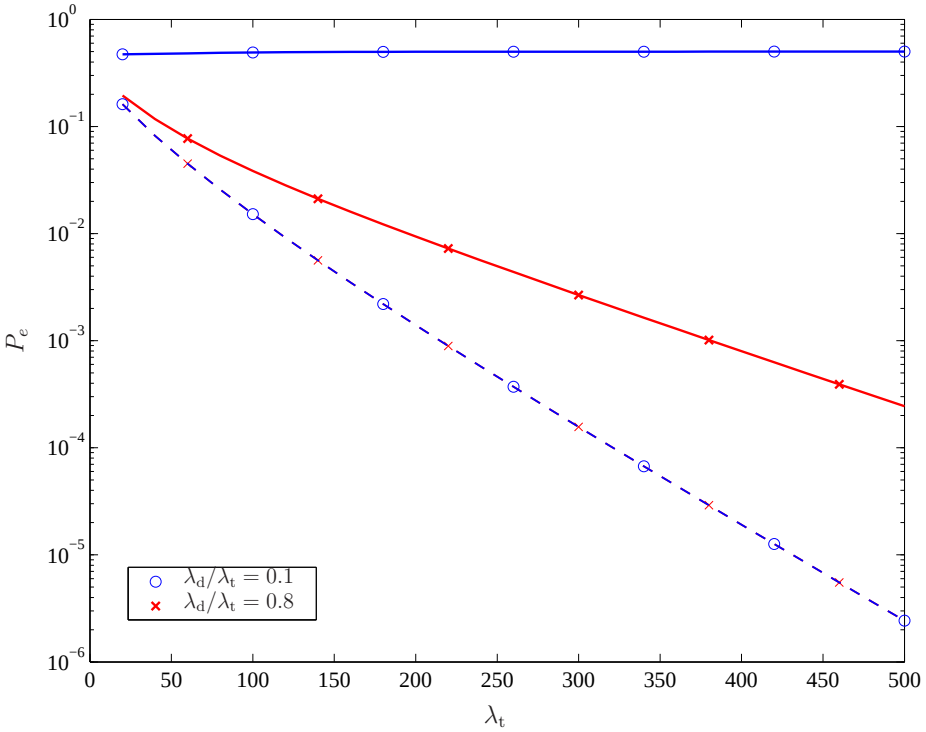

Figure 6-4: Performance of PFA and CFA with respect to the average number of nodes. The solid and dashed lines indicate PFA and CFA respectively. The flooding protocol parameter set used is $(T_h, \lambda_h, D_r) = (3, 11, 0.9)$, and SNR = -15 dB.

that the probability of error decays with increasing λ_t regardless of the PoI intensity. This shows that CFA provides reliability in WSN especially when the PoI intensity may be weak or unknown.

Next, we consider the effect of PoI intensity on the performance of both architectures when $\lambda_t = 500$ and SNR = -15 dB in Fig. 6-5. Two sets of consensus flooding protocol parameters are used for comparison in CFA. It can be seen that CFA is insensitive to the PoI intensity, and the protocol with higher delivery ratio performs better at the expense of a higher energy consumption due to the increased degree of connection λ_h required. Similar to Fig. 6-4, we can observe that PFA performs better as the PoI intensity increases, showing that the reliability of PFA depends heavily on the PoI intensity. Note that this performance also depends on the threshold at the fusion center, which we have assumed to be zero for this case. If the fusion center has more information about the sensor field and the PoI,[16] it can then optimize this

[16]Here, information refers to the individual probability of detection of each node and the *a priori*

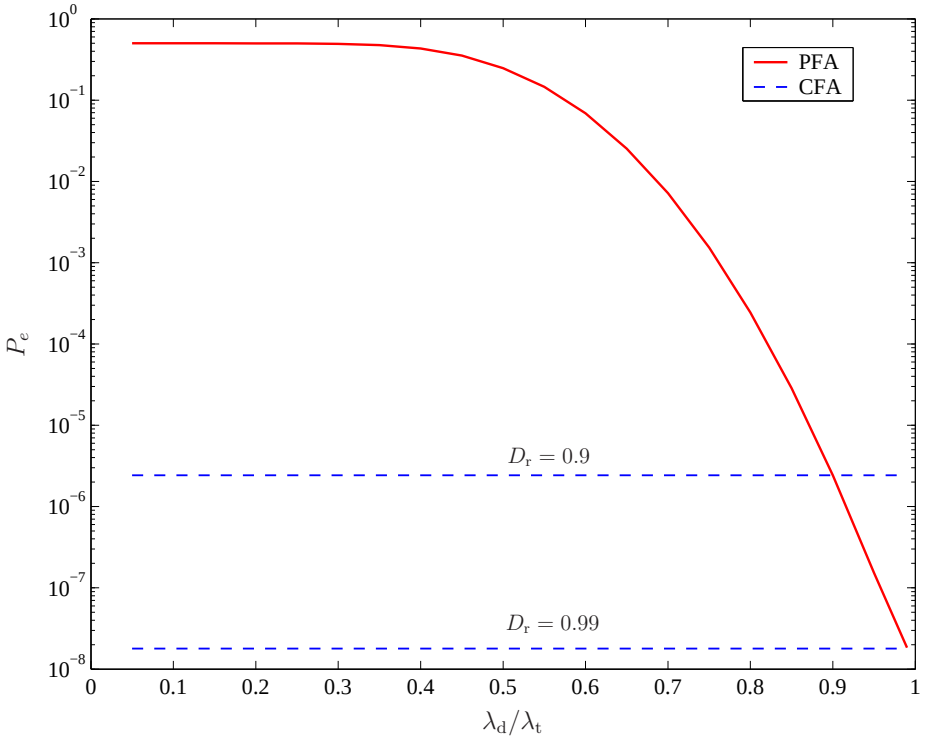

Figure 6-5: Effect of PoI intensity through λ_d/λ_t and delivery ratio of the consensus flooding protocol on the performance of PFA and CFA when $\lambda_t = 500$ and SNR = -15 dB. The solid and dashed lines indicate PFA and CFA respectively. The flooding protocol parameter sets used are $(T_h, \lambda_h, D_r) = (3, 11, 0.9)$ and $(T_h, \lambda_h, D_r) = (3, 15, 0.99)$.

threshold to obtain a better performance than that shown in Fig. 6-5.

The effect of PoI intensity, delivery ratio, network connectivity, and flooding energy on the energy efficiency of CFA at $P_e = 1 \times 10^{-4}$ and $\lambda_t = 500$ is plotted in Figs. 6-6 and 6-7. In Fig. 6-6, we compare two sets of consensus flooding protocol parameters with different D_r and λ_h. Using (6.17), we can determine the values of E_{flood}/E_{min} for $\lambda_h = 11$ and 15, respectively. By letting the δ that corresponds to $\lambda_h = 11$ to be 0.1, we can then obtain the new δ that corresponds to $\lambda_h = 15$ using the values of E_{flood}/E_{min}. From Fig. 6-6, we can observe that as the PoI intensity increases, the average energy gain due to cooperation decreases since PFA becomes more reliable. It can also be seen that higher deliver ratio offers a greater average energy efficiency due to cooperation. However, this average energy gain due to coop-

probabilities of the hypotheses.

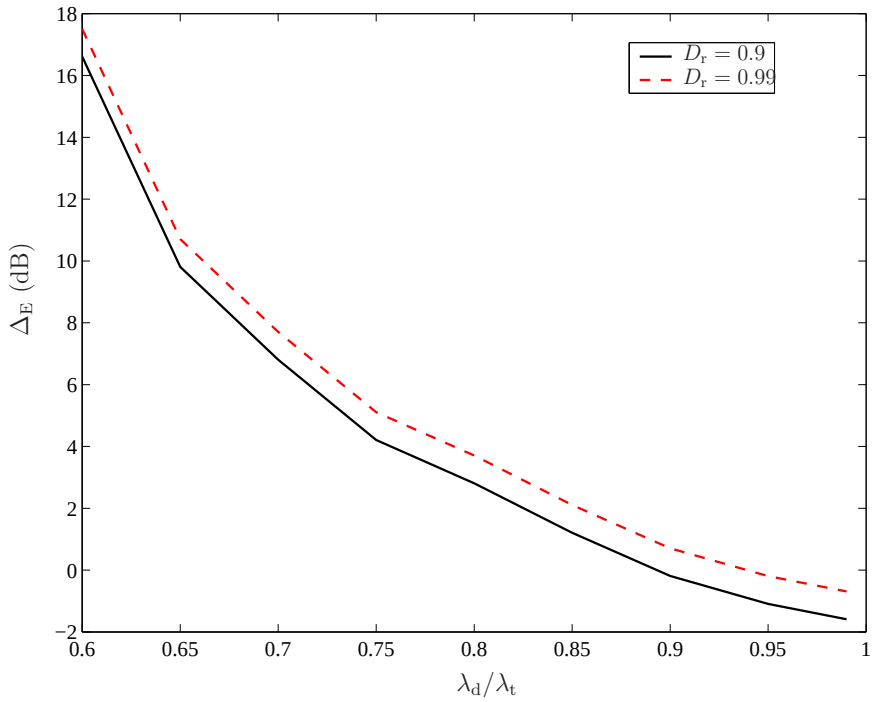

Figure 6-6: Effect of PoI intensity through λ_d/λ_t and delivery ratio on energy efficiency of CFA when $P_e = 1 \times 10^{-4}$ and $\lambda_t = 500$. The flooding protocol parameter sets used are $(T_h, \lambda_h, D_r) = (3, 11, 0.9)$ and $(T_h, \lambda_h, D_r) = (3, 15, 0.99)$.

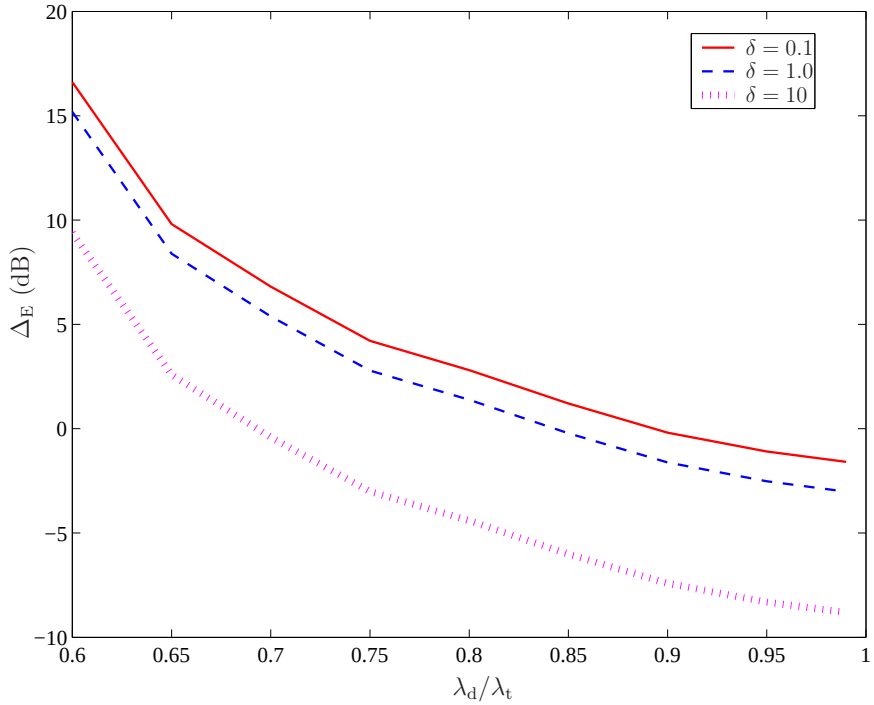

Figure 6-7: Effect of PoI intensity through λ_d/λ_t and flooding energy on energy efficiency of CFA when $P_e = 1 \times 10^{-4}$ and $\lambda_t = 500$. The flooding protocol parameter set used is $(T_h, \lambda_h, D_r) = (3, 11, 0.9)$.

eration can go below 0 dB at a certain region of high PoI intensity, since the increase in average energy consumption needed to execute flooding outweighs the gain in energy efficiency resulting from cooperation. To further investigate this phenomenon, we consider different values of δ ($\delta = 0.1$, $\delta = 1$ and $\delta = 10$) with the consensus flooding protocol parameter set $(T_{\mathrm{h}}, \lambda_{\mathrm{h}}, D_{\mathrm{r}}) = (3, 11, 0.9)$ in Fig. 6-7. It can be seen clearly in Fig. 6-7 that the average energy gain due to cooperation decreases as δ increases. Recall that δ mainly depends on the node transmitter power, bit rate and packet length. This result shows that these parameters have to be carefully designed to make δ small, in order for CFA to be more energy efficient than PFA. Depending on the PoI intensity, PFA can be more energy efficient than CFA, especially for larger values of δ. For example, when $\delta = 10$, it is more energy efficient to implement PFA in regions with PoI intensity $\lambda_{\mathrm{d}}/\lambda_{\mathrm{t}} \geq 0.7$.

Lastly, we consider the effect of node density on the energy efficiency of CFA at $P_{\mathrm{e}} = 1 \times 10^{-4}$ and $\lambda_{\mathrm{d}}/\lambda_{\mathrm{t}} = 0.8$ with the consensus flooding protocol parameter set $(T_{\mathrm{h}}, \lambda_{\mathrm{h}}, D_{\mathrm{r}}) = (3, 11, 0.9)$ in Fig. 6-8. As λ_{t} increases, the average energy gain due to cooperation decreases and tends to reach a floor. Similar to Fig. 6-7, we also observe here that the average energy gain due to cooperation decreases as δ increases.

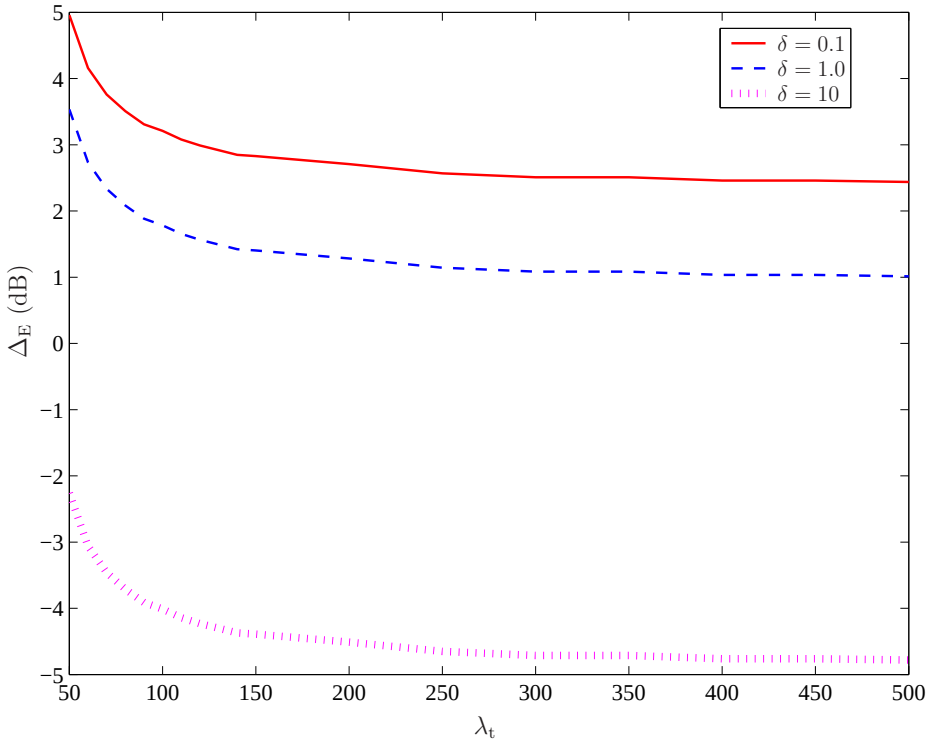

Figure 6-8: Effect of node density and flooding energy cost on energy efficiency of CFA when $P_{\mathrm{e}} = 1 \times 10^{-4}$ and $\lambda_{\mathrm{d}}/\lambda_{\mathrm{t}} = 0.8$. The flooding protocol parameter set used is $(T_{\mathrm{h}}, \lambda_{\mathrm{h}}, D_{\mathrm{r}}) = (3,\ 11,\ 0.9)$.

Chapter 7

Conclusions

This final chapter summarizes the contributions of the dissertation and highlights numerous areas for further research.

7.1 Contributions

In Chapter 2, we developed RPA algorithms that maximize the output SNR of coherent and noncoherent AF relay networks under both individual and aggregate relay power constraints. We showed that the coherent AF RPA problem, in the presence of perfect global CSI, can be formulated as a quasiconvex optimization problem. Thus, these RPA problems can be solved efficiently using the bisection method via a sequence of convex feasibility problems, in the form of SOCPs. We also showed that the noncoherent AF RPA problem, in the presence of perfect global CSI, can be approximately decomposed into $2L$ quasiconvex optimization subproblems. Each subproblem can be solved efficiently by the bisection method via a sequence of convex feasibility problems in the form of SOCP. Even with optimal RPA, we showed that the noncoherent AF relay network performs much worse than the coherent AF case. For the coherent AF case, we have distributed beamforming, which helps to reduce the severity of deep fades. Therefore, some form of diversity techniques needs to be exploited to further reduce the outages for the noncoherent AF case, e.g., time diversity or spatial receiver diversity. By applying the robust optimization methodol-

ogy, we showed that the robust counterparts of our convex feasibility problems with ellipsoidal uncertainty sets can be formulated as SDPs. Our results revealed that ignoring global CSI uncertainties and solving the relay power optimization problem often leads to poor performance. As a result, this work highlights the importance of robust algorithm designs in practical wireless networks.

In Chapter 3, we formulated the AF RPA problem as the total relay transmission power minimization problem subject to a QoS constraint. With the CE output SNR constraint, we proposed practical algorithms that track only large-scale fading. With perfect knowledge of the large-scale fading, we showed that the optimization problems for the coherent and noncoherent AF relay networks can be cast as an SOCP and an LP, respectively. The conditions for verifying the feasibility of these problems and the optimality of the solutions are also derived. Furthermore, we extended these optimization problems to take into account uncertainties in the knowledge of large-scale fading. For ellipsoidal uncertainty sets, we showed that the robust counterparts of our optimization problems for the coherent and noncoherent AF relay networks can be formulated as an SDP and an SOCP, respectively. Numerical results showed that the proposed algorithms provide significant power savings over the naive scheme that employs maximum transmission power at each relay node. In addition, our robust algorithms provide effective and feasible solutions, yielding good performance in the presence of uncertainties associated with the global CSI.

In Chapter 4, we analyzed the performance of TR and DTR signaling in dense multipath UWB channels. We derived the BEP expression for the TR signaling with AcR via the Gaussian approximation and sampling expansion approaches. We showed the limitation of the Gaussian approximation whose validity depends on the assumption of a large time-bandwidth product or large number of transmitted pulses per symbol. Based on the sampling expansion approach, we developed an analytical framework to derive a closed-form expression for the BEP of TR and DTR signaling with AcR for a broad class of fading channels. We extended our methodology to derive the BEP of TR and DTR signaling with modified AcR. We compared the performance of TR signaling with AcR with that of the ARake and PRake receivers

using our computationally simple lower bound. This allowed us to obtain the SNR penalty associated with TR signaling with an AcR, as compared to ARake and PRake receivers for the BEP range of interest.

In Chapter 5, we developed a quasi-analytical method as well as an approximate analytical method to evaluate the BEP of TR and DTR signaling in the presence of NBI. We showed that the approximate analytical method is particularly useful in obtaining BEP expressions that provide insight into the effect of NBI on the performance of TR signaling schemes. We showed that the approximation is in good agreement with the quasi-analytical results. We quantified the effects of NBI and channel PDP on the optimum integration interval of an AcR, showing that NBI imposes a practical limit on the amount of multipath energy that can be captured by an AcR. In particular, we showed that the optimum integration interval strongly depends on the channel PDP and the SNR, as well as the SIR. We compared TR and DTR signaling in terms of their sensitivity to NBI and revealed that the BEP improvement provided by DTR signaling is entirely different in noise-limited and interference-limited regimes.

In Chapter 6, we investigated a binary decentralized detection problem in a dense, randomly deployed and bandwidth-constrained WSN when the sensor observations are spatially varying. We compared two different fusion architectures, namely, the parallel fusion architecture and the cooperative fusion architecture, in bandwidth-constrained WSNs, where each node is restricted to sending a 1-bit information to the fusion center. We derived expressions for the probability of decision error at the fusion center and analyzed the average energy consumption for each architecture. We quantified the effect of PoI intensity, realistic link models, consensus flooding protocol, and network connectivity on the system reliability and average energy consumption for both fusion architectures. We showed that cooperation using our proposed consensus flooding protocol is particularly advantageous in scenarios where the PoI intensity may be weak or unknown. Consequently, this work identifies a fruitful approach for obtaining insight into the design of cooperative WSNs, as well as the understanding of the trade-off issues among reliability and energy efficiency in the presence of spatially varying sensor observations, network connectivity, and realistic link models.

7.2 Future work

For future research on the design of cooperative networks, we have summarized some interesting areas and extensions that are worth pursuing.

- **Robust Resource Allocation:** In our robust counterpart formulation, we assume that there is no distributional information of the global CSI uncertainty, and adopt the robust optimization methodology developed in [7, 8]. However, when there is some distributional information of the global CSI uncertainty, one can then employ stochastic optimization and safeguard constraints against violation using chance or probabilistic constraints [114, 155, 156]. The general difficulty of such a probabilistic approach is that computational tractable chance constraints only exist for some known distributions, and we often end up with non-convex chance constraints in most cases. Another possible direction is to design distributed power allocation algorithms instead of centralized design as studied in this dissertation. In the distributed design, the dual decomposition method provides a computationally tractable way to solve this power allocation problem [157]. In addition, it may be interesting to investigate how to extend such distributed algorithms to incorporate CSI uncertainties. Another possible direction is to generalize the formulation in this dissertation to the case of multiple-antenna relay nodes. It is well-known that multiple antennas can offer significant improvements in terms of spectral efficiency and link reliability. Therefore, it is interesting to study how resource allocation and efficient transmission designs can further increase the performance gains for such systems, as well as to understand how these gains depend on the number of antennas. Extension to the case of multiple source-destination pairs and multihop may be fruitful. Besides focusing on AF relaying, it would be interesting to consider other relaying schemes in the above studies.

- **Wideband Communications:** Since UWB systems need to coexist and contend with many narrowband communication systems, it is important to analyze the performance of TR signaling schemes in the presence of various narrowband

systems for successful deployment of UWB systems. As a result, it is important to study the performance in the case of multiple NBI, particularly using an interesting interference model has been considered in [158–160]. Moreover, an analytical comparison with energy detector is also worth investigating since both energy detector and AcR have been considered as potential low-complexity and low-sampling rate solutions in IEEE 802.15.4a standardization process. Some results along this direction can be found in [161, 162]. Besides investigating effect of NBI, it may be worthwhile to study the effect of other wideband systems or multiuser interference on UWB systems using either energy detector or AcR. In addition, it would be interesting to see how we can incorporate TR signaling into wideband cooperative networks design by taking into account the multipath fading channels and different relaying schemes.

- **Energy Efficiency:** In this dissertation, we have considered that the links from the nodes to the fusion center are subjected to identical large-scale fading. In general, the nodes are randomly distributed and the fusion center may be deployed such that the channels from different sensor nodes to the fusion center are subjected to different large-scale and small-scale fading. It would be of interest to examine ways in which current work can be extended to settings that include such effects. In addition, knowledge of channel state information at the sensor nodes through feedback may allow the nodes to exploit opportunistic transmission. This dissertation has not examined the scenario with mobility. Therefore, it would be interesting to investigate how mobility can affect our results. Another interesting avenue would be to extend our framework to a distributed multi-target classification problem [163]. This would be very relevant in practical WSNs where more than one target or event must be classified. It would be interesting to see what types of communication and detection strategies at the sensor nodes are needed under different power, network, and complexity constraints.

Appendix A

Mathematical Preliminaries

A.1 Generalized Convexity

In this appendix, we provide some mathematical preliminaries on generalized convexity.

Definition 3. *The lower-level set of a function $f : \mathbb{R}^N \to \mathbb{R}$ is defined as $L(f, \alpha) = \{\boldsymbol{x} \in \mathbb{R}^N : f(\boldsymbol{x}) \leq \alpha\}$. Similarly, the upper-level set of a function $f : \mathbb{R}^N \to \mathbb{R}$ is defined as $U(f, \alpha) = \{\boldsymbol{x} \in \mathbb{R}^N : f(\boldsymbol{x}) \geq \alpha\}$.*

Definition 4. *Let $\mathcal{S}$ be a convex subset of $\mathbb{R}^N$. A function $f : \mathcal{S} \to \mathbb{R}$ is said to be quasiconvex if and only if its lower-level sets $L(f, \alpha)$ are convex sets for every $\alpha \in \mathbb{R}$. Similarly, f is said to be quasiconcave if and only if its upper-level sets $U(f, \alpha)$ are convex sets for every $\alpha \in \mathbb{R}$.*

Definition 5. *Alternatively, a function $f : \mathcal{S} \to \mathbb{R}$ is said to be quasiconvex if and only if*

$$f(\lambda \boldsymbol{x} + (1 - \lambda)\boldsymbol{y}) \leq \max\{f(\boldsymbol{x}), f(\boldsymbol{y})\}, \tag{A.1}$$

for every $\boldsymbol{x}, \boldsymbol{y} \in \mathcal{S}$, and $0 \leq \lambda \leq 1$. Similarly, f is said to be quasiconcave if and only if

$$f(\lambda \boldsymbol{x} + (1 - \lambda)\boldsymbol{y}) \geq \min\{f(\boldsymbol{x}), f(\boldsymbol{y})\}, \tag{A.2}$$

for every $\boldsymbol{x}, \boldsymbol{y} \in \mathcal{S}$*, and* $0 \leq \lambda \leq 1$*.*

Definition 6. *If* $\mathcal{S} \subseteq \mathbb{R}^N$ *is a convex set, then* $f : \mathcal{S} \to \mathbb{R}$ *is concave on* $\mathcal{S}$ *if* $f(\lambda \boldsymbol{x} + (1-\lambda)\boldsymbol{y}) \geq \lambda f(\boldsymbol{x}) + (1-\lambda) f(\boldsymbol{y})$ *for every* $\boldsymbol{x}, \boldsymbol{y} \in \mathcal{S}$*, and* $0 \leq \lambda \leq 1$*. Similarly,* $f : \mathcal{S} \to \mathbb{R}$ *is convex on* $\mathcal{S}$ *if* $f(\lambda \boldsymbol{x} + (1-\lambda)\boldsymbol{y}) \leq \lambda f(\boldsymbol{x}) + (1-\lambda) f(\boldsymbol{y})$ *for every* $\boldsymbol{x}, \boldsymbol{y} \in \mathcal{S}$*, and* $0 \leq \lambda \leq 1$*.*

A.2 Conic Programming

Mathematically, SOCPs are a class of convex programming problems in which a linear objective function is minimized over the intersection of SOC constraints [114, 164]. The second-order cone (also known as quadratic, ice-cream, or Lorentz cone) $\mathcal{K}$ is defined as the norm cone for the Euclidean norm and is given by

$$\mathcal{K} = \left\{ \boldsymbol{u} \in \mathbb{R}^N,\ t \in \mathbb{R}_+ : \|\boldsymbol{u}\| \leq t \right\}. \tag{A.3}$$

The notation $\succeq_{\mathcal{K}}$ in (A.3) denotes the generalized inequality with respect to $\mathcal{K}$ as follows:

$$\begin{bmatrix} t \\ \boldsymbol{u} \end{bmatrix} \succeq_{\mathcal{K}} 0 \Leftrightarrow \|\boldsymbol{u}\| \leq t. \tag{A.4}$$

Therefore, an SOCP is a conic problem in which the standard form is given by [114]:

$$\begin{aligned} \min_{\boldsymbol{x}} \quad & \boldsymbol{q}^T \boldsymbol{x} \\ s.t. \quad & \begin{bmatrix} \boldsymbol{c}_i^T \boldsymbol{x} + d_i \\ \boldsymbol{A}_i \boldsymbol{x} + \boldsymbol{b}_i \end{bmatrix} \succeq_{\mathcal{K}} 0, \quad i \in \{1, 2, \ldots, M\}, \end{aligned} \tag{A.5}$$

where $\boldsymbol{x} \in \mathbb{R}^N$ is the optimization variable, and the data parameters are $\boldsymbol{q} \in \mathbb{R}^N$, $\boldsymbol{A}_i \in \mathbb{R}^{N_i \times N}$, $\boldsymbol{b}_i \in \mathbb{R}^{N_i}$, $\boldsymbol{c}_i \in \mathbb{R}^N$, and $d_i \in \mathbb{R}$. In addition, it is well-known that SOCP also includes several important standard convex optimization problems, such as LP, quadratic programming (QP), and quadratically constrained quadratic programming

(QCQP). In addition, we can always represent an SOC constraint in (A.4) in terms of a linear matrix inequality (LMI), as follows [114]:

$$\begin{bmatrix} t \\ \boldsymbol{u} \end{bmatrix} \succeq_{\mathcal{K}} 0 \Leftrightarrow \begin{bmatrix} t\boldsymbol{I}_N & \boldsymbol{u} \\ \boldsymbol{u}^T & t \end{bmatrix} \succeq 0. \tag{A.6}$$

As a result, SOCP can always be represented as a SDP.[1] However, it has been shown that is it computationally more efficient to solve SOCP compared to SDP by interior-point methods [114, 164].

Lemma 6. *The function $f(\boldsymbol{x}) = \boldsymbol{x}^T\boldsymbol{x}$ is SOC representable.*

Proof. The epigraph of $f(\boldsymbol{x})$, denoted by $\text{Epi}(f)$, is given by

$$\begin{aligned}
\text{Epi}(f) &= \left\{(\boldsymbol{x}, t) \in \mathcal{S} \times \mathbb{R} : \boldsymbol{x}^T\boldsymbol{x} \leq t\right\} \\
&= \left\{(\boldsymbol{x}, t) \in \mathcal{S} \times \mathbb{R} : \boldsymbol{x}^T\boldsymbol{x} + \frac{(t-1)^2}{4} \leq \frac{(t+1)^2}{4}\right\} \\
&= \left\{(\boldsymbol{x}, t) \in \mathcal{S} \times \mathbb{R} : \left\| \begin{matrix} \boldsymbol{x} \\ \frac{t-1}{2} \end{matrix} \right\| \leq \frac{t+1}{2}\right\} \\
&= \left\{(\boldsymbol{x}, t) \in \mathcal{S} \times \mathbb{R} : \begin{bmatrix} \frac{t+1}{2} \\ \boldsymbol{x} \\ \frac{t-1}{2} \end{bmatrix} \succeq_{\mathcal{K}} 0\right\}
\end{aligned}$$

where we have used the fact that $t = \frac{(t+1)^2}{4} - \frac{(t-1)^2}{4}$ and the generalized inequality in (A.4) to represent $\text{Epi}(f)$ as a cone. □

A.3 Robust Optimization

A generic mathematical programming problem is given by

$$\begin{aligned}
&\text{minimize}_{\boldsymbol{x}} \quad f_0(\boldsymbol{x}) \\
&\text{subject to} \quad f_i(\boldsymbol{x}) \geq 0, \qquad \forall i \in \{1, 2, \ldots, m\},
\end{aligned} \tag{A.7}$$

[1] SDP problems are a class of convex optimization problems in which a linear function is minimized over the cone of positive semi-definite matrices.

where $\boldsymbol{x}$ is the optimization variable, f_0 is the objective function, and $\{f_i\}$ are inequality constraint functions. In the nominal model, it is assumed that the nominal data is completely known, and it is possible to solve (A.7). However, in practice, each $\{f_i\}$ can be perturbed and the optimal solutions based on the nominal model in (A.7) may become infeasible or even useless [165].

A more appropriate design approach is to ensure that the optimal solutions remain feasible and yield good performance in all possible realizations of unknown perturbations. We make distinction from stochastic uncertainty where the probability distributions of the underlying stochastic perturbations are known. This requirement often creates heavy burden on the system designer since in many realistic applications, such information is unavailable or too costly to obtain. In the following, we treat uncertainty as a collection of data, which we call the uncertainty set. The size of the uncertainty set corresponds to the amount of uncertainty about the data.[2] Mathematically, the robust counterpart of the optimization problem in (A.7) with uncertain data can be formulated as [7, 8]:

$$\begin{array}{lll} \min_{\boldsymbol{\zeta}} & f_0(\boldsymbol{\zeta}, \boldsymbol{D}_0) & \\ \text{s.t.} & f_i(\boldsymbol{\zeta}, \boldsymbol{D}_i) \geq 0, & \forall i \in \{1, 2, \ldots, m\}, \\ & \boldsymbol{D}_j \in \mathcal{U}_j, & \forall j = 0, 1, \ldots, m, \end{array} \tag{A.8}$$

where $\{\boldsymbol{D}_i\}$ are the uncertain data associated with the uncertainty sets $\{\mathcal{U}_i\}$. The feasible set and optimal solutions of (A.8) are called the robust feasible set and robust optimal solutions, respectively. Note that this methodology does not assume that the data uncertainty is of stochastic nature, and it only looks for solutions which remain feasible for all possible data within the uncertainty set.

One might see that the cardinality of $\mathcal{U}_i$ can be potentially large and hence, the robust counterpart may end up with infinitely many inequalities, in which case, it is known as semi-infinite optimization problem. It is well-known that semi-infinite problems, even convex ones, are not always tractable. This limits severely on the size of problem we could address under the robust framework. Nevertheless, it has been

[2]The singleton uncertainty set corresponds to the case of perfect knowledge of the data.

shown that there are important problems coupled with reasonable choices of uncertainty sets, that retain polynomial complexity [7,8]. In such cases, there usually exist equivalent robust counterparts, which are explicit convex optimization problems, that are polynomially solvable using efficient algorithms such as interior-point methods. One such example is an ellipsoidal uncertainty set, defined as follows [7,8]:

$$\mathcal{U}_i = \left\{ \boldsymbol{D}_i = \boldsymbol{D}_{i,0} + \sum_{j=1}^{N} \delta_j \boldsymbol{D}_{i,j} : \|\boldsymbol{\delta}\| \leq \rho \right\} \tag{A.9}$$

where $\boldsymbol{D}_{i,0}$ is the nominal data, $\boldsymbol{D}_{i,j}$ is the jth direction of data perturbation, and $\boldsymbol{\delta}$ is the perturbation vector. The level of feasibility of each robust constraint in (A.8) is controlled by adjusting ρ deterministically. Although the uncertain-but-bounded model of uncertainty in (A.9) requires *a priori* knowledge of ρ, it is much easier to point out the support of the distribution of $\boldsymbol{\delta}$ rather than the distribution itself. For example, we may estimate the size of the ellipsoidal uncertainty set from the data obtained from preliminary knowledge of the imperfect CSI estimation and/or from extensive wireless channel measurement campaigns. Besides resulting in mathematical simplification, the ellipsoidal uncertainty set is also well-motivated by practical CSI error models [117].

Appendix B

BEP Derivation of TR Signaling

B.1 Output statistics of the AcR

In this appendix, we expand the output statistics of Z_{TR} as

$$
\begin{aligned}
Z_1 &\triangleq \sum_{j=0}^{\frac{N_{\mathrm{s}}}{2}-1} \int_{-\infty}^{\infty} \int_{j2T_{\mathrm{f}}+T_{\mathrm{r}}+c_j T_{\mathrm{p}}}^{j2T_{\mathrm{f}}+T_{\mathrm{r}}+c_j T_{\mathrm{p}}+T} \Big[h(\tau) s_{\mathrm{TR}}(t-\tau) h(\tau) s_{\mathrm{TR}}(t-T_{\mathrm{r}}-\tau) \Big] dt d\tau \\
&= \sum_{j=0}^{\frac{N_{\mathrm{s}}}{2}-1} \Bigg[\sum_{l=1}^{L_{\mathrm{CAP}}} \alpha_l^2 \int_{j2T_{\mathrm{f}}+c_j T_{\mathrm{p}}}^{j2T_{\mathrm{f}}+c_j T_{\mathrm{p}}+T} s_{\mathrm{TR}}(t-\tau_l) s_{\mathrm{TR}}(t+T_{\mathrm{r}}-\tau_l) dt \\
&\quad + \sum_{l=1}^{L_{\mathrm{CAP}}} \sum_{m=1}^{L_{\mathrm{CAP}}} \alpha_l \alpha_m \int_{j2T_{\mathrm{f}}+c_j T_{\mathrm{p}}}^{j2T_{\mathrm{f}}+c_j T_{\mathrm{p}}+T} s_{\mathrm{TR}}(t-\tau_l) s_{\mathrm{TR}}(t+T_{\mathrm{r}}-\tau_m) dt \Bigg] \\
&= \frac{E_{\mathrm{s}}}{2} d_0 \sum_{l=1}^{L_{\mathrm{CAP}}} \alpha_l^2 \qquad \text{(B.1)} \\
Z_2 &\triangleq \sum_{j=0}^{\frac{N_{\mathrm{s}}}{2}-1} \int_{-\infty}^{\infty} \int_{j2T_{\mathrm{f}}+T_{\mathrm{r}}+c_j T_{\mathrm{p}}}^{j2T_{\mathrm{f}}+T_{\mathrm{r}}+c_j T_{\mathrm{p}}+T} h(\tau) s_{\mathrm{TR}}(t-\tau) \widetilde{n}(t-T_{\mathrm{r}}) dt d\tau \\
&= \sum_{j=0}^{\frac{N_{\mathrm{s}}}{2}-1} \sum_{l=1}^{L_{\mathrm{CAP}}} \alpha_l \int_{j2T_{\mathrm{f}}+c_j T_{\mathrm{p}}}^{j2T_{\mathrm{f}}+c_j T_{\mathrm{p}}+T} s_{\mathrm{TR}}(t+T_{\mathrm{r}}-\tau_l) \widetilde{n}(t) dt \qquad \text{(B.2)} \\
Z_3 &\triangleq \sum_{j=0}^{\frac{N_{\mathrm{s}}}{2}-1} \int_{-\infty}^{\infty} \int_{j2T_{\mathrm{f}}+T_{\mathrm{r}}+c_j T_{\mathrm{p}}}^{j2T_{\mathrm{f}}+T_{\mathrm{r}}+c_j T_{\mathrm{p}}+T} h(\tau) s_{\mathrm{TR}}(t-T_{\mathrm{r}}-\tau) \widetilde{n}(t) dt d\tau
\end{aligned}
$$

$$= \sum_{j=0}^{\frac{N_s}{2}-1} \sum_{l=1}^{L_{\mathrm{CAP}}} \alpha_l \int_{j2T_f+c_jT_p}^{j2T_f+c_jT_p+T} s_{\mathrm{TR}}(t-\tau_l)\widetilde{n}(t+T_r)dt \tag{B.3}$$

$$Z_4 \triangleq \sum_{j=0}^{\frac{N_s}{2}-1} \int_{j2T_f+T_r+c_jT_p}^{j2T_f+T_r+c_jT_p+T} \widetilde{n}(t)\widetilde{n}(t-T_r)dt$$

$$= \sum_{j=0}^{\frac{N_s}{2}-1} \int_{j2T_f+c_jT_p}^{j2T_f+c_jT_p+T} \widetilde{n}(t)\widetilde{n}(t+T_r)dt. \tag{B.4}$$

B.2 Conditional Variances of the output of AcR

In this appendix, we derive the conditional variances of Z_2, Z_3, and Z_4 as shown below

$$\mathbb{V}\left\{Z_2|\{\alpha_l\}_{l=1}^{L_{\mathrm{CAP}}}\right\}$$
$$= \sum_{j=0}^{\frac{N_s}{2}-1}\sum_{j'=0}^{\frac{N_s}{2}-1}\sum_{l=1}^{L_{\mathrm{CAP}}} \alpha_l^2 \int_{j2T_f+c_jT_p}^{j2T_f+c_jT_p+T}\int_{j'2T_f+c_{j'}T_p}^{j'2T_f+c_{j'}T_p+T} s_{\mathrm{TR}}(t+T_r-\tau_l)s_{\mathrm{TR}}(u+T_r-\tau_l)R_{\widetilde{n}}(t-u)dtdu$$
$$\simeq \frac{E_s}{4}N_0 \sum_{l=1}^{L_{\mathrm{CAP}}} \alpha_l^2 \tag{B.5}$$

$$\mathbb{V}\left\{Z_3|\{\alpha_l\}_{l=1}^{L_{\mathrm{CAP}}}\right\}$$
$$= \sum_{j=0}^{\frac{N_s}{2}-1}\sum_{j'=0}^{\frac{N_s}{2}-1}\sum_{l=1}^{L_{\mathrm{CAP}}} \alpha_l^2 \int_{j2T_f+c_jT_p}^{j2T_f+c_jT_p+T}\int_{j'2T_f+c_{j'}T_p}^{j'2T_f+c_{j'}T_p+T} s_{\mathrm{TR}}(t-\tau_l)s_{\mathrm{TR}}(u-\tau_l)R_{\widetilde{n}}(t-u)dtdu$$
$$\simeq \frac{E_s}{4}N_0 \sum_{l=1}^{L_{\mathrm{CAP}}} \alpha_l^2. \tag{B.6}$$

Since the noise components are zero-mean, jointly Gaussian r.v.'s, and by using the result for the fourth-moment of jointly Gaussian random variables [166], the conditional variance of Z_4 can be derived as

$$\mathbb{V}\left\{Z_4|\{\alpha_l\}_{l=1}^{L_{\mathrm{CAP}}}\right\}$$
$$= \sum_{j=0}^{\frac{N_s}{2}-1}\sum_{j'=0}^{\frac{N_s}{2}-1} \int_{j2T_f+c_jT_p}^{j2T_f+c_jT_p+T}\int_{j'2T_f+c_{j'}T_p}^{j'2T_f+c_{j'}T_p+T} R_{\widetilde{n}}^2(t-u) + R_{\widetilde{n}}(t-u-T_r)R_{\widetilde{n}}(t-u+T_r)dtdu$$
$$\simeq \frac{N_s}{4}N_0^2WT. \tag{B.7}$$

Note that in the above derivations, we have assumed that $W \gg 1/T_{\rm g}$ so $R_{\tilde{n}}(\tau)$ in (4.8) is approximately equal to zero for $|\tau| \geq T_{\rm g}$.

B.3 Sampling Expansion Approach

In this appendix, we show how we can use the sampling expansion approach to represent a signal of finite duration with a fixed number of samples. Using this approximation, we can easily represent the signal energy in a finite duration with a finite sum of squares of samples. In the following, we begin with the low-pass signals before proceeding to the bandpass signals.

B.3.1 Lowpass Signals

Consider a low-pass real signal $x(t)$ which is bandlimited over $[-W_{\rm b}, W_{\rm b}]$. Recall from the inverse Fourier Transform, we can represent this signal as

$$x(t) = \int_{-W_{\rm b}}^{W_{\rm b}} X(f) e^{j2\pi ft} df, \tag{B.8}$$

where $X(f)$ is the Fourier transform of $x(t)$. From the Sampling theorem, it is well known that $x(t)$ can be represented by the Whittaker-Shannon-Kotel'nikov sampling series [167–169] as

$$x(t) = \sum_{m=-\infty}^{\infty} x_m {\rm sinc}(2W_{\rm b}t - m), \tag{B.9}$$

where ${\rm sinc}(x) = \sin(\pi x)/\pi x$ and $x_m = x(m/2W_{\rm b})$ denotes the mth sample of $x(t)$, sampled at a Nyquist rate of $2W_{\rm b}$. In the mathematical literature, the series in (B.9) is also known as a cardinal series since the sampling functions are the cardinal sine functions or sinc functions.[1]

Now, if $x(t)$ is of almost finite duration T, we can approximate $x(t)$ by truncating

[1]Note that the set of orthonormal functions in the expansion of (B.9) is $\{\sqrt{2W_{\rm b}}{\rm sinc}(2W_{\rm b}t - m)\}$ with corresponding coefficients $\frac{1}{\sqrt{2W_{\rm b}}} x\left(\frac{m}{2W_{\rm b}}\right)$.

the cardinal series in (B.9) to about $2W_{\rm b}T$ terms. This is the famous "Dimensionality Theorem" or "$2W_{\rm b}T$-Theorem" [166,169,170]. It is clear that non-zero signals cannot be both bandlimited and timelimited at the same time. As a result, a different set of orthonormal functions known as prolate spheroidal wave functions instead of sampling functions have been studied [171–174]. In [171–174], the authors showed that $2W_{\rm b}T$ terms suffice to approximate the energy in a finite duration of a bandlimited process.[2] Although the sampling approach lacks mathematical precision in the notion of both bandlimited and timelimited signals, it has been shown to be very useful in gaining engineering insight into a variety of problems [166,169,170,175]. In the following, we show how the sampling approach can be used to approximate a bandlimited signal $x(t)$ with approximate duration T by a sum of $2W_{\rm b}T$ terms as follows:

$$x(t) \cong \sum_{m=1}^{2W_{\rm b}T} x_m \text{sinc}(2W_{\rm b}t - m), \qquad 0 \le t \le T. \tag{B.10}$$

Using the fact that

$$\int_{-\infty}^{\infty} \text{sinc}(2W_{\rm b}t - i)\text{sinc}(2W_{\rm b}t - j)dt = \begin{cases} 1/2W_{\rm b}, & i = j \\ 0, & i \neq j, \end{cases} \tag{B.11}$$

we can then approximate the signal energy in the interval $[0, T]$ by

$$\mathcal{E} = \int_0^T x^2(t)dt \cong \frac{1}{2W_{\rm b}} \sum_{m=1}^{2W_{\rm b}T} x_m^2. \tag{B.12}$$

In addition, we can also use the sampling approach to calculate

$$U = \int_0^T x(t)y(t)dt \cong \frac{1}{2W_{\rm b}} \sum_{m=1}^{2W_{\rm b}T} x_m y_m, \tag{B.13}$$

where $y_m = y(m/2W_{\rm b})$ denotes the mth sample of a bandlimited signal $y(t)$, sampled

[2]Since UWB channel can contain several hundreds paths of significant strength [37, 38], the number of degrees of freedom available in a given time-bandwidth product is also large and thus allow us to apply the "Dimensionality Theorem" to represent the received bandpass signals as $2WT$-tuple real vectors.

at a Nyquist rate of $2W_{\rm b}$.

Next, we consider bandlimited low-pass white Gaussian noise, $n(t)$, with power spectral density $N_0/2$ over $[-W_{\rm b}, W_{\rm b}]$. Similarly, we can represent $n(t)$ over interval $[0,T]$ in terms of $2W_{\rm b}T$ samples as follows:

$$n(t) \cong \sum_{m=1}^{2W_{\rm b}T} n_m \text{sinc}(2W_{\rm b}t - m), \qquad 0 \le t \le T, \tag{B.14}$$

where $n_m = n(m/2W_{\rm b})$ is the mth sample of $n(t)$, sampled at a Nyquist rate of $2W_{\rm b}$ over $[0,T]$, and n_m is a Gaussian r.v. with zero-mean and variance N_0W, i.e., $n_m \sim \mathcal{N}(0, N_0W)$. Note that the noise samples are i.i.d. across m. The noise energy in $[0,T]$ can then be written as

$$\int_0^T n^2(t)dt \cong \sum_{m=1}^{2W_{\rm b}T} \left(\frac{n_m}{\sqrt{2W_{\rm b}}}\right)^2, \tag{B.15}$$

where (B.15) is the sum of $2W_{\rm b}T$ squared independent Gaussian r.v.'s, each with zero-mean and variance $N_0/2$, which is equivalent to a central chi-squared distribution with $2W_{\rm b}T$ degrees of freedom. Using (B.10) and (B.14), we can represent the received signal as

$$r(t) \cong \sum_{m=1}^{2W_{\rm b}T} (x_m + n_m)\,\text{sinc}(2W_{\rm b}t - m), \qquad 0 \le t \le T, \tag{B.16}$$

and the normalized received signal energy can be approximated as

$$\frac{1}{\sigma_n^2}\int_0^T r^2(t)dt \cong \frac{1}{2W_{\rm b}\sigma_n^2}\sum_{m=1}^{2W_{\rm b}T}(x_m + n_m)^2, \tag{B.17}$$

where we let $\sigma_n^2 = N_0/2$. The sum in (B.17) now has a noncentral chi-square distribution with $2W_{\rm b}T$ degrees of freedom and a non-centrality parameter given by

$$\mu = \frac{1}{\sigma_n^2}\int_0^T x^2(t)dt = \frac{2\mathcal{E}}{N_0}. \tag{B.18}$$

Furthermore, we can calculate the normalized U in (B.13) with noise as follows

$$\begin{aligned}\frac{1}{\sigma_n^2}\int_0^T r_1(t)r_2(t)dt &\cong \frac{1}{2W_{\mathrm{b}}\sigma_n^2}\sum_{m=1}^{2W_{\mathrm{b}}T}(x_m+n_{1,m})(y_m+n_{2,m})\\ &= \frac{1}{2W_{\mathrm{b}}\sigma_n^2}\sum_{m=1}^{2W_{\mathrm{b}}T}(x_m y_m + y_m n_{1,m} + x_m n_{2,m} + n_{1,m}n_{2,m}),\end{aligned} \tag{B.19}$$

where $r_1(t) = x(t) + n_1(t)$ and $r_2(t) = y(t) + n_2(t)$. Note that (4.21) in Chapter 4.3.2 takes a form similar to (B.19).

B.3.2 Bandpass Signals

Deterministic Case

Consider a real bandpass signal $x(t)$ with bandwidth W at carrier frequency f_{c} (assuming that $f_{\mathrm{c}} > W/2$). We can write $x(t)$ in terms of its complex baseband equivalent representation as follows [166, 176–179]:

$$\begin{aligned}x(t) &= k\ \mathfrak{Re}\left\{x_{\mathrm{b}}(t)e^{j2\pi f_{\mathrm{c}}t}\right\}\\ &= \frac{k}{2}\left[x_{\mathrm{b}}(t)e^{j2\pi f_{\mathrm{c}}t} + x_{\mathrm{b}}^*(t)e^{-j2\pi f_{\mathrm{c}}t}\right]\\ &= k\left[x_{\mathrm{I}}(t)\cos(2\pi f_{\mathrm{c}}t) - x_{\mathrm{Q}}(t)\sin(2\pi f_{\mathrm{c}}t)\right],\end{aligned} \tag{B.20}$$

where k is a normalization factor and $x_{\mathrm{b}}(t) = x_{\mathrm{I}}(t) + jx_{\mathrm{Q}}(t)$ is the complex baseband equivalent signal of $x(t)$ over frequency range of $[-W/2, W/2]$. The signal components $x_{\mathrm{I}}(t)$ and $x_{\mathrm{Q}}(t)$ are called the in-phase (I) and quadrature (Q) components of $x_{\mathrm{b}}(t)$, respectively, where $x_{\mathrm{I}}(t) = \mathfrak{Re}\{x_{\mathrm{b}}(t)\}$ and $x_{\mathrm{Q}}(t) = \mathfrak{Im}\{x_{\mathrm{b}}(t)\}$.

Taking the Fourier transform of $x(t)$ gives

$$\begin{aligned}X(f) &= \int_{-\infty}^{\infty} x(t)e^{-j2\pi ft}dt\\ &= \frac{k}{2}\int_{-\infty}^{\infty}\left[x_{\mathrm{b}}(t)e^{j2\pi f_{\mathrm{c}}t} + x_{\mathrm{b}}^*(t)e^{-j2\pi f_{\mathrm{c}}t}\right]e^{-j2\pi ft}dt\end{aligned}$$

$$= \frac{k}{2}\left[X_{\mathrm{b}}(f - f_{\mathrm{c}}) + X_{\mathrm{b}}^{*}(-f - f_{\mathrm{c}})\right]. \tag{B.21}$$

This is the basic frequency domain relationship between the spectrum of the real bandpass signal $X(f)$ and the spectrum of the complex baseband equivalent signal $X_{\mathrm{b}}(f)$. Figure B-1 shows the relationship between the spectrum of the bandpass signal $X(f)$, its scaled version $X_{\mathrm{A}}(f)$ which is restricted to positive frequencies, and its complex baseband equivalent signal $X_{\mathrm{b}}(f)$.[3] Now, we will use Fig. B-1 to interpret equation (B.20). Starting from an arbitrary complex baseband equivalent signal $x_{\mathrm{b}}(t)$ with Fourier transform $X_{\mathrm{b}}(f)$ as shown in the bottom of the figure, we first construct $X_{\mathrm{A}}(f)$ by translating $X_{\mathrm{b}}(f)$ to f_{c} as depicted in the middle of the figure. We then use $X_{\mathrm{A}}(f)$ to construct a conjugate symmetric bandpass signal $X(f)$ and scale the amplitude by $k/2$ to proceed from the middle of the figure to the top.[4] This simple example shows how we can use (B.20) to generate a real-valued bandpass signal for any given complex baseband signal.

Likewise, we can also obtain the complex baseband equivalent representation given any real-valued bandpass signal by reversing the frequency domain operations in the above example. Specifically, suppose that $x(t)$ is an arbitrary real bandpass signal. Thus, $x(t)$ must satisfy the conjugate symmetry condition, so knowledge of only the non-negative frequencies of $X(f)$ is sufficient for reconstruction of $X(f)$. In fact, such knowledge is supplied by the analytic-equivalent signal $x_{\mathrm{A}}(t)$ with Fourier transform given by

$$X_{\mathrm{A}}(f) = 2U(f)X(f) = \begin{cases} 2X(f), & f > 0 \\ 0, & \text{otherwise,} \end{cases} \tag{B.22}$$

where $U(f)$ is the unit step function. Equivalently, (B.22) can be expressed in the

[3]The inverse Fourier transform of $X_{\mathrm{A}}(f)$ is known as the analytic-equivalent signal for $x(t)$.

[4]Since $x(t)$ is a real-valued signal, its Fourier transform must satisfy conjugate symmetry condition, i.e., $X(f) = X^{*}(-f)$. Note that this conjugate symmetry condition implies that $\mathfrak{Re}\{X(f)\} = \mathfrak{Re}\{X(-f)\}$ (real part is symmetric) and $\mathfrak{Im}\{X(f)\} = -\mathfrak{Im}(X(-f))$ (imaginary part is antisymmetric).

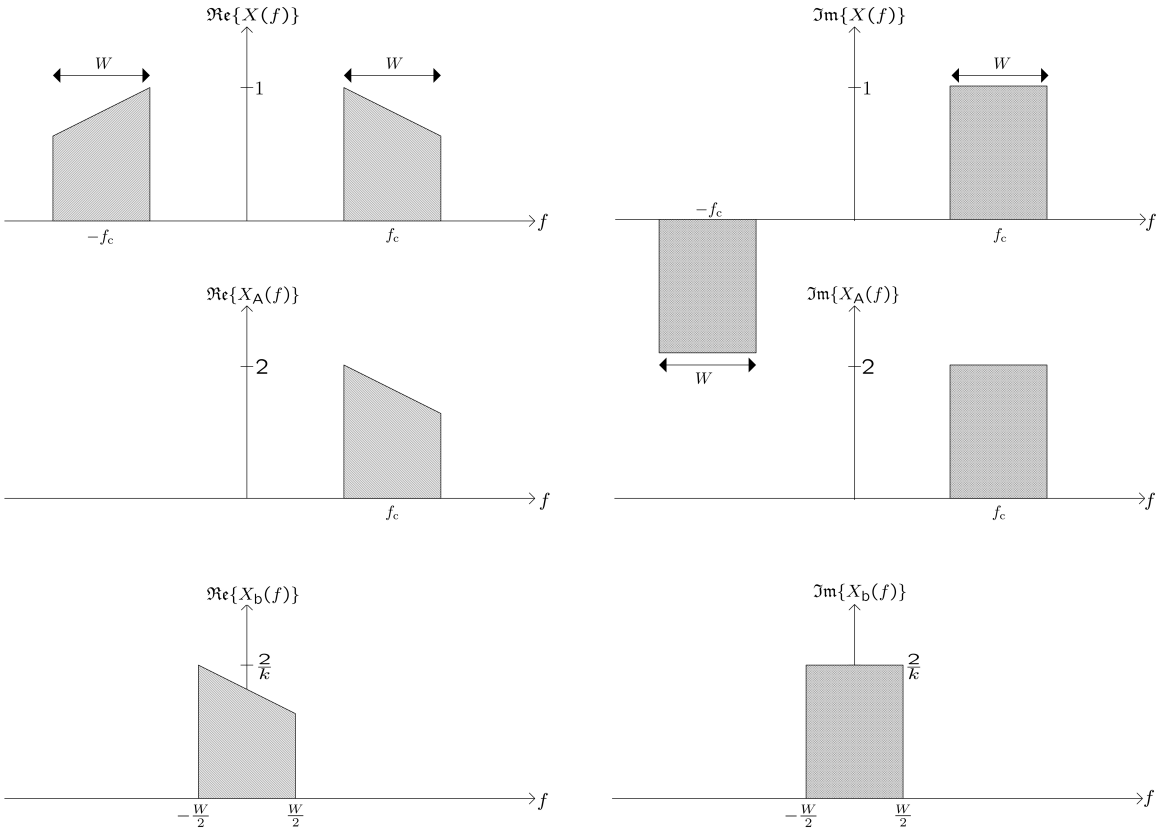

Figure B-1: Frequency domain relationship between a real bandpass signal $x(t)$ and its complex equivalent signals $x_{\mathrm{A}}(t)$ and $x_{\mathrm{b}}(t)$.

time-domain as

$$x_{\mathrm{A}}(t) = \int_{-\infty}^{\infty} X_{\mathrm{A}}(f) e^{j2\pi ft} df = \left[\delta(t) + \frac{j}{\pi t}\right] * x(t), \tag{B.23}$$

where the inverse Fourier transform of $U(f)$ is $\frac{1}{2}\left[\delta(t) + \frac{j}{\pi t}\right]$. Note that the imaginary part of the analytic signal is denoted by $\breve{x}(t) \triangleq 1/\pi t * x(t)$.[5] From (B.23), the original real bandpass signal $x(t)$ is clearly the real part of the analytic equivalent signal as given by

$$x(t) = \mathfrak{Re}\{x_{\mathrm{A}}(t)\}. \tag{B.24}$$

Now, by letting $x_{\mathrm{A}}(t) = k x_{\mathrm{b}}(t) e^{j2\pi f_c t}$, we obtain the equivalent relationship in (B.20).

[5] $\breve{x}(t)$ is also called the Hilbert transform of $x(t)$ since the filter with impulse response $1/\pi t$ is basically a $\pm\pi/2$ phase shifter for all frequencies in the input signal.

Moreover, the equivalent frequency-domain relationship between $x_{\mathrm{A}}(t)$ and $x_{\mathrm{b}}(t)$ is given by

$$X_{\mathrm{b}}(f) = \frac{1}{k} X_{\mathrm{A}}(f + f_{\mathrm{c}}). \tag{B.25}$$

Thus, $X_{\mathrm{b}}(f)$ is obtained by translating $X_{\mathrm{A}}(f)$ to the left by f_{c}. Again, we refer to Fig. B-1 to illustrate the relationship between $X(f)$, $X_{\mathrm{A}}(f)$, and $X_{\mathrm{b}}(f)$. However, we now go from top to bottom: starting from an arbitrary conjugate symmetric $X(f)$, we construct $X_{\mathrm{A}}(f)$, and then $X_{\mathrm{b}}(f)$. In summary, we can obtain a complex baseband equivalent signal $x_{\mathrm{b}}(t)$ that satisfies (B.20) and (B.21) starting from an arbitrary real bandpass signal $x(t)$.

Next, we turn to the relationship between the energy of $x(t)$ and $x_{\mathrm{b}}(t)$ as follows:

$$\mathcal{E} = \int_{-\infty}^{\infty} x^2(t)dt = \frac{k^2}{2} \int_{-\infty}^{\infty} |X_{\mathrm{b}}(f - f_{\mathrm{c}})|^2 df = \frac{k^2}{2} \int_{-\infty}^{\infty} |x_{\mathrm{b}}(t)|^2 dt, \tag{B.26}$$

where we have used the Parseval's relation and (B.21) to obtain the above results. From (B.26), we can see that although the normalization factor k appears to be arbitrary, it leads to different scaling factor between the energies of $x_{\mathrm{b}}(t)$ and $x(t)$.

In the following, we briefly summarize the different normalization factors k used in the literature [166, 176–179].

- When $k = 2$ [176], the energy of $x(t)$ is twice that of $x_{\mathrm{b}}(t)$. During down-conversion, the baseband signal $x_{\mathrm{I}}(t)$ can be retrieved by multiplying $x(t)$ by $\cos(2\pi f_{\mathrm{c}} t)$ and ideal low-pass filtering at baseband $[-W/2, W/2]$. Similarly, the baseband signal $x_{\mathrm{Q}}(t)$ can be retrieved by multiplying $x(t)$ by $-\sin(2\pi f_{\mathrm{c}} t)$ and ideal low-pass filtering at baseband $[-W/2, W/2]$. In this way, we have ensured that the transmitted and received signals have equal energies.

- When $k = \sqrt{2}$ [166, 177], the energies of $x(t)$ and $x_{\mathrm{b}}(t)$ are equal. For down-conversion, $x_{\mathrm{I}}(t)$ and $x_{\mathrm{Q}}(t)$ can be obtained simply by modulating $x(t)$ by $\sqrt{2}\cos(2\pi f_{\mathrm{c}} t)$ and $-\sqrt{2}\sin(2\pi f_{\mathrm{c}} t)$ followed by ideal low-pass filtering at baseband $[-W/2, W/2]$, respectively.

- When $k = 1$ [178, 179], the energy of $x(t)$ is half that of $x_{\rm b}(t)$. For down-conversion, $x_{\rm I}(t)$ and $x_{\rm Q}(t)$ can be obtained by modulating $x(t)$ by $2\cos(2\pi f_{\rm c}t)$ and $-2\sin(2\pi f_{\rm c}t)$ followed by ideal low-pass filtering at baseband $[-W/2, W/2]$, respectively.

Random Case

So far, we have focused on the complex representation of deterministic real bandpass signals. Here, we will show how the results from the deterministic case can be extended to bandpass random processes. Consider a real bandpass, wide-sense stationary (WSS) random process $x(t)$, we can equivalently represent $x(t)$ using (B.20) as follows:

$$\begin{aligned} x(t) &= \mathfrak{Re}\left\{k x_{\rm b}(t) e^{j2\pi f_c t}\right\} \\ &= \mathfrak{Re}\left\{x_{\rm A}(t)\right\}, \end{aligned} \tag{B.27}$$

where $x_{\rm A}(t)$ and $x_{\rm b}(t)$ are now complex random processes. Similar to (B.22), we pass $x(t)$ through a linear-time invariant (LTI) filter with transfer function $2U(f)$ to obtain analytic-equivalent signal $x_{\rm A}(t)$ with power spectral density given by

$$S_{x_{\rm A}}(f) = 4|U(f)|^2 S_x(f) = 4U(f)S_x(f), \tag{B.28}$$

where $S_x(f)$ denotes the power spectral density of $x(t)$ and $x_{\rm A}(t)$ is WSS[6] (See Fig. B-2). Using the fact that $x_{\rm b}(t) = \frac{1}{k} x_{\rm A}(t) e^{-j2\pi f_c t}$, the autocorrelation function of $x_{\rm b}(t)$ is

$$\begin{aligned} R_{x_{\rm b}}(t,\tau) &= \frac{1}{k^2}\,\mathbb{E}\left\{x_{\rm A}(t) e^{-j2\pi f_c t} x_{\rm A}^*(t-\tau) e^{j2\pi f_c (t-\tau)}\right\} \\ &= \frac{1}{k^2}\,\mathbb{E}\left\{x_{\rm A}(t) x_{\rm A}^*(t-\tau)\right\} e^{-j2\pi f_c \tau} \\ &= \frac{1}{k^2} R_{x_{\rm A}}(\tau) e^{-j2\pi f_c \tau}. \end{aligned} \tag{B.29}$$

[6]The output of any LTI system whose input is WSS is still WSS.

Thus, $x_{\rm b}(t)$ is also WSS with power spectral density equal to

$$\begin{aligned} S_{x_{\rm b}}(f) &= \int_{-\infty}^{\infty} R_{x_{\rm b}}(\tau) e^{-j2\pi f\tau} d\tau \\ &= \frac{1}{k^2} S_{x_{\rm A}}(f + f_{\rm c}), \end{aligned} \tag{B.30}$$

which shows that the power spectral density of $x_{\rm b}(t)$ is the version of $S_{x_{\rm A}}(f)$ translated to the origin (See Fig. B-2). Note that (B.28) and (B.30) show that the power spectral density of $x_{\rm b}(t)$ is $4/k^2$ times the one-sided power spectral density of $x(t)$.

Next, we consider the I and Q components of $x_{\rm b}(t)$ and show the relation between the autocorrelation function of $x(t)$ and the autocorrelation and cross-correlation functions of $x_{\rm I}(t)$ and $x_{\rm Q}(t)$. First, we derive the autocorrelation function of $x(t)$ using (B.20) as follows:

$$\begin{aligned} &R_x(t,\tau) \\ &= R_x(\tau) \\ &= k^2 \mathbb{E}\Big\{ [x_{\rm I}(t)\cos(2\pi f_{\rm c}t) - x_{\rm Q}(t)\sin(2\pi f_{\rm c}t)] \\ &\qquad \times [x_{\rm I}(t-\tau)\cos(2\pi f_{\rm c}(t-\tau)) - x_{\rm Q}(t-\tau)\sin(2\pi f_{\rm c}(t-\tau))] \Big\} \\ &= k^2 \big[R_{x_{\rm I}}(t,\tau)\cos(2\pi f_{\rm c}t)\cos(2\pi f_{\rm c}(t-\tau)) + R_{x_{\rm Q}}(t,\tau)\sin(2\pi f_{\rm c}t)\sin(2\pi f_{\rm c}(t-\tau)) \\ &\qquad - R_{x_{\rm I},x_{\rm Q}}(t,\tau)\cos(2\pi f_{\rm c}t)\sin(2\pi f_{\rm c}(t-\tau)) - R_{x_{\rm Q},x_{\rm I}}(t,\tau)\sin(2\pi f_{\rm c}t)\cos(2\pi f_{\rm c}(t-\tau)) \big] \\ &= \frac{k^2}{2} \Big\{ \big[R_{x_{\rm I}}(t,\tau) + R_{x_{\rm Q}}(t,\tau) \big] \cos(2\pi f_{\rm c}\tau) + \big[R_{x_{\rm I}}(t,\tau) - R_{x_{\rm Q}}(t,\tau) \big] \cos(2\pi f_{\rm c}(2t-\tau)) \\ &\qquad - \big[R_{x_{\rm Q},x_{\rm I}}(t,\tau) - R_{x_{\rm I},x_{\rm Q}}(t,\tau) \big] \sin(2\pi f_{\rm c}\tau) \\ &\qquad - \big[R_{x_{\rm Q},x_{\rm I}}(t,\tau) + R_{x_{\rm I},x_{\rm Q}}(t,\tau) \big] \sin(2\pi f_{\rm c}(2t-\tau)) \Big\}. \end{aligned} \tag{B.31}$$

Since $x(t)$ is WSS, $R_{x_{\rm I}}(t,\tau)$, $R_{x_{\rm I}}(t,\tau)$, $R_{x_{\rm I},x_{\rm Q}}(t,\tau)$, and $R_{x_{\rm Q},x_{\rm I}}(t,\tau)$ must depend only on τ. In addition, the right-hand side of (B.31) must only be a function of τ and this condition is satisfied only if the following equalities hold:

$$R_{x_{\rm I}}(\tau) = R_{x_{\rm Q}}(\tau) \tag{B.32}$$

$$R_{x_{\rm I},x_{\rm Q}}(\tau) = -R_{x_{\rm Q},x_{\rm I}}(\tau). \tag{B.33}$$

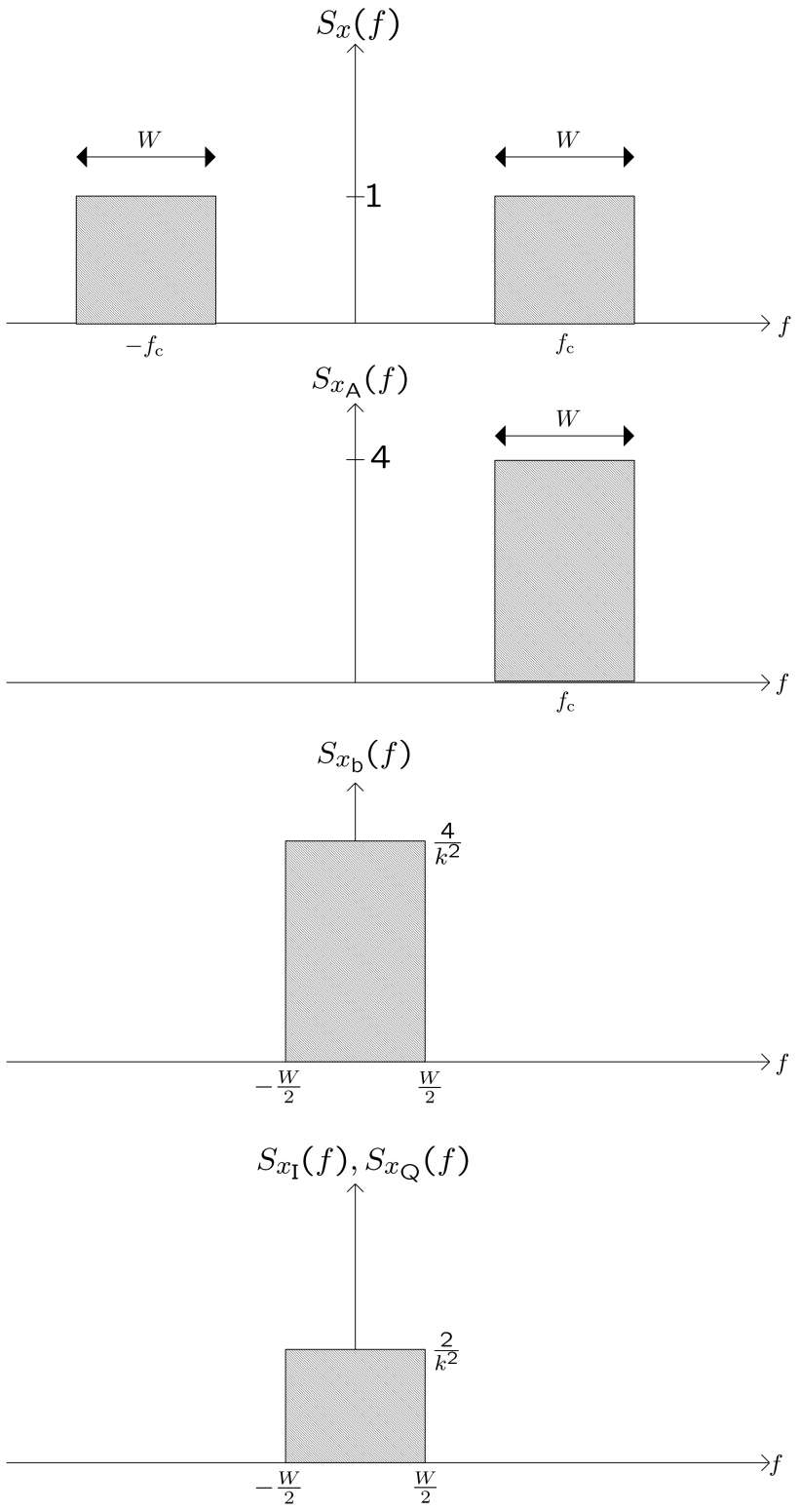

Figure B-2: Power spectrum relationship between a real bandpass random signal $x(t)$ and its complex equivalent random signals $x_{\mathrm{A}}(t)$ and $x_{\mathrm{b}}(t)$. (Note that all amplitudes are normalized to $S_x(f_{\mathrm{c}})$)

As a result, (B.31) reduces to

$$R_x(\tau) = k^2\big[R_{x_\mathrm{I}}(\tau)\cos(2\pi f_\mathrm{c}\tau) - R_{x_\mathrm{Q},x_\mathrm{I}}(\tau)\sin(2\pi f_\mathrm{c}\tau)\big]. \tag{B.34}$$

Furthermore, we can also derive the relation between the autocorrelation function of $x_\mathrm{b}(t)$ and the autocorrelation and cross-correlation functions of $x_\mathrm{I}(t)$ and $x_\mathrm{Q}(t)$ as follows:

$$\begin{aligned} R_{x_\mathrm{b}}(t,\tau) &= \mathbb{E}\left\{[x_\mathrm{I}(t) + jx_\mathrm{Q}(t)]\,[x_\mathrm{I}(t-\tau) - jx_\mathrm{Q}(t-\tau)]\right\} \\ &= R_{x_\mathrm{I}}(\tau) + R_{x_\mathrm{Q}}(\tau) + j\Big[R_{x_\mathrm{Q},x_\mathrm{I}}(\tau) - R_{x_\mathrm{I},x_\mathrm{Q}}(\tau)\Big] \\ &= 2\Big[R_{x_\mathrm{I}}(\tau) + jR_{x_\mathrm{Q},x_\mathrm{I}}(\tau)\Big], \end{aligned} \tag{B.35}$$

where we have used the equalities in (B.32) and (B.33) to obtain (B.35). By incorporating the results in (B.29), (B.34) and (B.35), we have

$$\begin{aligned} R_x(\tau) &= \frac{k^2}{4}\left[R_{x_\mathrm{b}}(\tau)e^{j2\pi f_\mathrm{c}\tau} + R^*_{x_\mathrm{b}}(\tau)e^{-j2\pi f_\mathrm{c}\tau}\right] \\ &= \frac{k^2}{2}\mathfrak{Re}\left\{R_{x_\mathrm{b}}(\tau)e^{j2\pi f_\mathrm{c}\tau}\right\} \\ &= \frac{1}{2}\mathfrak{Re}\left\{R_{x_\mathrm{A}}(\tau)\right\}, \end{aligned} \tag{B.36}$$

which shows the equivalent relation between $x(t)$, $x_\mathrm{A}(t)$, and $x_\mathrm{b}(t)$ in terms of their respective autocorrelation functions. Finally, using (B.36) (See Fig. B-2), we obtain the power spectral density of $x(t)$ as follows:

$$\begin{aligned} S_x(f) &= \frac{k^2}{4}\int_{-\infty}^{\infty}\left[R_{x_\mathrm{b}}(\tau)e^{j2\pi f_\mathrm{c}\tau} + R^*_{x_\mathrm{b}}(\tau)e^{-j2\pi f_\mathrm{c}\tau}\right]e^{-j2\pi f\tau}d\tau \\ &= \frac{k^2}{4}\left[S_{x_\mathrm{b}}(f - f_\mathrm{c}) + S_{x_\mathrm{b}}(-f - f_\mathrm{c})\right]. \end{aligned} \tag{B.37}$$

For example, when the bandpass random process is white Gaussian noise $n(t)$ with

double-sided power spectral density given by

$$S_n(f) = \begin{cases} \frac{N_0}{2}, & f_c - W/2 \leq |f| \leq f_c + W/2 \\ 0, & \text{otherwise.} \end{cases} \tag{B.38}$$

From (B.27) and (B.30), its analytic-equivalent signal $n_A(t)$ has power spectral density equal to

$$S_{n_A}(f) = \begin{cases} 2N_0, & f_c - W/2 \leq f \leq f_c + W/2 \\ 0, & \text{otherwise,} \end{cases} \tag{B.39}$$

and its complex baseband equivalent signal $n_b(t)$ has power spectral density equal to

$$S_{n_b}(f) = \begin{cases} \frac{2N_0}{k^2}, & -W/2 \leq f \leq W/2 \\ 0, & \text{otherwise.} \end{cases} \tag{B.40}$$

Since the power spectrum of $n(t)$ is symmetric around f_c, it follows that the power spectrum of $n_b(t)$ is an even function from (B.30). This implies that $R_{n_b}(\tau)$ is real for all τ, and so (B.35) yields $R_{n_Q,n_I}(\tau) = 0$. This means that $n_I(t)$ and $n_Q(t)$ are independent since $n_I(t)$ and $n_Q(t)$ are uncorrelated Gaussian processes. In this case, the real and imaginary parts of $n_b(t)$ each have power spectral density equal to

$$S_{n_I}(f) = S_{n_Q}(f) = \begin{cases} \frac{N_0}{k^2}, & -W/2 \leq f \leq W/2 \\ 0, & \text{otherwise.} \end{cases} \tag{B.41}$$

Sampling Expansion

In the following, we use (B.20) to express a real determinstic bandpass signal $x(t)$ with bandwidth W and duration T as follows:

$$x(t) = k\big[x_{\rm I}(t)\cos(2\pi f_{\rm c}t) - x_{\rm Q}(t)\sin(2\pi f_{\rm c}t)\big], \tag{B.42}$$

where $x_{\rm I}(t)$ and $x_{\rm Q}(t)$ have a frequency range of $[-W/2, W/2]$. From (B.10) and letting $W_{\rm b} = W/2$, we can approximate $x_{\rm I}(t)$ and $x_{\rm Q}(t)$ over a duration T as

$$\begin{aligned} x_{\rm I}(t) &\cong \sum_{m=1}^{WT} x_{{\rm I},m}{\rm sinc}(Wt-m), \qquad 0 \le t \le T \\ x_{\rm Q}(t) &\cong \sum_{m=1}^{WT} x_{{\rm Q},m}{\rm sinc}(Wt-m), \qquad 0 \le t \le T, \end{aligned} \tag{B.43}$$

where $x_{{\rm I},m} = x_{\rm I}(m/W)$ and $x_{{\rm Q},m} = x_{\rm Q}(m/W)$. It follows from (B.12) and (B.26) that the signal energy of $x(t)$ in the interval $[0, T]$ can be approximated by

$$\mathcal{E} = \int_0^T x^2(t)dt \cong \frac{k^2}{2}\sum_{m=1}^{WT}\left[\left(\frac{x_{{\rm I},m}}{\sqrt{W}}\right)^2 + \left(\frac{x_{{\rm Q},m}}{\sqrt{W}}\right)^2\right], \tag{B.44}$$

and the correlation of $x(t)$ and $y(t)$ in (B.13) becomes

$$U = \int_0^T x(t)y(t)dt \cong \frac{k^2}{2W}\sum_{m=1}^{WT}\left(x_{{\rm I},m}y_{{\rm I},m} + x_{{\rm Q},m}y_{{\rm Q},m}\right), \tag{B.45}$$

where $y_{{\rm I},m} = y_{\rm I}(m/W)$ and $y_{{\rm Q},m} = y_{\rm Q}(m/W)$.

Similarly, a bandpass WSS Gaussian noise $n(t)$ with double-sided power spectral density $N_0/2$ can be represented as

$$n(t) = k\big[n_{\rm I}(t)\cos(2\pi f_{\rm c}t) - n_{\rm Q}(t)\sin(2\pi f_{\rm c}t)\big], \tag{B.46}$$

and the complex baseband equivalent signals $n_{\rm I}(t)$ and $n_{\rm Q}(t)$ with a frequency range of $[-W/2, W/2]$ over interval $[0, T]$ can be approximated using (B.14) with $W_{\rm b} = W/2$

as

$$n_{\mathrm{I}}(t) \cong \sum_{m=1}^{WT} n_{\mathrm{I},m}\mathrm{sinc}(Wt-m), \qquad 0 \le t \le T$$
$$n_{\mathrm{Q}}(t) \cong \sum_{m=1}^{WT} n_{\mathrm{Q},m}\mathrm{sinc}(Wt-m), \qquad 0 \le t \le T, \tag{B.47}$$

where $n_{\mathrm{I},m} = n_{\mathrm{I}}(m/W)$ and $n_{\mathrm{Q},m} = n_{\mathrm{Q}}(m/W)$ are the mth samples of $n_{\mathrm{I}}(t)$ and $n_{\mathrm{Q}}(t)$, sampled at a Nyquist rate W over $[0,T]$, respectively. In addition, $n_{\mathrm{I},m}$ and $n_{\mathrm{Q},m}$ are i.i.d. Gaussian r.v.'s with zero-mean and variance N_0W/k^2, respectively. Similar to the argument in (B.44), the noise energy in $[0,T]$ can be written as

$$\int_0^T n^2(t)dt \cong \frac{k^2}{2}\sum_{m=1}^{WT}\left[\left(\frac{n_{\mathrm{I},m}}{\sqrt{W}}\right)^2 + \left(\frac{n_{\mathrm{Q},m}}{\sqrt{W}}\right)^2\right], \tag{B.48}$$

which is equivalent to having a central chi-squared distribution with $2WT$ degrees of freedom. Using (B.43) and (B.47), the received complex baseband equivalent signals over interval $[0,T]$ can be expressed as

$$r_{\mathrm{I}}(t) \cong \sum_{m=1}^{WT} (x_{\mathrm{I},m} + n_{\mathrm{I},m})\,\mathrm{sinc}(Wt-m), \qquad 0 \le t \le T$$
$$r_{\mathrm{Q}}(t) \cong \sum_{m=1}^{WT} (x_{\mathrm{Q},m} + n_{\mathrm{Q},m})\,\mathrm{sinc}(Wt-m), \qquad 0 \le t \le T, \tag{B.49}$$

where $r(t) = k\big[r_{\mathrm{I}}(t)\cos 2\pi f_{\mathrm{c}}t - r_{\mathrm{Q}}(t)\sin 2\pi f_{\mathrm{c}}t\big]$ is the received bandpass signal. Therefore, the normalized received signal energy can be approximated as

$$\begin{aligned}\frac{1}{\sigma_n^2}\int_0^T r^2(t)dt &= \frac{1}{2\sigma_n^2}\int_0^T \left[r_{\mathrm{I}}^2(t) + r_{\mathrm{Q}}^2(t)\right]dt \\ &= \frac{1}{2\sigma_n^2}\int_0^T \left[x_{\mathrm{I}}(t) + n_{\mathrm{I}}(t)\right]^2 dt \\ &\quad + \frac{1}{2\sigma_n^2}\int_0^T \left[x_{\mathrm{Q}}(t) + n_{\mathrm{Q}}(t)\right]^2 dt \\ &\cong \frac{k^2}{2W\sigma_n^2}\sum_{m=1}^{WT}\left[(x_{\mathrm{I},m} + n_{\mathrm{I},m})^2 + (x_{\mathrm{Q},m} + n_{\mathrm{Q},m})^2\right],\end{aligned} \tag{B.50}$$

where (B.50) has a noncentral chi-square distribution with $2WT$ degrees of freedom and a non-centrality parameter given by

$$\mu = \frac{1}{\sigma_n^2}\int_0^T x^2(t)dt = \frac{2\mathcal{E}}{N_0}. \tag{B.51}$$

Furthermore, the normalized U in (B.19) becomes

$$\begin{aligned}
&\frac{1}{\sigma_n^2}\int_0^T r_1(t)r_2(t)dt \\
&\cong \frac{k^2}{2W\sigma_n^2}\sum_{m=1}^{WT}[(x_{\mathrm{I},m}+n_{\mathrm{I},1,m})(y_{\mathrm{I},m}+n_{\mathrm{I},2,m})+(x_{\mathrm{Q},m}+n_{\mathrm{Q},1,m})(y_{\mathrm{Q},m}+n_{\mathrm{Q},2,m})] \\
&= \frac{k^2}{2W\sigma_n^2}\sum_{m=1}^{2WT}(\widetilde{x}_m\widetilde{y}_m+\widetilde{y}_m\widetilde{n}_{1,m}+\widetilde{x}_m\widetilde{n}_{2,m}+\widetilde{n}_{1,m}\widetilde{n}_{2,m}),
\end{aligned} \tag{B.52}$$

where $\widetilde{x}_{2m-1} \triangleq x_{\mathrm{I},m}$, $\widetilde{x}_{2m} \triangleq x_{\mathrm{Q},m}$, $\widetilde{y}_{2m-1} \triangleq y_{\mathrm{I},m}$, and $\widetilde{y}_{2m} \triangleq y_{\mathrm{Q},m}$ for $m = 1, \ldots, WT$. Note that (4.21) in Chapter 4.3.2 has a form similar to (B.52) with $k = 1$.

B.4 Derivation of (4.28)

In this appendix, we derive the expression for (4.28), where Y_1 and Y_2 are defined in (4.26) and (4.27) with pdfs $f_{\mathrm{NC}}(y_1, \mu, n)$ and $f_{\mathrm{C}}(y_2, n)$ respectively. Consider two new r.v.'s R_1 and R_2 where $R_1 = \sqrt{Y_1}$ and $R_2 = \sqrt{Y_2}$, the pdfs of R_1 and R_2 can be found by using transformation of r.v. as follows

$$f_{R_1}(r_1) = 2r_1 f_{\mathrm{NC}}(r_1^2, \mu, n) \tag{B.53}$$

$$f_{R_2}(r_2) = 2r_2 f_{\mathrm{C}}(r_2^2, n). \tag{B.54}$$

Using (B.54), $F_{R_2}(r_2)$ can be obtained as

$$F_{R_2}(r_2) = 1 - e^{-r_2^2}\sum_{i=0}^{n-1}\frac{r_2^{2i}}{i!}. \tag{B.55}$$

By using (B.53) and (B.55), we can rewrite

$$\begin{aligned}\mathbb{P}\left\{Y_1 < Y_2\right\} &= \int_0^\infty 2r_1^n e^{-\left(r_1^2+\mu\right)} \left(\frac{1}{\mu}\right)^{(n-1)/2} I_{n-1}\left(2r_1\sqrt{\mu}\right) e^{-r_1^2} \sum_{i=0}^{n-1} \frac{r_1^{2i}}{i!} dr_1 \\ &= e^{-\mu} \sum_{i=0}^{n-1} \frac{2}{i!} \left(\frac{1}{\mu}\right)^{(n-1)/2} \int_0^\infty r_1^{n+2i} e^{-2r_1^2} I_{n-1}\left(2r_1\sqrt{\mu}\right) dr_1. \end{aligned} \tag{B.56}$$

By using the result from [180], we have the following integral given by

$$\int_0^\infty x^{n+2i} e^{-2x^2} I_{n-1}\left(2x\sqrt{\mu}\right) dx = \frac{1}{2^n} \left[\frac{i!\left(4\mu\right)^{(n-1)/2}}{2^{n+i}}\right] e^{\frac{\mu}{2}} \sum_{k=0}^{i} \frac{(i+n-1)!}{(i-k)!(n-1+k)!} \frac{(\mu/2)^k}{k!}. \tag{B.57}$$

By substituting (B.57) into (B.56), we have

$$\mathbb{P}\left\{Y_1 < Y_2\right\} = \frac{e^{-\frac{\mu}{2}}}{2^n} \sum_{i=0}^{n-1} \frac{\left(\frac{\mu}{2}\right)^i}{i!} \sum_{k=i}^{n-1} \frac{1}{2^k} \frac{(k+n-1)!}{(k-i)!(n+i-1)!}. \tag{B.58}$$

Appendix C

BEP Derivation of TR signaling with NBI

C.1 Derivation of (5.5) and (5.6)

In this appendix, the derivation of the non-centrality parameters $\mu_{\mathrm{TR},Y_1}^{(\mathrm{NBI})}$ in (5.5) and $\mu_{\mathrm{TR},Y_2}^{(\mathrm{NBI})}$ in (5.6) are shown. We begin first with the derivation of $\mu_{\mathrm{TR},Y_1}^{(\mathrm{NBI})}$ which can be written as

$$\mu_{\mathrm{TR},Y_1}^{(\mathrm{NBI})} = \underbrace{\frac{1}{2\sigma_{\mathrm{TR}}^2}\sum_{j=0}^{\frac{N_\mathrm{s}}{2}-1}\int_0^T w_j^2(t)dt}_{\triangleq\mu_\mathrm{A}} + \underbrace{\frac{1}{8\sigma_{\mathrm{TR}}^2}\sum_{j=0}^{\frac{N_\mathrm{s}}{2}-1}\int_0^T \left(\xi_{1,j}(t)+\xi_{2,j}(t)\right)^2 dt}_{\triangleq\mu_\mathrm{B}}$$
$$+ \underbrace{\frac{1}{2\sigma_{\mathrm{TR}}^2}\sum_{j=0}^{\frac{N_\mathrm{s}}{2}-1}\int_0^T w_j(t)\left(\xi_{1,j}(t)+\xi_{2,j}(t)\right)dt}_{\triangleq\mu_\mathrm{C}}, \tag{C.1}$$

where we can futher simplify μ_A and μ_B in (C.1) as follows:

$$\mu_\mathrm{A} = \frac{1}{2\sigma_{\mathrm{TR}}^2}\sum_{j=0}^{\frac{N_\mathrm{s}}{2}-1}\int_0^T w_j^2(t)dt = \frac{E_\mathrm{s}}{N_0}\sum_{l=1}^{L_{\mathrm{CAP}}}\alpha_l^2,$$
$$\mu_\mathrm{B} \approx \frac{\alpha_\mathrm{J}^2 N_\mathrm{s} J_0 T}{2N_0} + \frac{\alpha_\mathrm{J}^2 N_\mathrm{s} J_0 T}{2N_0}\cos(2\pi f_\mathrm{J} T_\mathrm{r}). \tag{C.2}$$

Note that we have simply used the result in (4.25) to obtain μ_{A} in (C.2). However, to obtain μ_{B} in (C.2), we need to expand all the terms of μ_{B} in (C.1) as follows:

$$\frac{1}{8\sigma_{\mathrm{TR}}^2}\sum_{j=0}^{\frac{N_{\mathrm{s}}}{2}-1}\int_0^T \xi_{1,j}^2(t)dt = \frac{\alpha_{\mathrm{J}}^2 J_0}{2N_0}\sum_{j=0}^{\frac{N_{\mathrm{s}}}{2}-1}\Big[T + \frac{\sin\left(4\pi f_{\mathrm{J}}(T + j2T_{\mathrm{f}} + c_j T_{\mathrm{p}}) + 2\theta\right)}{4\pi f_{\mathrm{J}}} - \frac{\sin\left(4\pi f_{\mathrm{J}}(j2T_{\mathrm{f}} + c_j T_{\mathrm{p}}) + 2\theta\right)}{4\pi f_{\mathrm{J}}}\Big] \approx \frac{\alpha_{\mathrm{J}}^2 N_{\mathrm{s}} J_0 T}{4N_0},$$

$$\frac{1}{8\sigma_{\mathrm{TR}}^2}\sum_{j=0}^{\frac{N_{\mathrm{s}}}{2}-1}\int_0^T \xi_{2,j}^2(t)dt \approx \frac{\alpha_{\mathrm{J}}^2 N_{\mathrm{s}} J_0 T}{4N_0}, \tag{C.3}$$

where we have made the above approximations by observing that $T \gg \frac{1}{4\pi f_{\mathrm{J}}}$ and $|\sin(\phi)| \leq 1$. In addition,

$$\frac{1}{4\sigma_{\mathrm{TR}}^2}\sum_{j=0}^{\frac{N_{\mathrm{s}}}{2}-1}\int_0^T \xi_{1,j}(t)\xi_{2,j}(t)dt \approx \mu_{\mathrm{D}}. \tag{C.4}$$

where $\mu_{\mathrm{D}} = \frac{\alpha_{\mathrm{J}}^2 N_{\mathrm{s}} J_0 T}{2N_0}\cos(2\pi f_{\mathrm{J}} T_{\mathrm{r}})$ when $T\cos(2\pi f_{\mathrm{J}} T_{\mathrm{r}}) \gg \frac{1}{4\pi f_{\mathrm{J}}}$. Otherwise, μ_{D} is on the same order as $\frac{1}{4\pi f_{\mathrm{J}}}$, which is negligible compared to the first term of μ_{B} in (C.2). As a result, we can ignore the latter case and consider only the scenario when $T\cos(2\pi f_{\mathrm{J}} T_{\mathrm{r}}) \gg \frac{1}{4\pi f_{\mathrm{J}}}$ as shown in (C.2).

Next, we can rewrite μ_{C} in (C.1) as

$$\mu_{\mathrm{C}} = \frac{2\alpha_{\mathrm{J}}\sqrt{2E_{\mathrm{p}}J_0}}{N_0}\sum_{j=0}^{\frac{N_{\mathrm{s}}}{2}-1} a_j \sum_{l=1}^{L_{\mathrm{CAP}}} \alpha_l \int_0^{T_{\mathrm{p}}} p(t)\Big[\cos\left(2\pi f_{\mathrm{J}}(t + \tau_l + j2T_{\mathrm{f}} + c_j T_{\mathrm{p}}) + \theta\right) + \cos\left(2\pi f_{\mathrm{J}}(t + \tau_l + j2T_{\mathrm{f}} + c_j T_{\mathrm{p}} + T_{\mathrm{r}}) + \theta\right)\Big]dt. \tag{C.5}$$

In order to further simplify (C.5), we first look at how we can solve for $\int_0^{T_{\mathrm{p}}} p(t)\ \cos(2\pi f_{\mathrm{J}}\, t + \phi)\, dt$ as follows:

$$\int_0^{T_{\mathrm{p}}} p(t)\ \cos(2\pi f_{\mathrm{J}}\, t + \phi)\, dt \overset{(a)}{=} \frac{1}{2}\int_{-\infty}^{\infty} p(t)\ \left[e^{\jmath 2\pi f_{\mathrm{J}} t + \jmath\phi} + e^{-\jmath 2\pi f_{\mathrm{J}} t - \jmath\phi}\right]\ dt \overset{(b)}{=} \frac{1}{2}\int_{-\infty}^{\infty} \hat{P}(f)\ \left[e^{\jmath\phi}\delta(f - f_{\mathrm{J}}) + e^{-\jmath\phi}\delta(f + f_{\mathrm{J}})\right]\ df$$

$$\stackrel{(c)}{=} \frac{1}{2}\hat{P}(f_{\mathrm{J}})\, e^{\jmath\phi} + \frac{1}{2}\hat{P}^{*}(f_{\mathrm{J}})\, e^{-\jmath\phi}$$
$$\stackrel{(d)}{=} \Re\left\{|\hat{P}(f_{\mathrm{J}})|\, e^{\jmath\phi} e^{\jmath \arg \hat{P}(f_{\mathrm{J}})}\right\}$$
$$\stackrel{(e)}{=} |\hat{P}(f_{\mathrm{J}})|\, \cos\Big(\phi + \arg \hat{P}(f_{\mathrm{J}})\Big)$$

where (a) follows from the assumption that $p(t)$ is zero outside the interval $[0, T_{\mathrm{p}}]$; (b) follows from the Parseval's relationship; (c) follows from the fact that $p(t)$ is real so $\hat{P}(-f) = \hat{P}^{*}(f)$; (d) follows from the definition of the real part of a complex number; and (e) express in terms of cosine. Now, by substituting this result into (C.5) and using the fact that $\cos A + \cos B = 2\cos((A+B)/2)\cos((A-B)/2)$, we obtain

$$\begin{aligned}
\mu_{\mathrm{C}} &= \frac{2\alpha_{\mathrm{J}}|\hat{P}(f_{\mathrm{J}})|\sqrt{2E_{\mathrm{p}}J_0}}{N_0} \sum_{j=0}^{\frac{N_{\mathrm{s}}}{2}-1} a_j \sum_{l=1}^{L_{\mathrm{CAP}}} \alpha_l \\
&\qquad \times \Big[\cos\Big(2\pi f_{\mathrm{J}}(\tau_l + j2T_{\mathrm{f}} + c_j T_{\mathrm{p}}) + \theta + \arg \hat{P}(f_{\mathrm{J}})\Big) \\
&\qquad\quad + \cos\Big(2\pi f_{\mathrm{J}}(\tau_l + j2T_{\mathrm{f}} + c_j T_{\mathrm{p}} + T_{\mathrm{r}}) + \theta + \arg \hat{P}(f_{\mathrm{J}})\Big)\Big] \\
&= \frac{4\alpha_{\mathrm{J}}|\hat{P}(f_{\mathrm{J}})|\sqrt{2E_{\mathrm{p}}J_0}\cos(\pi f_{\mathrm{J}} T_{\mathrm{r}})}{N_0} \sum_{j=0}^{\frac{N_{\mathrm{s}}}{2}-1} a_j \sum_{l=1}^{L_{\mathrm{CAP}}} \alpha_l \\
&\qquad \times \cos\left(2\pi f_{\mathrm{J}}(\tau_l + j2T_{\mathrm{f}} + c_j T_{\mathrm{p}} + T_{\mathrm{r}}/2) + \varphi\right), \quad \text{(C.6)}
\end{aligned}$$

where $|\widehat{P}(f_{\mathrm{J}})|$ is the magnitude of the frequency response of $p(t)$ at frequency f_{J}. The composite random phase is given by $\varphi \triangleq \arg\{\widehat{P}(f_{\mathrm{J}})\} + \theta$, where $\arg\{\widehat{P}(f_{\mathrm{J}})\}$ is the angle of the frequency response of $p(t)$ at frequency f_{J}, and φ is uniformly distributed over $[0, 2\pi)$. In summary, we obtain $\mu^{(\mathrm{NBI})}_{\mathrm{TR},Y_1}$ in (5.5) using (C.2) and (C.6).

Using (C.1), (C.2) and (C.6), we can determine the validity of the approximate analytical method using the following ratios:

$$\begin{aligned}
\frac{\mu_{\mathrm{A}}}{\mu_{\mathrm{C}}} &= \left| \frac{\sum_{l=1}^{L_{\mathrm{CAP}}} \alpha_l^2}{\alpha_{\mathrm{J}} \cos(\pi f_{\mathrm{J}} T_{\mathrm{r}}) \sum_{j=0}^{\frac{N_{\mathrm{s}}}{2}-1} a_j \sum_{l=1}^{L_{\mathrm{CAP}}} \alpha_l \cos\left(2\pi f_{\mathrm{J}}\left(\tau_l + j2T_{\mathrm{f}} + c_j T_{\mathrm{p}} + \frac{T_{\mathrm{r}}}{2}\right) + \varphi\right)} \right| \\
&\qquad \times \frac{N_{\mathrm{s}}}{4|\widehat{P}(f_{\mathrm{J}})|} \sqrt{\frac{T_{\mathrm{f}}\mathsf{SIR}}{2}}, \quad \text{(C.7)}
\end{aligned}$$

$$\frac{\mu_{\mathrm{B}}}{\mu_{\mathrm{C}}} = \left| \frac{\alpha_{\mathrm{J}} \cos(\pi f_{\mathrm{J}} T_{\mathrm{r}})}{\sum_{j=0}^{\frac{N_{\mathrm{s}}}{2}-1} a_j \sum_{l=1}^{L_{\mathrm{CAP}}} \alpha_l \cos\left(2\pi f_{\mathrm{J}} \left(\tau_l + j2T_{\mathrm{f}} + c_j T_{\mathrm{p}} + \frac{T_{\mathrm{r}}}{2}\right) + \varphi\right)} \right| \times \frac{N_{\mathrm{s}} L_{\mathrm{CAP}} T_{\mathrm{p}}}{4|\widehat{P}(f_{\mathrm{J}})|} \sqrt{\frac{1}{2T_{\mathrm{f}}\mathsf{SIR}}} \tag{C.8}$$

For a given set of system parameters, we simply need to check if $\mu_{\mathrm{A}} + \mu_{\mathrm{B}} \gg \mu_{\mathrm{C}}$ using (C.7) and (C.8). For example, this can arise when Walsh-Hadamard sequences are used for $\{a_j\}$. To elaborate on this example, we first numerically average (over $\{\alpha_l\}$ and α_{J}) the quantities within $|\cdot|$ of (C.7) and (C.8) for a typical set of system parameters ($T_{\mathrm{f}} = 100$ns, $T_{\mathrm{p}} = 0.5$ns, $T_{\mathrm{r}} = 40$ns, possible $f_{\mathrm{J}} = 1.575$ GHz, 3.5 GHz, and 5.745 GHz) and considering $c_j = 1$ for all j and Walsh-Hadamard sequences for $\{a_j\}$. Results have shown that the value of $|\cdot|$ in (C.7) and (C.8) is always greater than 1. Approximating these factors by 1 and $|\widehat{P}(f_{\mathrm{J}})| \approx \sqrt{T_{\mathrm{p}}}$, we focus on the rest of the terms in (C.7) and (C.8). Since T_{f} is usually on the order of 100 times T_{p}, and N_{s} and L_{CAP} are usually larger than $4\sqrt{2}$, we can verify that $\mu_{\mathrm{A}} + \mu_{\mathrm{B}} \gg \mu_{\mathrm{C}}$ and neglect μ_{C} when $\mathsf{SIR} \geq -20$ dB.

Using similar approach leading to (C.3) and (C.4), we can approximate $\mu_{\mathrm{TR},Y_2}^{(\mathrm{NBI})}$ in (5.6) straightforwardly as follows:

$$\begin{aligned} \mu_{\mathrm{TR},Y_2}^{(\mathrm{NBI})} &= \frac{1}{8\sigma_{\mathrm{TR}}^2} \sum_{j=0}^{\frac{N_{\mathrm{s}}}{2}-1} \int_0^T (\xi_{2,j}(t) - \xi_{1,j}(t))^2 dt \\ &\approx \frac{\alpha_{\mathrm{J}}^2 N_{\mathrm{s}} J_0 T}{2N_0} - \frac{\alpha_{\mathrm{J}}^2 N_{\mathrm{s}} J_0 T}{2N_0} \cos(2\pi f_{\mathrm{J}} T_{\mathrm{r}}). \end{aligned} \tag{C.9}$$

C.2 Derivation of (5.12) and (5.13)

In this appendix, the non-centrality parameters $\mu_{\mathrm{TR},Y_3}^{(\mathrm{NBI})}$ in (5.12) and $\mu_{\mathrm{TR},Y_4}^{(\mathrm{NBI})}$ in (5.13) are derived. Following similar steps in Appendix D.1, $\mu_{\mathrm{TR},Y_3}^{(\mathrm{NBI})}$ can be written as

$$\mu_{\mathrm{TR},Y_3}^{(\mathrm{NBI})} = \underbrace{\frac{1}{2\sigma_{\mathrm{TR}}^2} \sum_{j=0}^{\frac{N_{\mathrm{s}}}{2}-1} \int_0^T w_j^2(t) dt}_{\triangleq \widetilde{\mu_{\mathrm{A}}}} + \underbrace{\frac{1}{8\sigma_{\mathrm{TR}}^2} \sum_{j=0}^{\frac{N_{\mathrm{s}}}{2}-1} \int_0^T (\xi_{2,j}(t) - \xi_{1,j}(t))^2 dt}_{\triangleq \widetilde{\mu_{\mathrm{B}}}}$$

$$+\underbrace{\frac{1}{2\sigma_{\mathrm{TR}}^2}\sum_{j=0}^{\frac{N_\mathrm{s}}{2}-1}\int_0^T w_j(t)\left(\xi_{2,j}(t)-\xi_{1,j}(t)\right)dt}_{\triangleq\widetilde{\mu_\mathrm{C}}}$$

$$\approx \frac{E_\mathrm{s}}{N_0}\sum_{l=1}^{L_\mathrm{CAP}}\alpha_l^2+\frac{\alpha_\mathrm{J}^2 N_\mathrm{s}J_0T}{2N_0}-\frac{\alpha_\mathrm{J}^2 N_\mathrm{s}J_0T}{2N_0}\cos(2\pi f_\mathrm{J}T_\mathrm{r})$$
$$+\frac{4\alpha_\mathrm{J}|\widehat{P}(f_\mathrm{J})|\sqrt{2E_\mathrm{p}J_0}\sin\left(-\pi f_\mathrm{J}T_\mathrm{r}\right)}{N_0}\sum_{j=0}^{\frac{N_\mathrm{s}}{2}-1}a_j\sum_{l=1}^{L_\mathrm{CAP}}\alpha_l$$
$$\times\sin\left(2\pi f_\mathrm{J}\left(\tau_l+j2T_\mathrm{f}+c_jT_\mathrm{p}+T_\mathrm{r}/2\right)+\varphi\right), \quad \text{(C.10)}$$

where $\widetilde{\mu_\mathrm{A}}$ and $\widetilde{\mu_\mathrm{B}}$ in (C.10) follows straightforwardly from (C.2) and (C.9), and we have used the results in (C.5) and (C.6) and the fact that $\cos B-\cos A=2\sin((A+B)/2)\sin((A-B)/2)$ to obtain $\widetilde{\mu_\mathrm{C}}$ in (C.10). Next, $\mu_{\mathrm{TR},Y_4}^{(\mathrm{NBI})}$ in (5.13) is given by

$$\mu_{\mathrm{TR},Y_4}^{(\mathrm{NBI})}=\frac{1}{8\sigma_{\mathrm{TR}}^2}\sum_{j=0}^{\frac{N_\mathrm{s}}{2}-1}\int_0^T\left(\xi_{2,j}(t)+\xi_{1,j}(t)\right)^2dt$$
$$\approx\frac{\alpha_\mathrm{J}^2N_\mathrm{s}J_0T}{2N_0}+\frac{\alpha_\mathrm{J}^2N_\mathrm{s}J_0T}{2N_0}\cos(2\pi f_\mathrm{J}T_\mathrm{r}), \quad \text{(C.11)}$$

where the above result follows directly from (C.2).

C.3 Derivation of (5.18), (5.19), (5.20), and (5.21)

Under the approximate analytical method, we can approximate the conditional non-centrality parameters of Y_1 as

$$\mu_{\mathrm{DTR},Y_1}^{(\mathrm{NBI})}\approx\underbrace{\frac{1}{2\sigma_{\mathrm{DTR}}^2}\sum_{j=0}^{N_\mathrm{s}-1}\int_0^T w_j^2(t)dt}_{\triangleq\mu_\mathrm{A}}$$
$$+\underbrace{\frac{1}{8\sigma_{\mathrm{DTR}}^2}\sum_{j=0}^{N_\mathrm{s}-1}\int_0^T\left(\xi_{1,j}(t)+\xi_{2,j}(t)\right)^2dt}_{\triangleq\mu_\mathrm{B}}, \quad \text{(C.12)}$$

where $\mu_{\rm A}$ and $\mu_{\rm B}$ are obtained using similar approach as shown in Appendix C.1. For brevity, we only give the results as follows:

$$\begin{aligned}\mu_{\rm A} &= \frac{1}{2\sigma^2_{\rm DTR}}\sum_{j=0}^{N_{\rm s}-1}\int_0^T w_j^2(t)dt = \frac{2E_{\rm s}}{N_0}\sum_{l=1}^{L_{\rm CAP}}\alpha_l^2,\\ \mu_{\rm B} &\approx \frac{\alpha_{\rm J}^2 N_{\rm s}J_0T}{N_0} + \frac{\alpha_{\rm J}^2 N_{\rm s}J_0T}{N_0}\cos(2\pi f_{\rm J}N_{\rm s}T_{\rm f}).\end{aligned} \tag{C.13}$$

where the differences between (C.13) and (C.2) lies in a doubled captured signal energy, double degrees of freedom, and the delay separation is now $N_{\rm s}T_{\rm f}$ instead of $T_{\rm r}$. As a result, we have the following desired results:

$$\begin{aligned}\mu^{\rm (NBI)}_{{\rm DTR},Y_2} &= \frac{1}{8\sigma^2_{\rm DTR}}\sum_{j=0}^{N_{\rm s}-1}\int_0^T (\xi_{2,j}(t)-\xi_{1,j}(t))^2dt\\ &\approx \frac{\alpha_{\rm J}^2 N_{\rm s}J_0T}{N_0} - \frac{\alpha_{\rm J}^2 N_{\rm s}J_0T}{N_0}\cos(2\pi f_{\rm J}N_{\rm s}T_{\rm f})\end{aligned} \tag{C.14}$$

$$\begin{aligned}\mu^{\rm (NBI)}_{{\rm DTR},Y_3} &\approx \frac{1}{2\sigma^2_{\rm DTR}}\sum_{j=0}^{N_{\rm s}-1}\int_0^T w_j^2(t)dt + \frac{1}{8\sigma^2_{\rm DTR}}\sum_{j=0}^{N_{\rm s}-1}\int_0^T (\xi_{2,j}(t)-\xi_{1,j}(t))^2\,dt\\ &\approx \frac{2E_{\rm s}}{N_0}\sum_{l=1}^{L_{\rm CAP}}\alpha_l^2 + \frac{\alpha_{\rm J}^2 N_{\rm s}J_0T}{N_0} - \frac{\alpha_{\rm J}^2 N_{\rm s}J_0T}{N_0}\cos(2\pi f_{\rm J}N_{\rm s}T_{\rm f})\end{aligned} \tag{C.15}$$

$$\begin{aligned}\mu^{\rm (NBI)}_{{\rm DTR},Y_4} &= \frac{1}{8\sigma^2_{\rm DTR}}\sum_{j=0}^{N_{\rm s}-1}\int_0^T (\xi_{1,j}(t)+\xi_{2,j}(t))^2dt\\ &\approx \frac{\alpha_{\rm J}^2 N_{\rm s}J_0T}{N_0} + \frac{\alpha_{\rm J}^2 N_{\rm s}J_0T}{N_0}\cos(2\pi f_{\rm J}N_{\rm s}T_{\rm f}).\end{aligned} \tag{C.16}$$

Bibliography

[1] S. Cui, J. Xiao, A. Goldsmith, Z.-Q. Luo, and H. V. Poor, "Estimation diversity and energy efficiency in distributed sensing," *IEEE Trans. Signal Process.*, vol. 55, no. 9, pp. 4683–4695, Sep. 2007.

[2] Y.-W. Hong, W.-J. Huang, F.-H. Chiu, and C.-C. J. Kuo, "Cooperative communications in resource-constrained wireless networks," *IEEE Signal Process. Mag.*, vol. 24, no. 3, pp. 47–57, May 2007.

[3] J. Yuan and W. Yu, "Joint source coding, routing, and power allocation in wireless sensor networks," *IEEE Trans. Commun.*, to appear.

[4] H. Wu, C. Qiao, S. De, and O. Tonguz, "Integrated cellular and ad hoc relaying systems: iCAR," *IEEE J. Sel. Areas Commun.*, vol. 19, no. 10, pp. 2105–2115, Oct. 2001.

[5] J. Bae, R. Berry, and M. Honig, "Power allocation, rate, and coverage for relay-assisted downlink data transmission," in *Proc. IEEE Int. Conf. on Commun.*, vol. 10, Istanbul, TURKEY, May 2006, pp. 4451–4456.

[6] R. Pabst, B. H. Walke, D. C. Schultz, P. Herhold, H. Yanikomeroglu, S. Mukherjee, H. Viswanathan, M. Lott, W. Zirwas, M. Dohler, H. Aghvami, D. D. Falconer, and G. P. Fettweis, "Relay-based deployment concepts for wireless and mobile broadband radio," *IEEE Commun. Mag.*, vol. 42, no. 9, pp. 80–89, Sep. 2004.

[7] A. Ben-Tal and A. Nemirovski, "Robust convex optimization," *Math. Oper. Res.*, vol. 21, no. 4, pp. 769–805, Nov. 1998.

[8] L. E. Ghaoui, F. Oustry, and H. Lebret, "Robust solutions to uncertain semidefinite programs," *SIAM J. Optim.*, vol. 9, no. 1, pp. 33–52, 1998.

[9] J. N. Laneman, D. N. C. Tse, and G. W. Wornell, "Cooperative diversity in wireless networks: Efficient protocols and outage behavior," *IEEE Trans. Inf. Theory*, vol. 50, no. 12, pp. 3062–3080, Dec. 2004.

[10] V. Stanković, A. Høst-Madsen, and Z. Xiong, "Cooperative diversity for wireless ad hoc networks," *IEEE Signal Process. Mag.*, vol. 23, no. 5, pp. 37–49, Sep. 2006.

[11] A. Bletsas, H. Shin, and M. Z. Win, "Outage optimality of opportunistic amplify-and-forward relaying," *IEEE Commun. Lett.*, vol. 11, no. 3, pp. 261–263, Mar. 2007.

[12] ——, "Cooperative communications with outage-optimal opportunistic relaying," *IEEE Trans. Wireless Commun.*, vol. 6, no. 9, Sep. 2007.

[13] J. Luo, R. S. Blum, L. Cimini, L. Greenstein, and A. Haimovich, "Decode-and-forward cooperative diversity with power allocation in wireless networks," *IEEE Trans. Wireless Commun.*, vol. 6, no. 3, pp. 793–799, Mar. 2007.

[14] R. Madan, N. Mehta, A. F. Molisch, and J. Zhang, "Energy-efficient cooperative relaying over fading channels with simple relay selection," in *Proc. IEEE Global Telecomm. Conf.*, San Francisco, CA, Nov. 2006, pp. 1–6.

[15] I. Maric and R. D. Yates, "Forwarding strategies for Gaussian parallel-relay networks," in *Proc. Conf. on Inform. Sci. and Sys.*, Princeton, NJ, Mar. 2004.

[16] M. Dohler, A. Gkelias, and H. Aghvami, "Resource allocation for FDMA-based regenerative multihop links," *IEEE Trans. Wireless Commun.*, vol. 3, no. 6, pp. 1989–1993, Nov. 2004.

[17] M. Chen, S. Serbetli, and A. Yener, "Distributed power allocation for parallel relay networks," in *Proc. IEEE Global Telecomm. Conf.*, vol. 3, St. Louis, MO, Nov. 2005, pp. 1177–1181.

[18] T. C.-Y. Ng and W. Yu, "Joint optimization of relay strategies and resource allocations in cooperative cellular networks," *IEEE J. Sel. Areas Commun.*, vol. 25, no. 2, pp. 328–339, Feb. 2007.

[19] A. Høst-Madsen and J. Zhang, "Capacity bounds and power allocation for wireless relay channels," *IEEE Trans. Inf. Theory*, vol. 51, no. 6, pp. 2020–2040, Jun. 2005.

[20] D. Brown, "Resource allocation for cooperative transmission in wireless networks," in *Proc. Asilomar Conf. on Signals, Systems and Computers*, vol. 2, Pacific Grove, CA, Nov. 2004, pp. 1473–1477.

[21] P. A. Anghel, M. Kaveh, and Z.-Q. Luo, "Optimal relayed power allocation in interference-free non-regenerative cooperative systems," in *Proc. IEEE Workshop on Signal Processing Advances in Wireless Commun.*, Lisboa, PORTUGAL, Jul. 2004, pp. 21–25.

[22] I. Hammerstrom and A. Wittneben, "On the optimal power allocation for non-regenerative OFDM relay links," in *Proc. IEEE Int. Conf. on Commun.*, vol. 10, Istanbul, TURKEY, Jun. 2006, pp. 4463–4468.

[23] K. G. Seddik, A. K. Sadek, W. Su, and K. J. R. Liu, "Outage analysis and optimal power allocation for multi-node amplify-and-forward relay networks," *IEEE Signal Process. Lett.*, vol. 14, no. 6, pp. 377–380, Jun. 2007.

[24] I. Maric and R. D. Yates, "Bandwidth and power allocation for cooperative strategies in Gaussian relay networks," in *Proc. Asilomar Conf. on Signals, Systems and Computers*, vol. 2, Pacific Grove, CA, Nov. 2004, pp. 1907–1911.

[25] A. Bletsas and A. Lippman, "Implementing cooperative diversity antenna arrays with commodity hardware," *IEEE Commun. Mag.*, vol. 44, no. 12, pp. 33–40, Dec. 2006.

[26] M. Gastpar and M. Vetterli, "On the capacity of large Gaussian relay networks," *IEEE Trans. Inf. Theory*, vol. 51, no. 3, pp. 765–779, Mar. 2005.

[27] A. F. Dana and B. Hassibi, "On the power efficiency of sensory and ad hoc wireless networks," *IEEE Trans. Inf. Theory*, vol. 52, no. 7, pp. 2890–2914, Jul. 2006.

[28] H. Bölcskei, R. Nabar, O. Oyman, and A. Paulraj, "Capacity scaling laws in MIMO relay networks," *IEEE Trans. Wireless Commun.*, vol. 5, no. 6, pp. 1433–1444, Jun. 2006.

[29] W. M. Gifford, M. Z. Win, and M. Chiani, "Diversity with practical channel estimation," *IEEE Trans. Wireless Commun.*, vol. 4, no. 4, pp. 1935–1947, Jul. 2005.

[30] ——, "Antenna subset diversity with non-ideal channel estimation," *IEEE Trans. Wireless Commun.*, to appear.

[31] M. Z. Win and R. A. Scholtz, "Impulse radio: How it works," *IEEE Commun. Lett.*, vol. 2, no. 2, pp. 36–38, Feb. 1998.

[32] ——, "Ultra-wide bandwidth time-hopping spread-spectrum impulse radio for wireless multiple-access communications," *IEEE Trans. Commun.*, vol. 48, no. 4, pp. 679–691, Apr. 2000.

[33] P. Withington, H. Fluhler, and S. Nag, "Enhancing homeland security with advanced UWB sensors," *IEEE Microwave Mag.*, vol. 4, no. 3, pp. 51–58, Sep. 2003.

[34] S. Roy, J. R. Foerster, V. S. Somayazulu, and D. G. Leeper, "Ultrawideband radio design: the promise of high-speed, short-range wireless connectivity," *Proc. IEEE*, vol. 92, no. 2, pp. 295–311, Feb. 2004.

[35] M. Z. Win and R. A. Scholtz, "On the robustness of ultra-wide bandwidth signals in dense multipath environments," *IEEE Commun. Lett.*, vol. 2, no. 2, pp. 51–53, Feb. 1998.

[36] ——, "On the energy capture of ultra-wide bandwidth signals in dense multipath environments," *IEEE Commun. Lett.*, vol. 2, no. 9, pp. 245–247, Sep. 1998.

[37] ——, "Characterization of ultra-wide bandwidth wireless indoor communications channel: A communication theoretic view," *IEEE J. Sel. Areas Commun.*, vol. 20, no. 9, pp. 1613–1627, Dec. 2002.

[38] D. Cassioli, M. Z. Win, and A. F. Molisch, "The ultra-wide bandwidth indoor channel: from statistical model to simulations," *IEEE J. Sel. Areas Commun.*, vol. 20, no. 6, pp. 1247–1257, Aug. 2002.

[39] S. Gezici, Z. Tian, G. B. Giannakis, H. Kobayashi, A. F. Molisch, H. V. Poor, and Z. Sahinoglu, "Localization via ultra-wideband radios: a look at positioning aspects for future sensor networks," *IEEE Signal Process. Mag.*, vol. 22, pp. 70–84, Jul. 2005.

[40] D. B. Jourdan, D. Dardari, and M. Z. Win, "Position error bound for UWB localization in dense cluttered environments," in *Proc. IEEE Int. Conf. on Commun.*, vol. 8, Istanbul, TURKEY, Jun. 2006, pp. 3705–3710.

[41] D. Dardari and M. Z. Win, "Threshold-based time-of-arrival estimators in UWB dense multipath channels," in *Proc. IEEE Int. Conf. on Commun.*, vol. 10, Istanbul, TURKEY, Jun. 2006, pp. 4723–4728.

[42] D. Dardari, C.-C. Chong, and M. Z. Win, "Analysis of threshold-based TOA estimator in UWB channels," in *Proc. of European Signal Processing Conf.*, Florence, ITALY, Sep. 2006.

[43] B. Basore, "Noise-like signals and their detection by correlation," Ph.D. dissertation, MIT, Cambridge, MA, May 1952.

[44] C. K. Rushforth, "Transmitted-reference techniques for random or unknown channels," *IEEE Trans. Inf. Theory*, vol. 10, no. 1, pp. 39–42, Jan. 1964.

[45] R. Gagliardi, "A geometrical study of transmitted reference communication system," *IEEE Trans. Commun.*, vol. 12, no. 4, pp. 118–123, Dec. 1964.

[46] A. Polydoros and K. T. Woo, "LPI detection of frequency-hopping signals using autocorrelation techniques," *IEEE J. Sel. Areas Commun.*, vol. 3, no. 5, pp. 714 – 726, Sep. 1985.

[47] W. M. Gifford and M. Z. Win, "On transmitted-reference UWB communications," in *Proc. 38th Asilomar Conf. on Signals, Systems and Computers*, Pacific Grove, CA, Nov. 2004, pp. 1526–1531.

[48] R. Hoctor and H. Tomlinson, "Delay-hopped transmitted-reference RF communications," in *Proc. IEEE Conf. on Ultra Wideband Sys. and Technol.*, Baltimore, MD, Jun. 2002, pp. 265–270.

[49] J. D. Choi and W. E. Stark, "Performance of ultra-wideband communications with suboptimal receivers in multipath channels," *IEEE J. Sel. Areas Commun.*, vol. 20, no. 9, pp. 1754–1766, Dec. 2002.

[50] L. Yang and G. B. Giannakis, "Optimal pilot waveform assisted modulation for ultrawideband communications," *IEEE Trans. Wireless Commun.*, vol. 3, no. 4, pp. 1236 – 1249, Jul. 2004.

[51] Y.-L. Chao and R. A. Scholtz, "Ultra-wideband transmitted reference systems," *IEEE Trans. Veh. Technol.*, vol. 54, no. 5, pp. 1556–1569, Sep. 2005.

[52] A. A. D'Amico and U. Mengali, "GLRT receivers for UWB systems," *IEEE Commun. Lett.*, vol. 9, no. 6, pp. 487–489, Jun. 2005.

[53] M. Ho, V. S. Somayazulu, J. Foerster, and S. Roy, "A differential detector for an ultra-wideband communications system," *Proc. IEEE Semiannual Veh. Technol. Conf.*, pp. 1896–1900, May 2002.

[54] G. D. Hingorani and J. Hancock, "A transmitted reference system for communication in random or unknown channels," *IEEE Trans. Commun. Technol.*, vol. 13, no. 3, pp. 293 – 301, Sep. 1965.

[55] G. D. Hingorani, "Error rates for a class of binary receivers," *IEEE Trans. Commun. Technol.*, vol. 15, no. 2, pp. 209 – 215, Apr. 1967.

[56] M. M. Hämäläinen, R. Tesi, and J. Iianatti, "On the UWB system performance studies in AWGN channel with interference in UMTS band," in *Proc. IEEE Conf. on Ultra Wideband Sys. and Technol.*, Baltimore, MD, May 2002, pp. 321–325.

[57] M. M. Hämäläinen, R. Tesi, J. Iianatti, and V. Hovinen, "On the performance comparison of different UWB data modulation schemes in AWGN channel in the presence of jamming," in *Proc. IEEE Radio and Wireless Conf.*, Boston, MA, Aug. 2002, pp. 83–86.

[58] M. M. Hämäläinen, V. Hovinen, R. Tesi, J. H. J. Iinatti, and M. Latva-aho, "On the UWB system coexistence with GSM900, UMTS/WCDMA, and GPS," *IEEE J. Sel. Areas Commun.*, vol. 20, no. 9, pp. 1712–1721, Dec. 2002.

[59] R. Giuliano and F. Mazzenga, "On the coexistence of power-controlled ultrawide-band systems with UMTS, GPS, DCS1800, and fixed wireless systems," *IEEE Trans. Veh. Technol.*, vol. 54, no. 1, pp. 62–81, Jan. 2005.

[60] A. Taha and K. M. Chugg, "A theoretical study on the effects of interference on UWB multiple access impulse radio," in *Proc. Asilomar Conf. on Signals, Systems and Computers*, vol. 1, Pacific Grove, CA, Nov. 2002, pp. 728–732.

[61] J. R. Foerster, "The performance of a Direct Sequence spread ultra-wideband system in the presence of multipath, narrowband interference and multi-user interference," in *Proc. IEEE Conf. on Ultra Wideband Sys. and Technol.*, Baltimore, MD, May 2002, pp. 87–91.

[62] L. Zhao and A. M. Haimovich, "Performance of ultra-wideband communications in the presence of interference," *IEEE J. Sel. Areas Commun.*, vol. 20, no. 9, pp. 1684–1691, Dec. 2002.

[63] J. D. Choi and W. E. Stark, "Performance analysis of ultra-wideband spread-spectrum communications in narrowband interference," in *Proc. IEEE Military Commun. Conf.*, vol. 2, Anaheim, CA, Oct. 2002, pp. 1075–1080.

[64] A. Giorgetti, M. Chiani, and M. Z. Win, "The effect of narrowband interference on wideband wireless communication systems," *IEEE Trans. Commun.*, vol. 53, no. 12, pp. 2139–2149, Dec. 2005.

[65] A. Giorgetti and D. Dardari, "The impact of OFDM interference on TH-PPM/BPAM transmission systems," in *Proc. IEEE Semiannual Veh. Technol. Conf.*, vol. 2, Stockholm, SWEDEN, May 2005, pp. 1037–1042.

[66] C. R. C. M. da Silva and L. B. Milstein, "The effects of narrowband interference on UWB communication systems with imperfect channel estimation," *IEEE J. Sel. Areas Commun.*, vol. 24, no. 4, pp. 717–723, Apr. 2006.

[67] Q. Li and L. A. Rusch, "Multiuser detection for DS-CDMA UWB in the home environment," *IEEE J. Sel. Areas Commun.*, vol. 20, no. 9, pp. 1701–1711, Dec. 2002.

[68] X. Chu and R. D. Murch, "The effect of NBI on UWB time-hopping systems," *IEEE Trans. Wireless Commun.*, vol. 3, no. 5, pp. 1431–1436, Sep. 2004.

[69] I. Bergel, E. Fishler, and H. Messer, "Narrowband interference mitigation in impulse radio," *IEEE Trans. Commun.*, vol. 53, no. 8, pp. 1278–1282, Aug. 2005.

[70] C. R. C. M. da Silva and L. B. Milstein, "Spectral-encoded UWB communication systems: Real-time implementation and interference suppression," *IEEE Trans. Commun.*, vol. 53, no. 8, pp. 1391–1401, Aug. 2005.

[71] N. Boubaker and K. B. Letaief, "MMSE multipath diversity combining for multi-access TH-UWB in the presence of NBI," *IEEE Trans. Wireless Commun.*, vol. 5, no. 4, pp. 712–719, Apr. 2006.

[72] R. A. Scholtz, "The orgins of spread-spectrum communications," *IEEE Trans. Commun.*, vol. 30, no. 5, pp. 822–854, May 1982.

[73] R. Wilson and R. Scholtz, "Template estimation in ultra-wideband radio," in *Proc. Asilomar Conf. on Signals, Systems and Computers*, vol. 2, Pacific Grove, CA, Nov. 2003, pp. 1244–1248.

[74] M. Pausini and G. J. M. Janssen, "On the narrowband interference in transmitted reference UWB receivers," in *Proc. IEEE Int. Conf. on Utra-Wideband*, Zürich, SWITZERLAND, Sep. 2005, pp. 571–575.

[75] C.-Y. Chong and S. P. Kumar, "Sensor networks: evolution, opportunities, and challenges," *Proc. IEEE*, vol. 91, no. 8, pp. 1247–1256, Aug. 2003.

[76] I. F. Akyildiz, W. Su, Y. Sankarasubramaniam, and E. Cayirci, "A survey on sensor networks," *IEEE Commun. Mag.*, vol. 40, no. 8, pp. 102–114, Aug. 2002.

[77] D. C. D. Estrin and M. Srivastava, "Overview of sensor networks," *IEEE Computer*, vol. 37, no. 8, pp. 41–49, Aug. 2004.

[78] R. Verdone, A. Conti, D. Sangiorgi, and D. Dardari, "Process estimation through a self-organizing collaborative wireless sensor network," in *Proc. IEEE Global Telecomm. Conf.*, vol. 5, Dallas, TX, Dec. 2004, pp. 3193–3199.

[79] R. R. Tenney and N. R. Sandell, "Detection with distributed sensors," *IEEE Trans. Aerosp. Electron. Syst.*, vol. 17, no. 4, pp. 501–510, Aug. 1981.

[80] J. N. Tsitsiklis, "Decentralized detection," *Advances in Statistical Signal Processing*, vol. 2, pp. 297–344, 1993.

[81] R. Viswanathan and P. K. Varshney, "Distributed detection with multiple sensors - Part I : Fundamentals," *Proc. IEEE*, vol. 85, no. 1, pp. 54–63, Jan. 1997.

[82] R. S. Blum, S. A. Kassam, and H. V. Poor, "Distributed detection with multiple sensors - Part II: Advanced topics," *Proc. IEEE*, vol. 85, no. 1, pp. 64–79, Jan. 1997.

[83] J.-F. Chamberland and V. V. Veeravalli, "Decentralized detection in sensor networks," *IEEE Trans. Signal Process.*, vol. 51, no. 2, pp. 407–416, Feb. 2003.

[84] ——, "Asymptotic results for decentralized detection in power constrained wireless sensor networks," *IEEE J. Sel. Areas Commun.*, vol. 22, no. 6, pp. 1007–1015, Aug. 2004.

[85] B. Chen, R. Jiang, T. Kasetkasem, and P. K. Varshney, "Channel aware decision fusion in wireless sensor networks," *IEEE Trans. Signal Process.*, vol. 52, no. 12, pp. 3454–3458, Dec. 2004.

[86] R. Niu, B. Chen, and P. K. Varshney, "Fusion of decisions transmitted over Rayleigh fading channels in wireless sensor networks," *IEEE Trans. Signal Process.*, vol. 54, no. 3, pp. 1018–1027, Mar. 2006.

[87] Y. Sung, L. Tong, and A. Swami, "Asymptotic locally optimal detector for large-scale sensor networks under the Poisson regime," *IEEE Trans. Signal Process.*, vol. 53, no. 6, pp. 2005–2017, Jun. 2005.

[88] R. Niu and P. K. Varshney, "Distributed detection and fusion in a large wireless sensor network of random size," *EURASIP J. Wireless Commun. and Networking*, vol. 2005, no. 4, pp. 462–472.

[89] H. E. Gamal, "On the scaling laws of dense wireless sensor networks: The data gathering channel," *IEEE Trans. Inf. Theory*, vol. 51, no. 3, pp. 1229–1234, Mar. 2005.

[90] S. Servetto, "Distributed signal processing algorithms for the sensor broadcast problem," in *Proc. Conf. on Inform. Sci. and Sys.*, Baltimore, ML, Mar. 2003.

[91] P. Swaszek and P. Willett, "Parley as an approach to distributed detection," *IEEE Trans. Aerosp. Electron. Syst.*, vol. 31, no. 1, pp. 447–457, Jan. 1995.

[92] D. A. Pados, K. W. Halford, D. Kazakos, and P. Papantoni-Kazakos, "Distributed binary hypothesis testing with feedback," *IEEE Trans. Syst., Man, Cybern.*, vol. 25, no. 1, pp. 21–42, Jan. 1995.

[93] Y.-W. Hong, A. Scaglione, and P. K. Varshney, "A communication architecture for reaching consensus in decision for a large network," in *Proc. IEEE Workshop on Statistical Signal Processing*, Paris, FRANCE, Jul. 2005, pp. 1220–1225.

[94] R. E. V. Dyck, "Detection performance in self-organized wireless sensor networks," in *Proc. Conf. on Inform. Sci. and Sys.*, Baltimore, ML, Mar. 2001.

[95] T. Q. S. Quek, H. Shin, M. Z. Win, and M. Chiani, "Optimal power allocation for amplify-and-forward relay networks via conic programming," in *Proc. IEEE Int. Conf. on Commun.*, Glasgow, SCOTLAND, Jun. 2007, pp. 5058–5063.

[96] ——, "Robust power allocation for amplify-and-forward relay networks," in *Proc. IEEE Int. Conf. on Commun.*, Glasgow, SCOTLAND, Jun. 2007, pp. 957–962.

[97] T. Q. S. Quek, M. Z. Win, and M. Chiani, "Robust power allocation algorithms for wireless relay networks," *IEEE Trans. Commun.*, submitted for publication.

[98] T. Q. S. Quek, H. Shin, and M. Z. Win, "Robust wireless relay networks: Slow power allocation with guaranteed QoS," *IEEE J. Select. Topics Signal Processing*, vol. 1, no. 4, pp. 700–714, Dec. 2007.

[99] T. Q. S. Quek and M. Z. Win, "Performance analysis of ultrawide bandwidth transmitted-reference communications," in *Proc. IEEE Semiannual Veh. Technol. Conf.*, vol. 3, Milan, ITALY, May 2004, pp. 1285–1289.

[100] ——, "Ultrawide bandwidth transmitted-reference signaling," in *Proc. IEEE Int. Conf. on Commun.*, vol. 6, Paris, FRANCE, Jun. 2004, pp. 3409–3413.

[101] ——, "Analysis of UWB transmitted-reference communication systems in dense multipath channels," *IEEE J. Sel. Areas Commun.*, vol. 23, no. 9, pp. 1863–1874, Sep. 2005.

[102] T. Q. S. Quek, M. Z. Win, and D. Dardari, "UWB transmitted-reference signaling schemes - Part I: Performance analysis," in *Proc. IEEE Int. Conf. on Utra-Wideband*, Zürich, SWITZERLAND, Sep. 2005, pp. 587–592.

[103] ——, "UWB transmitted-reference signaling schemes - Part II: Narrowband interference analysis," in *Proc. IEEE Int. Conf. on Utra-Wideband*, Zürich, SWITZERLAND, Sep. 2005, pp. 593–598.

[104] ——, "Unified analysis of UWB transmitted-reference schemes in the presence of narrowband interference," *IEEE Trans. Wireless Commun.*, vol. 6, no. 6, pp. 2126–2139, Jun. 2007.

[105] T. Q. S. Quek, D. Dardari, and M. Z. Win, "Energy efficiency of dense wireless sensor networks: To cooperate or not to cooperate," in *Proc. IEEE Int. Conf. on Commun.*, vol. 10, Istanbul, TURKEY, Jun. 2006, pp. 4479–4484.

[106] ——, "Cooperation in bandwidth-constrained wireless sensor networks," in *Proc. IEEE Inter. Workshop Wireless Ad Hoc Sensor Net.*, New York, NY, Jun. 2006.

[107] ——, "Energy efficiency of cooperative dense wireless sensor networks," Vancouver, CANADA, Jul. 2006, pp. 1323–1330.

[108] ——, "Energy efficiency of dense wireless sensor networks: To cooperate or not to cooperate," *IEEE J. Sel. Areas Commun.*, vol. 25, no. 2, pp. 459–470, Feb. 2007.

[109] M. O. Hasna and M.-S. Alouini, "Optimal power allocation for relayed transmissions over Rayleigh-fading channels," *IEEE Trans. Wireless Commun.*, vol. 3, no. 6, pp. 1999–2004, Nov. 2004.

[110] D. P. Bertsekas, A. Nedic, and A. E. Ozdaglar, *Convexity, Duality, and Lagrange Multipliers*, 1st ed. Belmont, MA 02178-9998: Athena Scientific, 2003.

[111] S. Boyd and L. Vandenberghe, *Convex Optimization*. Cambridge, UK: Cambridge University Press, 2004.

[112] L. A. Shepp, "Private conversation," AT&T Labs-Research, Jul. 1999, Red Bank, NJ.

[113] M. S. Klamkin and D. J. Newman, "The philosophy and applications of transform theory," 1960, unpublished manuscript.

[114] M. S. Lobo, L. Vandenberghe, S. Boyd, and H. Lebret, "Applications of second-order cone programming," *Linear Algebra and Its Appl.*, vol. 284, pp. 193–228, Nov. 1998.

[115] K. Glashoff and K. Roleff, "A new method for Chebyshev approximation of complex-valued functions," *Mathematics of Computation*, vol. 36, no. 153, pp. 233–239, Jan. 1981.

[116] R. L. Streit and A. H. Nuttall, "A note on the semi-infinite programming approach to complex approximation," *Mathematics of Computation*, vol. 40, no. 162, pp. 599–605, Apr. 1983.

[117] A. Pascual-Iserte, D. P. Palomar, A. I. Pérez-Neira, and M. Ángel Lagunas, "A robust maximin approach for MIMO communiations with imperfect channel state information based on convex optimization," *IEEE Trans. Signal Process.*, vol. 54, no. 1, pp. 346–360, Jan. 2006.

[118] A. Ben-Tal, A. Nemirovski, and C. Roos, "Robust solutions of uncertain quadratic and conic-quadratic problems," *SIAM J. Optim.*, vol. 13, no. 2, pp. 535–560, 2002.

[119] A. Ben-Tal and A. Nemirovski, "Robust optimization - Methodology and applications," *Math. Program. Ser B*, vol. 92, no. 3, pp. 453–480, 2002.

[120] J. Sturm, "Using SeDuMi 1.02, a MATLAB toolbox for optimization over symmetric cones," *Optim. Meth. Softw.*, vol. 11-12, pp. 625–653, Aug. 1999.

[121] A. F. Molisch, *Wireless Communications*, 1st ed. Piscataway, New Jersey, 08855-1331: IEEE Press, J. Wiley and Sons, 2005.

[122] A. Goldsmith, *Wireless Communications*. Cambridge, UK: Cambridge University Press, 2006.

[123] R. U. Nabar, H. Bölcskei, and F. W. Kneubühler, "Fading relay channels: Performance limits and space-time signal design," *IEEE J. Sel. Areas Commun.*, vol. 22, no. 6, pp. 1099–1109, Aug. 2004.

[124] S. Kandukuri and S. Boyd, "Optimal power control in interference-limited fading wireless channels with outage-probability specifications," *IEEE Trans. Wireless Commun.*, vol. 1, no. 1, pp. 46–55, Jan. 2002.

[125] J. Papandriopoulos, J. Evans, and S. Dey, "Optimal power control for Rayleigh-faded multiuser systems with outage constraints," *IEEE Trans. Wireless Commun.*, vol. 4, no. 6, pp. 2705–2715, Nov. 2005.

[126] M. Andersin and Z. Rosberg, "Time variant power control in cellular networks," in *Proc. IEEE Int. Symp. on Personal, Indoor and Mobile Radio Commun.*, vol. 1, Taipei, TAIWAN, Oct. 1996, pp. 193–197.

[127] S. V. Hanly, "Capacity and power control in spread spectrum macrodiversity radio networks," *IEEE Trans. Commun.*, vol. 44, no. 2, pp. 247–256, Feb. 1996.

[128] R. A. Horn and C. R. Johnson, *Matrix Analysis*, 1st ed. Cambridge: Cambridge University Press, 1990.

[129] J. Zander, "Performance of optimum transmitter power control in cellular radio systems," *IEEE Trans. Veh. Technol.*, vol. 41, no. 1, pp. 57–62, Feb. 1992.

[130] D. Bertsimas and J. N. Tsitsiklis, *Introduction to Linear Optimization*, 1st ed. Belmont, MA 02178-9998: Athena Scientific, 1997.

[131] Y.-L. Chao and R. Scholtz, "Novel UWB transmitted-reference signaling schemes," in *Proc. Asilomar Conf. on Signals, Systems and Computers*, vol. 1, Pacific Grove, CA, Nov. 2004, pp. 652–656.

[132] C.-C. Chong and S. K. Yong, "A generic statistical-based UWB channel model for high-rise apartments," *IEEE Trans. Antennas Propag.*, vol. 53, no. 8, pp. 2389–2399, Aug. 2005.

[133] C.-C. Chong, Y.-E. Kim, S. K. Yong, and S.-S. Lee, "Statistical characterization of the UWB propagation channel in indoor residential environment," *Wireless Commun. and Mobile Computing*, vol. 5, no. 5, pp. 503–512, Aug. 2005.

[134] S. R. Aedudodla, S. Vijayakumaran, and T. F. Wong, "Acquisition of direct-sequence transmitted reference ultra-wideband signals," *IEEE J. Sel. Areas Commun.*, vol. 24, no. 4, pp. 759–765, Apr. 2006.

[135] N. He and C. Tepedelenlioglu, "Performance analysis of non-coherent UWB receivers at different synchronization levels," *IEEE Trans. Wireless Commun.*, vol. 5, no. 6, pp. 1266–1273, Jun. 2006.

[136] M. Casu and G. Durisi, "Implementation aspects of a transmitted-reference UWB receiver," *Wireless Commun. Mobile Comput.*, vol. 5, no. 5, pp. 537–549, Aug. 2005.

[137] M. K. Simon and M.-S. Alouini, *Digital Communication over Fading Channels: A Unified Approach to Performance Analysis*, 1st ed. New York, NY, 10158: John Wiley & Sons, Inc., 2000.

[138] M. Z. Win, G. Chrisikos, and N. R. Sollenberger, "Performance of Rake reception in dense multipath channels: Implications of spreading bandwidth and selection diversity order," *IEEE J. Sel. Areas Commun.*, vol. 18, no. 8, pp. 1516–1525, Aug. 2000.

[139] D. Cassioli, M. Z. Win, F. Vatalaro, and A. F. Molisch, "Performance of selective Rake reception in a realistic UWB channel," in *Proc. IEEE Int. Conf. on Commun.*, vol. 2, New York, NY, May 2002, pp. 763–767.

[140] J. Gil-Pelaez, "Note on the inversion theorem," *Biometrika*, vol. 38, no. 3, pp. 481–482, Dec. 1951.

[141] D. Dardari, A. Giorgetti, M. Chiani, T. Q. S. Quek, and M. Z. Win, "A stop-and-go transmitted-reference UWB receiver," in *Proc. IEEE Int. Conf. on Utra Wideband*, Waltham, MA, Sep. 2006, pp. 309–314.

[142] P. Haschberger, M. Bundschuh, and V. Tank, "Infrared sensor for the detection and protection of wildlife," *J. Opt. Eng.*, vol. 35, no. 3, pp. 882–889, Mar. 1996.

[143] M. Hawkes and A. Nehorai, "Wideband source localization using a distributed acoustic vector-sensor array," *IEEE Trans. Signal Process.*, vol. 51, no. 6, pp. 1479–1491, Jun. 2003.

[144] R. Nemzek, J. Dreicer, D. C. Torney, and T. Warnock, "Distributed detection sensor networks for detection of mobile radioactive sources," *IEEE Trans. Nucl. Sci.*, vol. 51, no. 4, pp. 1693–1700, Aug. 2004.

[145] S. M. Brennan, A. M. Mielke, and D. C. Torney, "Radioactive source detection by sensor networks," *IEEE Trans. Nucl. Sci.*, vol. 52, no. 3, pp. 813–819, Jun. 2005.

[146] J. Orriss and S. K. Barton, "Probability distributions for the number of radio transceivers which can communicate with one another," *IEEE Trans. Commun.*, vol. 51, no. 4, pp. 676–681, Apr. 2003.

[147] Y.-C. Tseng, S.-Y. Ni, Y.-S. Chen, and J.-P. Sheu, "The broadcast storm problem in a mobile ad hoc network," *Wireless Networks*, vol. 8, no. 2/3, pp. 153–167, Mar. 2002.

[148] B. Williams and T. Camp, "Comparison of broadcasting techniques for mobile ad hoc networks," in *Proc. ACM Symp. on Mobile Ad Hoc Networking and Computing*, Lausanne, SWITZERLAND, Jun. 2002, pp. 194–205.

[149] D. Miorandi and E. Altman, "Coverage and connectivity of Ad Hoc networks in presence of channel randomness," in *Proc. IEEE Joint Conf. of the IEEE Computer and Commun. Societies*, vol. 1, Miami, FL, Mar. 2005, pp. 491–502.

[150] C. Bettstetter and C. Hartmann, "Connectivity of wireless multihop networks in a shadow fading environment," *Wireless Networks*, vol. 11, no. 5, pp. 571–579, Sep. 2005.

[151] M. Zorzi and S. Pupolin, "Optimum transmission ranges in multihop packet radio networks in the presence of fading," *IEEE Trans. Commun.*, vol. 43, no. 7, pp. 2201–2205, Jul. 1995.

[152] D. Maltz, J. Broch, and D. Johnson, "Lessons from a full-scale mutlihop wireless ad-hoc network testbed," *IEEE Personal Commun. Mag.*, vol. 8, no. 1, pp. 48–59, Feb. 2001.

[153] A. Ephremides, "Energy concerns in wireless networks," *IEEE Commun. Mag.*, vol. 9, no. 4, pp. 48–59, Aug. 2002.

[154] A. J. Goldsmith and S. B. Wicker, "Design challenges for energy-constrained ad hoc wireless networks," *IEEE Commun. Mag.*, vol. 9, no. 4, pp. 8–27, Aug. 2002.

[155] A. Charnes and W. Cooper, "Chance-constrained programming," *Management Science*, vol. 6, no. 1, pp. 73–79, Oct. 1959.

[156] J. Birge and F. Louveaux, *Introduction to Stochastic Programming*. New York: Springer-Verlag, 1997.

[157] D. P. Palomar and M. Chiang, "A tutorial on decomposition methods for network utility maximization," *IEEE J. Sel. Areas Commun.*, vol. 24, no. 8, pp. 1439–1451, Aug. 2006.

[158] E. Sousa, "Performance of a spread spectrum packet radio network link in a Poisson field of interferers," *IEEE Trans. Inf. Theory*, vol. 38, no. 6, pp. 1743–1754, Nov. 1992.

[159] J. Ilow, D. Hatzinakos, and A. Venetsanopoulos, "Performance of FH SS radio networks with interference modeled as a mixture of Gaussian and alpha-stable noise," *IEEE Trans. Commun.*, vol. 46, no. 4, pp. 509–520, Apr. 1998.

[160] P. C. Pinto, C.-C. Chong, A. Giorgetti, M. Chiani, and M. Z. Win, "Narrowband communication in a Poisson field of ultrawideband interferers," in *Proc. IEEE Int. Conf. on Utra Wideband*, Waltham, MA, Sep. 2006, pp. 387–392.

[161] A. Rabbachin, T. Q. S. Quek, P. Pinto, I. Oppermann, and M. Z. Win, "UWB energy detector in the presence of multiple narrowband interferers," in *Proc. IEEE Int. Conf. on Utra Wideband*, SINGAPORE, Sep. 2007, pp. 857–862.

[162] ——, "Effect of Aggregate Narrowband Interference on the UWB Autocorrelation Receiver," in *Proc. IEEE Int. Conf. on Utra Wideband*, Hannover, GERMANY, Sep. 2008, submitted.

[163] J. H. Kotecha, V. Ramachandran, and A. M. Sayeed, "Distributed multitarget classification in wireless sensor networks," *IEEE J. Sel. Areas Commun.*, vol. 23, no. 4, pp. 703–713, Apr. 2005.

[164] F. Alizadeh and D. Goldfarb, "Second-order cone programming," *Math. Program. Ser B*, vol. 95, no. 1, pp. 3–51, 2003.

[165] A. Ben-Tal and A. Nemirovski, "Robust solutions of linear programming problems contaminated with uncertain data," *Math. Program. Ser B*, vol. 88, pp. 411–424, 2000.

[166] J. M. Wozencraft and I. M. Jacobs, *Principles of Communication Engineering*, 1st ed. London: John Wiley & Sons, Inc., 1965.

[167] E. T. Whittaker, "On the functions which are represented by the exapansions of the interpolation theory," *Proc. Roy. Soc. Edinburgh*, vol. 35, pp. 181–194, 1915.

[168] V. Kotel'nikov, "On the carrying capacity of the "ether" and wire in telecommunications," *Material for the First All-Union Conference of Questions of Communication, Izd. Red. Upr. Svyazi RKKA*, 1933.

[169] C. E. Shannon, "Communications in the presence of noise," *Proc. IRE*, vol. 37, pp. 10–21, Jan. 1949.

[170] R. G. Gallager, *Information Theory and Reliable Communication*, 1st ed. New York, NY, 10158: John Wiley & Sons, Inc., 1968.

[171] D. Slepian and H. Pollak, "Prolate spheroidal wave functions, Fourier analysis and uncertainty: Part I," *Bell Sys. Tech. Journal*, vol. 40, pp. 43–64, Jan. 1961.

[172] H. Landau and H. Pollak, "Prolate spheroidal wave functions, Fourier analysis and uncertainty: Part II," *Bell Sys. Tech. Journal*, vol. 40, pp. 65–84, Jan. 1961.

[173] ——, "Prolate spheroidal wave functions, Fourier analysis and uncertainty: Part III," *Bell Sys. Tech. Journal*, vol. 41, pp. 1295–1336, Jul. 1962.

[174] D. Slepian, "On bandwidth," *Proc. IEEE*, vol. 64, no. 3, pp. 292–300, Mar. 1976.

[175] H. Urkowitz, "Energy detection of unknown deterministic signals," *Proc. IEEE*, vol. 55, no. 4, pp. 523–531, Apr. 1967.

[176] R. G. Gallager, *Principles of Digital Communication.* 6.450 MIT Course Notes, 2007.

[177] D. Tse and P. Viswanath, *Fundatmentals of Wireless Communications.* New York, NY: Cambridge University Press, 2005.

[178] S. Benedetto and E. Biglieri, *Principles of Digital Transmission with Wireless Applications*, 1st ed. New York, NY, 10013: Kluwer Academic/Plenum Publishers, 1999.

[179] J. G. Proakis, *Digital Communications*, 4th ed. New York, NY, 10020: McGraw-Hill, Inc., 2001.

[180] W. Lindsey, "Error probabilities for rician fading multichannel reception of binary and N-ary signals," *IEEE Trans. Inf. Theory*, vol. 11, no. 4, pp. 339–350, Oct. 1964.